UNIVERSITY OF CALIFORNIA, SAN DIEGO

Tracing Compartmentalized Metabolism in Mutant IDH Cancer Cells

A dissertation submitted in partial satisfaction of the requirements for the degree of Doctor of Philosophy

in

Bioengineering with a Specialization in Multi-Scale Biology

by

Seth Jameson Parker

Committee in charge:

Professor Christian M. Metallo, Chair
Professor Pieter C. Dorrestein
Professor Kun-Liang Guan
Professor Bernhard O. Palsson
Professor Reuben J. Shaw

2016

The dissertation of Seth Jameson Parker is approved, and it is acceptable in quality and form for publication on microfilm and electronically:

_____

_____

_____

_____

_____

Chair

University of California, San Diego

2016

DEDICATION

I dedicate this dissertation to my family for their incredible love and support, sacrifices, and unwavering commitment to my success.

TABLE OF CONTENTS

LIST OF FIGURES

LIST OF TABLES

ACKNOWLEDGEMENTS

I thank the chair of my dissertation committee, Professor Christian M. Metallo, for his support and mentorship throughout my Ph.D. training. I thank Christian for the many opportunities he has provided me to develop both scientifically and professionally. I owe much of my success at UC San Diego to Christian and his mentorship. I would like to thank the current and past members of the Metallo lab. I would like to thank the postdoctoral students, specifically Dr. Hui "Sunny" Zhang, Dr. Martina Wallace, Dr. Thekla Cordes, and Dr. Le You for discussing a vast array of scientific topics with me and expanding my scientific views. I would like to thank the graduate students in the lab including Courtney Green, Mehmet Badur, Nate Vacanti, and Chris Ahn for their help and discussions. I would like to thank the undergraduates who have helped me, including Austin Lefebvre, Spencer Lee, Courtney Green, Erika Handly, and Kimberly Wang, and wish them the best in their careers.

I would like to thank my collaborators for their invaluable guidance and scientific support. Thank you Dr. Anne Murphy and Dr. Ajit Divakaruni for your patience in training and assisting me with Seahorse experiments and for discussing mitochondrial physiology with me. To Dr. Matthew Vander Heiden, Dr. Caroline Lewis, Shawn Davidson, and several of the other Vander Heiden lab members: thank you for your scientific guidance, contributions to projects, and for including me at the Keystone conferences. I would like to thank Dr. Reuben Shaw and Dr. Rob Svensson for teaching me how to view metabolism from the viewpoint of a biologist, for our scientific dicussions, and for including me in our many fruitful collaborations.

Chapter 1, in full, is a reprint of the material as it appears in "Metabolic consequences of oncogenic IDH mutations", Pharmacology Therapeutics, vol. 152, 2015. Seth J. Parker is the primary author of this publication. Christian M. Metallo is the corresponding author of this publication.

Chapter 2, excluding subsection titled "Compromised Reductive TCA Metabolism in Endogenous IDH1 mutant cells", is a reprint of the material as it appears in "IDH1 Mutations Alter Citric Acid Cycle Metabolism and Increase Dependence on Oxidative Mitochondrial

Metabolism", Cancer Research, vol. 74, issue 12, 2014. Seth J. Parker and Alexandra R. Grassian are the primary authors of this publication. Shawn M. Davidson, Ajit S. Divakaruni, Courtney R. Green, Xiamei Zhang, Kelly L. Slocum, Minying Pu, Fallon Lin, Chad Vickers, Carol Joud-Caldwell, Franklin Chung, Hong Yin, Erika D. Handly, Christopher Straub, Joseph D. Growney are co-authors of this publication. Matthew G. Vander Heiden, Anne N. Murphy, Raymond Pagliarini, and Christian M. Metallo are corresponding authors of this publication. Subsection titled "Compromised Reductive TCA Metabolism in Endogenous IDH1 Mutant Cells" includes material generated by Seth J. Parker.

Chapter 3, in full, is a reprint of the material as it appears in "Tracing Compartmentalized NADPH Metabolism in the Cytosol and Mitochondria of Mammalian Cells", Molecular Cell, vol. 55, issue 2, 2014. Seth J. Parker and Caroline A. Lewis are primary authors of this publication. Brian P. Fiske, Douglas McCloskey, Dan Y. Gui, Courtney R. Green, Natalie I. Vokes, and Adam M. Feist are co-authors on this publication. Matthew G. Vander Heiden and Christian M. Metallo are corresponding authors on this publication.

Chapter 4 contains material generated by Seth J. Parker.

VITA

Education

University of California, San Diego
La Jolla, CA
Ph.D. Bioengineering with a Specialization in Multi-Scale Biology
September, 2016

University of Colorado at Boulder
Boulder, CO
B.S. Chemical and Biological Engineering
May, 2011

Peer-Reviewed Publications (*denotes equal contribution)

Zhang H*, Badur MG*, Divakaruni AS, Parker SJ, Jager C, Hiller K, Murphy AN, Metallo CM, Distinct metabolic states support self-renewel and lipogenesis in human pluripotent stem cells under different culture conditions, Cell Reports. 2016

Jiang L, Shestov A, Swain P, Yang C, Parker SJ, Wang QA, Terada L, Adams ND, McCabe MT, Pietrak B, Schmidt S, Metallo CM, Dranka BP, Schwartz B, DeBerardinis RJ, Cytosolic reductive carboxylation is required for mitochondrial redox homeostasis during anchorage-independent cell growth, Nature. 2016.

Parker SJ, Metallo CM, Chasing one-carbon units to understand the role of serine in epigenetics, Molecular Cell. 2015.

Lussey-Lepoutre C*, Hollinshead KER*, Ludwig C*, Menara M*, Morin A, Castro-Vega L, Parker SJ, Janina M, Martinelli C, Ottolenghi C, Metallo CM, Gimenez-Roqueplo A, Favier J, Tennant DA, Loss of succinate dehydrogenase activity results in dependency on pyruvate carboxylation for cellular anabolism, Nature Communications. 2015.

Parker SJ, Metallo CM, Metabolic consequences of oncogenic IDH mutations, Pharmacology & Therapeutics. 2015.

Lewis CA*, Parker SJ*, Fiske BP, McCloskey D, Gui DY, Green CR, Vokes NI, Feist AM, Vander Heiden MG, Metallo CM, Tracing compartmentalized NADPH metabolism in the cytosol and mitochondria of mammalian cells, Molecular Cell. 2014.

Vacanti NM, Divakaruni AS, Green CR, Parker SJ, Henry RR, Ciaraldi TP, Murphy AN, Metallo CM, Regulation of substrate utilization by the mitochondrial pyruvate carrier, Molecular Cell. 2014.

Grassian AR*, Parker SJ*, Davidson SM, Divakaruni AS, Green CR, Zhang X, Slocum KL, Pu M, Lin F, Vickers C, Joud-Caldwell C, Chung F, Yin H, Handly ED, Straub C, Growney JD, Vander Heiden MG, Murphy AN, Pagliarini R, Metallo CM, IDH1 mutations alter citric acid cycle metabolism and increase dependence on oxidative mitochondrial metabolism, Cancer Research. 2014.

Commisso C, Davidson SM*, Soydaner-Azeloglu RG*, Parker SJ*, Kamphorst JJ, Hackett S, Grabocka E, Nofal M, Drebin JA, Thompson CB, Rabinowitz JD, Metallo CM, Vander Heiden MG, Bar-Sagi D, Macropinocytosis of protein is an amino acid supply route in Ras-transformed cells, Nature. 2013.

Ungermannova D*, Parker SJ*, Nasveschuk CG, Wang W, Quade B, Zhang G, Kuchta RD, Phillips AJ, Liu X, Largazole and its derivatives selectively inhibit ubiquitin activating enzyme (E1), PLoS One. 2012.

Ungermannova D, Parker SJ, Nasveschuk CG, Chapnick DA, Phillips AJ, Kuchta RD, Liu X, Identification and mechanistic studies of a novel ubiquitin E1 inhibitor. Journal of Biomolecular Screening. 2012.

Poster Presentations (*denotes equal contribution)

Parker SJ, Dviakaruni AS*, Svensson RU*, Lefebvre AE, Murphy AN, Shaw RJ, Metallo CM, Alternative mitochondrial oxidative pathways are critical for LKB1-deficient tumor survival. Keystone Symposia: New Frontiers in Understanding Tumor Metabolism. Banff, Alberta, Canada. February 2016.

Parker SJ, Dviakaruni AS*, Svensson RU*, Lefebvre AE, Murphy AN, Shaw RJ, Metallo CM, Alternative mitochondrial oxidative pathways are critical for LKB1-deficient tumor survival. Abcam Cancer Metabolism. Cambridge, England. October 2015.

Parker SJ, Dviakaruni AS*, Svensson RU*, Lefebvre AE, Murphy AN, Shaw RJ, Metallo CM, Regulation of mitochondrial metabolism by the LKB1 tumor suppressor. Keystone Symposia: Tumor Metabolism. Vancouver, British Columbia, Canada. January 2015.

Parker SJ*, Lewis CA*, Fiske BP, McCloskey D, Gui DY, Green CR, Vokes NI, Feist AM, Vander Heiden MG, Metallo CM, Compartmentalized metabolic cofactor tracing using ^{2}H glucose. NIH/NIBIB Training Grantees Meeting. Washington, D.C. June 2014.

Parker SJ*, Lewis CA*, Fiske BP, McCloskey D, Gui DY, Green CR, Vokes NI, Feist AM, Vander Heiden MG, Metallo CM, Compartmentalized metabolic cofactor tracing using ^{2}H glucose. Keystone Symposia: Tumor Metabolism. Whistler, British Columbia, Canada. March 2014.

Grassian AR*, Parker SJ*, Davidson SM, Divakaruni AS, Green CR, Zhang X, Slocum KL, Pu M, Lin F, Vickers C, Joud-Caldwell C, Chung F, Yin H, Handly ED, Straub C, Growney JD, Vander Heiden MG, Murphy AN, Pagliarini R, Metallo CM, IDH1 mutations alter citric acid

cycle metabolism and increase dependence on oxidative mitochondrial metabolism. Keystone Symposia: Tumor Metabolism. Whistler, British Columbia, Canada. March 2014.

Parker SJ, Dviakaruni AS*, Svensson RU*, Lefebvre AE, Murphy AN, Shaw RJ, Metallo CM, Regulation of mitochondrial metabolism by the LKB1 tumor suppressor. Keystone Symposia: Tumor Metabolism. Keystone, Colorado. February 2013.

Parker SJ, Ungermannova D, Liu X, Largazole and its derivatives selectively inhibit ubiquitin activating enzyme (E1). UCCC Cancer Research Fellowship Symposium. Denver, CO. August 2011.

Parker SJ, Ungermannova D, Kuchta RD, Phillips AJ, Liu X. Profiling the synthetic lethality of largazole. Chemistry and Biochemistry Department Retreat. Winter Park, CO.

Parker SJ, Ungermannova D, Liu X. Largazole inhibits the ubiquitination of p27. HHMI Undergraduate Research Symposium. Boulder, CO.

Parker SJ, Liang X, Weimer, AW. Improving the bioactivity of titanium by atomic layer deposition surface modification. Discovery Learning Apprenticeship Symposium. Boulder, CO.

ABSTRACT OF THE DISSERTATION

Tracing Compartmentalized Metabolism in Mutant IDH Cancer Cells

by

Seth Jameson Parker

Doctor of Philosophy in Bioengineering with a Specialization in Multi-Scale Biology

University of California, San Diego, 2016

Professor Christian M. Metallo, Chair

Cellular metabolism comprises of a network of reactions responsible for converting nutrients into energy and building blocks necessary for cells to carry out specific functions and to proliferate. In many diseases, including cancer, metabolism is dysfunctional and distinct from normal, non-diseased cells largely due to the presence of mutations impacting the regulation of cellular signaling and metabolic pathways. The chapters of this dissertation are independent bodies of work that explore how specific mutations and environmental stresses can influence the flow of nutrients through the metabolic network. Chapter 1, titled "Metabolic Consequences of Oncogenic IDH Mutations", is a review on a set of mutations in a specific metabolic enzyme observed in several different types of human cancers and how these mutations affect the flow of major nutrients through the metabolic network. The chapter also discusses possible ther-

apeutic targets present in metabolism and current efforts to treat cancers that harbor these mutations. Chapter 2, titled "IDH1 Mutations Alter Citric Acid Cycle Metabolism and Increase Dependence on Oxidative Mitochondrial Metabolism", explores how mutations in the cytosolic enzyme isocitrate dehydrogenase 1 (IDH1) affects central carbon metabolism in response to the low oxygen tensions commonly experienced in tumors. Cancer cells harboring mutations in IDH1 exhibited a greater reliance on oxidative mitochondrial metabolism under low oxygen tensions and were significantly more sensitive to mitochondrial inhibitors, such as the biguanide phenformin. Chapter 3, titled "Tracing Compartmentalized NADPH Metabolism in the Cysotol and Mitochondria of Mammalian Cells", describes the development of a tracing technique utilizing deuterium-labeled substrates and mass spectrometry to understand how NADPH and NADH, two cofactors critical for a variety of cellular processes, are metabolized in intact cells. In addition, Chapter 3 discusses the development of a reporter system to detect metabolism of NADPH in distinct organelles, such as the cytosol and mitochondria, in order to elucidate the activity of NADPH-dependent isozymes that exist in both compartments. Lastly, Chapter 3 explores the directionality of folate-mediated one carbon metabolism, a pathway critical for synthesizing nucleotides and supplying NAD(P)H, utilizing the reporter system. Chapter 4, titled "Hypoxic Reprogramming of Redox Metabolism in Mutant IDH2 Cells", applies the deuterium tracing technique discussed in Chapter 3 to understand how redox metabolism, specifically NADH and NADPH metabolism, is reprogrammed in response to low-oxygen tensions. Furthermore, the reporter system is applied to understand how mitochondrial NADPH pools are affected by mutations in the mitochondrial enzyme IDH2 in cancer. Chapter 4 highlights an interesting, often overlooked, aspect of metabolism: the compartmentalization of metabolic pathways.

Chapter 1

Metabolic Consequences of Oncogenic IDH Mutations

Abstract

Specific point mutations in isocitrate dehydrogenase 1 and 2 (*IDH1* and *IDH2*) occur in a variety of cancers, including acute myeloid leukemia (AML), low-grade gliomas, and chondrosarcomas. These mutations inactivate wild-type enzymatic activity and convey neomorphic function to produce D-2-hydroxyglutarate (D-2HG), which accumulates at millimolar levels within tumors. D-2HG can impact α-ketoglutarate-dependent dioxygenase activity and subsequently affect various cellular functions in these cancers. Inhibitors of the neomorphic activity of mutant IDH1 and IDH2 are currently in Phase I/II clinical trials for both solid and blood tumors. As IDH1 and IDH2 represent key enzymes within the tricarboxylic acid (TCA) cycle, mutations have significant impact on intermediary metabolism. The loss of some wild-type metabolic activity is an important, potentially deleterious and therapeutically exploitable consequence of oncogenic IDH mutations and requires continued investigation in the future. Here we review how IDH1 and IDH2 mutations influence cellular metabolism, epigenetics, and other biochemical functions, discussing these changes in the context of current efforts to therapeutically target cancers bearing these mutations.

Introduction

Mutations in oncogenes and tumor suppressors facilitate the rapid growth of cancer cells and their survival in response to environmental stress. To maintain this phenotype tumor cells initiate a metabolic program that supplies the energy, reducing equivalents, and biosynthetic precursors necessary to divide (Tennant et al., 2010). In the early 20th century Otto Warburg observed that cancer cells (and normal proliferating cells) selectively metabolized glucose to lactate even under aerobic conditions (Warburg, 1956). This phenomenon, also known as the "Warburg Effect" is common to many (but not all) tumors. Since Warburg's discovery, biochemists have painstakingly annotated the network of biochemical reactions comprising cellular metabolism. Though not yet complete, this information provides a biochemical roadmap to study metabolic dysfunction in the context of diseases using a range of datasets (Bordbar et al., 2014; Yizhak et al., 2010). Most oncogenes and tumor suppressors directly impact cellular metabolism, and several hallmark cancer mutations have been observed to occur in metabolic enzymes. Homozygous loss-of-function mutations in fumarate hydratase (FH) or one of the five subunits comprising the succinate dehydrogenase (SDH) complex can lead to the development of specific cancers, representing the first time that metabolic enzymes were classified as bonafide tumor suppressors (King et al., 2006). More recently, mutations in isocitrate dehydrogenase 1 and 2 (IDH1, IDH2) have been discovered in various cancers. These exclusively heterozygous mutations do not follow a traditional loss-of-function mechanism, and the downstream effects of these mutations on tumor initiation, metabolism, and growth are currently being investigated. Here we review how mutations in IDH1 and IDH2 impact intermediary metabolism and other cell functions. Finally, the metabolic and epigenetic consequences of mutant IDH1 and IDH2 are discussed in the context of current efforts to therapeutically target cancers harboring these mutations.

Mutation of Isocitrate Dehydrogenase 1 and 2

Mutation of *IDH1* and *IDH2* were initially identified through exome sequencing of colon tumor and glioblastoma multiforme (GBM) (Parsons et al., 2008; Sjoblom et al., 2006). Since these discoveries, IDH mutations have been observed in several other tumor types, including acute myeloid leukemia (AML), chondrosarcoma, and intrahepatic cholangiocarcinoma (Amary et al., 2011; Borger et al., 2012; Mardis et al., 2009; Parsons et al., 2008; Yan et al., 2009). These mutations are somatically acquired and occur on distinct arginine residues of IDH1 (R132) and IDH2 (R172 or R140). Interestingly, *IDH1* mutations occur at much higher incidences than *IDH2* mutations in low grade gliomas, cholangiocarcinoma, and chondrosarcoma; however, *IDH1* and *IDH2* mutations occur at similar rates in AML (Molenaar et al., 2014; Ward et al., 2010). Due to the frequency of observation in low grade gliomas, IDH mutations are thought to play a significant role in early tumorigenesis and precede other oncogenic mutations (Balss et al., 2008; Juratli et al., 2013; Watanabe et al., 2009).

In contrast to SDH and FH mutants, which exhibit traditional homozygous loss-of-function mutations, IDH mutants retain one wild-type allele and rarely exhibit loss of heterozygosity (Jin et al., 2013; Mullen and DeBerardinis, 2012). Furthermore, the occurrence of mutations on distinct IDH1 and IDH2 residues within the active site provided evidence that these changes elicit a gain-of-function phenotype in each enzyme. Subsequently, an analysis of the x-ray structure of mutant IDH1 in conjunction with metabolomics profiling demonstrated that (D)-2-hydroxyglutarate (D- or R-2HG) was produced by mutant IDH1 and accumulated at high levels in mutant tumors, confirming a gain-of-function mechanism (Dang et al., 2009). Similar production of D-2HG was demonstrated in cells and tumors harboring *IDH2* mutations (Ward et al., 2010).

Wild-type IDH1 and IDH2 normally catalyze the reversible, NADP+-dependent oxidative decarboxylation of isocitrate to alpha-ketoglutarate in either the cytosol (IDH1) or mitochondria (IDH2). However, the mutant IDH enzyme loses oxidative activity and instead reduces alpha-ketoglutarate (αKG, also known as 2-oxoglutarate) to D-2HG, consuming one molecule of NADPH in the process (Figure 1.1). Under normal conditions human cells produce low

levels of both D-2HG and L-2HG (or S-2HG) due to enzyme promiscuity, but 2HG (referring to both D-2HG and L-2HG) fails to accumulate due to the activity enantiomer-specific FAD-dependent 2-hydroxyglutarate dehydrogenases (*L2HGDH* and *D2HGDH*) that convert 2HG to αKG (Van Schaftingen et al., 2013). Deficiency in *L2HGDH* or *D2HGDH* due to homozygous loss-of-function mutation causes patients to develop 2HG aciduria characterized by an accumulation of either enantiomer in body fluids (Rzem et al., 2007; Struys, 2006). About 50% of patients with D-2HG aciduria have autosomal recessive mutations in *D2HGDH*; however, the majority of patients with normal D-2HGDH enzyme but high D-2HG harbored mutations in *IDH2* (either R140Q or R140G) (Kranendijk et al., 2010). Patients with D-2HG aciduria either show no symptoms or exhibit developmental delay, epilepsy, cardiomyopathy, and other clinical symptoms (Kranendijk et al., 2010). In contrast, patients with L-2HG aciduria have an increased risk of developing certain brain cancers, suggesting that 2HG may act as a driver of tumorigenesis (DeBerardinis and Thompson, 2012; Moroni et al., 2004). Most patients who developed metastatic brain tumors exhibited high levels of L-2HG, not D-2HG, and tumors that develop are of a different type than those commonly associated with IDH mutation (Cairns and Mak, 2013). Thus, D-2HG accumulation from mutant IDH may not be sufficient to drive malignancy and may require additional oncogenic mutations. Indeed, IDH mutations observed in low-grade gliomas frequently precede 1p/19q co-deletion and/or *TP53* mutation which give rise to either oligoastrocytomas/oligodendrogliomas or low grade astrocytomas, respectively (Cairns and Mak, 2013; Labussiere et al., 2010; Lai et al., 2011). These tumors follow distinct transformation programs with 1p/19q co-deleted tumors commonly activating PI3K/Akt or Ras and p53 mutant tumors amplifying receptor tyrosine kinases (*i.e.*, MET and PDGFR) (Wakimoto et al., 2014). Further transformation of IDH mutant low-grade gliomas into secondary glioblastomas requires EGFR amplification, PTEN loss, and/or additional genetic alterations (Lai et al., 2011).

Sequencing of *IDH1* and *IDH2* in AML patients indicated that these mutations occurred in a subset of tumors that were distinct from those harboring loss-of-function *TET2* mutations, suggesting that D-2HG accumulation disrupts the function of TET2 or another αKG-dependent dioxygenase (Figueroa et al., 2010). Several studies have subsequently indicated that both

L-2HG and D-2HG can act as competitive inhibitors of αKG-dependent dioxygenases, including the EglN family of prolyl hydroxylases (PHDs), the TET family of DNA demethylases, and the JmjC family of histone demethylases (Chowdhury et al., 2011; Koivunen et al., 2012; Lu et al., 2012; Xu et al., 2011). As such, D-2HG acts in a manner similar to the succinate and fumarate that accumulate in the context of SDH and FH mutant tumors, respectively (Selak et al., 2005; Xiao et al., 2012). Indeed, D-2HG accumulation resulting from mutant IDH expression has been observed to promote DNA and/or histone hypermethylation phenotypes (Figueroa et al., 2010; Lu et al., 2013; Turcan et al., 2012). At least in the context of SDH mutant cells, this inhibitory effect on dioxygenase activity can be ameliorated by addition of cell-permeable αKG analogs (MacKenzie et al., 2007). In addition, histone hypermethylation associated with IDH1 mutant expression in U87 glioma cells was reversed by octyl-αKG addition (Xu et al., 2011). In contrast to the inhibitory mechanisms noted above, D-2HG has been observed to activate EglN in many cell and *in vivo* models, leading to hypoxia inducible factor-1α (HIF1α) degradation and the promotion of tumor development (Koivunen et al., 2012; Losman et al., 2013). On the other hand, other studies have observed increases in HIF1α levels in IDH1 mutant U87 cells (Xu et al., 2011; Zhao et al., 2009) or in brain-specific Nestin-IDH1$^{R132H/wt}$ transgenic mouse embryos (Sasaki et al., 2012a). In contrast, an analysis of IDH1-R132H and HIF1α expression in serial sections of IDH1-R132H positive gliomas suggested that IDH1-R132H expression was not sufficient for HIF1α stabilization (Williams et al., 2011). Overall, the role of IDH mutants and 2HG on HIF1α stabilization is complex and can be influenced by cell type, tissue, and the local microenvironment. The epigenetic dysregulation caused by αKG antagonism has been proposed to be one mechanism through which D-2HG contributes to tumorigenesis in mutant IDH tumors (Figure 1.1). However, the specific αKG-dependent dioxygenases that contribute to tumor development are likely to be context-dependent (*e.g.* tissue specific). As this family of enzymes catalyzes a wide variety of reactions and includes protein- and DNA-modifying enzymes as well as metabolic enzymes (reviewed by Losman and Kaelin (2013)), additional insights are needed to determine the mechanistic drivers of tumorigenesis downstream of mutant IDH (Losman and Kaelin, 2013).

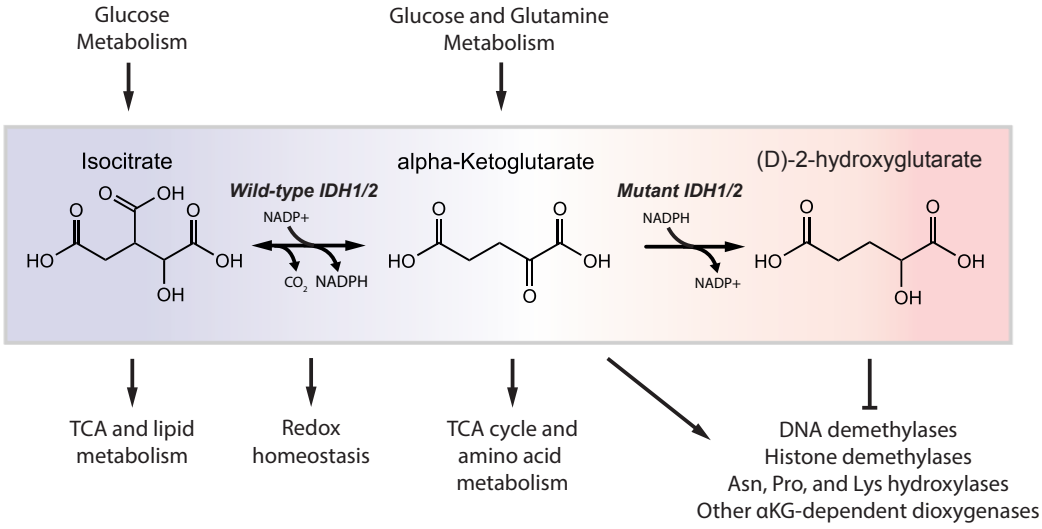

Figure 1.1: Multiple Cellular Pathways are Affected by Mutations in *IDH1* and *IDH2*. Metabolites involved in these reactions are critical for glucose, glutamine, NADPH, amino acid, and lipid metabolism as well as epigenetic regulation.

IDH Mechanism and Regulation

The crystal structures of human IDH1 and pig IDH2, which shares >97% identity with human IDH2, have yielded insights into the enzymatic and regulatory mechanisms of these NADP+-dependent enzymes (Ceccarelli et al., 2002; Xu et al., 2004). Structural studies of IDH1 suggest that its IDH1 follows a self-regulation feedback mechanism whereby isocitrate binds directly to Arg132, inducing a conformational change that allows the Asp279 residue to interact with Ca^{2+} cofactor and participate in catalysis (Xu et al., 2004). Kinetic studies suggest that isocitrate, and to a greater extent NADP+, regulate the activity and directionality of IDH1 (Rendina et al., 2013). The point mutations in IDH1 and IDH2 have significant effects on enzyme catalytic function and mechanism (Dang et al., 2009; Rendina et al., 2013). Arg132 directly interacts with isocitrate, and amino acid substitutions from any of the mutations observed in gliomas prevented isocitrate from binding (Dang et al., 2009; Zhao et al., 2009). Thus, IDH1 mutants become insensitive to physiological isocitrate levels and exhibit a >80% decreased capacity to carry out the oxidative reaction (Zhao et al., 2009). Consequently, the

NADPH production by oxidative IDH activity is diminished, resulting in a ~38% reduction in the NADPH generation capacity in *IDH1*-mutant versus wild-type glioblastoma tumor tissue (Bleeker et al., 2010).

IDH1 mutants exhibit a sequential kinetic mechanism whereby NADPH first binds, reductively trapping αKG into D-2HG before allowing it to undergo carboxylation to form ICT (Rendina et al., 2013). IDH1-R132 variants (H, C, G, S, L) exhibit significantly different kinetic parameters for αKG and, consequently, produce different levels of D-2HG in cells expressing IDH1-R132 (Pusch et al., 2014). These mechanistic insights offer an explanation as to why D-2HG is preferentially produced by mutant IDH1 enzymes. In addition to the IDH1-R132 and IDH2-R172 and R140Q mutants, other IDH mutation sites have been predicted and/or demonstrated to exhibit neomorphic activity, including IDH1-R100, IDH1-Y179, and IDH1-G97 (Rendina et al., 2013; Ward et al., 2012). IDH1-Y179 and IDH1-G97 mutants exhibited lower K_m values for isocitrate (*i.e.*, improved binding); suggesting that neomorphic function is not reliant on an impaired utilization of isocitrate (Rendina et al., 2013). Ultimately, the changes in wild-type and neomorphic function of IDH1 and IDH2 described above influence cell signaling, epigenetics, and enzyme activity to directly and indirectly drive metabolic reprogramming within tumors (Figure 1.2).

Glucose Metabolism

Glycolytic flux is commonly upregulated in tumors downstream of various signaling pathways. For example, phosphoinositide 3-kinase (PI3K) is activated in many tumors and plays a significant role in maintaining the glycolytic phenotype of cancers through protein kinase B (PKB/Akt) signaling (Engelman, 2009). This oncogenic signal stimulates glycolysis, in part, by promoting the expression of glucose and other nutrient transporters and stimulating the activity of glycolytic enzymes including hexokinase and PFKFB3 (Cairns et al., 2011; DeBerardinis et al., 2008; Elstrom et al., 2004; Vander Heiden et al., 2009). While hyperactivation of PI3K/Akt signaling contributes to the aggressiveness of gliomas (Bleau et al., 2009; Koul, 2008), U87 glioma cells expressing IDH1-R132H exhibited decreased Akt levels at both the

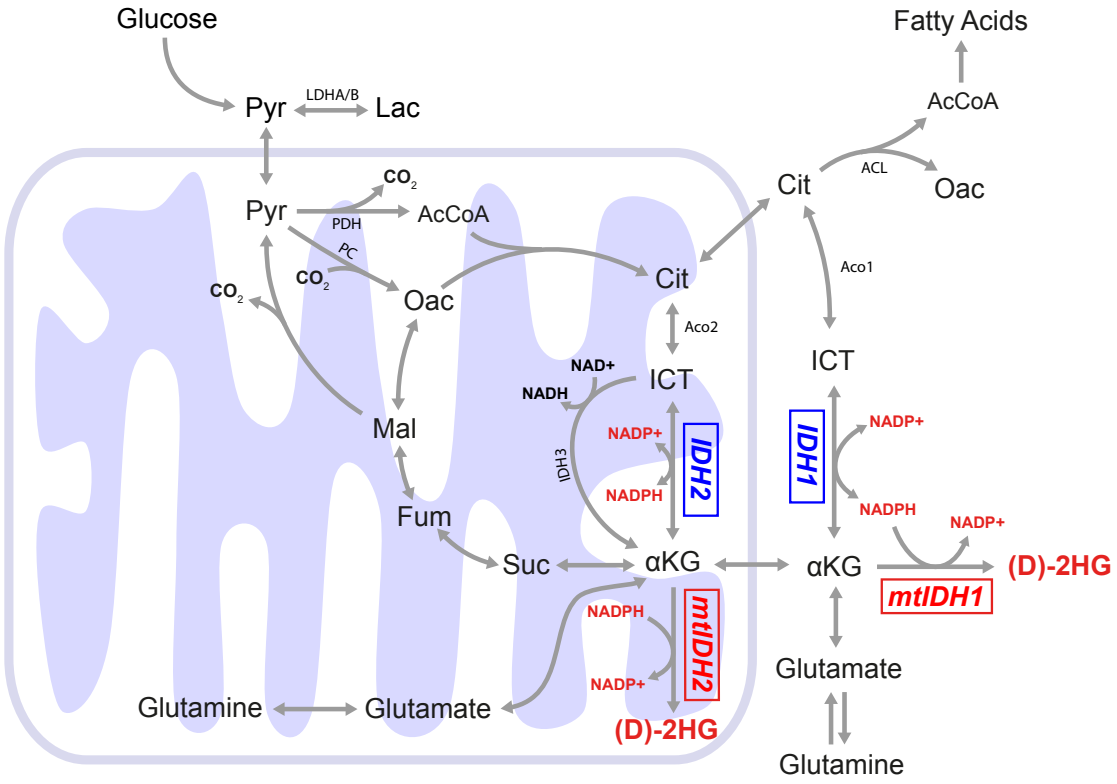

Figure 1.2: Biochemical Pathways Involved in Intermediary Metabolism. Glycolysis and glucose entry into the TCA cycle is regulated by the activity of lactate dehydrogenase (LDHA and LDHB), pyruvate dehydrogenase (PDH), and pyruvate carboxylation (PC). IDH1 and IDH2 are cytosolic and mitochondrial enzymes, respectively, that are critical for the metabolism of glucose- and glutamine- derived carbons. NADPH produced by either IDH1 or IDH2 is critical for maintaining the redox state in subcellular compartments. AcCoA: acetyl-coenzyme A, ÎśKG: alpha-ketoglutarate, Cit: citrate, D-2HG: D-2-hydroxyglutarate, Fum: fumarate, ICT: isocitrate, Lac: lactate, Mal: malate, Oac: oxaloacetate, Pyr: pyruvate, Suc: succinate.

mRNA and protein level (Bralten et al., 2011). Furthermore, expression of mutant IDH1 in LN-319 glioblastoma cells caused a decrease in Akt phosphorylation, suggesting that mutant tumors may exhibit less of a glycolytic metabolic phenotype compared to IDH1 wild-type tumors (Birner et al., 2014). Importantly, the majority of tumors harboring both IDH mutations and 1p/19q co-deletion exhibit activation of PI3K/Akt; thus, the role of Akt on glucose metabolism in mutant IDH tumors may also rely on external factors (*i.e.* additional oncogenic mutations, tumor microenvironment).

Lactate dehydrogenase A (*LDHA*) is commonly upregulated in cancer cells downstream of HIF1α and Myc signaling (Cairns et al., 2011; Dang et al., 2008; Kim et al., 2007); this enzyme helps maintain glycolysis via NAD+ regeneration (Metallo and Vander Heiden, 2013). One recent study observed that IDH mutant gliomas and tumor-derived brain tumor stem cells silence *LDHA* expression through promoter hypermethylation (Chesnelong et al., 2014). In addition, one study identified that AML patients with *IDH1* or *IDH2* mutant tumors exhibited lower LDH activity compared to wild-type *IDH1* or *IDH2* tumors, suggesting a common phenotype between IDH mutants mediated by αKG/2HG (Chou et al., 2011). An analysis of gene expression in *IDH1* mutant and *IDH1* wild-type glioma samples demonstrated that factor inhibiting HIF-1 (FIH-1/HIFAN) was upregulated in IDH1 mutant tumors (Mustafa et al., 2014). FIH-1 inhibits the activity of HIF1α by preventing its transactivation in an αKG-dependent manner (Mahon et al., 2001), and HIF1α levels are known to be decreased in IDH1 mutant gliomas, enhancing tumorigenesis (Koivunen et al., 2012). This phenotype is thought to result from increased EglN activity fueled by 2HG-αKG isomerization (Tarhonskaya et al., 2014). Putatively as a consequence of HIF1α suppression, IDH1 mutant gliomas expressed high levels of *LDHB* relative to *LDHA* as compared to IDH1 wild-type gliomas or normal brain tissue (Mustafa et al., 2014). Acting as the final step in converting glucose to lactate, *LDHA* silencing may act to mitigate aerobic glycolysis. Although both isoforms of LDH (LDHA and LDHB) can metabolize the conversion of pyruvate to lactate, the LDHB isoform is more sensitive to substrate inhibition by pyruvate and is more capable of converting lactate to pyruvate (Dang, 2013).

Pyruvate dehydrogenase (PDH) is a major point of entry for glucose-derived pyruvate oxidation in the TCA cycle. PDH activity is regulated by its phosphorylation state and HIF1α

stimulates expression of PDK1, leading to inactivating phosphorylation of PDH (Kim et al., 2006; Papandreou et al., 2006; Rardin et al., 2009; Semenza et al., 1994). Thus, alteration of HIF1α expression in mutant IDH cells and tumors may influence PDH activity and lead to changes in flux of glucose-derived pyruvate into the mitochondria. In addition to mitochondrial acetyl-CoA generated by PDH, cells need oxaloacetate (OAC) to maintain TCA cycle flux. Cancer cells can obtain OAC through various mechanisms, including glucose anaplerosis via pyruvate carboxylase or glutaminolysis, and pyruvate carboxylase is required for cells growing in glutamine-deprived conditions (Cheng et al., 2011). Furthermore, *in vivo* tracing studies in an orthotopic model of human glioblastoma using ^{13}C-labeled glucose have indicated that pyruvate carboxylase and PDH are highly active in GBM (Marin-Valencia et al., 2012). One recent study demonstrated that IDH mutant overexpression in astrocytes results in an increased fractional flux through pyruvate carboxylase and an increase in PC expression, suggesting this pathway is critical for IDH mutant cells to maintain TCA activity (Izquierdo-Garcia et al., 2014). Consistent with this observation, we observed increased pyruvate cycling through malic enzymes and PC in HCT116 cells harboring heterozygous *IDH1* mutations (Grassian et al., 2014).

Glutaminolysis, Reductive Carboxylation, and TCA Metabolism

Glutamine is another major contributor to TCA metabolism in cancer cells and enters this pathway at αKG. As such, glutamine-glutamate-αKG metabolism represents a critical node in IDH mutant tumors. Glutamine is converted to glutamate during the biosynthesis of nucleotides, hexosamines, and asparagine; alternatively this reaction may be catalyzed in mitochondria via glutaminase (GLS). Transaminases or glutamate dehydrogenase (GLUD) can convert glutamate to the TCA intermediate and IDH substrate/product αKG. These pathways are highly active in most cancer cells as a result of oncogenic mutations or limited glucose oxidation (Gaglio et al., 2011; Son et al., 2013a). Hypoxic microenvironments common to solid tumors promote glutamine flux into TCA metabolism such that it becomes the predominant carbon source for the glutaminolysis (Fan et al., 2013; Grassian et al., 2014; Le et al., 2012) and reductive carboxylation pathways (Metallo et al., 2012; Mullen et al., 2012; Scott et al., 2011; Wise

et al., 2011).

Not surprisingly, much of the D-2HG produced by mutant IDH1 and IDH2 in cells is derived from glutamine (Grassian et al., 2014). Due to its clinical prevalence and the availability of cell models more studies have focused on the impact of mutant IDH1 on TCA metabolism compared to mutant IDH2. Beyond αKG generation, flux through both glutaminolytic and reductive carboxylation pathways are significantly impacted by IDH mutations. When oxygen is replete, evidence suggests that IDH flux predominantly occurs in the oxidative direction, with minimal (but some) exchange observable. Given the impact of mutant IDH1 on WT activity it is not surprising that such cells become more reliant on the glutaminolysis pathway. Recent studies have highlighted differences in this pathway when cells express or harbor *IDH1* mutations. For example, a glioblastoma cell line and transformed astrocytes both exhibited increased sensitivity to pharmacological or siRNA-mediated inhibition of glutaminase (Seltzer et al., 2010). In addition, Chen et al. recently observed that gliomas harboring *IDH1* mutations overexpressed glutamate dehydrogenase 1 and 2 (GLUD1 and GLUD2), and orthotopic growth of mutant glioma lines were sensitive to *GLUD1* or *GLUD2* knockdown (Chen et al., 2014). We observed a similar increase in the dependence of IDH1 mutant cells on glutaminolysis in our analysis of a panel of HCT116 cells, providing evidence that these changes arise due to a direct impact on metabolism rather than indirectly through cell lineage-specific mechanisms (Grassian et al., 2014). Notably, this dependence on oxidative glutamine metabolism was exacerbated by culture under hypoxia, such that mutant IDH1 cells exhibited decreased growth and increased respiration under hypoxia (Grassian et al., 2014).

IDH1 has been implicated in catalyzing the reductive carboxylation of αKG to isocitrate, a pathway that facilitates conversion of glutamine to biosynthetic intermediates under conditions of hypoxia or mitochondrial dysfunction (Metallo et al., 2012; Mullen et al., 2012; Scott et al., 2011). As the IDH reactions in human cells involve the interplay of NADH, NADPH, αKG, and isocitrate in two important cellular compartments, the localization, interconnectivity (*i.e.*, via NAD(P)H shuttling), regulation, and function of the reductive carboxylation pathway is still actively investigated. *In vitro* enzyme studies have demonstrated that mutant/wild-type heterodimers of both IDH1 and IDH2 are unable to catalyze the reductive carboxylation reaction

(Leonardi et al., 2012). Given the demonstrated role of IDH1 in this reaction, mutant IDH1 cells exhibit a strong defect in the conversion of glutamine to isocitrate, citrate, and acetyl-CoA under various conditions. Indeed, the extent that heterozygous mutant IDH HCT116 cells and IDH1-R132C HT1080 fibrosarcoma cells activate this pathway under hypoxia was compromised when compared to cells with IDH2 mutations or wild-type IDH (Grassian et al., 2014). Changes in glutamine metabolism under hypoxia were also observed in an additional study that employed HCT116 IDH1-R132H cells (Reitman et al., 2014). Furthermore, IDH1 mutant cells exhibited increased sensitivity to inhibitors of respiration, conditions known to promote reductive carboxylation (Fendt et al., 2013a; Gameiro et al., 2013; Mullen et al., 2012). This sensitivity could be due to the cells' inability to synthesize acetyl-CoA through reductive carboxylation or alternatively due to their increased dependence on respiration under hypoxia. TCA metabolism is coupled with cellular respiration. As noted above, we observed increased sensitivity to ETC/respiration inhibitors and changes in oxygen consumption rates in IDH1 mutant HCT116 cells under hypoxia (Grassian et al., 2014). More recently, Chan et al. and other studies have demonstrated that D-2HG produced by mutant IDH inhibits complex IV (also known as cytochrome c oxidase, COX) of the ETC (Chan et al., 2015; da Silva et al., 2002; Wajne et al., 2002). This mechanism induced mutant IDH leukemia cell lines (patient-derived and engineered) to become sensitive to Bcl-2 inhibitors, initially identified as a target in a shRNA screen (Chan et al., 2015).

In addition to fatty acid and cholesterol synthesis, acetyl-CoA is an important building block for phospholipids, amino acids, and protein acetylation (Kaelin and McKnight, 2013). Interestingly, N-acetylated amino acids including N-acetyl-aspartyl-glutamate (NAAG) and N-acetyl-aspartate (NAA) were significantly decreased in human glioma cells expressing IDH1-R132H (Reitman et al., 2011). These results suggest that mutant IDH tumors may exhibit perturbed acetyl-CoA metabolism, potentially due to changes in pathway fluxes fueling acetyl-CoA pools. In addition to differences in acetyl-CoA metabolism, IDH mutant tumors exhibited a significantly altered phospholipid profile compared to wild-type IDH tumors. Specifically, pools of the phospholipid metabolites phosphoethanolamine and glycerophosphocholine were significantly perturbed in mutant IDH versus wild-type IDH tumors (Esmaeili et al., 2014). Several of the

oncogenic signaling pathways altered in IDH mutant tumors also impact fatty acid synthesis and uptake. For example, ATP-citrate lyase (ACL) acts as the major supplier of cytosolic AcCoA for fatty acid synthesis and is a major Akt substrate, and Akt also induces other fatty acid synthesis enzymes (*i.e.* FAS, ACC) via mTORC1 activation of SREBP-1 (Berwick et al., 2002; Porstmann et al., 2008; Ru et al., 2013). In addition to *de novo* synthesis, fatty acids and cholesterol can be scavenged from extracellular sources, and PI3K/Akt signaling can upregulate expression of the LDL receptor—supplying cells with cholesterol—via SREBP-1 (Guo et al., 2011). Of note, IDH1 is a transcriptional target of SREBP-1a and to a lesser extent SREBP-2, purportedly to supply NADPH for reductive biosynthesis in the cytosol (Shechter et al., 2003).

In part due to a lack of isogenic or cell-based models, fewer studies have addressed the impact of heterozygous mutations in IDH2 on intermediary metabolism. Generally, cells expressing IDH2-R172 accumulate more or similar amounts of D-2HG than those with mutant IDH1, though IDH2-R140Q mutants produce the least (Ward et al., 2010). *In vitro* enzyme studies and ectopic expression of mutants has indicated that differences in gene expression and compartment localization/conditions may influence the differential D-2HG production by IDH1-R132 mutants versus IDH2-R172 mutants (Ward et al., 2013). In addition to effects on D-2HG accumulation, some evidence indicates that the intermediary metabolism of cells with mutant IDH1 versus IDH2 differs as well. As noted above, detectable and significant effects on TCA metabolism were observed in an isogenic HCT116 cell panel cultured under normoxia and hypoxia. In contrast, the profile of glucose and glutamine-driven TCA metabolism in cells with either IDH2-R172 or IDH2-R140Q mutations was similar to that of parental cells cultured normally or in the presence of exogenous D-2HG (Grassian et al., 2014). No *in vitro* growth defect was observed under hypoxia, and the cells readily used the reductive carboxylation pathway for *de novo* lipogenesis. Similar trends were observed when comparing HT1080 (IDH1-R132C) fibrosacroma and SW1353 (IDH2-R172S) chondrosarcoma cells.

In the context of analyzing flux changes in heterozygous IDH mutant tumors versus those with WT IDH1 and IDH2 it is important to consider that a heterozygous mixture of homo- and heterodimers will exist within cells. Notably, the binding affinity of IDH1-R132 and IDH1-WT monomers was not significantly different, suggesting that a diversity of homo- and hetero- IDH1

dimers exists in *IDH1* mutant tumors (Jin et al., 2011). In contrast, IDH2-R172 weakly binds IDH2-WT, indicating that there is a greater enrichment of WT-WT homodimers in mutant IDH2 tumors (Jin et al., 2011). Furthermore, differences in substrate availability for the IDH reaction are likely significant when comparing metabolism in the cytosol/peroxisome (IDH1) and mitochondrial matrix (IDH2). The ability to resolve such differences remains a challenge, as it is unclear to what extent reductive carboxylation is catalyzed in the mitochondria versus cytosol (Metallo and Vander Heiden, 2013). While defects in this pathway arise in mutant IDH1 cells but not mutant IDH2 cells, the expression of several mitochondrial enzymes (*e.g.* transhydrogenase, αKG-dehydrogenase complex) influences reductive carboxylation flux (Gameiro et al., 2013; Mullen et al., 2012). Despite the observed *in vitro* differences in metabolism and growth, HCT116 cells containing either *IDH1* or *IDH2* mutations panel grew significantly slower as xenografts when compared to parental cells (Grassian et al., 2014). These findings highlight the importance of microenvironment on metabolism and the impact of IDH mutations as well as the need for better cell/tumor models.

Other Metabolic Pathways

Beyond glucose, glutamine, and acetyl-CoA metabolism, αKG and 2HG can influence a number of other metabolic pathways. As noted above, D-2HG may inhibit (or promote the activity of) other members of the αKG-dependent dioxygenase family. These enzymes catalyze diverse functions that include various metabolic reactions beyond demethylation (Losman and Kaelin, 2013; Rose et al., 2011). For example, the activity of several proline and lysine hydroxylases are perturbed in the context of IDH mutations, leading to compromised collagen maturation and impacts on extracellular matrix (ECM) processing. Notably, a significant impact on ECM was observed in an IDH mutant knock-in model (Sasaki et al., 2012b). The dioxygenase family also includes enzymes involved in fatty acid metabolism, RNA modifications, and carnitine biosynthesis (Losman and Kaelin, 2013; Rose et al., 2011). Furthermore, αKG is a substrate for a large number of enzymes outside of dioxygenases, including transaminases. Notably, BCAT1 expression is high in glioblastoma and suppressed by ectopic mutant IDH1 over-

expression, suggesting that αKG or D-2HG levels influence branched chain amino acid (BCAA) metabolism (Tonjes et al., 2013). The activities of aspartate aminotransaminase (AST) and glutamate dehydrogenase (GDH), enzymes that utilize αKG as a substrate, were decreased in IDH1 mutant U87 cells due to changes in expression (AST) or posttranslational modifications (GDH) (Chaumeil et al., 2014). More focused, functional characterization of these pathways may highlight additional metabolic perturbations in IDH mutant tumors.

NADPH Metabolism

In addition to the aforementioned TCA intermediates, the reactions catalyzed by IDH1 and IDH2 require NADPH as a cofactor (Figure 1.2). The pyridine nucleotide cofactor NADP(H) is critical for important cellular processes supporting redox homeostasis and biosynthesis of lipids and nucleotides (Pollak et al., 2007a). NADP(H) exists as either the oxidized (NADP+) or reduced (NADPH) form, and the ratio of this redox couple heavily influences cellular physiology. The regeneration rate of reduced NADPH is extraordinarily high in proliferating cancer cells such that the pool turns over in approximately 20 minutes (Fan et al., 2014; Lewis et al., 2014). Classically, NADPH was thought to be regenerated primarily by the oxidative pentose phosphate pathway (PPP); however, recent evidence suggests that several other enzymes are also major contributors (Fan et al., 2014; Lewis et al., 2014; Pollak et al., 2007a). These enzymes include malic enzymes (ME), isocitrate dehydrogenases (IDH), aldehyde dehydrogenases (ALDH), and methylene tetrahydrofolate dehydrogenases (MTHFD) (Lunt and Vander Heiden, 2011; Pollak et al., 2007a; Tibbetts and Appling, 2010). Importantly, many of these enzymes have isoforms that exist in specific organelles (*e.g.*, ME1 is cytosolic while ME2 and ME3 are mitochondrial), and since NADP(H) cannot transport directly across subcellular organelle membranes the maintenance of redox homeostasis in each organelle is distinctly regulated.

Mutation in either IDH1 or IDH2 deactivates the NADPH-production capacity of these enzymes; thus, mutant IDH cells may need to reroute flux through compensatory NADP+-dependent enzymes or suffer a decrease in available NADPH. In order to prevent oxidative damage from reactive oxygen species (ROS) generated during proliferation cells must maintain

pools of reduced glutathione (GSH), the most abundant cellular antioxidant (Balendiran et al., 2004). Reduced glutathione can either be synthesized *de novo* or regenerated from oxidized glutathione (GSSG) via NADPH and glutathione reductase. A reduction in NADPH availability could lead to an increase in oxidative stress by decreasing GSH pools. In fact, one study of clonally selected cells overexpressing wild-type or IDH1-R132H glioma cells indicated that NADPH levels were decreased relative to wild-type IDH1 cells (Shi et al., 2014). Consequently, ROS and GSH levels were increased and decreased, respectively, in cells expressing mutant IDH1 (Shi et al., 2014). Furthermore, mutant IDH1 cells exhibited increased sensitivity to temozolomide (TMZ) and cis-diamminedichloroplatinum (CDDP), which can induce oxidative stress in tumor cells (Shi et al., 2014; SongTao et al., 2012). A similar sensitivity was observed when cells ectopically expressing mutant IDH1 or IDH2 were exposed to radiation (Li et al., 2013). These data provide some indication that oncogenic IDH1 perturbs NADPH homeostasis; however, the extent that these findings correlate with survival and treatment responsiveness remains unclear (Dubbink et al., 2009; Houillier et al., 2010). Ultimately, additional molecular studies are required to elucidate whether this increased sensitivity to oxidative stress is due to an inability to compensate metabolically or because of orthogonal effects of the mutation on cell physiology/epigenetics.

An *in vivo* knock-in model of IDH1-R132H exhibited increased NADP+/NADPH ratio, decreased GSH, and decreased ascorbate in whole brains, consistent with a decrease in NADPH production and redox control capacity (Sasaki et al., 2012a). However, intracellular ROS levels in total brains of IDH1-R132H knock-in mice were significantly reduced relative to IDH1-WT knock-in brains (Sasaki et al., 2012a). Inhibition of IDH1-R132H may increase total ROS levels and, along with reduced NADPH and GSH levels, increase oxidative stress in these tumors and lead to cell death. High levels of ROS can damage lipids, proteins, and DNA and can lead to the activation of apoptosis and disruption of the cell cycle (Finkel and Holbrook, 2000). In addition, high levels of mitochondrial ROS may contribute significantly to mitochondrial dysfunction, as mtDNA is more readily damaged than nuclear DNA (Kim et al., 2015). Mutation of mtDNA has been observed to contribute to tumorigenicity in several cancer types (Sabharwal and Schumacker, 2014); to this end, mutant IDH2 cells in particular may

exhibit compromised mitochondrial NADPH homeostasis, which may lead to increased mtDNA mutation and mitochondrial dysfunction.

Allelic Inhibitors of Mutant IDH1 and IDH2

Given the distinct, gain-of-function activity caused by IDH mutations, several efforts have identified selective pharmacological agents that target mutant IDH1 and IDH2 enzymes. One of the first compounds (AGI-5198) to be discovered specifically inhibited IDH1-R132H and IDH1-R132C mutant enzymes, reduced 2HG levels in glioma cells, and impaired growth of IDH1 mutant but not IDH1 WT glioma xenografts (Rohle et al., 2013). AGI-5198 suppression of 2HG levels did not completely ameliorate the DNA hypermethylation phenotype in mutant IDH1 glioma cells, suggesting that mutant IDH1-mediated epigenetic dysregulation is not easily reversed (Rohle et al., 2013). Since AGI-5198 was discovered, several other inhibitors have been identified that reduce D-2HG production in both in vitro and *in vivo* models (Popovici-Muller et al., 2012; Zheng et al., 2013). Shortly after the discovery of AGI-5198, medicinal chemistry optimization yielded the first inhibitor of IDH2-R140Q (AGI-6780) that reversed the hematopoietic differentiation induced by IDH2-R140Q in TF-1 erythroleukemia cells (Wang et al., 2013). Several additional inhibitors of the IDH2-R172K and IDH2-R140Q, the two highest frequency *IDH2* mutations, have recently been discovered, including IDH2-C100 and AG-221, a derivative of AGI-6780, which both exhibit efficacy in cell and *in vivo* models (Patent WO 2013102431) (Yen et al., 2013). In aggressive IDH2 mutant primary AML xenografts models, AG-221 treatment reduced 2HG levels >90%, reversed histone and DNA hypermethylation, and conferred significant survival benefits to mice (Yen et al., 2013).

Clinical data from Phase I/II trials are emerging at a rapid rate, providing encouraging results for AML. As we continue to gain a better appreciation of the response of solid and blood tumors to these inhibitors, alternative approaches worth investigating are combinatorial treatments that target the metabolic deficiencies in IDH mutant tumors. While resistance to changes the epigenetic state of IDH mutant cells may emerge, these tumors are unlikely to regain the wild-type IDH1 or IDH2 activity that was originally lost to mutation. Therefore,

pharmacological inhibition of the specific metabolic pathways on which IDH1 or IDH2 mutant cells are critically dependent may prove efficacious.

Conclusion

The discovery, functional characterization, and clinical development of therapies surrounding oncogenic IDH mutations highlight the great potential impact of advanced scientific technologies on medicine. In order to fully exploit the metabolic and physiological defects of IDH mutant tumors additional studies are required to identify and target such biochemical pathways in cellular and preclinical models. Improved biological models are still required, since patient-derived IDH mutant tumor cells grow slowly, ectopic expression of mutant enzymes is unstable and ineffective at producing high D-2HG levels, and isogenic, engineered cell lines lack appropriate biological context. Ultimately, molecular level analyses of how IDH mutations impact the metabolism, epigenetics, and oncogenic development of tumors will lead to additional insights into the pathogenesis of other transforming events (*e.g.* SDH and FH-deficient tumors) and inborn errors of metabolism (L-2HG and D-2HG aciduria).

Acknowledgements

Chapter 1, in full, is a reprint of the material as it appears in "Metabolic consequences of oncogenic IDH mutations", Pharmacology Therapeutics, vol. 152, 2015. Seth J. Parker is the primary author of this publication. Christian M. Metallo is the corresponding author of this publication.

Chapter 2

IDH1 Mutations Alter Citric Acid Cycle Metabolism and Increase Dependence on Oxidative Mitochondrial Metabolism

Abstract

Oncogenic mutations in isocitrate dehydrogenase 1 and 2 (IDH1/2) occur frequently in several tumor types, but the metabolic consequences of these genetic modifications are not fully clear. To address this question, we performed ^{13}C metabolic flux analysis (MFA) on an isogenic cell panel containing heterozygous IDH1/2 mutations. We observe that IDH1, but not IDH2, mutant cells exhibit increased oxidative tricarboxylic acid (TCA) metabolism and decreased reductive glutamine metabolism in hypoxia. Selective inhibition of mutant IDH1 enzyme function cannot reverse the defect in reductive carboxylation activity. Furthermore, this metabolic reprogramming increases the sensitivity of IDH1 mutant cells to hypoxia or electron transport chain (ETC) inhibition *in vitro*. IDH1 mutant cells also grow poorly as subcutaneous xenografts within hypoxic *in vivo* microenvironments. These results suggest that exploiting metabolic defects specific to IDH1 mutant cells could be an interesting avenue to explore therapeutically.

Significance

This study identifies metabolic alterations induced by heterozygous IDH1 mutations, specifically increased oxidative mitochondrial metabolism and a decrease in reductive glutamine metabolism under hypoxia, which is not reversed by a mutant-IDH1 inhibitor. This metabolic phenotype increases the sensitivity of IDH1 mutant cells to several inhibitors of the electron transport chain, suggesting that these metabolic alterations could offer an additional means of therapeutically targeting IDH1 mutant tumors.

Introduction

Mutations in the metabolic enzymes isocitrate dehydrogenase 1 and 2 (IDH1/2) have been identified in a variety of tumor types, including acute myeloid leukemia (AML), gliomas, cholangiocarcinomas, and chondrosarcomas (Arai et al., 2012; Cairns et al., 2012; Hayden et al., 2009; Parsons et al., 2008; Yan et al., 2009; Mardis et al., 2009; Amary et al., 2011; Borger et al., 2012; Wang et al., 2013). These mutations are almost exclusively heterozygous point mutations that occur in specific residues within the catalytic pocket and are suggestive of activating, oncogenic mutations. Although IDH mutants are no longer capable of efficiently carrying out the normal oxidative reaction (converting isocitrate and NADP+ to α-ketoglutarate [αKG], CO_2 and NADPH), IDH mutations result in a novel gain-of-function involving the reductive, NADPH-dependent conversion of αKG to (D)2-hydroxyglutarate (2-HG) (Ward et al., 2010; Dang et al., 2009). 2-HG is not typically present at high levels in normal cells but accumulates considerably in cells with IDH1/2 mutations as well as in the tumors of patients with IDH1/2 mutations, and has thus been termed an "oncometabolite" (Ward et al., 2010; Dang et al., 2009; Yen and Schenkein, 2012).

Research into the oncogenic function of mutant IDH1/2 has focused in large part on the effects of 2-HG. Numerous reports have linked 2-HG accumulation to epigenetic changes, which are thought to contribute to alterations in cellular differentiation status (Xu et al., 2011; Figueroa et al., 2010; Lu et al., 2012; Turcan et al., 2012; Chowdhury et al., 2011;

Sasaki et al., 2012b; Wang et al., 2013; Losman et al., 2013; Koivunen et al., 2012; Rohle et al., 2013). Additional mutant IDH phenotypes have also been reported, including changes in collagen maturation and hypoxia inducible factor 1α (HIF-1α) stabilization (Koivunen et al., 2012; Sasaki et al., 2012a). These changes likely occur through inhibition of αKG-dependent dioxygenase activity by high levels of 2-HG. However, the diverse roles that αKG-dependent dioxygenases play in the cell and the numerous phenotypes associated with mutant IDH and 2-HG suggest that the phenotypes downstream of 2-HG induction could be cell type- or context-specific. We hypothesize that metabolic alterations induced by IDH mutations may also be present and might be a general phenotype that offers additional approaches to target these tumors. Previous work suggests that overexpression of mutant IDH alters the levels of several metabolites (Reitman et al., 2011) and leads to increased sensitivity to glutaminase inhibitors (Seltzer et al., 2010). Studies by Leonardi and colleagues have indicated that the IDH1 mutant enzymes compromise the ability of this enzyme to catalyze the reductive carboxylation reaction (Leonardi et al., 2012). However, it is unclear how IDH mutations affect central carbon metabolism in the heterozygous cellular setting, and further exploration into how these metabolic differences could be therapeutically exploited is warranted. An important distinction between IDH1 and IDH2 is their localization in the cytosol/peroxisome and mitochondria, respectively, which may influence the ultimate metabolic phenotype of tumor cells with mutations in either enzyme.

Systems-based approaches that employ stable isotope tracers (*e.g.*, [^{13}C]glutamine), mass spectrometry, and network modeling to estimate metabolic fluxes offer a unique means of characterizing intracellular metabolism (Zamboni, 2011). To understand the metabolic impact of heterozygous IDH mutation *in vitro* we have applied ^{13}C metabolic flux analysis (MFA) to a panel of cell lines that differ only with respect to their IDH1 and IDH2 mutant status. Using this approach we have characterized how cells with wild-type (WT) and mutant IDH1/2 respond to hypoxia and pharmacological induction of mitochondrial dysfunction.

Results

Mutant IDH1 Compromises Metabolic Reprogramming Under Hypoxia

We and others have previously demonstrated that TCA metabolism is reprogrammed under hypoxia and flux through wild-type IDH1 and/or IDH2 become critical in these contexts (Metallo et al., 2012; Wise et al., 2011; Mullen et al., 2012; Scott et al., 2011; Fendt et al., 2013b; Gameiro et al., 2013). Oncogenic mutations in IDH1 and IDH2 mitigate these enzymes' WT function and, in particular, the ability to catalyze the reductive carboxylation reaction while inducing a neomorphic activity that results in the accumulation of D-2-HG (Dang et al., 2009; Leonardi et al., 2012). Therefore, we hypothesized that cancer cells harboring mutations in either IDH1 or IDH2 may be compromised in their ability to modulate metabolism under low oxygen tensions. To identify metabolic liabilities induced by IDH1 mutations we applied ^{13}C MFA to isogenic HCT116 colon cancer cells with WT IDH1/2 (parental) or a heterozygous IDH1 mutation, IDH1 R132H/+ (clone 2H1). The IDH1 mutant, but not wild-type, cells have previously been shown to produce high levels of 2-HG (Grassian et al., 2012). To gauge relative flux through the TCA cycle, each cell line was cultured in the presence of [U-$^{13}C_5$]glutamine (uniformly ^{13}C labeled glutamine) under normoxic or hypoxic (2% oxygen) conditions for 72 hours, and isotope enrichment in various metabolites was determined via mass spectrometry (Figure 2.1A). Both cell lines displayed decreased oxidative TCA flux (as evidenced by decreased M3 αKG) in hypoxia (Figure S2.3A). While minimal changes in labeling were detected when comparing the mass isotopomer distribution (MID) of citrate in each cell type grown in normoxia (designated as M0, M1, M2, etc. mass isotopomers, corresponding to ion fragments containing zero, one, or two ^{13}C, respectively), more significant deviations occurred in cells proliferating under hypoxia (Figure 2.1B). Parental cells under hypoxia exhibited increased M5 labeling indicative of reductive carboxylation (Figure 2.1B), as has been seen previously for many WT IDH1/2 cell lines (Metallo et al., 2012; Wise et al., 2011; Scott et al., 2011). In contrast, the IDH1 R132H/+ cells showed only a slight increase in the abundance of this mass isotopomer under hypoxia (Figure 2.1B). M5 citrate can also be produced via M6 citrate and glutaminolysis

(Le et al., 2012); however, no increase in the low basal levels of M6 citrate were observed in hypoxia (Figure 2.1B). We observed similar changes in the labeling of other TCA metabolites, including M3 fumarate, malate, and aspartate (derived from oxaloacetate), further supporting our finding that IDH1 mutant cells display compromised reductive glutamine metabolism in hypoxia (Figures 2.1A and S2.3B-D). To further quantify the metabolism of glutamine through the reductive carboxylation pathway in these cells we determined the contribution of [5-^{13}C]glutamine to palmitate synthesis using isotopomer spectral analysis (ISA), as this tracer specifically labels acetyl coenzyme A (AcCoA) through the reductive carboxylation pathway (Figure 2.1A) (Metallo and Vander Heiden, 2013). While parental cells increased the contribution of glutamine to lipogenic AcCoA almost 5-fold under hypoxia, cells with a mutant IDH1 allele were compromised in their ability to increase this reductive carboxylation flux (Figure 2.1C).

To characterize the metabolic phenotype of HCT116 cells with WT or IDH1 R132H/+ in a more comprehensive and unbiased manner, we incorporated uptake/secretion fluxes and mass isotopomer data into a network of central carbon metabolism. This model included glycolysis, the pentose phosphate pathway (PPP), TCA metabolism, and various biosynthetic fluxes using [U-$^{13}C_5$]glutamine and [1,2-$^{13}C_2$]glucose (for the oxidative PPP bifurcation), as these tracers provide optimal flux resolution throughout central carbon metabolism (Metallo et al., 2009). An elementary metabolite unit (EMU)-based algorithm was used to estimate fluxes and associated confidence intervals in the network (Young et al., 2008; Antoniewicz et al., 2006), and a detailed description of the model, assumptions, and the complete data set are included as Supplementary Material. As expected, glucose and lactate fluxes were significantly increased by hypoxia in both cell lines, and significant 2-HG secretion occurred only in IDH1 R132H/+ cells (Figure 2.1D). Notably, 2-HG secretion was elevated under hypoxia, consistent with previous observations of 2-HG accumulation at low oxygen tension (Wise et al., 2011).

The modeling data comparing parental HCT116 cells grown in normoxia and hypoxia highlights some of the important metabolic changes that occur at low oxygen tensions (Figures 2.1E-I, S2.4, Tables S2.2-S2.5). In the HCT116 parental cells, pyruvate dehydrogenase (PDH) and oxidative TCA metabolism are decreased under hypoxia, while pyruvate cycling through malic enzyme (ME) and pyruvate carboxylase (PC) are elevated under these conditions. Parental

cells increased reductive IDH flux several fold, such that net IDH flux slightly favored the direction of reductive carboxylation (Figures 2.1F, G, and I. As with the MID changes (Figure 2.1B), only modest changes in metabolism were detected when comparing parental HCT116 cells to IDH1 R132H/+ 2H1 grown under normoxia (Figures 2.1E-H, Tables S2.2-S2.5). However, mutant cells maintained high oxidative IDH and αKG-dehydrogenase (αKGDH) fluxes and were unable to induce reductive carboxylation under hypoxia relative to the parental cells (Figures 2.1E-G, I and Tables S2.2-S2.5). This oxidative TCA flux was maintained by increased glutamine anaplerosis and flux through ME and PC (Figures 2.1H and I and Tables S2.2-S2.5). Overall, these results demonstrate that significant reprogramming of TCA metabolism occurs in cells at 2% oxygen, and expression of IDH1 R132H/+ abrogates the cells' ability to respond appropriately to hypoxic stress.

Compromised Reductive TCA Metabolism is Specific to Cells with Mutant IDH1

The MFA results above suggest that heterozygous IDH1 mutations disrupt the metabolic response of cells to hypoxic stress. To determine whether this metabolic deficiency is common to cells with either IDH1 or IDH2 mutations, we interrogated a panel of previously reported IDH1 and IDH2 mutant isogenic cells (Grassian et al., 2012) and measured the ability of each to initiate reductive carboxylation under 2% oxygen. With the exception of IDH2 R140Q/+ cells, these mutant cell lines exhibit a ≥ 25-fold increase in 2-HG compared to parental HCT116 cells (Grassian et al., 2012). We cultured each clone with [U-$^{13}C_5$]glutamine under normoxia and hypoxia, quantifying M5 citrate abundance (see Figure 2.1A) to determine the relative extent of reductive carboxylation induction. All but one of the IDH1 mutant clones were consistently compromised in their ability to increase reductive carboxylation activity under hypoxia (Figure 2.2A). The one exception being the IDH1 R132H/+ 2C11 clone, which showed a weaker phenotype relative to the other IDH1 mutant clones (Figure 2.2A). This is likely explained by a lower level of IDH1 R132H protein (Figure 2.2B) and lower level of 2-HG than the IDH1 R132H/+ 2H1 clone (Grassian et al., 2012).

Unlike mutant IDH1 cells, HCT116 cells with IDH2 mutations exhibited levels of M5 citrate under hypoxia which were comparable to the parental cells (Figure 2.2A). Addition of

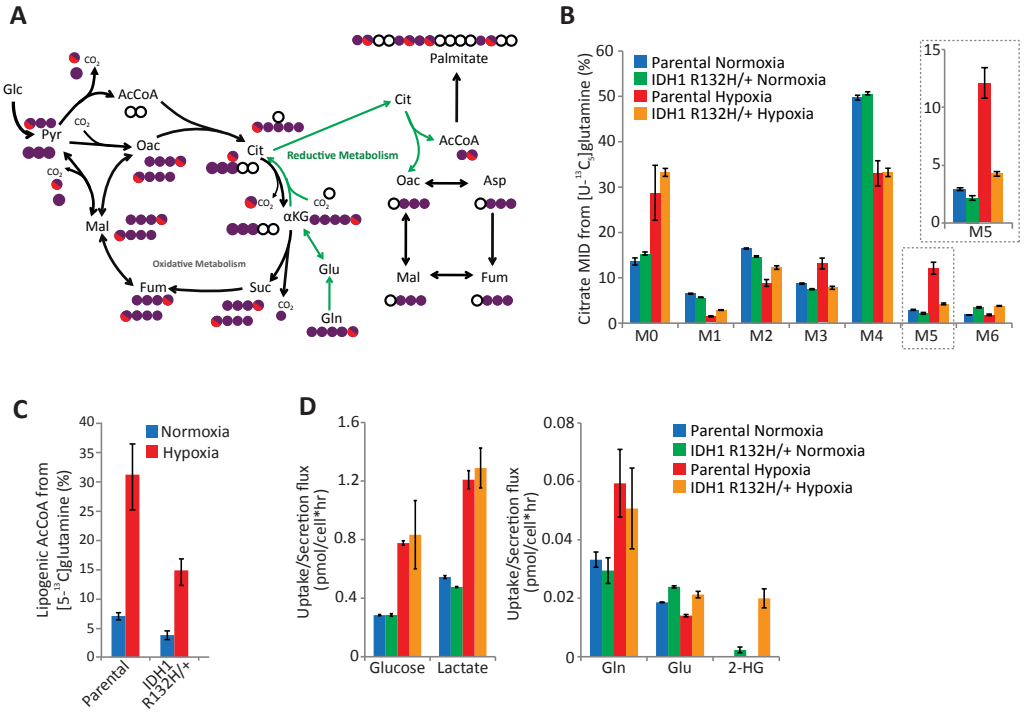

Figure 2.1: Isogenic IDH1 Mutation Compromises Metabolic Reprogramming Under Hypoxia. (A) Carbon atom (represented by circles) transitions and tracers used to detect changes in flux. [U-$^{13}C_5$]glutamine (purple circles) or [5-^{13}C]glutamine (circle with red). The fifth carbon is lost during oxidative TCA metabolism but is retained on citrate, AcCoA and palmitate in the reductive pathway (green arrows). (B) Citrate MID labeling from [U-$^{13}C_5$]glutamine from HCT116 Parental and HCT116 IDH1 R132H/+ clone 2H1 cells cultured in normoxia or hypoxia (2% oxygen) for 72 hours. Data are representative of more than three independent experiments. Inset highlights changes in %M5 Citrate. (C) Contribution of [5-^{13}C]glutamine to lipogenic AcCoA from cells cultured as in Figure 2.1B. (D) Uptake and secretion fluxes for cells cultured as in Figure 2.1B. (E, F, G and H) α-Ketoglutarate Dehydrogenase (E), Reductive IDH (F), Oxidative IDH (G), and Glutamine Anaplerosis (H) flux estimates and 95% confidence intervals by the ^{13}C MFA model. (I) Graphical representation of fluxes determined via MFA. Arrow thickness indicates level of flux in HCT116 cells cultured in hypoxia. Color indicates fold difference between hypoxic and normoxic parental HCT116 cells (left panel) or between hypoxic HCT116 IDH1 R132H/+ 2H1 cells and hypoxic HCT116 Parental cells (right panel). The * denotes metabolites that were modeled as existing in separate mitochondrial and cytosolic pools. (aKG) α-Ketoglutarate; (Cit) citrate; (Fum) fumarate; (Gluc) glucose; (Glu) glutamate; (Gln) glutamine; (Lac) lactate; (Mal) malate; (Oac) oxaloacetate; (Pyr) pyruvate. See also Supplemental Methods, Supplemental Figure S2.4 and Supplemental Tables S1-S4 for details of MFA model, results, and data.

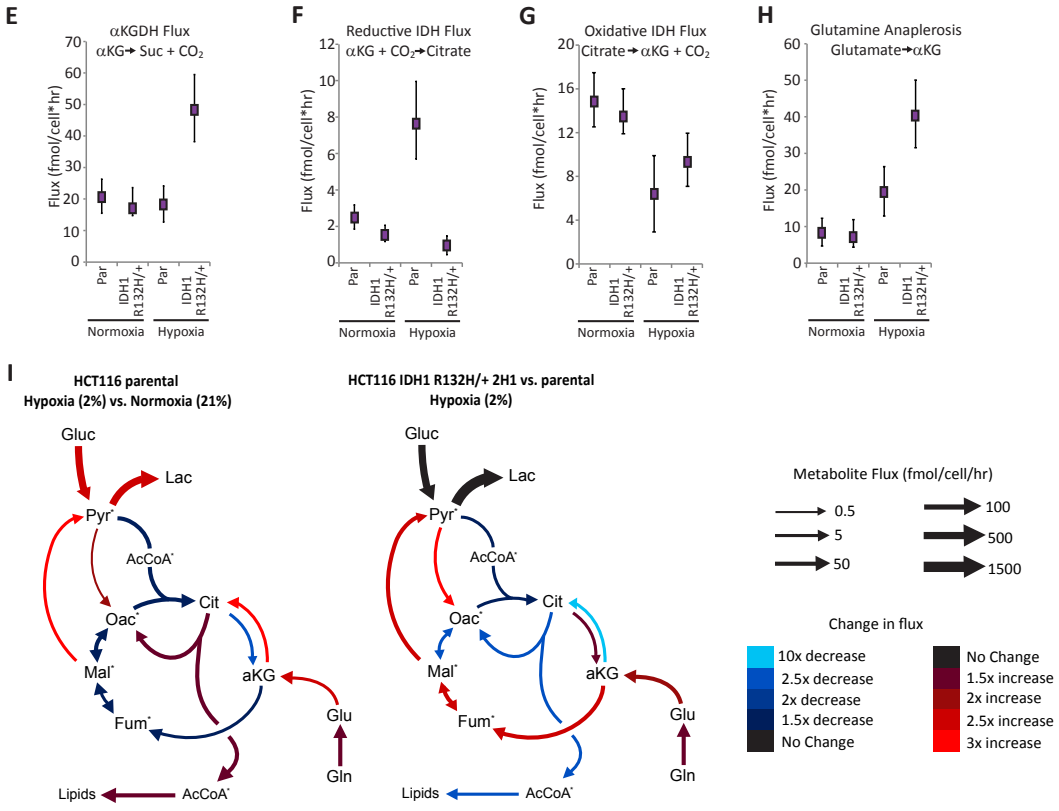

Figure 2.1: Isogenic IDH1 Mutation Compromises Metabolic Reprogramming Under Hypoxia, *continued*

10 mM D-2-HG to the culture media also had a minimal effect on TCA metabolism (Figure 2.2A). These data suggest that high 2-HG levels alone are unable to inhibit reductive carboxylation activity, even though this dose of exogenous D-2-HG is sufficient to induce the 2-HG-dependent epithelial-mesenchymal transition (EMT) phenotype previously described in these cell lines (Grassian et al., 2012). Consistent changes were observed when normalizing M5 citrate to M5 glutamate (Figure S2.5A) and levels of M6 citrate were not high in any of the clones (Figure S2.5B) providing evidence that such changes are specific to the IDH/aconitase node of metabolism. Similar trends were also observed when measuring the ratio of αKG/citrate under normoxia and hypoxia (Figure 2.2C), another metric that describes the extent of reductive versus oxidative IDH flux (Fendt et al., 2013b,a). Finally, the contribution of glutamine to lipogenic AcCoA under hypoxia was significantly lower in cells with IDH1 mutations but not those with IDH2 mutations or exogenous 2-HG (Figure 2.2D). Overall, the extent that each IDH1 mutant cell line produced 2-HG correlated with their ability to activate reductive carboxylation flux under hypoxia (Figure 2.2E), whereas IDH2 mutant cells did not adhere to this trend.

We next conducted shRNA-mediated knockdown of IDH1 and IDH2 in parental HCT116 cells to examine the roles of wild-type IDH1 and IDH2 in mediating reductive glutamine metabolism (Figures S2.5C-D). Knockdown of IDH1 decreased levels of M5 citrate in cell populations cultured with [U-$^{13}C_5$]glutamine, while cells expressing shRNAs targeting IDH2 exhibited the same or higher M5 citrate (Figure 2.2F). These results are consistent with previous studies in other cell lines (Metallo et al., 2012), highlighting the importance of WT IDH1 expression in reprogramming TCA metabolism under hypoxia and further suggests that IDH1 mutation selectively impedes WT IDH1 function in these cells.

To determine whether this mutant IDH1-induced metabolic deficiency is specific to the HCT116 genetic background or more broadly applicable to cells of different tissue origin, we performed similar analyses using MCF-10A immortalized mammary epithelial cells with heterozygous IDH1 mutations (Grassian et al., 2012). When cultured for 3 days under normoxia or hypoxia, two distinct IDH1 R132H/+ clones were compromised in their ability to generate M5 citrate or lipogenic AcCoA from [U-$^{13}C_5$]glutamine (Figures 2.2G-H and S2.5E). Thus, cells with heterozygous IDH1 mutations, but not IDH2 mutations or exogenous 2-HG, are compromised

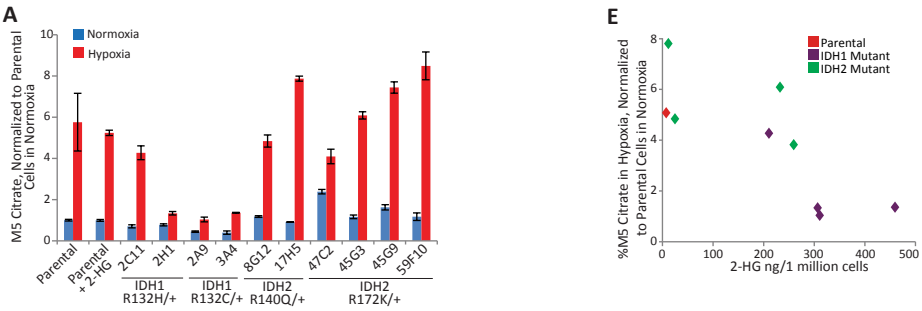

Figure 2.2: Compromised Reductive TCA Metabolism is Specific to Cells with Mutant IDH1. (A) Relative level of reductive glutamine metabolism, determined by M5 labeling of citrate from [U-$^{13}C_5$]glutamine in HCT116 Parental cells with or without 10mM D-2-HG, or HCT116 IDH1/2-mutant isogenic cells cultured in normoxia or hypoxia (2% oxygen). Percentage of M5 Citrate levels are normalized to HCT116 Parental cells in normoxia for each experiment. (B) Western blot of HCT116 Parental, HCT116 IDH1 R132H/+ clone 2C11, and HCT116 IDH1 R132H/+ clone 2H1 showing levels of IDH1 R132H and total levels of IDH1. (C) Ratio of α-ketoglutarate to citrate from cells cultured as in Figure 2.2A. (D) Contribution of [U-$^{13}C_5$]glutamine to lipogenic AcCoA from cells cultured as in Figure 2.2A. Four independent experiments are shown. (E) Correlation of reductive glutamine metabolism in 2% oxygen (as measured by %M5 citrate from [U-$^{13}C_5$]glutamine) to 2-HG ng/1 million cells. Note that HCT116 IDH2 R172K/+ 45G9 and 59F10 are not included in this figure. (F) Relative level of reductive glutamine metabolism, determined by M5 labeling of citrate from [U-$^{13}C_5$]glutamine in HCT116 Parental cells which were stably infected with doxycycline-inducible shRNA's targeting IDH1 or IDH2, or non-targeting control (NTC). Cells were cultured for 48 hours in normoxia or hypoxia (1% oxygen) in the presence of 100ng/ml doxycycline. Citrate labeling was determined via LC-MS. (G) Relative level of reductive glutamine metabolism, determined by M5 labeling of citrate from [U-$^{13}C_5$]glutamine in MCF-10A cells cultured in normoxia or hypoxia (2% oxygen) for 72 hours. (H) Contribution of [U-$^{13}C_5$]glutamine to lipogenic AcCoA from cells cultured as in Figure 2.2G.

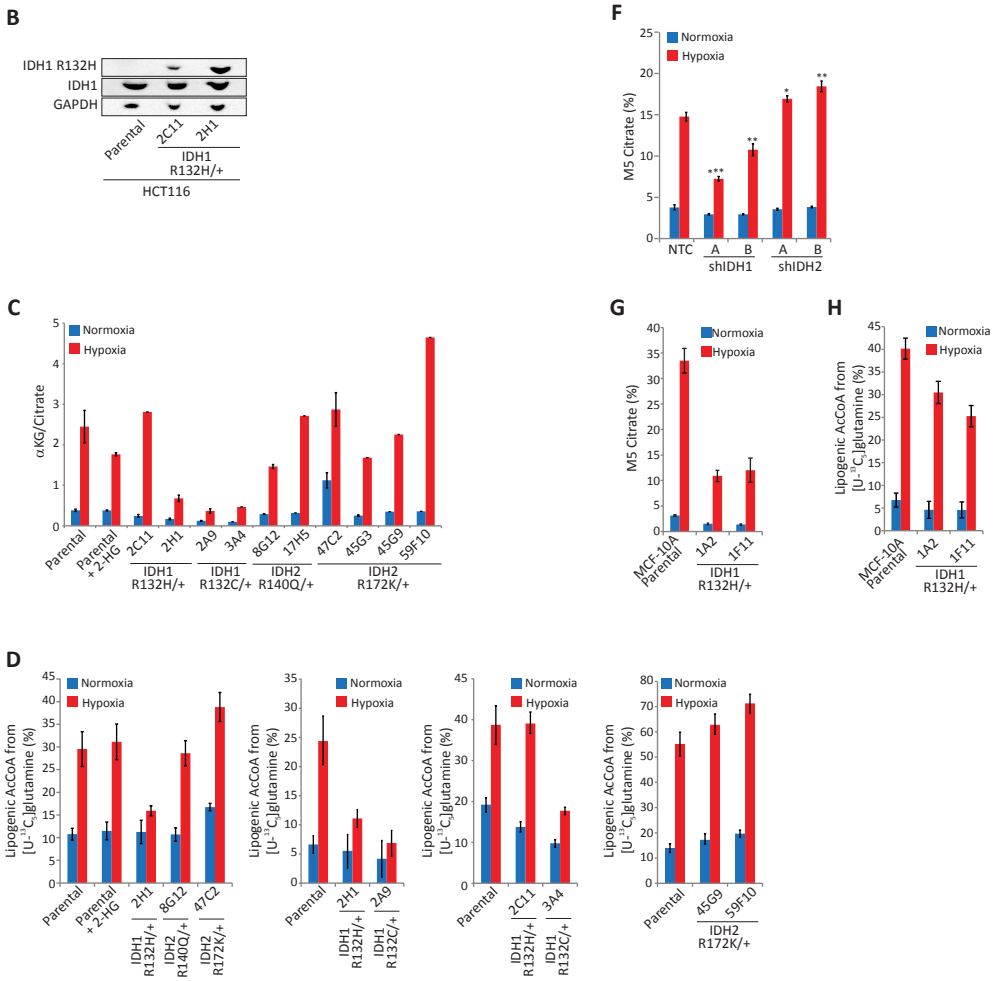

Figure 2.2: Compromised Reductive TCA Metabolism is Specific to Cells with Mutant IDH1, *continued*.

for glutamine reductive carboxylation under hypoxia.

Compromised Reductive TCA Metabolism in Endogenous IDH1 Mutant Cells

In order to determine if mutations in IDH1 affect metabolic switching to reductive carboxylation in hypoxia, we utilized an endogenous IDH1$^{R132C/+}$ mutant HT1080 fibrosarcoma cell line expressing a "corrected" IDH1 allele using the TALEN technology (Ma et al., 2015; Wang et al., 2015). HT1080 IDH1$^{+/-}$ cells were generated using TALEN and an IDH1 wild-type allele (WT), an IDH1-R132H allele (R132), a catalytic dead IDH1-R132H-T77A allele (T77), or vector (PB) were stably expressed using pBabe-puro. We observed a significant reduction in 2HG levels in IDH1 wild-type cell lines (PB, T77, WT) versus the IDH1 mutant cell line (R132) (Figure 2.3A). Interestingly, there was no significant impact on growth rates after correction of IDH1 mutation in contrast to the growth defect observed in HCT116 IDH1$^{R132H/+}$ cell lines (Figure 2.3B). We cultured the engineered HT1080 cell lines in the presence of [U-$^{13}C_5$]glutamine in normoxia and hypoxia and quantified labeling on citrate as a readout of relative oxidative and reductive glutamine metabolism (Figure 2.3C). Similar to the IDH1 mutant HCT116 cells, the HT1080$^{R132H/+}$ cells exhibited a blunted switch to reductive glutamine metabolism in hypoxia and an overall increase in oxidative glutamine metabolism as evidenced by M+4 and M+5 citrate labeling (Figure 2.3D-E). Furthermore, the contribution of glutamine to lipogenic acetyl-CoA via reductive carboxylation followed a similar trend (Figure 2.3F). Strikingly, correction of the mutant IDH1 allele resulted in significant rescue of reductive flux (Figure 2.3D-F). Furthermore, overexpression of the IDH1 wild-type allele (WT) promoted increased reductive carboxylation in both normoxia and hypoxia compared to PB and T77 cell lines (Figure 2.3D-F).

Cells with Endogenous IDH1 and IDH2 Mutations Respond Differently to Mitochondrial Stress

To examine whether these trends are observed in cell lines from cancers with endogenous IDH mutations we evaluated the ability of two cell lines harboring IDH1 or IDH2 mutations to activate reductive carboxylation under conditions of mitochondrial stress. When switched to hypoxic growth, HT1080 IDH1 R132C/+ fibrosarcoma cells exhibited a significantly decreased

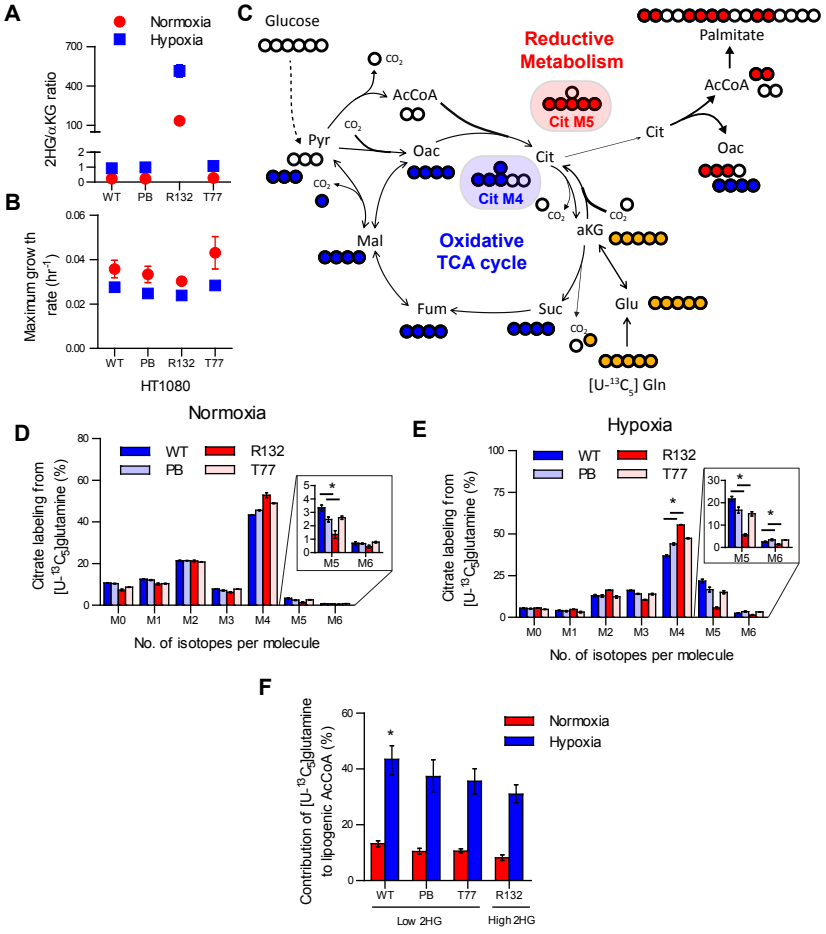

Figure 2.3: Correction of Mutant IDH1 Rescues Switch to Reductive Carboxylation in Hypoxia. (A) 2HG/αKG ratio in HT1080 PB, WT, R132, T77 cell lines measured with GC-MS. (B) Maximal exponential growth rate in engineered HT1080 cell lines after 72 hours. (C) Tracer diagram depicting atom transitions of [U-$^{13}C_5$]glutamine (orange circles) metabolized either oxidatively through the TCA cycle (blue circles) or reductively (red circles) to yield M+4 or M+5 citrate, respectively. (D-E) Citrate labeling from [U-$^{13}C_5$]glutamine in normoxia (D) or hypoxia (E) after 72 hours. (F) Contribution of reductive glutamine metabolism to lipogenic acetyl-CoA quantified by ISA.

ability to induce reductive glutamine metabolism in comparison to SW1353 IDH2 R172S/+ chondrosarcoma cells (Figures 2.4A and S2.6A). HT1080 cells also utilized less glutamine for *de novo* lipogenesis than the SW1353 cells in 1% oxygen tension (Figure 2.4B). Thus, a cell line with an endogenous mutation in IDH1, but not IDH2, displays compromised reductive glutamine metabolism in hypoxia.

In addition to low oxygen tensions, an alternative means of inducing reductive TCA metabolism is through the inhibition of oxidative phosphorylation (OXPHOS) (Mullen et al., 2012; Fendt et al., 2013a). To compromise OXPHOS, we generated ρ^0 cells that lack a functional electron transport chain from various cell lines using established methods (McClintock et al., 2002). As expected, oxidative mitochondrial metabolism was virtually extinguished, as evidenced by M3 and M3/M5 labeling of αKG in ρ^0 cells generated from IDH mutant cells (HT1080, SW1353) or other cancer cell lines with WT IDH1/2 (143B osteosarcoma, A549 non-small cell lung cancer) (Figures S2.6B-E). However, HT1080 IDH1 R132C/+ ρ^0 cells were compromised in their ability to generate citrate and palmitate through reductive glutamine metabolism, whereas SW1353 and both of the IDH1/2-WT ρ^0 cell lines were able to efficiently induce reductive carboxylation and use glutamine for lipid synthesis (Figures 2.4C-F). Both the HT1080 and SW1353 ρ^0 cells continued to use glucose for lipid synthesis, and this contribution was higher in the HT1080 ρ^0cells (Figure 2.4D). The increased glucose utilization in HT1080 ρ^0 cells compared to SW1353 ρ^0 cells was facilitated by anaplerosis through pyruvate carboxylase, as demonstrated by increased labeling in TCA intermediates from [3-^{13}C]glucose (Figures S2.6F-G). These results provide evidence that hypoxia and mitochondrial dysfunction drive reprogramming of the TCA cycle, and cells with spontaneously acquired IDH1 mutations are unable to efficiently reprogram metabolism to induce reductive glutamine carboxylation.

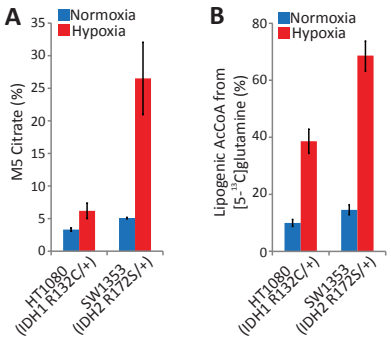

Figure 2.4: Cells with Endogenous IDH1 and IDH2 Mutations Respond Differently to Mitochondrial Stress. (A) Relative level of reductive glutamine metabolism, determined by M5 labeling of citrate from [U-$^{13}C_5$]glutamine in HT1080 and SW1353 cells cultured in normoxia or hypoxia (2% oxygen) for 72 hours. (B) Contribution of [5-^{13}C]glutamine to lipogenic AcCoA from HT1080 and SW1353 cells cultured in normoxia or hypoxia (1% oxygen) for 72 hours. (C) Relative level of reductive glutamine metabolism, determined by M5 labeling of citrate from [U-$^{13}C_5$]glutamine in HT1080 and SW1353 WT or ρ^0 cells. (D) Contribution of [U-$^{13}C_5$]glutamine and [U-$^{13}C_6$]glucose to lipogenic AcCoA from cells cultured as in Figure 2.4C. (E) Relative level of reductive glutamine metabolism, determined by M5 labeling of citrate from [U-$^{13}C_5$]glutamine in A549 and 143B WT or ρ^0 cells. (F) Contribution of [U-$^{13}C_5$]glutamine to lipogenic AcCoA from cells cultured as in Figure 2.4E.

Mutant IDH1 Affects TCA Metabolism *in vivo*

The metabolic deficiencies of IDH1 mutant cells occur at oxygen tensions that are likely to occur in solid tumors and some normal tissues (Hockel and Vaupel, 2001). To determine whether these metabolic phenotypes arise *in vivo* we generated subcutaneous xenografts using parental, IDH1 R132H/+ 2H1, and IDH1 R132C/+ 2A9 HCT116 cells. After tumors achieved a minimum diameter of 0.8 cm, mice were infused with [1-^{13}C]glutamine for 6 hours to achieve steady state isotope enrichment in plasma and tumor (Figures 2.5A-B) (Marin-Valencia et al., 2012). A targeted metabolomic analysis was performed on plasma and tumor extracts to quantify isotope enrichment and metabolite abundances. Significant 2-HG was detected only in the IDH1 mutant tumors (Figure 2.5C). Insufficient isotope enrichment was achieved in plasma and intratumoral glutamine/αKG to detect label on citrate via reductive carboxylation (Figures 2.5A, B and D). However, in agreement with the results obtained from *in vitro* studies, the αKG/citrate ratio was significantly lower in IDH1 mutant tumors compared to those generated using parental

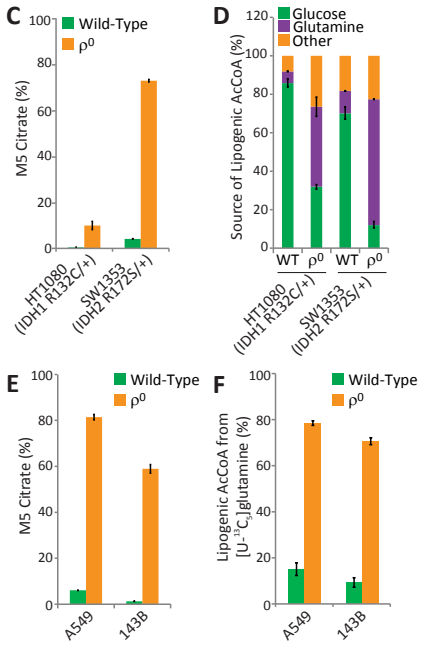

Figure 2.4: Cells with Endogenous IDH1 and IDH2 Mutations Respond Differently to Mitochondrial Stress, *continued*.

HCT116 cells (Figure 2.5E), indicating that TCA metabolism may also be perturbed in tumors comprised of IDH1 mutant cells. In addition, the contribution of glutamine anaplerosis to the αKG pool was significantly elevated in IDH1 R132H/+ and IDH1 R132C/+ tumors (Figure 2.5F), which was also observed in our MFA results (Figures 2.1H-I). Thus the available data are consistent with our *in vitro* MFA results and provide evidence that TCA metabolism is similarly compromised by IDH1 mutations *in vivo*.

Inhibition of Mutant IDH1 Does Not Rescue Reprogramming of TCA Metabolism

One possible explanation for the decrease in reductive carboxylation flux in IDH1 mutant cells is that localized substrate (αKG and NADPH) consumption by the mutant enzyme for production of 2-HG compromises this activity. Therefore, we examined whether pharmacological inhibition of mutant IDH1 could increase reductive carboxylation activity and rescue the ability of cells to use this pathway for growth under hypoxia. To test this hypothesis we treated IDH1

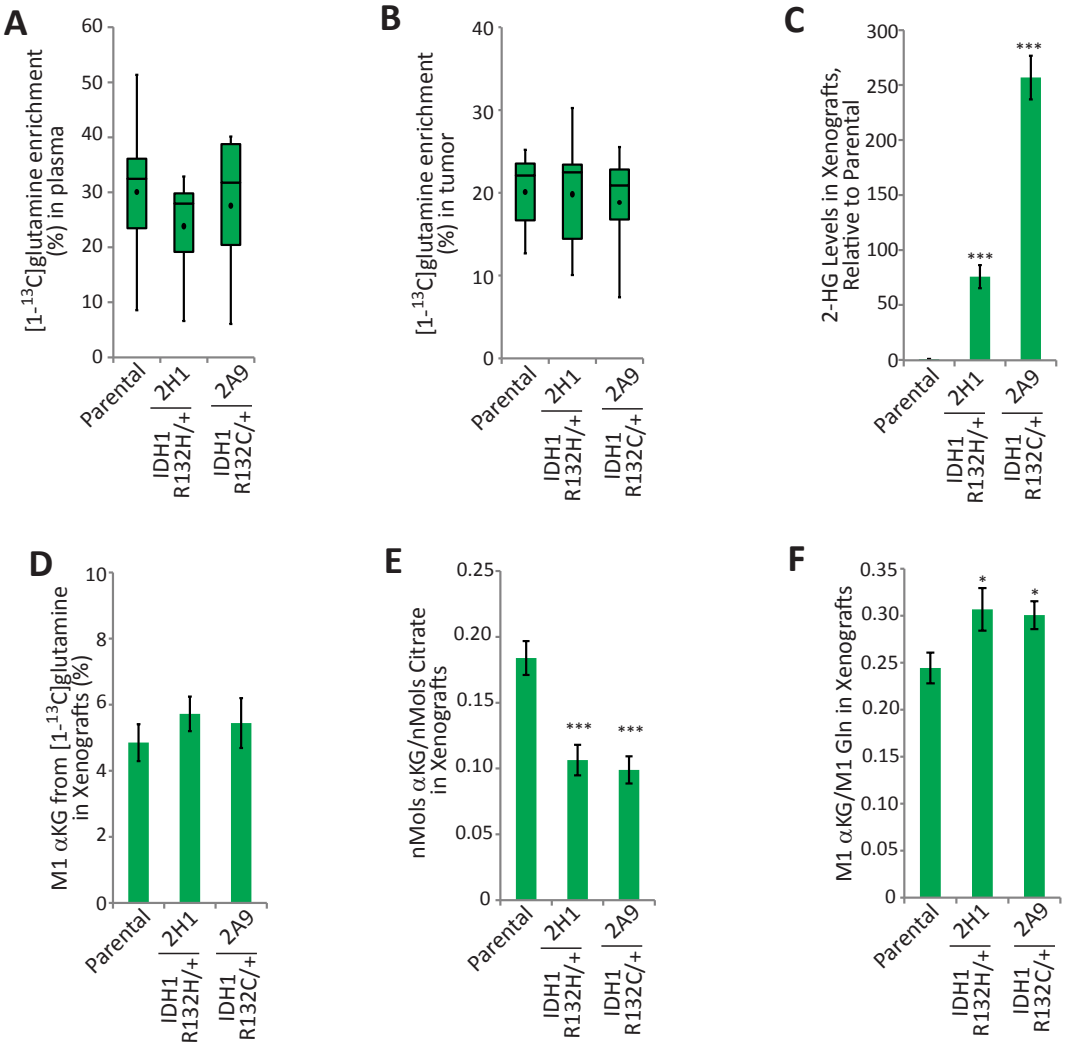

Figure 2.5: Mutant IDH1 Affects TCA Metabolism *in vivo*. (A and B) Box-whisker plots showing [1-^{13}C]glutamine enrichment in plasma (A) and tumor (B) from mice with xenografts derived from the indicated cell lines. Black dot: mean; Center line: median; Box: interquartile range; Whiskers: maximum and minimum values. (C) Relative 2-HG levels from xenografts, normalized to HCT116 parental xenografts. (D) Percentage of M1 αKG derived from [1-^{13}C]glutamine in tumor xenografts. (E) nMols αKG/nMols citrate ratio from xenografts grown from the indicated HCT116 cells. (F) Glutamine anaplerosis, as determined by M1 labeling of αKG relative to M1 labeling of glutamine from xenografts grown from the indicated HCT116 cells.

R132H/+ 2H1 or IDH1 R132C/+ 2A9 cells with a mutant IDH1 inhibitor (IDH1i A) similar to a previously described structural class (Figure 2.6A) (Rohle et al., 2013; Popovici-Muller et al., 2012). Doses of 10μM were able to decrease 2-HG levels more than 25-fold in both clones (Figure 2.6B). As would be expected from an engineered cell line that does not exhibit growth dependence on mutant IDH1 or 2-HG, 10μM of IDH1i A had no appreciable effect on the growth rate of either cell line (Figure 2.6C). Both short term (3 day) and long term (31 day) treatment with 10μM IDH1i A induced minimal changes in metabolite abundances beyond 2-HG (Figure 2.6D) and effectively reversed the mutant IDH-dependent EMT phenotype exhibited by these cells (Figure S2.7A).

IDH1i A did not rescue the ability of cells to initiate reductive TCA metabolism under hypoxia, as labeling of citrate (Figure 2.6E) and other metabolites (Figures S2.7B-D) from [U-$^{13}C_5$]glutamine was not increased compared to vehicle treatment. Other indices of reductive TCA metabolism, including the ratio of αKG/citrate and contribution of glutamine to lipid biosynthesis, also indicated that IDH1i A failed to rescue reductive carboxylation flux in these cells (Figures 2.6F-G). At 10μM, the dose that showed maximal 2-HG inhibition, IDH1i A mildly inhibited reductive carboxylation in the wild-type parental cells (Figures S2.7E-F), potentially due to off-target effects on WT IDH1 at high concentrations. To further address this issue we also treated the IDH1 mutant cells with an additional inhibitor of mutant IDH1 at more moderate concentrations (Figure 2.6H). We again observed no rescue in reductive glutamine metabolism (Figures 2.6I-K), providing evidence that inhibition of IDH1 mutant activity may be insufficient to remove the block in metabolic reprogramming in response to hypoxic stress.

Cells Expressing Mutant IDH1 are Sensitive to Pharmacological Inhibition of Mitochondrial Oxidative Metabolism

In comparing the growth rates of the HCT116 panel under normoxia and hypoxia, we observed that mutant IDH1 cells grew more poorly under conditions of low oxygen tension than parental cells or those expressing mutant IDH2 (Figure 2.7A). HCT116 IDH1 mutant xenografts also grew at a significantly slower rate than the HCT116 parental cells (Figure 2.7B), conditions that exhibited significant stabilization of hypoxia inducible factor-1α (HIF-1α) in both parental

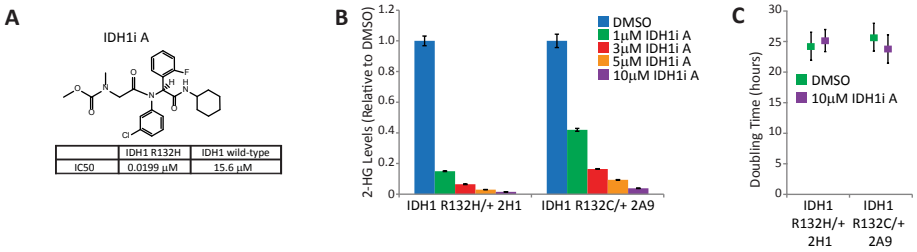

Figure 2.6: Inhibition of Mutant IDH1 Does Not Rescue Reprogramming of TCA Metabolism. (A) Structure and biochemical data for mutant IDH1 inhibitor, IDH1i A. Note that this is the (S) enantiomer. (B) 2-HG levels in HCT116 IDH1 R132H/+ 2H1 and HCT116 IDH1 R132C/+ 2A9 cell lines treated with the indicated concentrations of IDH1i A for three days. (C) Doubling time of cells cultured with or without 10μM of IDH1i A. (D) Change in total metabolite levels of HCT116 IDH1 R132H/+ 2H1 and HCT116 IDH1 R132C/+ 2A9 cells cultured in the presence or absence of 10μM of IDH1i A for 3 or 31 days, the final 72 hours of which the cells are grown in hypoxia (2% oxygen). (E) Citrate MID labeling from [U-$^{13}C_5$]glutamine from cells cultured as in Figure 2.6D. Dotted line over M5 citrate represents average %M5 citrate observed in HCT116 parental cells cultured in hypoxia. (F) αKG/citrate ratio from cells cultured as in Figure 2.6D. (G) Contribution of [U-$^{13}C_5$]glutamine to lipogenic AcCoA from cells cultured as in Figure 2.6D. (H) 2-HG levels in HCT116 IDH1 R132H/+ 2H1 and HCT116 IDH1 R132C/+ 2A9 cell lines treated with the indicated concentration of IDH1-C227 for three days. (I) Relative level of reductive glutamine metabolism, determined by M5 labeling of citrate from [U-$^{13}C_5$]glutamine in HCT116 IDH1 R132H/+ 2H1 and HCT116 IDH1 R132C/+ 2A9 cell lines treated in with 1μM of IDH1-C227 for 3 or 12 days, the final 72 hours of which the cells are grown in hypoxia (2% oxygen). (J) αKG/citrate ratio from cells cultured as in Figure 2.6I. (K) Contribution of [U-$^{13}C_5$]glutamine to lipogenic AcCoA from cells cultured as in Figure 2.6I.

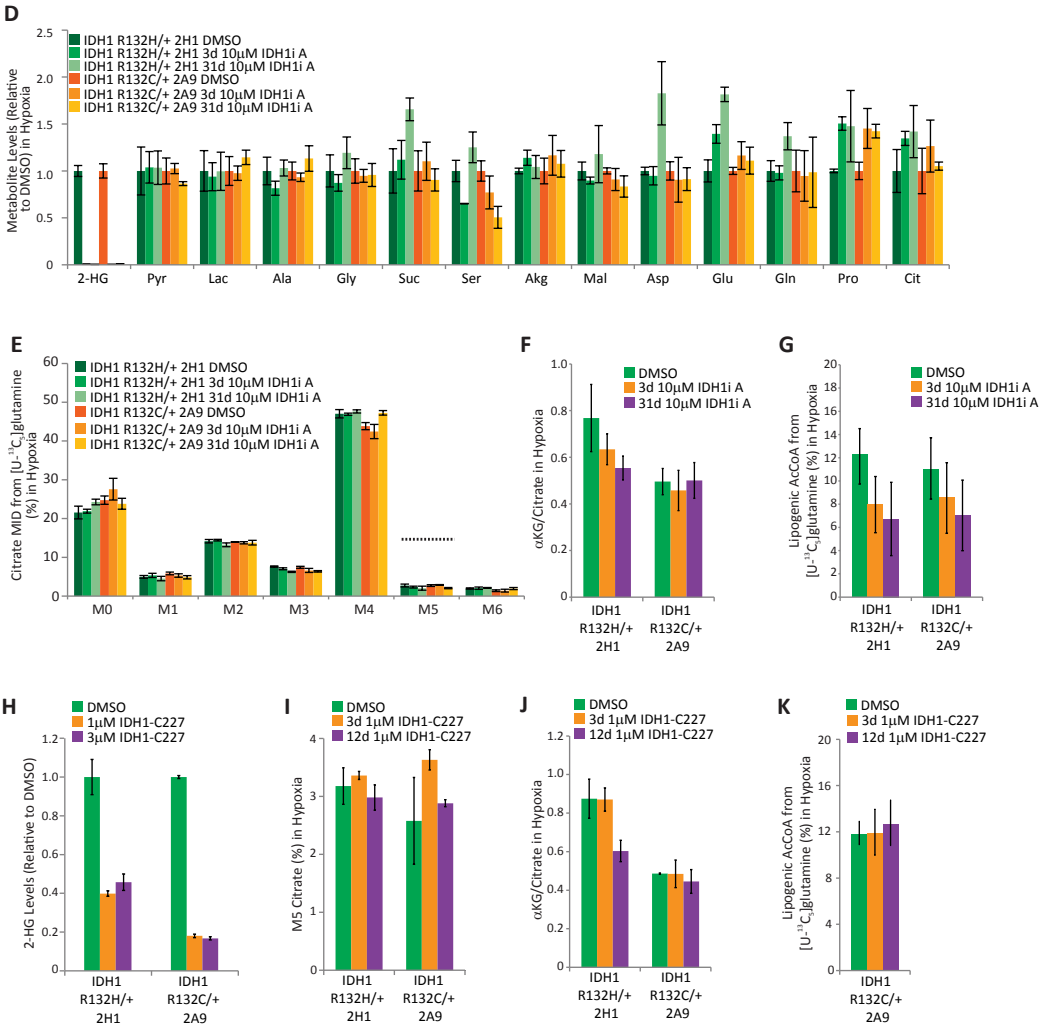

Figure 2.6: Inhibition of Mutant IDH1 Does Not Rescue Reprogramming of TCA Metabolism, *continued*.

and IDH1 mutant tumors (Figure 2.7C). The growth rate of IDH2 mutant cells as xenografts was also significantly decreased relative to the parental cells (Figure S2.8A), though our available data does not yet support a hypothesis for how IDH2 mutations affect *in vivo* growth.

The slow growth of IDH1 mutant cells in the xenograft model suggests that altered TCA metabolism may contribute to the slower growth of these cells under the decreased oxygen levels *in vivo*. IDH1 mutant cells also exhibited increased oxidative TCA metabolism under hypoxia compared to parental cells (Figures 2.1E and I), providing evidence that they are more dependent on OXPHOS. To further confirm this phenotype we measured oxygen consumption in parental and IDH1 mutant cells under both normoxia and hypoxia. Consistent with our MFA results, basal respiration was not significantly altered in parental and IDH1 mutant cells under normoxic conditions, though uncoupled respiration was decreased in the IDH1 mutant cells (Figsures S2.8B-E). Notably, mutant IDH1 cells exhibited significantly higher oligomycin-sensitive oxygen consumption under hypoxia compared to parental HCT116 cells, an effect not reproduced under normoxia (Figures 2.7D-E and S2.8F-G). Therefore, we hypothesized that, as with growth in hypoxia, cells harboring IDH1 mutations may be more susceptible to inhibition of oxidative mitochondrial metabolism than cells with WT IDH1/2 or mutant IDH2.

To address this question we cultured parental HCT116 cells and three IDH1 mutant clones in the presence of several compounds that inhibit Complex I of the electron transport chain (ETC) and OXPHOS. Confluency measurements were taken every 12 hours, and the maximum specific growth rate of each cell was determined using a generalized logistic growth model and compared to vehicle treatment for each cell line (Figure 2.7F). The proliferation rate of cells with mutant IDH1 was significantly more affected than that of parental HCT116 cells in response to discreet dose ranges of Complex I inhibitors. On the other hand, the IDH2 R172K/+ cells displayed no such increased sensitivity with the same treatments (Figure S2.8H). This altered sensitivity is not due to differences in target modulation, as 100nM rotenone effectively shut down oxidative TCA cycle flux in all cells tested (Figure S2.8I). Treatment of parental HCT116 cells with 100 nM rotenone also induced reductive carboxylation, whereas R132H/+ 2H1 and R132C/+ 2A9 HCT116 cells were less able to increase flux through this pathway (Figures S2.8J-K). Treatment with Antimycin A, an inhibitor of Complex III of the ETC, also inhibited

oxidative TCA metabolism (Figure S2.8L). Induction of reductive carboxylation by Antimycin A was observed in the parental, but not IDH1 mutant, cells (Figures S2.8M-N). However, this compound had differential effects on succinate labeling compared to rotenone (Figure S2.8O). Notably, IDH1 mutant cells did not exhibit increased sensitivity to Antimycin A (Figure S2.8P), suggesting that Complex III inhibition suppresses growth through distinct mechanisms compared to Complex I inhibitors (*e.g.* ROS generation, pyrimidine synthesis) (McClintock et al., 2002). Thus, these data indicate that IDH1, but not IDH2, mutant cells are selectively sensitive to Complex I inhibitors.

To determine whether IDH1 mutants are generally more sensitive to other treatments we examined the effect of the cell cycle inhibitor—flavopyridol—in the HCT116 panel of cells. IDH1 mutant cells did not display increased sensitivity in comparison to parental or IDH2 mutant cells (Figure S2.8Q), further suggesting that the differential sensitivity we observe is specific to inhibitors of mitochondrial metabolism. These results indicate that oncogenic IDH1 mutations induce cells to rely more heavily on Complex I of the ETC, rendering these cancer cells more susceptible to inhibition of this pathway compared to cells with WT IDH1/2 or mutant IDH2 alleles.

Finally, to evaluate whether these results are relevant to other cells, we interrogated the Cancer Cell Line encyclopedia (CCLE) (Barretina et al., 2012), which contains compound sensitivity data across more than 500 cell lines for four ETC inhibitors (Figure 2.7G) (Lai et al., 2013). Cell lines clustered well into sensitive and insensitive groups, suggesting these compounds show consistent behavior across a wide panel of cell lines. Notably, IDH1 mutant HT1080 cells fell into the sensitive group, whereas IDH2 mutant SW1353 cells fell into the insensitive group (Figure 2.7G). The differential effects of mitochondrial metabolism inhibitors were not likely due to HT1080 being generally more sensitive to compound treatments, as the sensitivities of HT1080 and SW1353 to a broad array of more than 1300 compounds were within one standard deviation of each other (Figure S2.8R). Furthermore, HT1080 cells were significantly more sensitive than SW1353 cells to phenformin treatment, a compound which was not included in the CCLE screening set (Figure 2.7H). Together, these data indicate that IDH1 mutation may substantially sensitize cells to inducers of mitochondrial stress.

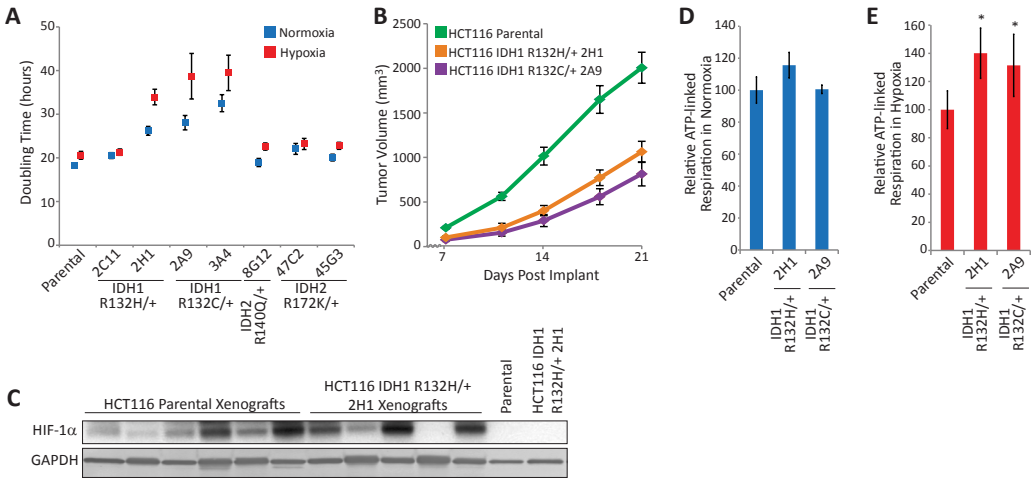

Figure 2.7: Cells Expressing Mutant IDH1 are Sensitive to Pharmacological Inhibition of Mitochondrial Oxidative Metabolism. (A) Doubling times of HCT116 cells cultured in normoxia or hypoxia (2% oxygen) for 72 hours. (B) Growth curves for HCT116 Parental and IDH1 mutant xenografts. (C) Western blot showing HIF-1α expression in HCT116 Parental and HCT116 IDH1 R132H/+ 2H1 cells grown in normoxia in cell culture (last two lanes) or as xenografts. (D) ATP-linked oxygen consumption for the indicated cell lines grown in normoxia. (E) ATP-linked oxygen consumption for the indicated cell lines grown in Hypoxia (3% O2). (F) Growth charts from cells cultured as indicated. Images were acquired every 12 hours to measure confluency. Change in growth relative to DMSO treatment ($\Delta X\%$) was calculated using a generalized logistics growth model for batch culture, and represents the change in the specific growth rate relative to the DMSO treatment for the indicated cell line. (G) Heatmap displaying IC_{50} values to four inhibitors of mitochondrial metabolism for more than 500 cancer cell lines (Cancer Cell Line Encyclopedia—CCLE); HT-1080 and SW1353 cells are indicated. (H) Growth of HT-1080 and SW1353 cells under the indicated concentration of phenformin for 48 hours.

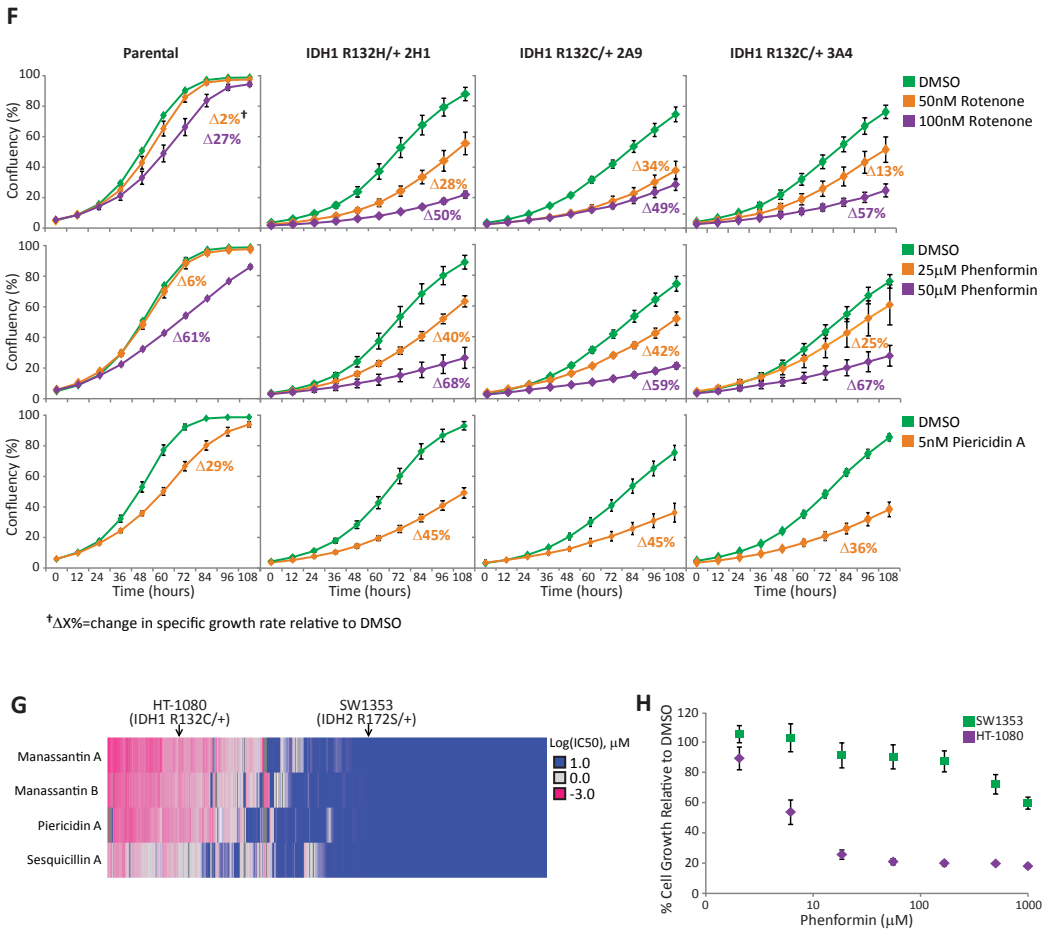

Figure 2.7: Cells Expressing Mutant IDH1 are Sensitive to Pharmacological Inhibition of Mitochondrial Oxidative Metabolism, *continued*.

Discussion

Since the discovery of oncogenic mutations in IDH1 and IDH2, significant efforts have been made to elucidate the mechanisms driving tumorigenesis in these cancers. Owing to the accumulation of D-2-HG in these tumors, researchers have focused on the role of this oncometabolite in regulating the phenotype of IDH1/2 mutant cancer cells. For example, high D-2-HG levels and other metabolites regulate the activity of αKG-dependent dioxygenases that control many distinct cellular processes (Yen and Schenkein, 2012). However, the diverse roles of these enzymes in mediating activities ranging from collagen hydroxylation and HIF stabilization to epigenetics regulation complicate identification of the specific process(es) driving tumorigenesis in each tumor type.

Despite the central role of these enzymes in cellular metabolism, surprisingly few investigations have addressed the metabolic changes that occur as a result of these genetic modifications. Here, we find that IDH1 mutations cause cells to increase flux through the oxidative TCA cycle, increase respiration, and compromise the conversion of glutamine to citrate, AcCoA and fatty acids under hypoxia compared to those with WT IDH1 (Figure 2.8). Others have previously shown that IDH1 mutant proteins are biochemically compromised with respect to this latter functionality, suggesting that cells harboring such mutations may be similarly defective under certain conditions (Leonardi et al., 2012). However the cellular consequences of this effect have not been well characterized within intact, heterozygous, IDH mutant cells. Proliferating cells must double their membrane lipids in order to successfully complete cell division, and evidence suggests that tumors may rely more on *de novo* lipogenesis than do non-neoplastic tissues and inhibition of lipid synthesis decreases tumor growth *in vivo* (Medes et al., 1953; Hatzivassiliou et al., 2005). Additionally, AcCoA is an important precursor for a number of other molecules including cholesterol, phospholipids, amino acid modifications, and histone acetylation (Kaelin and McKnight, 2013). Interestingly, previous studies have also found that overexpression of mutant IDH leads to a decrease in N-acetyl amino acids, and these changes were also observed when comparing wild-type human glioma tissue to that of tumors with mutant IDH1 (Reitman et al., 2011). This suggests that other AcCoA-dependent molecules may be similarly

perturbed in the IDH1 mutant setting. Our application of MFA to IDH1 mutant cells builds upon these results by addressing the functional consequences of heterozygous IDH1 mutations and in particular the metabolic limitations that arise in tumors cells with these genetic modifications. Given the importance of each of these AcCoA-dependent processes for cellular homeostasis and proliferation, we speculate that the reduced metabolic flexibility of these cells contributes to the decrease in growth rate that we observe in the IDH1 mutant cells under conditions of decreased oxidative mitochondrial metabolism.

Although 2-HG-mediated control of αKG-dependent dioxygenase activity clearly plays a role in tumorigenesis driven by IDH mutations (Xu et al., 2011; Figueroa et al., 2010; Lu et al., 2012; Turcan et al., 2012; Chowdhury et al., 2011; Sasaki et al., 2012b; Losman et al., 2013; Koivunen et al., 2012; Rohle et al., 2013; Sasaki et al., 2012a), our results provide insights into therapeutic strategies that exploit the metabolic vulnerabilities caused by partial loss of WT IDH1 function. Interestingly, we observe that IDH1 mutant cells do not exhibit pronounced metabolic differences in normoxia; however, growth in low oxygen tensions or with pharmacological inhibitors of mitochondrial metabolism results in the emergence of dramatic metabolic changes. Our MFA results identify several enzymes and pathways that are altered under hypoxia and in particular in the context of IDH1 mutations. Although compartment-specific IDH fluxes cannot be resolved with these data, these findings further highlight the importance of WT IDH1 activity in mediating reductive glutamine metabolism. Importantly, our results provide evidence that IDH1 mutations functionally compromise cellular metabolism under conditions of low oxygen levels, with the most pronounced effects being increased dependence on oxidative mitochondrial metabolism and an inability to induce reductive glutamine metabolism. We artificially induced such stresses using pharmacological inhibitors of Complex I or manipulation of the oxygen tensions and observed selective growth rate reductions in several IDH1 mutant cells, but not in parental or IDH2 mutant cancer cells. Other recent studies have also highlighted the importance of oxidative mitochondrial metabolism for tumor cell growth and survival both *in vitro* and *in vivo* (Marin-Valencia et al., 2012; Grassian et al., 2011).

These results suggest that compromised IDH1 function may affect the proliferative capacity of tumor cells and furthermore that IDH1 mutant tumors may be sensitive to inhibitors

that perturb mitochondrial metabolism. When comparing the metabolic phenotype of tumor xenografts derived from parental or IDH1 mutant cells to our *in vitro* results similar changes were detected, including increased glutamine anaplerosis and a decreased αKG to citrate ratio. The increase in glutamine anaplerosis we observe in the IDH1 mutant cells is in agreement with previous findings which suggest that IDH1 mutant cells display an increased sensitivity to glutaminase inhibitors (Seltzer et al., 2010). The similar metabolic changes that could be reliably measured in vivo suggest that the altered sensitivity we observe to inhibitors of mitochondrial metabolism *in vitro* may also be true *in vivo*. Additional studies are required to determine if cellular proliferation in the tumor microenvironment alone can drive hypoxia and induce reductive glutamine metabolism. Regardless, tumors would still be expected to increase their reliance on WT IDH1 (or cytosolic TCA) activity when treated with phenformin or other inhibitors of mitochondrial metabolism, suggesting that these strategies could be efficacious in IDH1 mutant cancers. As such, this increased susceptibility of cultured IDH1 mutant cells relative to parental cells or IDH2 mutant cells provides intriguing evidence of a potential therapeutic strategy associated with IDH1 mutational status and warrants further investigation in preclinical models.

We find that inhibition of mutant IDH1 is unable to reverse the observed metabolic phenotype. The DNA hypermethylator phenotype which is highly associated with IDH mutation is also not entirely reverted by a mutant IDH1 inhibitor (Rohle et al., 2013), providing further evidence that some, but not all, mutant IDH-dependent phenotypes may be reversed by inhibitors targeting 2-HG production. Mechanistically, this result also suggests that the metabolic defect we observe may be independent of 2-HG production. A previous study used biochemical assays to quantify the effects of IDH1 mutations on reductive carboxylation activity, and, in agreement with our findings here, demonstrated that the mutant enzymes are unable to catalyze the conversion of αKG and CO_2 to isocitrate (Leonardi et al., 2012). This study concluded that the subunits in a wild-type/mutant heterodimer function independently; however our modeling data indicate that heterozygous IDH1 mutations leads to a much greater than 50% inhibition of reductive glutamine metabolism (Figure 2.1F), suggesting a possible dominant effect of the mutant protein in cells or alternatively global metabolic reprogramming in response to the

compromised cytosolic IDH1 activity caused by these mutations.

Importantly, as small molecules capable of inhibiting mutant IDH1 enzymatic activity and preventing D-2-HG accumulation fail to rescue mutant cell metabolism under hypoxia, this suggests that combinatorial therapeutic strategies that block oncogenic D-2-HG production (*e.g.* via a mutant-selective inhibitor of enzyme function), while simultaneously targeting mutant IDH1-induced metabolic liabilities may be a viable option for therapy. Such an approach could involve IDH1 mutant inhibitor treatment to attenuate any pro-survival or dedifferentiation effects of D-2-HG, while increasing the tumor's reliance on WT IDH1 activity through an inhibitor of oxidative mitochondrial metabolism. As drugs which could target the mutant IDH1 metabolic phenotype are already in the clinic (metformin, phenformin) and inhibitors of mutant IDH1 are currently being developed (Rohle et al., 2013; Popovici-Muller et al., 2012), it is hoped that this hypothesis will be tested in the clinic in the near future.

Materials and Methods

Cell Culture

HCT116 and MCF-10A isogenic clones were obtained from Horizon Discovery Ltd and were not further tested or authenticated (Grassian et al., 2012). HCT116 cells were cultured in McCoy's 5A modified medium with 10% fetal bovine serum (FBS). D-2-HG treatments were done at 10 mM and replenished every 48 hours. MCF-10A cells were cultured as described previously (Grassian et al., 2012). HT-1080, SW1353, A549 and 143B cells were cultured in DMEM supplemented with 10% FBS. HT-1080 and SW1353 cells were obtained from the American Type Culture Collection (ATCC) and cells were tested and authenticated by single-nucleotide polymorphism fingerprinting. A549 cells were obtained from ATCC and were not further tested or authenticated. 143B cells were kindly provided by Dr. Leonard Guarente and were not further tested or authenticated. Cells were routinely cultured in normoxia (21% O_2) and then moved to hypoxia (1-3% O2, as indicated in the Figure Legends) for 48-72 hours where indicated. Generation of the ρ^0 cells is described in the Supplemental Methods in Supplement to Chapter 2. Xenograft assays are described in Supplemental Methods in Supplement to Chapter

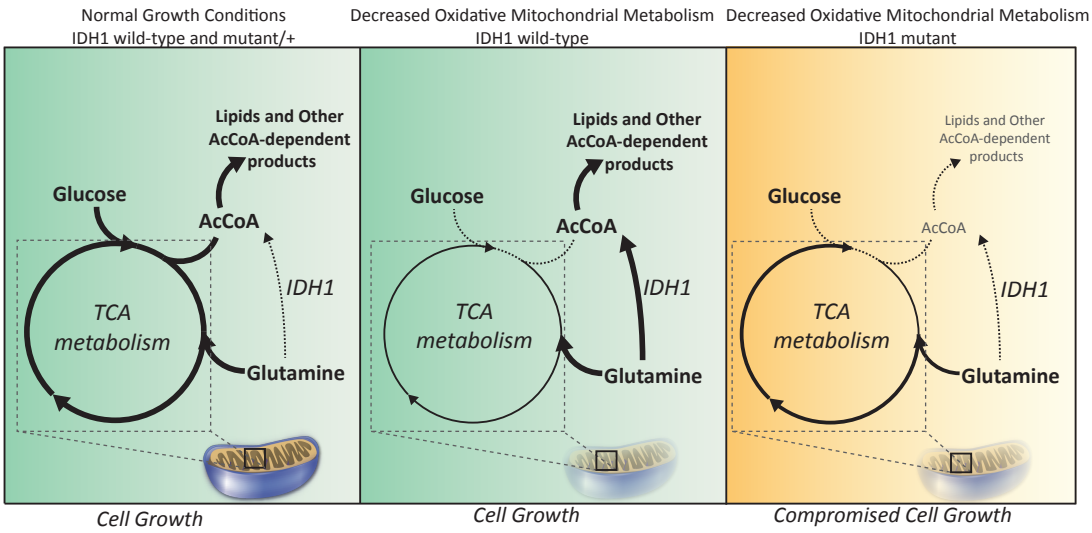

Figure 2.8: Mutant IDH1 Sensitizes Cells to Inhibition of Oxidative Mitochondrial Metabolism. Left panel: Under normal growth conditions, glucose is metabolized oxidatively in the mitochondria, and AcCoA and lipids are derived mainly from glucose carbons. Middle panel: In IDH1 WT cells, inhibition of oxidative mitochondrial metabolism (induced by growth in hypoxia or pharmacological inhibitors of the electron transport chain) limits glucose flux to the mitochondria, and cells instead rely on reductive glutamine metabolism via IDH1 to provide carbons for AcCoA generation and lipid synthesis. Right panel: When oxidative mitochondrial metabolism is inhibited, cells with a mutant IDH1 allele are unable to fully induce reductive glutamine metabolism, and are thus compromised for AcCoA and lipid production, leading to decreased cell growth.

2.

Steady state labeling of organic, amino and fatty acids was accomplished by culturing subconfluent cells in triplicate in tracer medium for 72 hours in a 6-well plate. Labeling studies of HCT116, SW1353, HT-1080, A549 and 143B cells were performed in glucose or glutamine-free DMEM containing 10% fetal bovine serum and 17.5mM [1,2-$^{13}C_2$]glucose, 4mM [U-$^{13}C_5$]glutamine, or 4mM [5-^{13}C]glutamine. For the HCT116 isogenic cells, the initial seeding density was 150,000 cells per well except for the IDH1 R132H/+ 2H1, IDH1 R132C/+ 2A9 and IDH1 R32C/+ 3A4, which were 250,000 cells per well. Labeling studies of the MCF-10A cells was done in glutamine-free DMEM containing 4mMmg/L [U-$^{13}C_5$]glutamine, 5% horse serum, 20 ng/ml epidermal growth factor (EGF), 10 µg/ml insulin, 0.5 µg/ml hydrocortisone and 100 ng/ml cholera toxin. Gas chromatography mass spectrometry (GC-MS) analysis is described in Supplemental Methods in Supplement to Chapter 2.

Metabolic Flux Analysis (MFA)

^{13}C MFA was conducted using INCA, a software package based on the elementary metabolite unit (EMU) framework (http://mfa.vueinnovations.com) (Antoniewicz et al., 2007). Intracellular concentrations of free metabolites and intra- and extra- cellular fluxes were assumed to be constant over the course of the tracing experiment. Fluxes through a metabolic network comprising of glycolysis, the pentose phosphate pathway, the TCA cycle, biomass synthesis, and fatty acid synthesis were estimated by minimizing the sum of squared residuals between experimental and simulated mass isotopomer distributions and extracellular fluxes using nonlinear least squares regression (Antoniewicz et al., 2006). The best global fit was found after estimating 100 times using random initial guesses for all fluxes in the network. A X^2 statistical test was applied to assess the goodness-of-fit using α of 0.01. The 95% confidence intervals for all fluxes in the network were estimated by evaluating the sensitivity of the sum of squared residuals to flux variations (Antoniewicz et al., 2006). Isotopomer Spectral Analysis (ISA) was performed as previously described (Metallo et al., 2012). See Supplemental Methods in Supplement to Chapter 2 for further details on MFA.

Reagents

The following reagents were used at the doses indicated and as described in the text/Figure legends: [1,2-$^{13}C_2$]glucose, [3-^{13}]glucose, [U-$^{13}C_5$]glutamine, [1-^{13}C]glutamine and [5-^{13}C]glutamine (all from Cambridge Isotope Laboratories); IDH-C277 (Xcessbio); HIF1α antibody (610958, BD Bioscinces). Synthesis of IDH1i A is described in the Supplemental Methods in Supplement to Chapter 2.

Determination of Oxygen Consumption

HCT 116 cells were grown at either normoxia or hypoxia (3% O2) and respiration was measured using an XF^{e}96 analyzer (Seahorse Bioscience). Cell growth and assays at 3% O2 were conducted using the Coy Dual Hypoxic Chambers for Seahorse XF^e Analyzer (Coy Laboratory Products, Inc.) as described in Supplemental Methods in Supplement to Chapter 2.

Proliferation Assays

To calculate doubling time, cells were trypsinized and viable cells were quantified on a ViCell (Beckman-Coulter). Doubling times are presented as the average of three or more independent experiments.

To generate longer term growth curves, cells were plated at 3000 cells per well in a 96-well plate in triplicate. 24 hours later, the indicated treatment was started and confluency measurements were taken every 12 hours for 108-216 hours using an Incucyte Kinetic Imaging System (Essen BioScience). Confluency data was modeled using a generalized logistic growth equation (2.1) and the maximum growth rate was estimated using nonlinear regression.

$$Y = \frac{U - L}{1 + e^{-\mu \max (t - t_0)}} + L \tag{2.1}$$

Where U and L represent upper and lower asymptotes, to represents the time at which cell confluency reaches 50%, and μ_{max} represents the maximum growth rate in h^{-1}.

Pharmacological profiling of the Cancer Cell Line Encyclopedia (CCLE) was performed as previously described (Barretina et al., 2012).The growth inhibition assays are described in Supplemental Methods in Supplement to Chapter 2.

Statistical Analysis

All results shown as averages of multiple independent experiments are presented as mean $\pm$ standard error; results shown as averages of technical replicates are presented as mean $\pm$ standard deviation. P-values were calculated using a Student's two-tailed t-test; (*) P-value between 0.005 and 0.05; (**) P-value between 0.001 and 0.005; (***) P-value $<$0.001. All errors associated with MFA and ISA of lipogenesis are 95% confidence intervals determined via sensitivity analysis.

Acknowledgements

We thank Karen Studer-Rabeler, Rosemary Barrett, Yue Liu, Olga Shebanova, Rao Pasupuleti, Guiqing Liang, Brandon Medeiros, Kristie Wetzel, Lei Xu, Jen Tullai, and Julie Downall for technical assistance. We thank Nicholas Keen, William Sellers, Jonathan Coloff, Julian Levell, Charles Stiles, Juliet Williams, Brant Firestone, Jonathan Solomon and the Novartis Postdoctoral Fellows for helpful discussions of this work. We thank the Cancer Cell Line Encyclopedia (CCLE) team at Novartis, especially Christopher Wilson, Felipa Mapa and Nathan Ross, for generation and analysis of the cell profiling data. We acknowledge support from Coy Laboratory Products, Inc. and Seahorse Bioscience for equipment and instrumentation. We thank Dr. Kun-Liang Guan for his generous contribution of the TALEN engineered HT1080 cell lines.

Chapter 2, excluding subsection titled "Compromised Reductive TCA Metabolism in Endogenous IDH1 mutant cells", is a reprint of the material as it appears in "IDH1 Mutations Alter Citric Acid Cycle Metabolism and Increase Dependence on Oxidative Mitochondrial Metabolism", Cancer Research, vol. 74, issue 12, 2014. Seth J. Parker and Alexandra R. Grassian are the primary authors of this publication. Shawn M. Davidson, Ajit S. Divakaruni,

Courtney R. Green, Xiamei Zhang, Kelly L. Slocum, Minying Pu, Fallon Lin, Chad Vickers, Carol Joud-Caldwell, Franklin Chung, Hong Yin, Erika D. Handly, Christopher Straub, Joseph D. Growney are co-authors of this publication. Matthew G. Vander Heiden, Anne N. Murphy, Raymond Pagliarini, and Christian M. Metallo are corresponding authors of this publication. Subsection titled "Compromised Reductive TCA Metabolism in Endogenous IDH1 Mutant Cells" includes material generated by Seth J. Parker.

Chapter 3

Tracing Compartmentalized NADPH Metabolism in the Cysotol and Mitochondria of Mammalian Cells

Summary

Eukaryotic cells compartmentalize biochemical processes in different organelles, often relying on metabolic cycles to shuttle reducing equivalents across intracellular membranes. NADPH serves as the electron carrier for the maintenance of redox homeostasis and reductive biosynthesis, with separate cytosolic and mitochondrial pools providing reducing power in each respective location. This cellular organization is critical for numerous functions but complicates analysis of metabolic pathways using available methods. Here we develop an approach to resolve NADP(H)-dependent pathways present within both the cytosol and the mitochondria. By tracing hydrogen in compartmentalized reactions that use NADPH as a cofactor, including the production of 2-hydroxyglutarate by mutant isocitrate dehydrogenase enzymes, we can observe metabolic pathway activity in these distinct cellular compartments. Using this system we determine the direction of serine/glycine interconversion within the mitochondria and cytosol, highlighting the ability of this approach to resolve compartmentalized reactions in intact cells.

Introduction

One of the defining characteristics of eukaryotic cell metabolism is the compartmentalization of reactions in different organelles. Although coordination of metabolic flux across organelles is critical for cell physiology, the inability to distinctly observe identical reactions present in more than one subcellular location has been a major barrier to understanding cell metabolism. Many of these compartmentalized reactions are oxidation/reduction (redox) reactions that utilize pyridine nucleotide-based cofactors to transfer electrons between metabolites to support biosynthesis, redox homeostasis, signal transduction, and ATP generation (Pollak et al., 2007a). For instance, reduction of NAD+ to NADH captures energy from catabolic reactions to drive ATP synthesis through mitochondrial oxidative phosphorylation, whilst NADPH is regenerated via a different set of reactions to maintain reduced glutathione (GSH) pools and support reductive biosynthesis (Lunt and Vander Heiden, 2011). As such, NADPH has been hypothesized to be limiting for proliferation, lipid biosynthesis, and survival in response to cell stress (Diehn et al., 2009; Jeon et al., 2012; Jiang et al., 2013; Schafer et al., 2009). These compartmentalized metabolic processes impact numerous cell and tissue functions; therefore, understanding how biochemical networks function across compartments is necessary to determine how metabolism contributes to disease pathologies.

The pool of NADP(H) in cells is small relative to flux through pathways that utilize this cofactor (Pollak et al., 2007a). Thus, interconversion between the oxidized and reduced states must be coupled across all reactions involving this cofactor, and changes in abundance may not be informative for assessing the use of NADPH in a particular pathway. Neither NAD(H) nor NADP(H) are known to be transported across intracellular membranes (Nikiforov et al., 2011; Pollak et al., 2007b), and multistep shuttles involving compartmentalized redox reactions are used to transfer electrons between the mitochondria and cytosol (Bissell et al., 1976; LaNoue et al., 1974; LaNoue and Schoolwerth, 1979). This organization facilitates the maintenance of different NADPH/NADP+ ratios in each subcellular location and allows for the execution of compartment-specific metabolic processes. Classically, cytosolic NADPH is thought to be regenerated primarily via the oxidative pentose phosphate pathway (PPP) (Lunt and Vander Heiden,

2011; Pollak et al., 2007a). Other potential sources of cytoplasmic NADPH exist in mammalian cells, including reactions catalyzed by specific isozymes of isocitrate dehydrogenase (IDH), malic enzyme (ME), aldehyde dehydrogenase (ALDH), and methylene tetrahydrofolate dehydrogenase (MTHFD) (Pollak et al., 2007a; Tibbetts and Appling, 2010). However, isoforms of several of these enzymes also catalyze identical reactions in the mitochondria and can potentially transfer reducing equivalents between the mitochondria and the cytosol. For example, the reductive carboxylation of alpha-ketoglutarate (αKG) to isocitrate by IDH2 consumes mitochondrial NADPH, with citrate/isocitrate subsequently transported to the cytosol where it can be oxidized by IDH1 to produce cytosolic NADPH (Sazanov and Jackson, 1994; Wise et al., 2011). Theoretically, the reverse cycle may be used to produce mitochondrial NADPH. Metabolic cycles such as this utilize compartment-specific enzymes, and existing methods for tracing metabolism rely on breaking apart cells and pooling metabolites from all compartments, making it impossible to reliably distinguish the net reaction flux through each enzyme or pathway.

Results

Tracing NADPH With ^{2}H-labeled Glucose

Because reaction mechanisms involving pyridine nucleotides transfer electrons as a hydride (H^-) ion, isotope-labeled hydrogen atoms can be used to follow electron movement in these reactions (Katz et al., 1965; Rendina et al., 1984). The transfer of ^{2}H and ^{3}H can also be used to observe redox reactions in central carbon metabolism, an approach that has been used to generate insight into NAD(P)H metabolism in eukaryotic cells (Ben-Yoseph et al., 1994; Ruhl et al., 2012). Glucose is the primary carbon source for glycolysis and the oxidative PPP in mammalian cells, with the latter pathway representing an important source of cytosolic NADPH. Non-labile hydrogen atoms on specific glucose carbons (the 1 and 3 positions, respectively) are transferred to NADPH by the oxidative PPP enzymes glucose-6-phosphate dehydrogenase (G6PD) and 6-phosphogluconate dehydrogenase (6PGD). The hydrogen atom on carbon-3 of glucose (which becomes carbon-1 of dihydroxyacetone phosphate in glycolysis) can exchange with water during isomerization to glyceraldehyde-3-phosphate (GAP) by triose

phosphate isomerase (TPI) (Katz et al., 1965). This prevents confounding labeling of downstream metabolites including TCA cycle intermediates, suggesting that tracing this hydrogen atom could provide a means of quantifying the contribution of 6PGD to the cellular NADPH pool (Figure 3.1A) (Katz et al., 1966; Katz and Rognstad, 1978). To test this possibility, we cultured H1299 non-small cell lung cancer cells in the presence of [3-^{2}H]glucose and observed labeling of NADPH using LC/MS-MS (Figure 3.1B). The rapid turnover of NADPH allows labeling from [3-^{2}H]glucose to reach isotopic steady state within 30 minutes, as evidenced by the lack of any increased label incorporated into NADPH after culturing cells in the presence of [3-^{2}H]glucose for 24 hours (Figure 3.1B). NADPH has two hydrogens that can be transferred when it acts as an electron donor. Once labeled, either the labeled or unlabeled hydrogen atom can be transferred depending on the stereospecificity of downstream NADPH-utilizing enzymes (You, 1985). Transfer of the unlabeled hydride from labeled NADPH generates labeled NADP+ (Figure S3.1A), and subsequent labeling of the second hydrogen on NADP+ yields NADPH heavy by two mass units (M2) at later time points (Figure 3.1B). Some labeling of ribose-5-phosphate and ribulose-5-phosphate was also observed at late time points, presumably via flux through the nonoxidative PPP (Figure S3.1B). This label incorporation into the ribose moieties of NADP(H) could account for a minor portion of the isotope enrichment observed at 24 hours as suggested by the small amount of M+2 labeling of NADP+ (Figure S3.1A), but these atoms would not be subject to transfer in downstream reactions utilizing NADPH as a cofactor. [3-^{2}H]glucose does not contribute to NAD(H) except by incorporation into the ribose moieties, and only a small amount of NAD(H) is labeled at late time points (Figure S3.1C), arguing that the majority of NADPH labeling from [3-^{2}H]glucose reflects hydride transfer. Importantly, metabolites in lower glycolysis such as pyruvate and lactate are not labeled from [3-^{2}H]glucose (see % values in Figure 3.1A) implying that the presence of label on downstream metabolites must arise as a result of hydride transfer from labeled NADPH. [1-^{2}H]glucose labels NADPH via G6PD in the oxidative PPP (Figures S3.1D-E), and similar to [3-^{2}H]glucose this label is detected on NADP+ and pentose phosphate pathway intermediates (Figures S3.1E-F). However, deuterium present on carbon-1 of [1-^{2}H]glucose can be lost due to reversibility of phosphoglucose isomerase, resulting in less glucose-6-phosphate labeling from [1-^{2}H]glucose in cells compared to

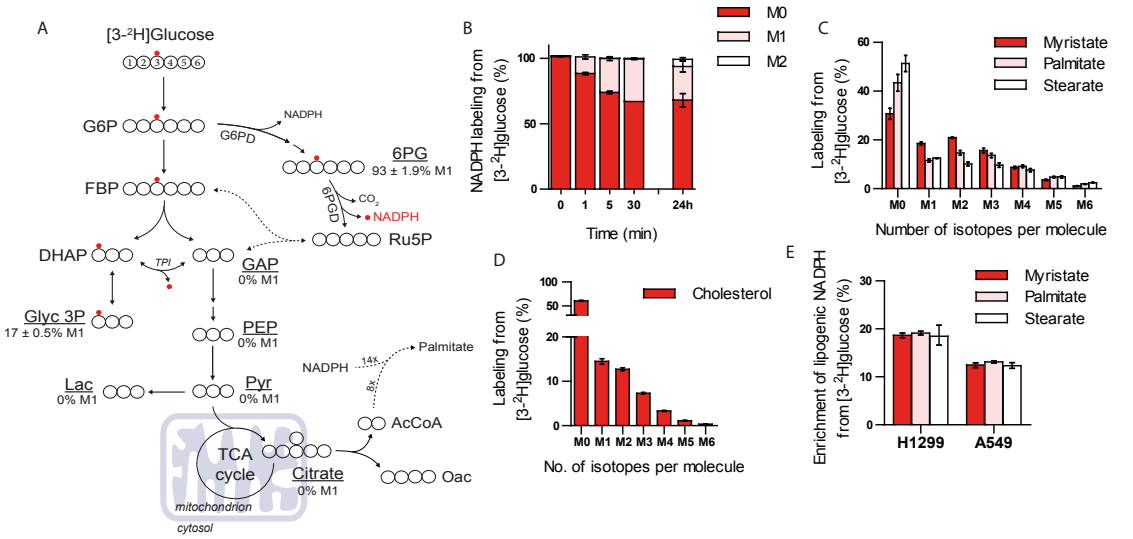

Figure 3.1: Use of ^{2}H Glucose to Label Cytosolic NADPH. (A) Atom-transition map depicting a model of deuterium transfer from [3-^{2}H]glucose through glycolysis and the pentose phosphate pathway. Open large circles represent carbon and small red circles indicate deuterium label from [3-^{2}H]glucose. Where measured, enrichment of M1 isotopomer (%) for glycolytic intermediates in parental H1299 cells is shown. (B) Labeling of NADPH from [3-^{2}H]glucose in parental H1299 cells over time. (C) Saturated fatty acid labeling (myristate; C14:0, palmitate; C16:0 and stearate C18:0) from [3-^{2}H]glucose in parental H1299 cells following incubation for 72 hours. (D) Cholesterol labeling from [3-^{2}H]glucose in parental H1299 cells cultured for 72 hours. (E) Enrichment of lipogenic [^{2}H]-NADPH by [3-^{2}H]glucose estimated by a model for saturated fatty acid synthesis (ISA) in parental H1299 and A549 cells following incubation with tracer for 72 hours. Data plotted in a-d represent mean ± SD of at least three biological replicates. For e, data presented are mean ± 95% confidence interval of at least three biological replicates.

labeling from [3-^{2}H]glucose (Figure S3.1G) (Ben-Yoseph et al., 1994; Hellerstein et al., 1986; Katz and Rognstad, 1976). In contrast to [3-^{2}H]glucose, the deuterium isotope from carbon-1 of glucose does not exchange with water in any of the reactions of glycolysis and is retained on carbon entering the TCA cycle (Figure S3.1D). Therefore, deuterium from [1-^{2}H]glucose has the potential to label downstream metabolites by either hydride transfer from NADPH or label retention on the carbon from glucose. As a result, use of [3-^{2}H]glucose is preferable for tracing NADPH produced by the oxidative PPP.

The NADPH labeling we observe is a subset of the total cellular pool. To gain insights into compartment-specific redox reactions we next quantified ^{2}H enrichment in specific metabolites downstream of NADPH-dependent reactions. For example, fatty acid and choles-

terol synthesis occur specifically in the cytosol and require NADPH. When H1299 cells are cultured with [3-^{2}H] glucose for 72 hours to allow for accumulation of new lipid molecules, we detected significant label on newly synthesized fatty acids; including myristate (C14:0), palmitate (C16:0), and stearate (C18:0); as well as cholesterol (Figures 3.1C-D). Importantly, no label from [3-^{2}H]glucose was detected on citrate (see % value in Figure 3.1A), suggesting that isotope enrichment on lipids was from the NADPH pool that was labeled by the oxidative PPP. We also detected labeling of fatty acids from [1-^{2}H]glucose (Figure S3.1H); however, tracing of G6PD-derived NADPH is complicated by deuterium from [1-^{2}H]glucose being retained on citrate and lipogenic acetyl-CoA (Figure S3.1D). We next applied isotopomer spectral analysis (ISA) to estimate the contribution of [3-^{2}H]glucose to the lipogenic NADPH pool used for palmitate synthesis, as fourteen NADPH molecules are required during the production of one palmitate molecule (Kharroubi et al., 1992; Metallo et al., 2012). The ISA model includes two parameters representing the deuterium enrichment of the NADPH pool and the percentage of palmitate that was synthesized *de novo* (Figure S3.2). Using this method we estimated the enrichment of lipogenic NADPH from [3-^{2}H]glucose ranged from 12-20% in A549 and H1299 cells (Figure 3.1E). ISA modelling of other saturated fatty acids (*e.g.* myristate and stearate) yielded similar estimations for the enrichment of lipogenic NADPH from [3-^{2}H]glucose (Figure 3.1E).

Use of ^{2}H Glucose to Trace NADH Metabolism

To maintain flux through glycolysis cytosolic NAD+ pools are regenerated primarily by three enzymes: lactate dehydrogenase (LDH), malate dehydrogenase (MDH), and/or the glycerol phosphate shuttle (Glyc3PDH) (Lunt and Vander Heiden, 2011; Metallo and Vander Heiden, 2013). Distinct hydrogen atoms on glucose are transferred to NAD+ during glycolysis via glyceraldehyde phosphate dehydrogenase (GAPDH). In theory, up to half of the hydrogen transferred to NADH via GAPDH comes from carbon four of glucose; however, exchange with water in the aldolase and TPI reactions decreases the net contribution of this hydrogen atom to NADH (Go et al., 2009) (Figure 3.2A). Upon culturing A549 and H1299 cells with [4-^{2}H]glucose, significant labeling of lactate, malate, and glycerol 3-phosphate was observed (Figure 3.2B). Label was detected on GAP in A549 cells; however, the level of GAP in H1299 cells was below the

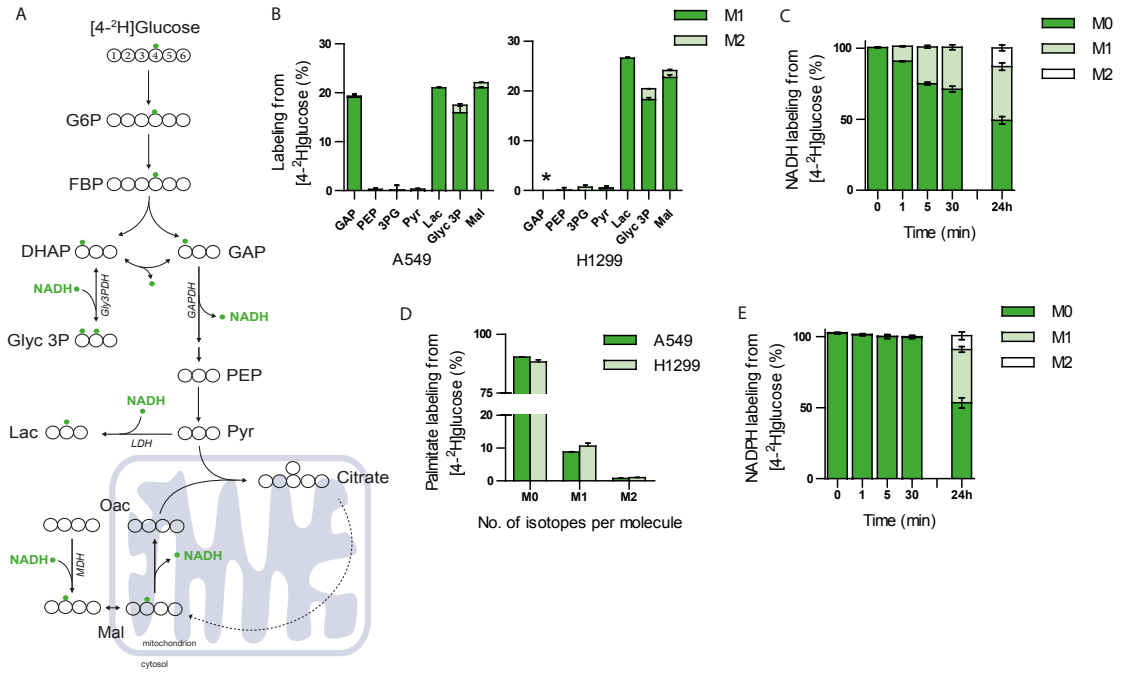

Figure 3.2: Use of ^{2}H Glucose to Label NADH. (A) Atom-transition map depicting a model of deuterium transfer from [4-^{2}H]glucose through glycolysis and NAD+-dependent shuttle systems (malate dehydrogenase MDH, glycerol 3-phosphate dehydrogenase Gly3PDH, and lactate dehydrogenase LDH). Open large circles represent carbon and small green circles indicate deuterium label from [4-^{2}H]glucose. (B) Labeling of glycolytic intermediates from [4-^{2}H]glucose in A549 (left panel) and H1299 (right panel) cells. Glyceraldehyde-3-phosphate (GAP) was below the limit of detection in H1299 cells, indicated by *. (C) Labeling of NADH from [4-^{2}H]glucose in parental H1299 cells over time. (D) Palmitate labeling from [4-^{2}H]glucose in A549 and H1299 cells following incubation with tracer for 72 hours. (E) Time course labeling of NADPH from [4-^{2}H]glucose in parental H1299. Data presented are mean $\pm$ SD of at least three biological replicates.

limit of detection. In addition, no label was detected on metabolites in lower glycolysis including PEP, 3PG, and pyruvate. This pattern fits with known reactions using NADH in central carbon metabolism (Figure 3.2A) and suggests that [4-^{2}H]glucose can be used to label the NADH pool produced by glycolysis in cells. Consistent with these findings, we observed rapid labeling from [4-^{2}H]glucose on NADH (Figure 3.2C), as well as label on NAD+ (Figure S3.3A) arising from donation of the unlabeled hydride from M+1 labeled NADH.

Interestingly, we observed isotope incorporation into fatty acid pools from [4-^{2}H]glucose (Figure 3.2D), suggesting that some label from NADH transfers to cytosolic NADPH through an unknown mechanism (Figure S3.3F). Whilst deuterium label from [4-^{2}H]glucose was detected on aspartate, citrate, and isocitrate due to the symmetry of fumarate (Figures S3.3B-D), carbons labeled in this manner do not contribute to lipogenic acetyl-CoA, demonstrating that the observed fatty acid labeling is derived from hydride transferring from NAD(H) to cytosolic NADP(H). We also observed some isotope enrichment on NADP+ and NADPH from [4-^{2}H]glucose (Figure 3.2E and Figure S3.3A); however, ribose 5-phosphate and ribulose 5-phosphate are also labeled from [4-^{2}H]glucose (Figure S3.3E). Furthermore, these direct measurements of total cellular NADP(H) cannot distinguish between cytosolic and mitochondrial pools, highlighting the need for methods to elucidate compartment-specific NADP(H) pools.

A Reporter System to Trace Compartmentalized Sources of NADPH

The above data demonstrate that we can observe cytosolic production of NADPH and NADH in intact cells. Although we were able to quantify the contribution of oxidative PPP enzymes to the lipogenic NADPH pool, deuterium tracing alone cannot distinguish other compartmentalized sources of NADPH. Therefore, we sought to develop a reporter system that can detect pathway-specific NADPH production in different subcellular compartments. To accomplish this, we took advantage of the neomorphic mutant IDH enzymes that produce (D)2-hydroxyglutarate (2HG) from αKG. This reaction reduces αKG by transferring a hydride from NADPH to form 2HG. As 2HG is a xenometabolite that is only present at very low levels in most cells (Matsunaga et al., 2012), it can be used as an end-product readout. By applying specific metabolic ^{2}H-tracers to cells and measuring enrichment of 2HG produced by ectopically

expressed mutant IDH1 (cytosol) or IDH2 (mitochondria), we reasoned that pathway-specific information on NADPH metabolism in each compartments could be obtained (Figure 3.3A).

We generated H1299 and A549 cell lines that express epitope-tagged mutant IDH1-R132H (mtIDH1-C) or mutant IDH2-R172K (mtIDH2-M) in a doxycycline-dependent manner (Figure S3.4A). We employed a weak promoter to minimize effects on endogenous IDH metabolism. Indeed, flag-tagged mtIDH1-C was expressed at levels that were not detectable with an antibody recognizing wild-type IDH1 enzyme in these cells (Figure S3.4A). mtIDH1-C is expected to be expressed in the cytoplasm and mtIDH2-M in the mitochondria, and we confirmed the localization of each using cell fractionation and Western blotting (Figure 3.3B). We also confirmed that the flag-tagged mutant IDH enzymes produce 2HG in a doxycycline-dependent manner in both H1299 and A549 cell lines (Figure 3.3C). Interestingly, mtIDH1-C produced less 2HG than mtIDH2-M in cells, consistent with observations that ectopically expressed IDH2 mutants produce more 2HG than IDH1 mutants due to their mitochondrial localization (Ward et al., 2013). In all cases 2HG levels were far below those observed in tumor cell lines expressing endogenous mutations in IDH1 (R132C/+, HT1080) or IDH2 (R172S/+, SW1353) (Figure 3.3D). Introduction of mutant IDH enzymes could impact NADPH or TCA metabolism; however, 2HG production flux observed in cell lines expressing IDH1 mutations at higher levels is small relative to other αKG-dependent reaction fluxes, suggesting mutant IDH expression has a minimal direct impact on αKG pools (Grassian et al., 2014). Furthermore, no significant change in [3-^{2}H]glucose contribution to cytosolic NADPH was observed in A549 cells following mtIDH1-C or mtIDH2-M expression (Figure S3.4G).

Although doxycycline can affect the metabolism and proliferation of some mammalian cancer cell lines in culture (Ahler et al., 2013), we saw no dox-dependent changes in the abundance of central carbon metabolites (Figure S3.4B) or in the proliferation rate (Figure S3.4C) of A549 or H1299 cells. Importantly, cells expressing dox-inducible GFP also showed no changes in metabolite pool sizes or proliferation rates (Figures S3.4B-C), indicating that when added at this concentration doxycycline does not significantly affect metabolism in this system. In addition, we observed no significant differences in pool sizes of NAD+, NADH, NADP+ or NADPH in H1299 mtIDH1-C and mtIDH2-M cells following the addition of doxycycline for

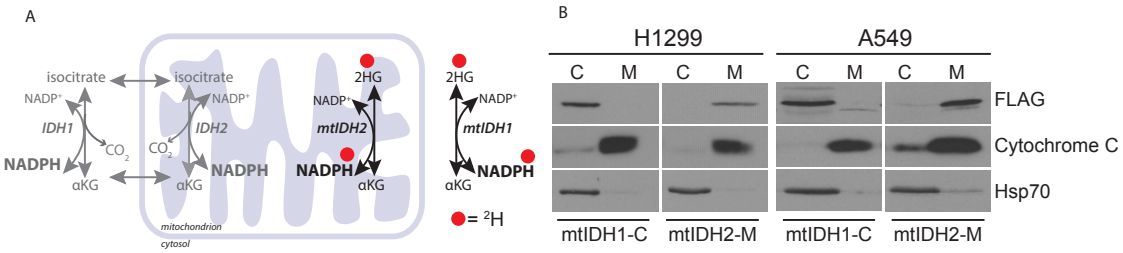

Figure 3.3: Generation and Characterization of Cell Lines Expressing Inducible Mutant IDH. (A) Schematic demonstrating the transfer of deuterium (red dots) from NADPH to 2HG via the reaction catalyzed by mutant IDH enzymes. mtIDH1 is localized to the cytoplasm and mtIDH2 is localized to the mitochondria. By expressing compartment specific mutant enzymes and combining this with deuterated glucose tracer, it is possible to track 2HG production, and therefore the source of the NADPH used to make the 2HG in the cytosol or the mitochondria. (B) Mutant IDH1-R132H is localized to the cytosol (mtIDH1-C) and mutant IDH2-R172K is localized to the mitochondria (mtIDH2-M) in H1299 and A549 cells. Cells were transduced with lentiviral constructs containing cDNA encoding C-terminal FLAG-tagged IDH1-R132H or IDH2-R172K under the control of a doxycycline-inducible promoter. Once stable cell lines were established, cells were treated with 0.1 μg/mL doxycycline for 24 hrs. Protein expression was analyzed by cellular fractionation and Western blotting using antibodies against FLAG, Cytochrome C (mitochondrial-specific marker) and Hsp70 (cytoplasmic-specific marker). C: Supernatant-100 fraction (cytoplasm); M: Mitochondria. White lines between blots in the horizontal direction indicate separate gels. (C) Cell lines expressing inducible IDH mutants produce 2HG in a doxycycline-dependent manner. H1299 and A549 cells stably expressing inducible mtIDH1-C or mtIDH2-M constructs were treated with doxycycline (0.1 μg/mL) for 24 hrs. Amounts of 2HG (total ion counts: TIC) are shown relative to GFP control cells treated with vehicle. (D) 2HG production, as measured by 2HG/αKG ratio, is much higher in cell lines harbouring endogenous mutations for IDH1 (R132C/+, HT1080) and IDH2 (R172S/+, SW1353) than cells expressing mtIDH1-C and mtIDH2-M. (E) NADPH produced by the pentose phosphate pathway (6PGD) is cytosolic. Cells were cultured in [3-^{2}H]glucose (10mM) for 24 hrs before adding doxycycline (0.1μg/mL) for 24 hours to induce mutant IDH expression and amount of M1 label (%) from [3-^{2}H]glucose incorporated into 2HG and αKG was measured. (F) NADH supports NADPH production in the mitochondria. Cells were incubated with 10mM [4-^{2}H]glucose for 24 hours and treated and analyzed as in E. Data represent mean ± SEM of at least three biological replicates.

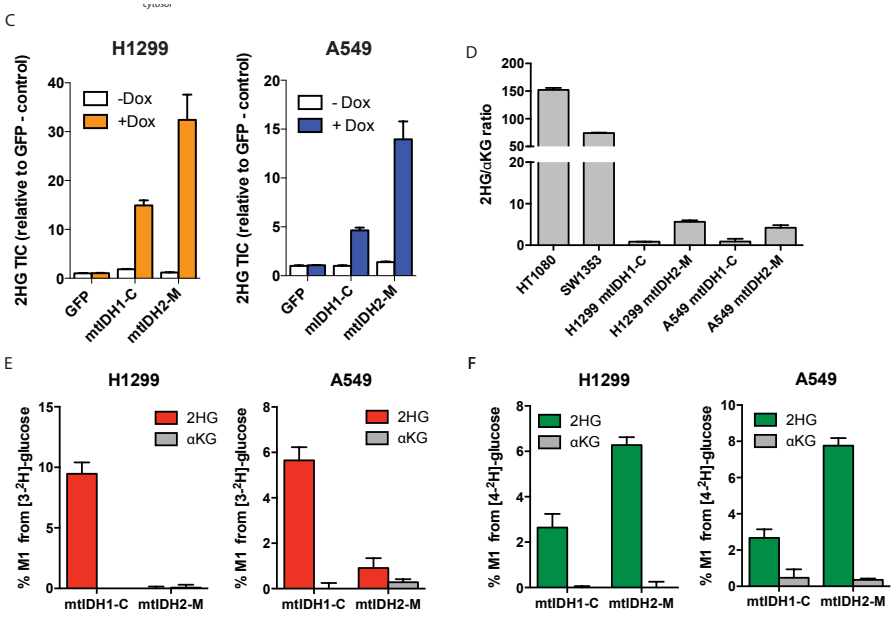

Figure 3.3: Generation and Characterization of Cell Lines Expressing Inducible Mutant IDH, *continued*.

24 hours, suggesting that dox-dependent production of 2HG was not altering the availability of these cofactors for use in other redox reactions (Figure S3.4D). This is supported by the reported k_{cat} of mutant IDH1 enzymes being small relative to wild type IDH1 (Dang et al., 2009) and suggests that any direct effects of these enzymes on cellular redox state are minimal.

Validation of Compartment-Specific Cofactor Tracing

To validate the ability of this system to trace compartment-specific NADPH metabolism we induced expression of the mutant IDH enzymes in cells cultured in the presence of [3-^{2}H]glucose and measured enrichment of ^{2}H in the 2HG pool. In order to ensure that the cells were at or near isotopic steady-state prior to induction of mutant IDH expression, the cells were incubated with tracer for 24 hours prior to the addition of doxycycline. Consistent with [3-^{2}H]glucose producing cytosolic NADPH via the oxidative PPP, 2HG was only significantly labeled from [3-^{2}H]glucose in the mtIDH1-C cell lines and not in the mtIDH2-M cell lines (Figure 3.3E). Importantly, little to no label was observed on αKG under these conditions, ensuring

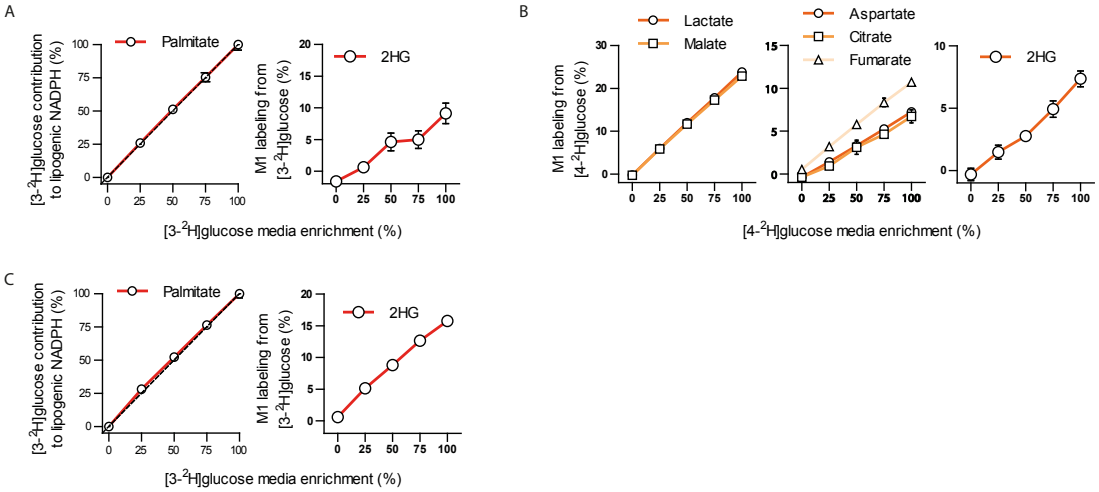

Figure 3.4: Kinetic Isotope Effect Minimally Affects 3-^{2}H-glucose and 4-^{2}H-glucose Metabolism. (A) [3-^{2}H]glucose was titrated with unlabeled glucose and added to H1299 cells expressing mtIDH1-C. Labeling from [3-^{2}H]glucose on lipogenic NADPH (left panel) and 2HG (right panel) was measured. Dashed lined (left panel) represents 1:1 contribution of lipogenic NADPH from [3-^{2}H]glucose to enrichment of [3-^{2}H]glucose in media. (B) [4-^{2}H]glucose was titrated with unlabeled glucose and added to H1299 cells expressing mtIDH2-M. Labeling from [4-^{2}H]glucose on lactate and malate (left panel); aspartate, citrate, and fumarate (middle panel); and 2HG (right panel) was measured. (C) [3-^{2}H]glucose was titrated with unlabeled glucose in HT1080 cells harbouring endogenous IDH1 mutations (R132C/+). Enrichment of lipogenic NADPH from [3-^{2}H]glucose (left panel) and M1 labeling on 2HG (right panel) was quantified at 0, 25, 50, 75, and 100 percent dilution with unlabeled glucose (left panel) in HT1080 cells cultured with [3-^{2}H]glucose diluted with unlabeled glucose at 0, 25, 50, 75, and 100 percent enrichment. Data presented are shown as mean ± SD of three biological replicates.

that label on 2HG was a direct result of hydride ion transfer from NADPH by the mutant enzyme. We next asked whether label from [4-^{2}H]glucose was incorporated into 2HG by either mtIDH1-C or mtIDH2-M. Notably, more 2HG was labeled from [4-^{2}H]glucose in mtIDH2-M cells than in mtIDH1-C cells (Figure 3.3F). These data suggest that transfer of H^- from NADH to NADPH occurs through a mitochondrial intermediate (*e.g.* malate) or via nicotinamide nucleotide transhydrogenase (NNT), and transfer of reducing equivalents from NADH to NADPH mostly supports the mitochondrial NADPH pool. Similar results were observed in cell lines with endogenous, heterozygous IDH1 and IDH2 mutations (Figures S3.4E-F).

In vitro steady state enzyme kinetics experiments have demonstrated that rate constants

for reactions involving ^{2}H transfer can be lower compared to studies conducted with unlabeled substrate (Rendina et al., 1984). This phenomenon has been an invaluable tool for elucidating biochemical reaction mechanisms, including many of the reactions responsible for label transfer in our system. However, given the diverse means through which metabolism is regulated and the challenges associated with understanding which enzymatic steps are rate limiting for pathways in intact cells, the relevance of isotope effects to intracellular metabolic fluxes is not clear. To determine the significance of this phenomenon in our system we cultured cells in different ratios of [3-^{2}H]glucose and unlabeled glucose and measured downstream labeling of lipogenic NADPH and 2HG in H1299 mtIDH1-C cells (Figure 3.4A). Similarly, we titrated [4-^{2}H]glucose with unlabeled substrate in H1299 mtIDH2-M cells and observed whether label transfer to lactate, malate, aspartate, fumarate, citrate, and 2HG was affected by different amounts of labeled substrate (Figure 3.4B). We reasoned that if reaction rates are affected by the presence of ^{2}H isotopes, the use of unlabeled substrates would be favored and less relative transfer of label would be observed as unlabeled substrate is titrated into the medium. However, in all cases transfer of label from either tracer decreased linearly as the tracer was diluted with unlabeled substrate, suggesting that kinetic isotope effects minimally impact the results of these experiments (Figures 3.4A-B). A linear decrease in lipogenic NADPH and 2HG labeling was also observed in endogenous mtIDH1 cells (HT1080) that exhibit much higher rates of 2HG production when we titrated [3-^{2}H]glucose, further supporting the notion that isotope effects minimally affect substrate fluxes through the reactions we traced in intact cells (Figure 3.4C).

Characterizing Serine/Glycine Metabolism in the Cytosol and Mitochondria

We next sought to use our reporter system to examine a compartmentalized metabolic cycle. Reactions that make up folate-mediated one carbon metabolism exist in both the cytosol and the mitochondria, although it is not clear from current literature whether these are linked in a cycle and/or in which direction the reactions proceed (Anderson et al., 2011; Nilsson et al., 2014; Tedeschi et al., 2013; Tibbetts and Appling, 2010). Serine and glycine interconversion via serine hydroxymethyltransferase (SHMT) has been observed in cultured cells (Jain et al., 2012; Levintow and Eagle, 1961; Perry et al., 2007) but ^{13}C tracing is unable to ascertain the

directionality, compartmentalization, and interconnectivity of this process. Indeed, upon culture with [U-$^{13}C_3$]serine we observed significant interconversion of serine and glycine in A549 mtIDH1-C and mtIDH2-M cells (Figure 3.5A). The reactions catalyzed by MTHFD1 (cytosolic) and MTHFD2/MTHFD2L (mitochondrial) utilize NAD(P)H (Figure 3.5B); therefore, we hypothesized that ^{2}H-labeled serine and glycine tracing in combination with our compartment reporter system would enable us to experimentally determine the direction of serine-glycine exchange reactions in the cytosol and mitochondria. Hydrogens on carbon-3 of serine are transferred to 5,10-methylenetetrahydrofolate (5,10-methyleneTHF) and subsequently to NADPH via MTHFD1/2 (Figure 3.5B). Additionally, the glycine cleavage system (GCS) exists in the mitochondria and could transfer hydrogen from carbon two of glycine to 5,10-methylene-THF and generate NADPH (Figure 3.5B) (Kikuchi et al., 2008).

To study these compartment-specific pathways, we cultured A549 mtIDH1-C and mtIDH2-M cells with either [3,3-$^2H_2$]serine or [2,3,3-$^2H_3$]serine and unlabeled glycine or [2,2-$^2H_2$]glycine and unlabeled serine and measured incorporation of ^{2}H in cytosolic or mitochondrial 2HG, respectively. Strikingly, we detected label from [3,3-$^2H_2$]serine and [2,3,3-$^2H_3$]serine on 2HG only in mtIDH2-M cells, strongly suggesting that serine to glycine conversion occurs primarily in the mitochondria in these cells with the MTHFD2/MTHFD2L reaction operating oxidatively (Figures 3.5C and Figure S3.5A-C). We did not observe labeling of 2HG from [2,2-$^2H_2$]glycine in cells expressing either mutant IDH (Figure 3.5C), indicating that either the majority of mitochondrial glycine is generated by SHMT2 (rather than glycine import) or the label is lost in the GCS. Consistent with the lack of label transfer from ^{2}H-labeled serine or glycine to 2HG in mtIDH1-C cells, we detected minimal contribution of these tracers in the lipogenic NADPH pool (Figure 3.5D). To further confirm the direction of MTHFD1, we cultured A549 mtIDH1-C and mtIDH2-M cells with [3-^{2}H]glucose, which specifically labels cytosolic NADPH. We observed transfer of ^{2}H from [3-^{2}H]glucose onto serine suggesting that cytosolic MTHFD1 can operate in the reductive direction in these cells (Figure 3.5E). The lack of glycine labeling from [3-^{2}H]glucose confirms label transfer to serine was obtained from 5,10-methyleneTHF (Figure 3.5E, S3.5D). The lack of labeling from either [2,3,3-$^2H_3$]serine or [3,3-$^2H_2$]serine on either fatty acids or 2HG produced by mtIDH1-C is

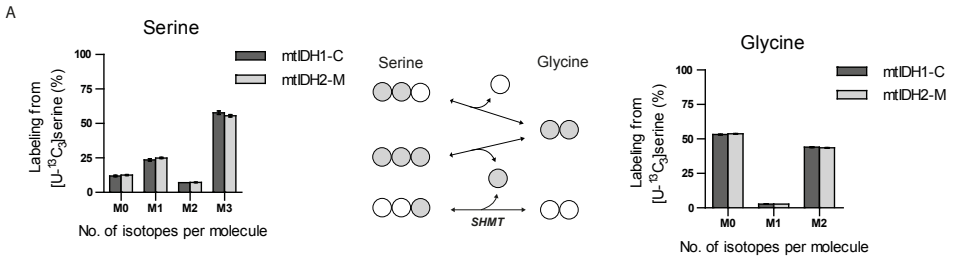

Figure 3.5: Characterizing Serine/Glycine Metabolism in the Cytosol/Mitochondria. (A) Serine (left panel) and glycine (right panel) labeling in A549 mtIDH1-C and mtIDH2-M cells cultured with [U-$^{13}C_2$]serine. Cells were incubated with [U-$^{13}C_2$]serine for 24 hours prior to dox-induction (0.1 μg/mL) for an additional 48 hours. Middle panel demonstrates interconversion of serine and glycine by SHMT. Data plotted represent mean ± SD for three biological replicates. (B) A schematic of folate-mediate one carbon metabolism in cytosolic and mitochondrial compartments catalyzed via SHMT and MTHFD. Deuterium transfer from [3,3-$^2H_2$]serine is shown for pathways containing SHMT and MTHFD and is indicated by small red or blue circles for cytosolic and mitochondrial isozymes, respectively. The extra deuterium on [2,3,3-$^2H_3$]serine is indicated by an orange (cytosolic) or a turquoise (mitochondrial) circle. Deuterium transfer from [2,2-$^2H_2$]glycine is shown for the glycine cleavage system (GCS) pathway indicated by small green circles. (C) 2HG labeling from [3,3-$^2H_2$]serine, [2,3,3-$^2H_3$]serine or [2,2-$^2H_2$]glycine in A549 mtIDH1-C and mtIDH2-M cells. Cells were incubated with either tracer for 24 hours prior to dox-induction (0.1 μg/mL) for an additional 48 hours. No label was detected on 2HG in mtIDH1-C cells from either [3,3-$^2H_2$]serine or [2,3,3-$^2H_3$]serine, nor was label detected on 2HG from [2,2-$^2H_2$]glycine in mtIDH1-C and mtIDH2-M cells (indicated by *). (D) Fatty acid labeling from A549 mtIDH1-C and mtIDH2-M cells cultured with either [3,3-$^2H_2$]serine, [2,3,3-$^2H_3$]serine, or [2,2-$^2H_2$]glycine. Cells were incubated with tracer for 24 hours prior to dox-induction (0.1 μg/mL) for an additional 48 hours. (E) Serine and glycine labeling in A549 mtIDH1-C and mtIDH2-M cells cultured with [3-^2H]glucose. Cells were incubated with tracer for 24 hours prior to dox-induction (0.1 μg/mL) for 48 hours. Data represent mean ± SEM of at least three biological replicates for panels C-E.

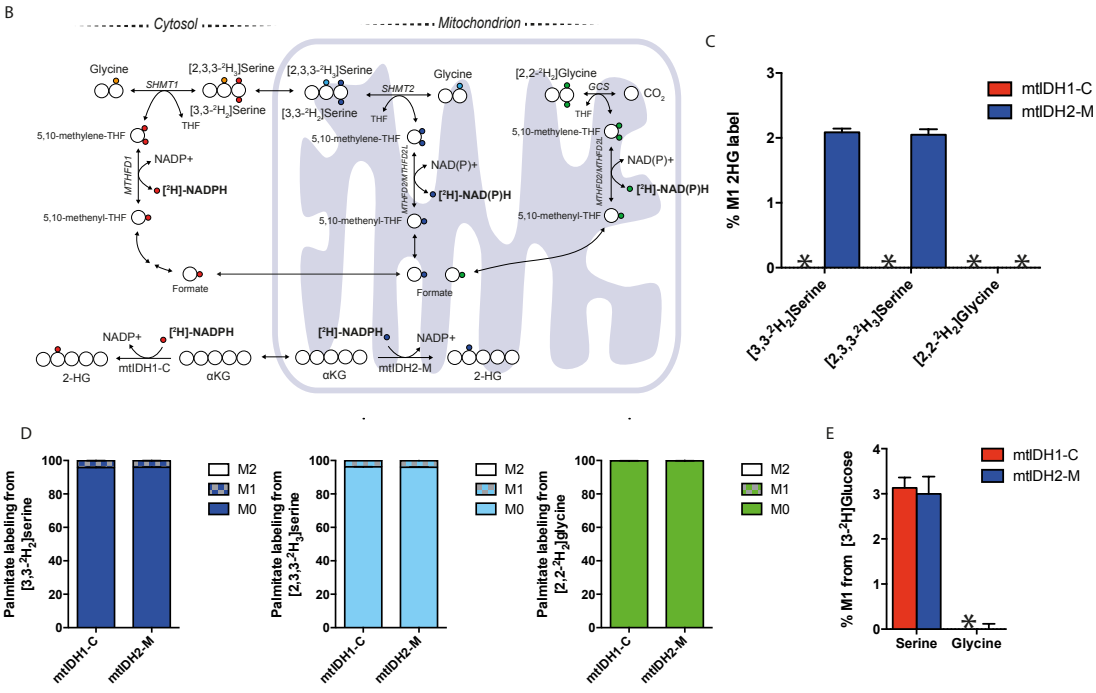

Figure 3.5: Characterizing Serine/Glycine Metabolism in the Cytosol/Mitochondria, *continued*.

also consistent with minimal contribution of MTHFD1 to the cytoplasmic NADPH pool in these cells, although channeling to other reactions cannot be ruled out by these methods. Shuttling of serine labeled by [3-^{2}]glucose by MTHFD1/SHMT1 into the mitochondria for catabolism by MTHFD2/SHMT2 may account for the small amount of label (<1%) we observe on mitochondrial 2HG in A549 mtIDH2-M cells cultured with [3-^{2}H]glucose (Figure 3.3E). Collectively, these data provide direct evidence that serine metabolism can contribute to regenerating mitochondrial NADPH in cells.

Discussion

We have developed a system that can distinguish compartmentalized pools of NADPH, demonstrating the directionality and interconnectivity of serine/glycine metabolism in the cytosol and mitochondria of intact cells. In the cells studied, conversion of serine to glycine occurs primarily in the mitochondria with the reaction catalyzed by MTHFD2/MTHFD2L con-

tributing to NADPH production in this compartment. Interestingly, label transfer from both [2,3,3-$^2H_3$]serine and [3,3-$^2H_2$]serine to mitochondrial 2HG was observed, suggesting that serine metabolism by SHMT2 is a contributor to the mitochondrial NADPH and glycine pools. These data also provide direct experimental support for the hypothesis that the cytoplasmic source of formate used for purine synthesis can be mitochondrially-derived in some cells. Previous efforts to ascertain directionality of folate-mediated one carbon metabolism have been unable to distinguish between compartments, relying on expression data (Nilsson et al., 2014), mathematical modeling (Scotti et al., 2013; Tedeschi et al., 2013), or isolated mitochondrial preparations (Barlowe and Appling, 1988). The importance of distinguishing compartmentalized redox pathways is highlighted by the large number of potential pathways that have been implicated in the shuttling of reducing equivalents between the cytosol and mitochondria (Tibbetts and Appling, 2010). For instance, compartment-specific metabolic cycling through citrate/αKG (Sazanov and Jackson, 1994; Ward et al., 2010), malate/pyruvate (Jiang et al., 2013; Son et al., 2013b), proline (Hagedorn and Phang, 1983; Nilsson et al., 2014), and serine have been suggested to be important for mammalian cell physiology. Although carbon tracing is increasingly combined with genetic approaches to implicate a role for compartment-specific isozymes in such processes, adaptation to genetic depletion strategies that break these cycles can confound interpretation. The reporter system described here circumvents these issues for reactions involving NAPDH by providing direct visualization of compartmentalized reaction activity and direction in intact cells.

Other subcellular compartments also have distinct metabolic needs in eukaryotic cells and could be probed with an analogous approach by engineering the localization of mutant IDH enzymes and/or monitoring ^2H transfer between other metabolites. The endoplasmic reticulum (ER) is an important site for protein folding, disulfide bond formation, long chain fatty acid extension, and sterol reduction; as such, the NADP+/NADPH ratio within the ER can influence diverse cellular and physiological processes (Banhegyi et al., 2009; Kardon et al., 2008; Szaraz et al., 2010). This approach may also be adapted to quantify the NADP+/NADPH ratio in particular organelles and the turnover rate of NADPH in specific compartments. Altering the cofactor selectivity of the mutant IDH enzyme, or relying on NADH-dependent production of another xenometabolite could similarly be used to visualize compartmentalized reactions that

utilize NADH. Finally, these data may be integrated with compartmentalized ^{13}C metabolic flux analysis (MFA) models to better understand the role of cofactor metabolism in metabolic engineering applications or disease models (Ruhl et al., 2012). Thus, this approach opens up new avenues to observe metabolic processes in complex cells and improve our understanding of metabolism in normal and disease states.

Materials and Methods

Cell Culture and Isotopic Labeling

All cell lines were maintained in DMEM supplemented with 10% FBS, 100 U/mL penicillin/streptomycin and 4 mM L-glutamine. The pSLIK-mtIDH cell lines (see below) were maintained as above, but FBS was substituted for Tet-free FBS (Clontech). Cell number was determined using an automated cell counter (Nexcelom) or by haemocytometer. For isotopic labeling experiments in the pSLIK-mtIDH cell lines, cells were cultured in 6-well plates in glucose- and glutamine- free DMEM, supplemented with 10% dialyzed Tet-free FBS, 100 U/mL penicillin/streptomycin, 4 mM L-glutamine and 10 mM or 15 mM of the appropriate deuterated glucose tracer ([3-^{2}H, 95% or 98%]glucose or [4-^{2}H, 94% or 98%]glucose) for 24 hour or 48-72 hour incubation, respectively (Omicron and Cambridge Isotope Laboratories, Inc.). For cholesterol labeling experiments, parental H1299 cells were cultured in DMEM supplemented with 1% FBS for two passages prior to 72 hour incubation with [3-^{2}H]glucose. Cells were cultured in tracer medium for 24 hours prior to the addition of doxycycline hyclate (0.1 μg/mL in water: Sigma) for 24 to 48 hours in order to induce mutant IDH expression and accumulate 2HG. Isotope-labeled glycine and serine tracer medium was prepared from custom phenol red-, glucose-, sodium pyruvate-, amino acid- and sodium bicarbonate-free DMEM (Hyclone Laboratories, Inc.) supplemented with 10% dialyzed Tet-free FBS, 3.7 g/L sodium bicarbonate, and DMEM-levels of L-arginine, L-cystine, L-glutamine, L-histidine, L-isoleucine, L-leucine, L-lysine, L-methionine, L-phenylalanine, L-threonine, L-tryptophan, L-tyrosine, and L-valine prepared as a 100x stock in aqueous acid (pH 2.0). A549 pSLIK mtIDH1-C and mtIDH2-M cells were cultured in serine- and glycine- free DMEM supplemented with either [2,3,3-$^2H_3$, 98%]serine or

[3,3-$^2H_2$, 98%]serine and unlabeled glycine (0.4 mM) (Cambridge Isotope Laboratories, Inc.), or [2,2-$^2H_2$, 98%]glycine and unlabeled serine (0.4 mM) (Cambridge Isotope Laboratories, Inc.). Cells were cultured in the presence of tracer medium for 24 hours prior to doxycycline addition (0.1 μg/mL) for a further 48 hours.

Generation of Cell Lines Stably Expressing Inducible Forms of Flag-Tagged Mutant IDH

To generate the doxycycline-inducible mutant IDH (mtIDH) cell lines, full-length cDNA for IDH1-R132H and IDH2-R172K was amplified by PCR and cloned into the p3xFLAG-CMV14 vector (Sigma) to generate C-terminal Flag-tagged constructs. cDNA for IDH1-R132H-FLAG and IDH2-R172K-FLAG was then amplified by PCR and cloned into the pEN_TTmcs entry vector for recombination into the pSLIK-hygro lentiviral vector (Both vectors from Addgene (Shin et al., 2006)). Lentiviruses were produced by transfecting HEK-293T cells with the pSLIK-hygro-IDH1-R132H or pSLIK-hygro-IDH2-R172K plasmids along with the lentiviral packaging plasmids pMDLg/pRRE and pRSV-Rev and the envelope plasmid pMD2.G (all from Addgene). Supernatants containing lentiviral particles were collected 48 hours after transfection and used to infect sub-confluent H1299 and A549 cells. Infected cells were allowed to recover for 24 hours before being placed under selection with 350 μg/mL hygromycin (Invitrogen) for ten days. Protein expression was induced using 0.1 μg/mL doxycycline hyclate (Sigma) for 24-48 hours.

Protein Expression Analysis and Cellular Fractionation

For whole cell extracts, cells were lysed in RIPA buffer. Mitochondrial and cytoplasmic fractions were prepared as previously described (Vander Heiden et al., 1997). Briefly, cells were harvested in buffer A (250 mM sucrose, 20 mM HEPES, 10 mM KCl, 1.5 mM MgCl2, 1 mM EDTA, 1 mM EGTA, 1 mM DTT, 1x EDTA-free protease inhibitor cocktail tablet (Roche)[pH 7.4]) and broken apart using a mechanical homogenizer (H Y Enterprise, Redwood City, CA). Following centrifugation at 750 xg to remove unlysed ells and nuclei, mitochondria were isolated by centrifuging at 10,000 xg for 25 mins. The resulting pellet was resuspended in buffer A

and represents the mitochondrial fraction. The remaining supernatant containing cytoplasmic and membrane proteins was centrifuged for 1 hour at 100,000 xg. The supernatant from this final spin represents the S100 fraction. Protein expression was analyzed by Western blotting using antibodies against FLAG (DYKDDDDK Tag: Cell Signaling), IDH1 (Santa Cruz), IDH2 (Abcam), Cytochrome C (clone 7H8.2C12, Abcam), Hsp 70 (Cell Signaling).

Metabolite Extraction and GC-MS Analysis

Polar metabolites and fatty acids were extracted using methanol/water/chloroform as previously described (Metallo et al., 2012). Parental and pSLIK-mtIDH cells were cultured in 6-well or 12-well plates and volumes of tracer media and extraction buffers were adjusted accordingly. Derivatization of both polar metabolites and fatty acids has been described previously (Metallo et al., 2012). Briefly, polar metabolites were derivatized to form methoxime-tBDMS derivatives by incubation with 2% methoxylamine hydrochloride (MP Biomedicals) in pyridine (or MOX reagent (Thermo Scientific) followed by addition of N-tert-butyldimethylsilyl-N-methyltrifluoroacetamide (MTBSTFA) with 1% tert-butyldimethylchlorosilane (t-BDMCS) (Regis Technologies). Non-polar fractions, including triacylglycerides and phospholipids were saponified to free fatty acids and esterified to form fatty acid methyl esters either by incubation with 2% H_2SO_4 in methanol or by using Methyl-8 reagent (Thermo Scientific). Derivatized samples were analysed by GC-MS using a DB-35MS column (30m x 0.25mm i.d. x 0.25 μm, Agilent J&W Scientific) installed in an Agilent 7890A gas chromatograph (GC) interfaced with an Agilent 5975C mass spectrometer (MS). Mass isotopomer distributions were determined by integrating metabolite ion fragments (Table S3.1) and corrected for natural abundance using in-house algorithms adapted from Fernandez et al. (Fernandez et al., 1996).

Extraction of NAD+, NADH, NADP+ and NADPH and Analysis by LC-MS/MS

The extraction protocol for NADPH was based on one previously described by Fendt et al. (Fendt et al., 2013a), and was optimized for analysis by LC-MS/MS. Briefly, cells were cultured in 6-well plates over the course of 30 minutes, washed once in ice cold water and immediately quenched in liquid nitrogen. 200 μL ice cold extraction buffer (40:40:20 acetoni-

trile/methanol/200 mM NaCl, 10 mM Tris-HCl, pH 9.2) was added directly to the cells. Cells were scraped on ice and cleared by centrifugation at 4°C. 50 µL of supernatant was transferred to a polypropylene vial and samples were analysed using a Q Exactive Benchtop LC-MS/MS (Thermo Fisher Scientific).

For measurement of NAD(P)H at 24 hours, cells were cultured in 10 cm plates. After 24 hour incubation with tracer, approximately $1x10^7$ cells were washed in ice cold 0.9% saline and immediately quenched in 1 mL of 80% methanol at -80°C. Cells were scraped on dry ice and cleared by centrifugation at 4°C. Cleared supernatant was transferred to Eppendorf tube, dried under vacuum using a CentriVap (Labconco), resuspended in water and immediately loaded onto a XSELECT HSS XP 150 mm ÃŮ 2.1 mm ÃŮ 2.5 µm (Waters, Milford, MA) with an UFLC XR HPLC (Shimadzu, Columbia, MD) coupled to an AB SCIEX Qtrap 5500 mass spectrometer (AB SCIEX, Framingham, MA) operating in negative ion mode. Mass isotopomer distributions were corrected for natural abundance using in-house software adapted from Fernandez et al. (Fernandez et al., 1996). Additional information regarding chromatographic separation, mass spectrometry, and data acquisition can be found in the Supplemental Experimental Procedures in the Supplement to Chapter 3.

Isotopomer Spectral Analysis (ISA)

The ISA method compares a measured palmitate mass isotopomer distribution to one that is simulated using a reaction network for palmitate synthesis whereby 14 NADPH molecules are consumed to form one palmitate molecule. Models were also generated for myristate and stearate synthesis whereby 12 or 16 NADPH molecules are consumed to form one myristate or stearate molecule, respectively. Parameters for the relative enrichment of the lipogenic NADPH pool from a given [^{2}H] tracer and the percentage of fatty acids that are *de novo* synthesized are extracted from a best fit model using the INCA metabolic flux analysis software package (Figure S3.2) (Young, 2014). The 95% confidence intervals for both parameters were estimated by evaluating the sensitivity of the sum of squared residuals between measured and simulated palmitate mass isotopomer distributions to small flux variations (Antoniewicz et al., 2006).

Cell Proliferation Assays

On day -1, 1/10 of a confluent 10cm dish of cells were seeded in six six-wells of a six-well plate. 24 hours later, cells were counted on an automated cell counter (Nexcelom) and this time-point was considered T_0. At T_0, all other time-points were media changed to $\pm$ dox media (0.1 μg/mL doxycycline hyclate (Sigma) in water). Cells were counted every 24 hours in technical duplicate and biological triplicate. Media was changed every 48 hours to prevent degradation of doxycycline in the media.

Acknowledgements

We thank Michael Pacold, Elizaveta Freinkman, David Sabatini, and Bernhard Palsson for providing access to equipment. We are grateful to Patrick Ward and Craig B. Thompson for providing the cDNA for IDH1-R132H and IDH2-R172K. Eric L. Bell and Sarah-Maria Fendt provided advice and reagents. This work was supported, in part, by NIH grants P30CA147882, U54-CA121852-09, and R01CA168653, as well as the Koch Institute/DFHCC Bridge Project, the Koch Institute Frontier Research Fund, the Burroughs Wellcome Fund, the Damon Runyon Cancer Research Foundation, American Cancer Society grant IRG 70-002, DOD grant W81XWH-13-1-0105, a University of California Cancer Research Coordinating Committee grant, and a Searle Scholar Award. The authors declare no conflict of interest.

Chapter 3, in full, is a reprint of the material as it appears in "Tracing Compartmentalized NADPH Metabolism in the Cytosol and Mitochondria of Mammalian Cells", Molecular Cell, vol. 55, issue 2, 2014. Seth J. Parker and Caroline A. Lewis are primary authors of this publication. Brian P. Fiske, Douglas McCloskey, Dan Y. Gui, Courtney R. Green, Natalie I. Vokes, and Adam M. Feist are co-authors on this publication. Matthew G. Vander Heiden and Christian M. Metallo are corresponding authors on this publication.

Chapter 4

Hypoxic Reprogramming of NADPH Metabolism in Mutant IDH Cells

Introduction

Pyridine nucleotides, such as NADP(H) and NAD(H), are critical cofactors involved in many biosynthetic and cellular processes including lipid and nucleotide biosynthesis required for proliferation. As detailed in Chapter 3, NADP(H) and NAD(H) cannot directly transport across subcellular organelle boundaries allowing cells to maintain distinct cytosolic, mitochondrial, and other compartmental pools (Pollak et al., 2007a). Canonical pathways that regenerate reduced NADPH include IDH, malic enzyme, and the pentose phosphate pathway (PPP) with the latter pathway thought to contribute the majority of cytosolic NADPH (Pollak et al., 2007a). Isoforms of these enzymes are localized in specific organelles and maintain the balance of NADP+/NADPH within each compartment. For example, IDH1 and IDH2/3 are localized to the cytoplasm and mitochondria, respectively. Specific biosynthetic reactions occur in specific compartments (*i.e.* fatty acid and cholesterol synthesis occur in the cytosol) and thus require compartmentalized pools of NADPH. In addition, glycolysis occurs in the cytosol requiring NAD+ regeneration via several cytosolic NADH-dependent shuttle systems (*i.e.* lactate dehydrogenase (LDH), the malate-aspartate shuttle, and the glycerol 3-phosphate dehydrogenase shuttle) (Lewis et al., 2014). The TCA cycle and oxidative phosphorylation rely on tight maintenance of the mitochondrial NAD+:NADH ratio in order to produce ATP.

Hypoxia is commonly experienced by cancers in vivo due to, in part, the lack of an

efficient vascular system and high nutrient and oxygen consumption rates (Carmeliet and Jain, 2000; Eales et al., 2016). Low oxygen microenvironments lead to several metabolic alterations with enhanced glycolytic rates representing a mutual response in both non-transformed and transformed tissues (DeBerardinis et al., 2008). In addition, the ratio of mitochondrial NAD+:NADH decreases in hypoxia leading to reduced mitochondrial oxidative phosphorylation (Frezza et al., 2011; Hollinshead and Tennant, 2016). Several of the metabolic alterations in hypoxia are caused by the activity of HIF1 which is stabilized under hypoxia. HIF1 regulates the expression of glucose transporters (GLUT1 and 3) and glycolytic enzymes (HK1, aldolase A and C, triose phosphate isomerase, and GAPDH) (Higashimura et al., 2011; Semenza et al., 1996; Gess et al., 2004). In addition, hypoxia leads to alterations in NADPH metabolism both in the cytosol and mitochondria. Generally, levels of ROS are thought to increase in hypoxia and NADPH would become critical for maintenance of ROS-detoxifying systems in this microenvironment (Chandel et al., 2000). How hypoxia reprograms NADPH production and the contribution of cytosolic and mitochondrial NADPH-producing pathways is largely unknown.

Folate-mediated one carbon metabolism (FOCM), involving the amino acids serine and glycine, represents one such pathway that has been reported to be critical for supplying mitochondrial NAD(P)H critical for maintaining mitochondrial redox and oxidative phosphorylation (Lewis et al., 2014; Fan et al., 2014). Serine lies at a critical pivot point within intermediary metabolism, linking biosynthetic flux from glycolysis to purine synthesis, folate-mediated one-carbon metabolism (FOCM), glutathione synthesis, and lipid metabolism (Tibbetts and Appling, 2010). Each of these metabolic processes may influence a number of biological functions, including epigenetic regulation and cellular redox status. Not surprisingly, a growing number of studies have demonstrated the importance of this pathway in cancer. Genes encoding several enzymes along these pathways are amplified or overexpressed in tumors, including phosphohydroxyglycerate dehydrogenase (PHGDH) (Locasale et al., 2011), serine hydroxymethyltransferase (SHMT), and methylene tetrahydrofolate dehydrogenase (MTHFD) (Nilsson et al., 2014). Expression of SHMT2, the mitochondrial isoform, is regulated by HIF-1α signaling and is involved in the maintenance of cellular NADPH:NADP+ ratios (Ye et al., 2014). Modulation of serine availability can impact *in vivo* tumor growth and the sensitivity to mitochondrial inhibitors (Gravel

et al., 2014; Maddocks et al., 2013). Several studies have also shed light on the impacts of serine on purine and NAD(P)H regeneration (Fan et al., 2014; Field et al., 2015; Lewis et al., 2014; Nilsson et al., 2014; Maddocks et al., 2016).

Mutations in specific compartmentalized NAD(P)H-dependent enzymes, including IDH1 and IDH2, influences redox metabolism in the cytosol and mitochondria. Specifically, heterozygous IDH2- R140 and R172 and IDH1-R132 mutations eliminate the oxidative capacity of IDH to produce NADPH leading to dysfunctional redox metabolism in either the cytosol or mitochondria (Chapter 1) (Parker and Metallo, 2015). As demonstrated in Chapter 3, ^{13}C tracing alone cannot distinguish metabolic flux in redundant pathways involving isoforms in many subcellular compartments (*i.e.* malic enzyme, IDH, ALDHs); thus, we developed a compartmentalized NADPH reporter system capable of deconvoluting such redundancies in intact cells (Lewis et al., 2014). The compartmentalized NADPH reporter system uniquely enables us to perform quantitative ^{2}H tracing studies to investigate redundant metabolic pathway activity and NADPH reprogramming in intact cells. Herein we utilize the cytosolic and mitochondrial NADPH reporter system to investigate NADPH reprogramming in IDH2 mutant cells, specifically in the mitochondria. Furthermore, we investigate how the contribution of NADPH producing pathways is influenced by hypoxic microenvironments and if mutations in IDH2 affect NADPH metabolic reprogramming in hypoxia. These studies provide insight into possible metabolic liabilities in mutant IDH2 cancers that could be targeted therapeutically to achieve a synthetic lethal effect.

Results

Hypoxia Reprograms NADH and NADPH Metabolism

In order to quantify the reprogramming of NADPH metabolism in response to hypoxic microenvironments, we cultured a panel of cancer cell lines in the presence of [3-^{2}H]glucose under normoxic of hypoxic (1% oxygen) for 48-72 hours and isotope enrichment of various metabolites was determined by mass spectrometry (Figure 4.1A). As demonstrated in Chapter 3, cytosolic NADPH produced by the pentose phosphate pathway (PPP) can be visualized by measuring labeling on *de novo* synthesized fatty acids (Lewis et al., 2014). Strikingly, we observed

a significant increase, ranging from 11—40%, in PPP contribution to cytosolic NADPH in response to hypoxic stress (Figure 4.1B). We cultured HCT116 cells, which exhibited the largest increase in PPP contribution under hypoxia, in the presence of [1,2-$^{13}C_2$]glucose and quantified the relative shunting of glucose carbon through the oxidative PPP. Interestingly, we did not observe a significant effect on the relative shunting through oxPPP in hypoxia (Figure 4.1C). Given that glycolytic flux increases in hypoxic microenvironments and we observed an increase in contribution, the absolute molar flux through the PPP is increased despite similar shunting of glycolytic intermediates (Chapter 2, Figure 2.1D). These results suggest that cells exhibit an increase in NADPH demand in hypoxic microenvironments. Interestingly, A549 cells did not exhibit an increase in PPP contribution under hypoxia; however (Figure 4.1B).

To quantify reprogramming of NADH metabolism and glycolytic metabolism in response to hypoxic microenvironments, we cultured A549 cells in the presence of [4-^{2}H]glucose under normoxic or hypoxic (1% oxygen) for 72 hours. Chapter 3 details the labeling through which [4-^{2}H]glucose labels NADH. Briefly, NAD+ is reduced to NADH via GAPDH in the cytosol transferring ^{2}H from [4-^{2}H]glucose to NADH. NAD+ regeneration via three main cytosolic NADH-dependent enzymes is required to maintain glycolytic flux. Under hypoxia, we observed a significant decrease in labeling of [4-^{2}H]glucose onto GAP (Figure 4.1D). As ^{2}H can be lost through water exchange during the TPI reaction, these results suggest that under hypoxia there is an increased exchange flux at the TPI step of glycolysis diluting ^{2}H labeling on GAP. Furthermore, we observed a significant decrease in labeling on cytosolic NADH as observed by decreased labeling on lactate, glycerol 3-phosphate, and malate (Figure 4.1D). We observed a significant decrease in NADH entry into the mitochondria via the malate-aspartate-shuttle and incorporation into TCA intermediates in hypoxia (Figure 4.1E). Taken together, these results suggest that cytosolic NADH metabolism is reprogrammed under hypoxia.

PPP Contributes to Cytosolic Reductive Carboxylation in Hypoxia

The malate-aspartate shuttle consists of a system of isozymes present in the cytosol and mitochondria that can act to shuttle reducing equivalents into the mitochondria through coupled reductive cytosolic and oxidative mitochondrial activity. Reductive carboxylation of glutamine

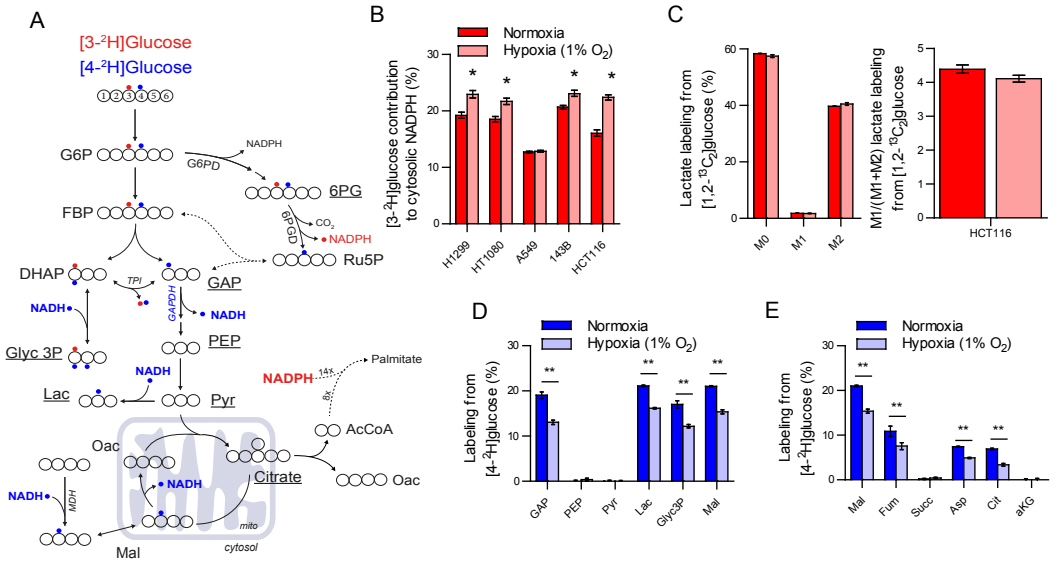

Figure 4.1: NADPH and NADH Metabolism is Reprogrammed Under Hypoxia. (A) Tracer diagram depicting atom-transitions for [3-^{2}H]glucose (^{2}H atoms colored red) and [4-^{2}H]glucose (^{2}H atoms colored blue) labeling of NADPH and NADH, respectively. (B) Contribution of [3-^{2}H]glucose to lipogenic NADPH quantified using isotopomer spectral analysis (ISA) in panel of cell lines. Cells cultured for 48-72 hours in presence of [3-^{2}H]glucose and incorporation into palmitate measured and modeled.(C) (left) Labeling of lactate from [1,2-$^{13}C_2$]glucose in HCT116 cells in normoxic or hypoxic conditions. M+1 lactate arises from shunting of glucose 6-phosphate through the oxidative branch of PPP and rejoining glycolysis as GAP. (right) Ratio of M1/(M1+M2) lactate labeling from [1,2-$^{13}C_2$]glucose represents relative shunting through oxPPP. (D) Labeling of glycolytic intermediates from [4-^{2}H]glucose after 72 hours in A549 cells. Label on GAP transfers onto NADH via GAPDH and subsequently labels lactate, glycerol 3-phosphate, and malate through LDH, glycerol 3-phosphate dehydrogenase, and MDH, respectively. (E) Labeling of TCA intermediates from [4-^{2}H]glucose arising from malate entering TCA cycle via the malate-aspartate shuttle.

and subsequent oxidative IDH activity represents another such redox shuttle that has been shown to be active under anchorage-independent conditions (Jiang et al., 2016). Furthermore, reductive carboxylation has been shown to facilitate lipogenesis under hypoxic microenvironments and mitochondrial dysfunction (Metallo et al., 2012). In 143B cells cultured in the presence of [U-$^{13}C_5$]glutamine, we observed a significant switch from oxidative to reductive glutamine metabolism in hypoxia as evidenced by decrease in M+4 and increase in M+5 citrate labeling (Figure 4.2A-B). Furthermore, we observed a significant increase in reductive carboxylation to lipogenic acetyl-CoA (Figure 4.2C). Reductive carboxylation can occur through either IDH1 or IDH2 in the cytosol or mitochondria, respectively. To determine the compartmentalization of reductive carboxylation, we cultured 143B cells with [3-^{2}H]glucose to label cytosolic NADPH and observed significant labeling of citrate under hypoxia (Figure 4.2D). These results suggest that the reductive carboxylation of aKG primarily occurs in the cytosol via IDH1 in the system tested.

G6PD Knockdown Reduces Reductive Carboxylation

As we observed contribution of NADPH labeled from [3-^{2}H]glucose to reductive carboxylation, we knocked down G6PD the first enzyme of the PPP in A549 cells stably expressing a non-targeting (shNT) or G6PD (shG6PD) hairpin and utilized ^{13}C and ^{2}H tracing to characterize effects on NADPH metabolism and impacts on RC flux (Figure 4.3A). Culturing G6PD knockdown A549 cells in the presence of [1,2-$^{13}C_2$]glucose confirmed that relative flux through the oxidative branch of the PPP was significantly reduced in G6PD knockdown cells (Figure 4.3B). Furthermore, G6PD knockdown significantly reduced the contribution of oxPPP to cytosolic NADPH by approximately 50% (Figure 4.3C, left). Treatment with the G6PD inhibitor, 6-aminonicotinamide (6AN), leads to a similar reduction in contribution from oxPPP to cytosolic NADPH (Figure 4.3C, right). Characterizing impacts on RC, we cultured G6PD knockdown cells in the presence of either [1-^{13}C]glutamine or [5-^{13}C]glutamine which yield two distinct readouts of RC activity (Figure 4.3D). Citrate labeling from [1-^{13}C]glutamine via RC increased under hypoxia in both control and G6PD knockdown cells; however, the increase in RC was blunted in G6PD knockdown cells (Figure 4.3E). Furthermore, [5-^{13}C]glutamine labeling of palmitate

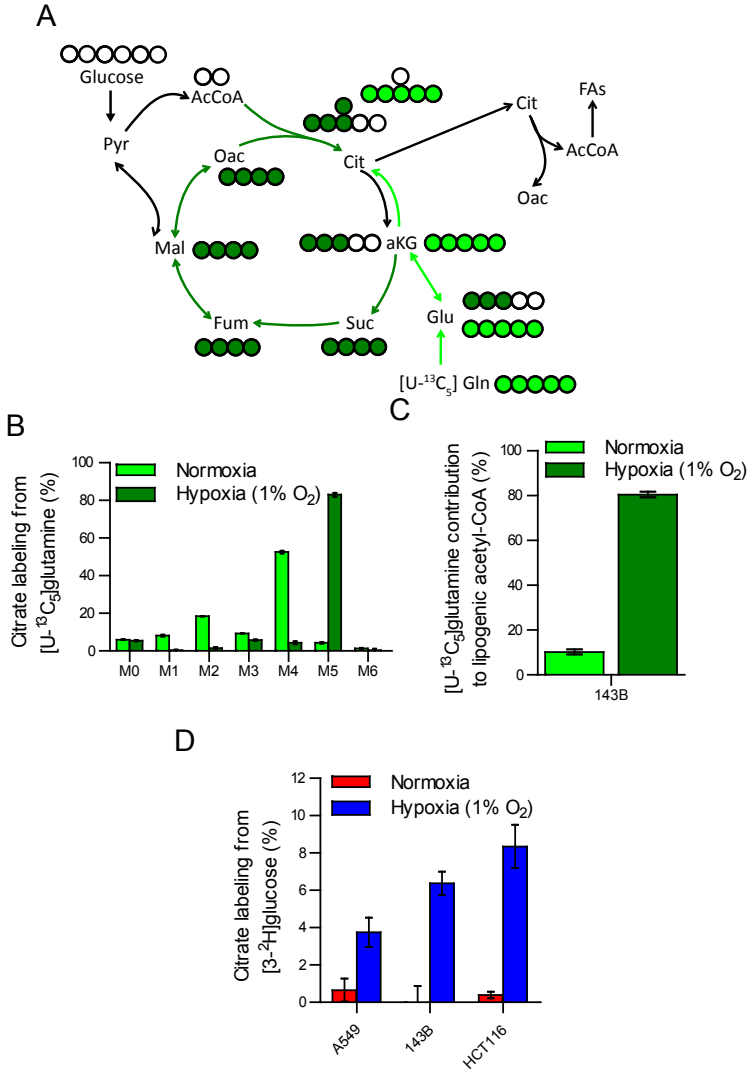

Figure 4.2: Reductive Carboxylation Occurs in the Cytosol in Hypoxia. (A) Tracer diagram depicting atom-transitions for [U-$^{13}C_5$]glutamine. Dark green circles represent labeling arising from oxidative TCA cycle flux. Light green circles represent labeling arising from reductive carboxylation flux. (B) Citrate labeling from [U-$^{13}C_5$]glutamine in 143B cells after 72 hours. (C) Contribution of glutamine carbon via reductive carboxylation to lipogenic acetyl-CoA quantified by ISA of palmitate labeling from [U-$^{13}C_5$]glutamine in 143B cells after 72 hours. (D) Citrate labeling in A549, 143B, and HCT116 cells cultured with [3-^{2}H]glucose after 72 hours in normoxia and hypoxia.

followed a similar trend whereby G6PD knockdown significantly reduced the contribution of RC to lipogenic acetyl-CoA (Figure 4.3F).

Hypoxia Promotes NADPH Shuttling Into the Mitochondrial via FOCM

FOCM can act as a cytosol:mitochondrial redox shuttle (Tibbetts and Appling, 2010). Since ^{13}C tracing is not sufficient to determine the directionality of isozymes present in the FOCM pathway (Lewis et al., 2014), we engineered 143B, HCT116, and A549 cell lines to express the dox-inducible cytosolic (mtIDH1-C) and mitochondrial (mtIDH2-M) NADPH probes discussed in Chapter 3. 143B mtIDH1-C and mtIDH2-M cell lines produced 2HG when treated with 0.1 μg/mL doxycycline (Figure 4.4A). Strikingly, hypoxia increased the amount of 2HG similar to that previously observed in endogenous mutant IDH cell lines (Figure 4.4A). In order to quantify the shuttling of cytosolic NADPH into the mitochondria, we cultured 143B mtIDH2-M cells in the presence of [3-^{2}H]glucose in normoxic and hypoxic conditions. Notably, we observed significantly increased labeling of serine (via MTHFD1) and citrate (via reductive IDH1) from cytosolic NADPH in hypoxia (Figure 4.4B). Furthermore, significant label incorporation in mitochondrial 2HG was observed from cytosolic NADPH (Figure 4.4B) suggesting increased shuttling of cytosolic NADPH into the mitochondria. To quantify FOCM pathway activity in response to hypoxia, we cultured 143B mtIDH1-C and mtIDH2-M cells in the presence of [2,3,3-$^{2}H_3$]serine (Figure 4.4C). Strikingly, the contribution of MTHFD2 to mitochondrial NADPH increased significantly in response to hypoxia (Figure 4.4D). Only minimal oxidative MTHFD1 activity was observed in hypoxia suggesting that the pathway was operating mainly to supply mitochondrial NADPH (Figure 4.4D). Knockdown of either MTHFD1 or SHMT2 in HCT116 or A549 mtIDH2-M cell lines, respectively, resulted in a significant decrease of cytosolic NADPH contribution to the mitochondrial NADPH pool. Taken together, these results suggest that FOCM contributes a significant portion of mitochondrial NADPH under hypoxia.

Cytosolic NADPH Shuttling is Critical for Mutant IDH2 Cells

In order to understand how mitochondrial NADPH metabolism is reprogrammed in IDH2 mutant versus wild-type cells, we first engineered IDH2 wild-type HCT116 cells to express our

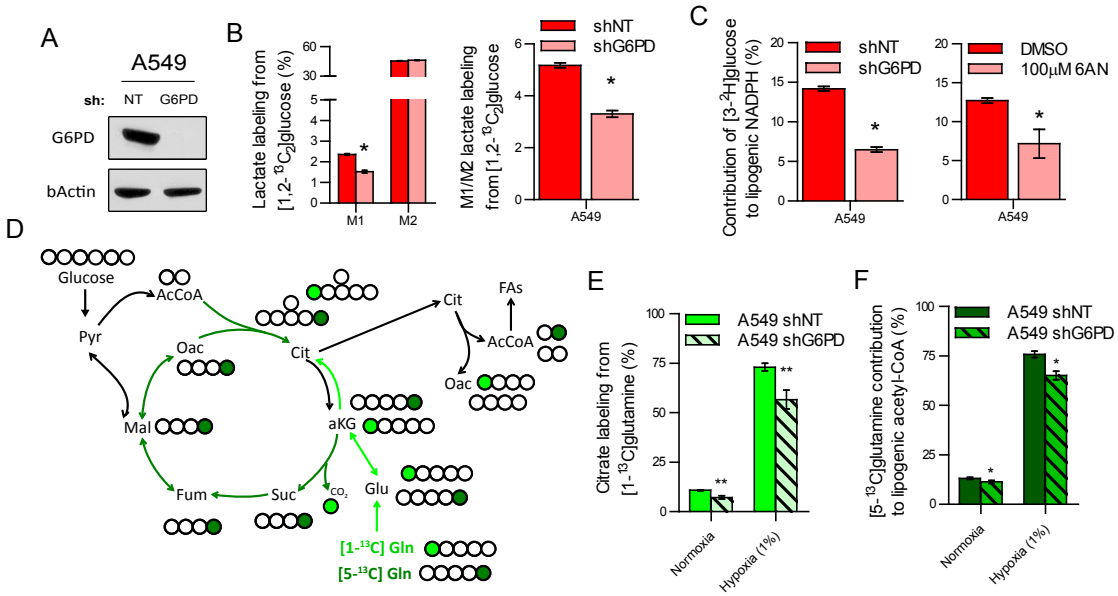

Figure 4.3: G6PD Knockdown Blunts Switch to Reductive Carboxylation Under Hypoxia. (A) Immunoblot of G6PD and βActin in A549 cells expressing control or G6PD-targeted hairpins. (B) (left) Labeling of lactate from [1,2-$^{13}C_2$]glucose in A549 shNT and shG6PD cells. (right) Ratio of M1/(M1+M2) lactate from [1,2-$^{13}C_2$]glucose. (C) (left) Contribution of [3-^{2}H]glucose to lipogenic NADPH in A549 shNT and shG6PD cells after 72 hours. (right) Contribution of [3-^{2}H]glucose to lipogenic NADPH in A549 cells treated with vehicle (DMSO) or 100 μM 6AN for 72 hours. (D) Tracer diagram depicting atom transitions for [1-^{13}C]glutamine (light green) and [5-^{13}C]glutamine (dark green). The ^{13}C label on [1-^{13}C]glutamine is retained on citrate only if glutamine is metabolized reductively as the label is lost as CO_2 via aKGDH (Figure 4.3D). In addition, the ^{13}C label on [5-^{13}C]glutamine will only label lipogenic acetyl-CoA if metabolized by reductive carboxylation. (E) Citrate labeling from [1-^{13}C]glutamine in A549 shNT and shG6PD cells cultured in normoxia or hypoxia for 72 hours. (F) Contribution of [5-^{13}C]glutamine to lipogenic acetyl-CoA via reductive carboxylation in A549 shNT and shG6PD cells cultured in normoxia or hypoxia for 72 hours.

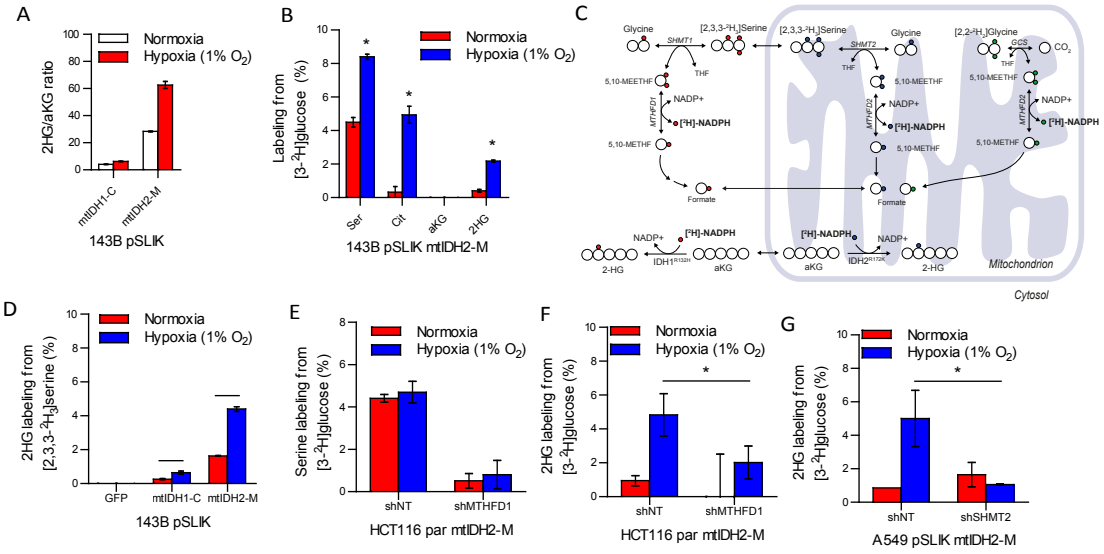

Figure 4.4: Redox Shuttling of Cytosolic NADPH into the Mitochondria. (A) 2HG/aKG ratio in 143B cells expressing either pSLIK-IDH1-R132H (mtIDH1-C) or pSLIK-IDH2-R172K (mtIDH2-M) in normoxia or hypoxia. (B) Labeling of serine, citrate, aKG, and 2HG in 143B mtIDH2-M cells cultured in the presence of [3-^{2}H]glucose in normoxia or hypoxia. (C) Tracer diagram for [2,3,3-$^2H_3$]serine depicting atom transitions through FOCM. Small blue dots represent ^{2}H atoms arising from oxidative MTHFD2 activity. Small red dots represent 2H atom-transitions arising from oxidative MTHFD1 activity. (D) 2HG labeling from [2,3,3-$^2H_3$]serine in 143B pSLIK cell lines cultured in normoxia or hypoxia for 48 hours. Dox induction (0.1 µg/mL) for 24 hours. (E) Serine labeling from [3-^{2}H]glucose in HCT116 parental mtIDH2-M cells expressing shNT or shMTHFD1 in normoxia or hypoxia for 48 hours. (F) 2HG labeling from [3-^{2}H]glucose in HCT116 parental mtIDH2-M cells expressing shNT or shMTHFD1 in normoxia or hypoxia for 48 hours. Dox induction (0.1 µg/mL) for 24 hours. (G) 2HG labeling from [3-^{2}H]glucose in A549 mtIDH2-M cells expressing shNT or shSHMT2 in normoxia or hypoxia for 48 hours. Dox induction (0.1 µg/mL) for 24 hours.

cytosolic and mitochondrial NADPH reporters discussed in Chapter 3. HCT116 parental (IDH2 wild-type cells) were engineered to express either pSLIK-IDH1-R132H or pSLIK-IDH2-R172K; hereby referred to as mtIDH1-C or mtIDH2-M (as reported in Chapter 3), respectively; and generated 2HG only in the presence of 0.1 μg/mL doxycycline (Figure 4.5A). We cultured HCT116 parental cells expressing the mtIDH2-M mitochondrial NADPH reporter and HCT116 cells engineered to express heterozygous $IDH2^{R172K/+}$ mutations (clones 59F10 and 45G9) in the presence of [3-^{2}H]glucose to quantify the contribution of cytosolic NADPH to the mitochondrial pool of NADPH. We observed that cytosolic NADPH redox shuttling accounted for approximately 3% of mitochondrial NADPH at normal oxygen tensions in both IDH2 wild-type and mutant cells; however, a significant increase in mitochondrial NADPH labeling from [3-^{2}H]glucose was observed in hypoxia (Figure 4.5B). In addition, we observed a significant increase in cytosolic NADPH contribution to mitochondrial NADPH in IDH2 mutant cells compared to wild-type cells (Figure 4.5B). These results suggest that cytosolic NADPH contributes a significant portion of mitochondrial NADPH in hypoxia and that mutant IDH2 cells rely on this redox shuttling significantly more than IDH2 wild-type cells.

To determine if FOCM activity was important in an endogenous IDH2 mutant context, we cultured SW1353 chondrosarcoma cells, which harbor a heterozygous $IDH2^{R172K/+}$ mutation, in the presence of [2,3,3-$^2H_3$]serine in normoxia and hypoxia. In addition, we knocked down the mitochondrial NAD(P)+-dependent enzyme MTHFD2 to determine if FOCM was involved in the mitochondrial NADPH labeling from [2,3,3-$^2H_3$]serine. We observed robust labeling of mitochondrial 2HG in normoxia and a significant increase in labeling under hypoxia (Figure 4.5C). Furthermore, MTHFD2 knockdown significantly blunted the labeling of mitochondrial 2HG from [2,3,3-$^2H_3$]serine (Figure 4.5C). Furthermore, MTHFD2 knockdown blunted FOCM flux as indicted by a significant decrease in M+1 serine labeling from [2,3,3-$^2H_3$]serine indicative of flux through MTHFD1/2 (Figure 4.5D).

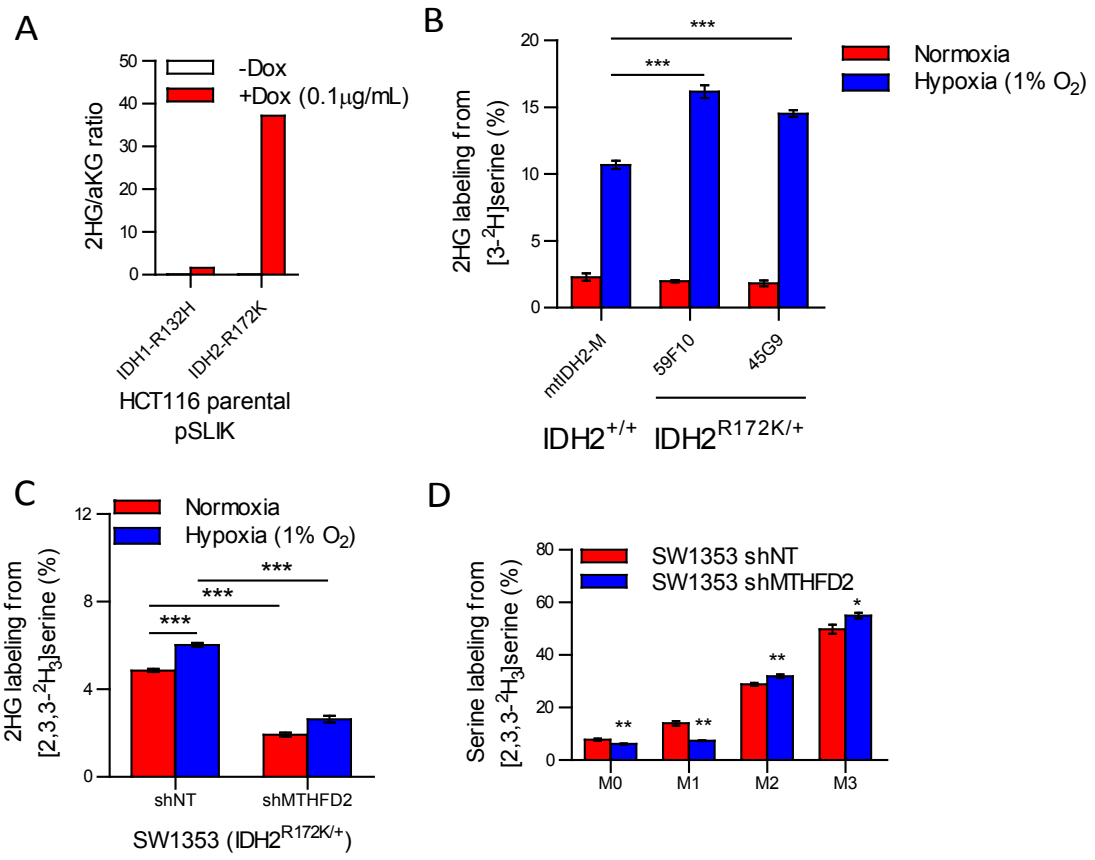

Figure 4.5: IDH2 Mutant Cells Rely More on Cytosolic Redox Shuttles to Supply Mitochondrial NADPH. (A) 2HG/aKG ratio in HCT116 parental cells expressing pSLIK-IDH1-R132H (mtIDH1-C) or pSLIK-IDH2-R172K (mtIDH2-M) treated with or without dox (0.1 μg/mL) for 72 hours. (B) 2HG labeling from [3-^{2}H]glucose in HCT116 parental mtIDH2-M cells or HCT116 IDH2$^{R172K/+}$ (clones 59F10 and 45G9) in normoxia or hypoxia for 48 hours. Dox induction (0.1 μg/mL) for 24 hours. (C) 2HG labeling in SW1353 shNT or shMTHFD2 cells cultured in presence of [2,3,3-^{2}H$_3$]serine in normoxia or hypoxia for 48 hours. (D) Serine labeling in SW1353 shNT or shMTHFD2 cells cultured in presence of [2,3,3-^{2}H$_3$]serine in normoxia or hypoxia for 48 hours.

Discussion

Adaptation to hypoxia is critical in order for cancer to survive during progression. Many of the metabolic responses to hypoxia are controlled by HIF-1 signaling which facilitates the switch to aerobic glycolysis by activating transcription of glucose transporters and several glycolytic enzymes. Here we show reprogramming of cytosolic NADPH and NADH metabolism in response to hypoxic microenvironments. We observed a significant increase in the reliance on the oxidative PPP pathway to supply cytosolic NADPH under hypoxia. In addition, the relative shunting of glycolytic carbon through the oxPPP was not significantly affected; however, molar glucose flux and lactate secretion are significantly increased in hypoxia suggesting that absolute NADPH production flux is increased and, thus, the demand for NADPH in hypoxia. Fatty acid synthesis, one of the major NADPH consuming pathways in the cell (Fan et al., 2014), is significantly decreased in hypoxia suggesting that other NADPH consumption pathways, including reactive oxygen species defense, may be driving the increased NADPH demand in hypoxia.

In addition to increased aerobic glycolysis, glutamine metabolism is reprogrammed in hypoxic environments routing flux reductively to form citrate necessary for maintaining *de novo* lipogenesis (Metallo et al., 2012). The switch to reductive glutamine metabolism has also been shown to activate in conditions of anchorage-independence (Jiang et al., 2016). Jiang et al. demonstrated that reductive carboxylation occurred in an IDH1-dependent manner and counteracted the substantial increase in mitochondrial ROS in anchorage independent conditions. This study and others have suggested that reductive carboxylation can act to shuttle cytosolic reducing equivalents into the mitochondria to support redox homeostasis through mitochondrial glutathione and thioredoxin regeneration; however, the role of mitochondrial NADPH has not been fully elucidated (Wallace, 2012; Wallace and Fan, 2010; Wallace et al., 2010). Our results suggest that reductive carboxylation occurs in the cytosol and blunting cytosolic NADPH production by the oxPPP compromises the switch in hypoxia. Furthermore, we observe transfer of cytosolic reducing equivalents into the mitochondria under hypoxia suggesting this pathway is important for supplying mitochondrial NADPH in addition to facilitating fatty acid synthesis. Serine and glycine metabolism have been proposed to form a redox cycle similar to reductive

carboxylation (Tibbetts and Appling, 2010; Fan et al., 2014; Lewis et al., 2014). We have observed labeling from cytosolic NADPH on citrate (via RC) and on serine (via reductive MTHFD1 activity) in hypoxia, suggesting that both of these pathways are active in hypoxia and could be responsible for supplying mitochondrial reducing equivalents that we observe.

For cancer cells that have a deficiency in one or many of these redox shuttles, such as the inability to switch to reductive carboxylation in IDH1 mutant cells or the increased reliance on FOCM in IDH2 mutant cells, inhibiting one or many of these pathways may selectively sensitize IDH mutant cancer cells to redox stress or conditions that promote ROS (*i.e.* hypoxia, anchorage-independence). The studies presented herein do not explore possible synthetic lethality, but the increased reliance of IDH2 mutants on FOCM for mitochondrial NADPH suggests that these cells may be selectively sensitive to inhibitors of FOCM. Unfortunately, no publically available inhibitors of MTHFD or SHMT exist; however, several are currently in development. Knockdown of SHMT2 has been shown to increase mitochondrial ROS and cause cell death in cancer cells under hypoxia supporting the notion that this pathway is critical for mitochondrial redox homeostasis and a viable therapeutic target (Ye et al., 2014).

Materials and Methods

Cell Culture

A549 and 143B cell lines were cultured in DMEM supplemented with 10% FBS and 1% Pen Strep. HCT116 isogenic clones were obtained from Horizon Discovery Ltd. Cells were routinely cultured in normoxia (21% O_2) and then moved to a Coy hypoxia chamber (1% O_2) for 48 to 72 hours.

Steady-state labeling of intracellular metabolites was achieved by culturing subconfluent cells in triplicate for 48-72 hours as indicated. Glucose- and glutamine- free DMEM containing 10% dialyzed FBS and 1% Pen Strep and 20 mM of either [1,2-$^{13}C_2$]glucose, [3-^{2}H]glucose, [4-^{2}H]glucose and 4mM unlabeled glutamine or 20 mM unlabeled glucose and 4mM of either [U-$^{13}C_5$]glutamine, [1-^{13}C]glutamine, or [5-^{13}C]glutamine. Extraction of intracellular metabolites and GC-MS analysis of labeled species was conducted using protocols presented in Chapter 2

and Chapter 3.

Reagents

[1,2-$^{13}C_2$]glucose, [U-$^{13}C_5$]glutamine, [1-^{13}C]glutamine, and [5-^{13}C]glutamine were acquired from Cambridge Isotope Laboratories. [3-^{2}H]glucose and [4-^{2}H]glucose were acquired from Omicron Biochemicals.

Isotopomer Spectral Analysis (ISA)

A model for palmitate biosynthesis, whereby eight acetyl-CoA molecules are consumed to form one palmitate molecule, was generated to estimate the rate of *de novo* synthesis from experimental palmitate mass isotopomer distributions. Parameters for the relative enrichment of lipogenic acetyl-CoA from a given ^{13}C tracer and the percentage of fatty acids that are *de novo* synthesized are extracted from a best-fit model using the INCA MFA software package (Young, 2014). The 95% confidence intervals for both parameters were estimated by sensitivity analysis of the sum of squared residuals between measured and simulated palmitate mass isotopomer distributions to small flux variations (Antoniewicz et al., 2006).

Production of Stable Knockdown Transformed Cells

Lentival shRNA plasmids targeting human SHMT2 (NM 005412.4—541s21c1: CCGGGTCTGACGTCAAGCGGATATCCTCGAGGATATCCGCTTGACGTCAGACTTTTTG), MTHFD1 (NM 005956.2—2559s1c1: CCGGGCAGATGACATTGAATTACTTCTCGAGAAGTAATTCAATGTCATCTGCTTTTTG), or MTHFD2 (NM 006636.2—772s1c1: CCGGGCAGTTGAAGAAACATACAATCTCGAGATTGTATGTTTCTTCAACTGCTTTTTG) or a non-targeting control construct were packaged in 293FT cells using FuGENE 6 as a transfection agent for the desired pLKO vector and VSV-G, gag/pol, and rev. The 293FT spent medium containing the lentiviral constructs was collected and filtered (0.45 μm) to remove any cells. Polybrene was added to a final concentration of 8 μg/ml. Cells in 6-well plates were cultured with 0.5 ml of the virus-containing medium for 4-6 hours before addition

of 2 ml of virus free medium. Cells were then selected and maintained in media containing 2 μg/ml puromycin.

Statistical Analysis

All results shown as averages of multiple technical replicates are presented as mean ± SD. P-values were calculated using a Student's two-tailed t test. * p-value between 0.05 and 0.01, ** p-value between 0.01 and 0.001, *** p-value < 0.001. All errors associated with ISA of de novo lipogenesis are 95% confidence intervals determined by sensitivity analysis.

Acknowledgements

Chapter 4 contains material generated by Seth J. Parker.

Chapter 5

Conclusions

The works presented in this dissertation highlight the influence of subcellular compartmentalization of metabolic processes and the impact of specific mutations and/or microenvironments on intermediary metabolism. Specifically, this dissertation focuses on metabolic reprogramming in hypoxic microenvironments and how mutations in isocitrate dehydrogenase (IDH) affect metabolic flux in response to stress.

The first chapter, "Metabolic Consequences of Oncogenic IDH Mutations", examines the molecular signaling and metabolic impacts of oncogenic mutations in a compartmentalized TCA cycle enzyme present in the cytosol or mitochondria. IDH mutations are particularly interesting as they represent one of only a few metabolic enzymes that are found to be mutated in cancer, others including succinate dehydrogenase (SDH) and fumarate hydratase (FH). Mainly, groups have focused on elucidating the impacts of 2-hydroxyglutarate (2HG)—a metabolic byproduct of IDH mutation—on signaling pathways, on how IDH mutation impacts cellular metabolism, and on the oncogenic development of tumors harboring these mutations. This chapter reviews some of these efforts and highlights the need for improved preclinical models and studies that identify exploitable metabolic and signaling defects in cancers that harbor IDH mutation.

The second chapter, "IDH1 Mutations Alter Citric Acid Cycle Metabolism and Increase Dependence on Oxidative Mitochondrial Metabolism", focuses on metabolic studies using ^{13}C stable isotope tracing and metabolic flux analysis to examine alterations in central carbon metabolism in mutant IDH cancer cells. These studies were done using a cell model engineered to express heterozygous IDH1 (IDH1-R132H/C) or IDH2 (IDH2- R140Q, R172K) mutation and

were also replicated in several cell models harboring endogenous IDH mutations. Surprisingly, there were only minor differences between IDH mutant and wild-type cells in flux through central carbon metabolism in basal conditions; however, when cells were cultured under low oxygen environments, a significant defect in mitochondrial metabolism in IDH1 mutant cells was observed. Mutant cells relied more on oxidative mitochondrial metabolism and were incapable of switching to reductive glutamine metabolism in hypoxic microenvironments, sensitizing cells to inhibitors of the electron transport chain (ETC). This metabolic deficiency was observed in additional cell models and also in vivo. Future work into effective dosing of mitochondrial inhibitors in vivo and possible synergistic co-treatments is needed in order to validate this proof of principle therapeutic target for treating mutant IDH1 cancers.

The third chapter, "Tracing Compartmentalized NADPH Metabolism in the Cytosol and Mitochondria of Mammalian Cells", discusses the use of a stable isotope tracing methodology to understand compartmentalized NADH and NADPH metabolism in intact cells. Importantly, NAD(H) and NADP(H) cannot cross intracellular membranes and cells maintain distinct ratios of NAD(P)+/NAD(P)H to execute compartment-specific metabolic processes. Previous techniques to measure NAD(P)H suffer from several technical limitations, including mixing organelle pools and long sample preparation time; therefore, this chapter discusses the use of reductive biosynthesis as a readout of NADPH metabolism that circumvents these limitations. Furthermore, this chapter discusses the development of NADPH reporters capable of tracing redox metabolism in specific compartments (*i.e.* the cytosol and mitochondria of cells) to observe the activity of complex, multi-compartment pathways in greater detail. Finally, the chapter highlights the utility of this technique by applying it to resolve the directionality of folate-mediated one carbon metabolism, which involves multistep, compartmentalized redox reactions existing in both the cytosol and mitochondria. Future work into developing reporters for other subcellular compartments, including the endoplasmic reticulum and nucleus, would be beneficial as metabolism in these organelles becomes more appreciated.

The fourth chapter, "Hypoxic Reprogramming of NADPH Metabolism in Mutant IDH2 Cells", investigates the impact of hypoxia and IDH2 mutations on cytosolic and mitochondrial NADPH metabolism. Several metabolic pathways, including folate-mediated one carbon

metabolism and reductive carboxylation, have been proposed to operate as a cycle shuttling reducing equivalents between the cytosol and mitochondria. Studies have shown cytosolic NADPH to shuttle into the mitochondria via reductive carboxylation in cells under conditions of anchorage-independence. Reductive carboxylation can also support *de novo* lipogenesis, and this chapter explores the compartmentalization of RC and how it can shuttle cytosolic NADPH to combat the increased redox stress experienced by cells under hypoxia. In addition, this chapter describes how inactivating mutations in IDH2, which eliminate the capacity of reductive carboxylation to facilitate reducing equivalent shuttling, results in a greater contribution of mitochondrial NADPH to come from FOCM shuttling. Future work investigating potential increased sensitivity of FOCM inhibitors in mutant IDH2 cells is needed in order to validate this pathway as therapeutically efficacious.

Supplement to Chapter 1

Abbreviations

ACC: acetyl-CoA carboxylase, ACO: aconitase, AML: acute myeloid leukemia, αKG: alpha-ketoglutarate, D-2HG: D-2-hydroxyglutarate, FAS: fatty acid synthase, Fum: fumarate, FH: fumarate hydratase, ICT: isocitrate, IDH: isocitrate dehydrogenase, L-2HG: L-2-hydroxyglutarate, LDH: lactate dehydrogenase, Mal: malate, Oac: oxaloacetate, Pyr: pyruvate, PC: pyruvate carboxylase, PDH: pyruvate dehydrogenase, SDH: succinate dehydrogenase.

Supplement to Chapter 2

Abbreviations

IDH, isocitrate dehydrogenase; 2-HG, 2-hydroxyglutarate; MFA, metabolic flux analysis; αKG, α-ketoglutarate; EMT, epithelial-mesenchymal transition; HIF-1α, hypoxia inducible factor 1α; WT, wild-type; ISA, isotopomer spectral analysis; AcCoA, acetyl coenzyme A; PPP, pentose phosphate pathway; TCA, the citric acid cycle; PDH, pyruvate dehydrogenase; ME, malic enzyme; PC, pyruvate carboxylase; OXPHOS, oxidative phosphorylation; ETC, electron transport chain.

Materials and Methods

Extracellular Flux Determination

Cells were seeded in triplicate at a density of 150,000 or 250,000 cells/well. After 72 hours, cells were counted by hemacytometer and conditioned medium was collected by centrifugation. Glucose and lactate concentrations were measured in fresh and spent medium (after 24-72 hours of culture) using a NOVA Biomedical BioProfile FLEX Analyzer or a Yellow Springs Instruments (YSI) 7100. Concentrations of glutamine, glutamate, 2-hydroxyglutarate, pyruvate, and alanine in fresh and spent medium were determined by GC-MS analysis of corresponding methoxime-tBDMS derivatives. Briefly, 25 μl of fresh and conditioned medium was extracted in 200 μl of cold 80% methanol (-80°C) containing 1 μg norvaline to serve as an internal standard. Concentrations were determined by comparing total ion counts to a calibration curve generated in parallel. The cell specific growth rate (μ) was measured assuming exponential growth and

uptake/secretion fluxes (q_i) for each of the aforementioned metabolites were quantified using the following equations (S2.1-S2.3):

$$\frac{dX}{dt} = \mu X \tag{S2.1}$$

$$\frac{dC_i}{dt} = q_i X_o e^{\mu t} \tag{S2.2}$$

$$\frac{dC_{Gln}}{dt} = -k_{Gln} C_{Gln} + q_{Gln} X_o e^{\mu t} \tag{S2.3}$$

Where C_i and X represent the concentration of the ith metabolite and the cell density, respectively. The spontaneous first-order degradation of glutamine to ammonia and pyrrolidonecarboxylic acid was estimated to be 0.002 h^{-1} and included in the calculation of the cellular uptake flux of glutamine (Ozturk and Palsson, 1990; Ahn and Antoniewicz, 2011).

Gas Chromatography Mass Spectrometry (GC-MS) Analysis

Extracted polar metabolites were derivatized to form methoxime-tBDMS derivatives by first dissolving the evaporated samples in 20 µl of 2% (w/v) methoxylamine hydrochloride (MP Biomedicals, Solon, OH) in pyridine and incubating at 37°C for 60-90 minutes. Samples were then silylated by addition of 30 µl of N-tert-butyldimethylsily-N-methyltrifluoroacetamide (MTB-STFA) with 1% tert-butyldimethylchlorosilane (tBDMS) (Regis Technologies, Morton Grove, IL) and incubated at 37°C for 30-45 minutes. Samples were centrifuged at 14,000 rpm for 5-15 minutes and clarified supernatant was transferred to GC sample vials for analysis. Extracted nonpolar metabolites were esterified to form fatty acid methyl esters (FAMEs) by adding 500 µl of 2% (w/v) H_2SO_4 in methanol and incubating at 50°C for 90-120 minutes. The reactions were quenched with 100 µl of saturated NaCl solution and FAMEs were extracted with two

hexane washes. Extracted hexanes were evaporated to dryness at room temperature, dissolved in 50-100 µl of hexane, and transferred to glass GC vials for analysis. Derivatized samples were analyzed by GC-MS using a DB-35MS (30m x 0.25mm i.d. x 0.25µm, Agilent JW Scientific) installed in an Agilent 7890A gas chromatograph (GC) interfaced with an Agilent 5975C mass spectrometer (MS) operating in electron impact mode scanning over the range 100-650 m/z for methoxime-tBDMS derivatives and 100-350 m/z for FAMEs. The GC oven temperature methods for methoxime-tBDMS and FAME derivatives were run as previously described (Metallo et al., 2012).

Metabolic Flux Analysis (MFA)

Table S2.1: Metabolite Fragment Ions Used for GC-MS Analysis. Carbons represented, chemical formula, and m/z for each metabolite included in Chapter 2.

Metabolite	Carbons	Formula	Mass (m/z)
Pyruvate	123	$C_6H_{12}O_3NSi$	174
Lactate	23	$C_{10}H_{25}O_2Si_2$	233
Lactate	123	$C_{11}H_{25}O_3Si_2$	261
Citrate	123456	$C_{20}H_{39}O_6Si_3$	459
Citrate	123456	$C_{26}H_{55}O_7Si_4$	591
aKG	12345	$C_{14}H_{28}O_5NSi_2$	346
Succinate	1234	$C_{12}H_{25}O_4Si_2$	289
Fumarate	1234	$C_{12}H_{23}O_4Si_2$	287
Malate	1234	$C_{18}H_{39}O_5Si_3$	419
Alanine	23	$C_{10}H_{26}ONSi_2$	232
Alanine	123	$C_{11}H_{26}O_2NSi_2$	260
Aspartate	12	$C_{14}H_{32}O_2NSi_2$	302
Aspartate	234	$C_{17}H_{40}O_3NSi_3$	390
Aspartate	1234	$C_{18}H_{40}O_4NSi_3$	418
Glutamate	12345	$C_{17}H_{36}O_2NSi_2$	330
Glutamate	12345	$C_{19}H_{42}O_4NSi_3$	432
Glutamine	12345	$C_{19}H_{43}O_3N_2Si_3$	431
2-HG	12345	$C_{19}H_{41}O_5Si_3$	433
Palmitate	1-16	$C_{17}H_{34}O_2$	270

^{13}C metabolic flux analysis was conducted under the following assumptions:

1. Cells were assumed to be at metabolic and isotopic steady state, *i.e.* intracellular free metabolite pool size and ^{13}C enrichments are constant.

2. Per cell extracellular flux of glucose, lactate, glutamine, glutamate, pyruvate, 2-HG, and

alanine were assumed to be constant over the course of the labeling experiment.

3. Cells were assumed to grow exponentially.

4. Succinate and fumarate are structurally symmetric and can be enzymatically converted to their subsequent products in either configuration.

5. Labeled CO_2 released during decarboxylation reactions is diluted upon release and does not reincorporate during carboxylation reactions.

6. Separate mitochondrial and cytosolic pools of aspartate, malate, fumarate, pyruvate, and acetyl-CoA were modeled with exchange fluxes for malate and pyruvate. The pool of succinate was comprised of an unlabeled dilution pool and a metabolically active pool (Noguchi et al., 2009).

7. Malic enzyme flux was assumed to be primarily mitochondrial, as minimal labeled lactate was detected from [U-$^{13}C_5$]glutamine. Alanine exhibited more significant label from [U-$^{13}C_5$]glutamine and the mitochondrial flux enabled us to address this discrepancy.

8. The extracellular flux of 2-HG was calculated assuming that all 2-HG produced by the cell is secreted.

9. Relative branching of glucose flux to the oxidative pentose phosphate pathway (PPP) relative to glycolysis was determined via the M1/M2 lactate ratio in HCT116 parental and IDH1 R132H/+ (2H1 clone) cells cultured in either normoxia or hypoxia with [1,2-$^{13}C_2$]glucose.

Abbreviations used in Tables S2.2-S2.5

2-HG, 2-hydroxyglutarate; 2-HG.x, 2-hydroxyglutarate secretion; 3PG, 3-phosphoglycerate; AcCoA.m, mitochondrial acetyl-coenzyme A; AcCoA.c, cytosolic acetyl-coenzyme A; aKG, α-ketoglutarate; Ala, alanine; Ala.x, alanine secretion; Asp.c, cytosolic aspartate; Asp.m, mitochondrial aspartate; Cit, citrate; CO2, carbon dioxide; DHAP, dihydroxyacetone phosphate; E4P, erythrose 4-phosphate; F6P, fructose 6-phopsphate;

Fum.c, cytosolic fumarate; Fum.m, mitochondrial fumarate; G6P, glucose 6-phosphate; GAP, glyceraldehyde 3-phosphate; Glc.x, glucose uptake; Gln, glutamine; Gln.x, glutamine uptake; Glu, glutamate; Glu.x, glutamate secretion; Lac, lactate; Lac.x, lactate secretion; Mal.c, cytosolic malate; Mal.m, mitochondrial malate; P5P, ribose 5-phosphate; Palm.d, dilution/already present Palmitate; Palm.s, de novo synthesized Palmitate; Pyr.c, cytosolic pyruvate; Pyr.m, mitochondrial pyruvate; Pyr.x, pyruvate secretion; S7P, sedoheptulose 7-phosphate; Suc, succinate; Suc.d, succinate dilution.

Determination of Oxygen Consumption

HCT 116 cells were grown at either normoxia or hypoxia (3% O2) and respiration was measured under these conditions using an XF^{e}96 analyzer (Seahorse Bioscience). All cell growth and assays at 3% O2 were conducted using the Coy Dual Hypoxic Chambers for Seahorse XF^e Analyzer (Coy Laboratory Products, Inc.). See set-up pictured below (Figure S2.1):

Figure S2.1: Coy Dual Hypoxic Chambers for Seahorse XF^e Analyzer.

Parental cells or IDH1 mutant cells were maintained in DMEM + 10% (v/v) fetal bovine serum + 2 mM GlutaMAX + 100U/mL penicillin, and 100μg/mL streptomycin and plated in 96-well XF assay plates subsequently kept at normoxia (parental—1.75x10^4 cells/well; IDH1 mutants—2.0x10^4 cells/well) or hypoxia (parental—1.25x10^4 cells/well; IDH1 mutants—1.5x10^4 cells/well). After two days, medium was changed to DMEM supplemented with 10 mM glucose, 4 mM glutamine, and 1.5 mM pyruvate prior to conducting the assay.

Respiration under hypoxia was measured using Wave 2.0 software with the XF^{e}96 in

Hypoxia Mode and the oxygen tension set to 3%. 250 mM sodium sulfite was added during the course of the experiment to provide a zero-point calibration of the system. Medium was buffered with 44 mM $NaHCO_3$, as the hypoxia chamber enclosing the instrument contained 5% CO_2. Respiration data under normoxia was obtained both on the benchtop (medium buffered with 10 mM HEPES) and in the Coy chamber, with bicarbonate-buffered medium and the oxygen tension set to 20.7% O2. The respiration data collected in the chamber and on the benchtop showed no qualitative difference, so the values were pooled for analysis. Five independent, biological replicates were conducted with 10 technical replicates per cell line. Immediately after the assay, total cell protein was calculated by lysing cells in 20μL/well RIPA buffer and protein was calculated using the bicinconinic acid (BCA) assay. All oxygen consumption values were normalized to microgram of total cell protein.

ATP-linked respiration was determined by the amount of oxygen consumption sensitive to 2μg/mL oligomycin. Maximal respiration was determined under normoxia as the amount of respiration stimulated by the protonophore FCCP (added in subsequent injections for final concentrations of 500 nM and 750 nM in the medium). Non-mitochondrial respiration was determined by shutting down mitochondrial electron transport with 2 μM rotenone and 1 μM antimycin A. The ratio of maximal respiration to ATP-linked respiration (*i.e.* the respiratory capacity) was also determined. Uncoupler-stimulated respiration was not calculated under 3% O2 because the well reached anoxia during the measurement phase.

Statistical analysis was conducted on the raw data by analysis of variance (ANOVA) of repeated measurements with Dunnett's post-hoc test ($p<0.05$). All respiration data are presented as mean ± S.E.M.

Biomass Equation

In order to quantify the per cell dry weight, 18-20 million HCT116 cells were pelleted by centrifugation and washed three times with cold acetone (-80°C) to remove free metabolites. Cell pellets were then evaporated to dryness overnight and weighed. The dry weight per cell was estimated to be approximately 400 pg. The dry cell mass composition (in %w/w) was estimated from the literature for hybridomas (Quek et al., 2010; Sheikh et al., 2005) and the stoichiometric

coefficients (in fmol/cell) were determined by multiplying the biomass composition by the per cell dry weight (Murphy et al., 2013).

RNA Interference and LC-MS Analysis of Citrate

IDH1/2 shRNAs were generated in pLKO-based lentiviral vectors containing a tetracycline-inducible promoter as described previously (Grassian et al., 2012). The targeting sequences for the IDH1/2 shRNAs were as follows: IDH1 shRNA A, GGAATC-CGGAATAAATACTAC; IDH1 shRNA B, GCCTGGCCTGAATATTATACT; IDH2 shRNA A, GTGGACATCCAGCTAAAGTAT; IDH2 shRNA B, CACCATACTGAAAGCCTACGA. The indicated cells lines were transduced with these shRNAs or a nontargeting control (NTC). After viral transduction, 0.6 μg/ml puromycin was added to select for polyclonal pools of cells with stable integration of the shRNA constructs. For all experiments, cells were grown in the presence of 100 ng/ml doxycycline where noted for the indicated number of days to induce shRNA expression. Quantitative PCR (qPCR) was performed as previously described (Grassian et al., 2012).

HCT116 Parental cells with NTC or IDH1/2 shRNA were cultured in glutamine free DMEM media supplemented with [U-$^{13}C_5$]glutamine under normoxia and hypoxia (1% oxygen). Cell pellets were lysed in 80% methanol in water (4:1 v/v) via 3 cycles of freeze-thawing in liquid nitrogen. Supernatants of the cell extracts were dried down and reconstituted in water for LC-MS/MS analysis. Citrate ^{13}C-labelled isotopologues were quantified using LC-MS/MS with an API4000 triple quadruple MS system (AB Sciex, Framingham, MA). Analytes of interests were individually tuned and the most sensitive MRM was selected for quantification. Citrate was separated on Phenomenex Luna PFP 2x150mmc column, 3μm particle size with 0.1% formic acid in water as mobile phase A (MPA) and 0.1% formic acid in acetonitrile as mobile phase B in a 7 minute gradient from 100% MPA to 90% MPA. The retention times were verified using authentic standards. Contributions from natural isotope distribution and mass spec cross-talk from isotopologues that are within 2 Da have been corrected for the data presentation.

Generation of ρ^0 Cells

To generate ρ^0 cells, cells were grown in DMEM with 10% fetal bovine serum, 100ïĄŋμ/ml uridine, 1mM sodium pyruvate and 50 ng/ml ethidium bromide for 4-6 weeks. To ensure inactivation of mitochondrial DNA, cells were cultured in DMEM without glucose, with 10% dialyzed fetal bovine serum and 25mM galactose; no surviving cells after 48 hours confirmed the of inactivation of mitochondrial DNA.

Growth-inhibition Assay

Cells (HT-1080 or SW1353) were plated at 3000 or 6000 cells per well in a 96-well plate. Each 96-well plate contained six replicates of treatment concentration gradient, vehicle control, and background control. Cells were allowed to attach overnight and phenformin- (Fluka) or vehicle- (DMSO, Sigma) containing media was added after approximately 16 hours. Following 48 hour incubation, media was removed and cells were fixed with ice-cold 4% paraformaldehyde (Electron Microscopy Sciences) in PBS for 15 minutes at room temperature. Then, 0.9% (w/v) crystal violet (Sigma) in water was added to each well and incubated for 8-10 minutes at room temperature. Crystal violet solution was removed and plates were washed and allowed to dry overnight. Absorbed dye was dissolved in a 4:1:1 ethanol:methanol:water mixture and the absorbance was measured at a fixed wavelength of 595 nm. Measured absorbance was background-corrected and normalized to vehicle control.

Xenograft Studies

Cells tested were free of mycoplasma and viral contamination in the IMPACT 1 PCR assay panel (RADIL, MU Research Animal Diagnostic Laboratory, Columbia, MO). For xenograft growth analysis, $2x10^6$ cells were injected subcutaneously in a suspension in PBS (cat. 17-516F, Lonza) solution. The total injection volume containing cells in suspension was 200 μl. For cell implantation, mice were anesthetized with continuous flow of 1.5-3.5% isoflurane/oxygen mixture using the integrated multi chambers anesthesia center (IMCAC) and induction chamber (Vetequip, Inc. Pleasanton, CA). Animal well-being and behavior, including grooming and

ambulation were monitored twice daily. Individual tumor volumes were measured twice a week by manual calipers and data collected in the Abivo data capture package. Tumor volumes were calculated as (length x width^2) x $\pi/6$. Individual body weights (BW) were measured twice a week. The percent change in BW was calculated as ($BW_{current}$-$BW_{initial}$)/$BW_{initial}$ x100.

For *in vivo* glutamine infusion studies, Parental HCT116, HCT116 IDH1 R132H/+ 2H1, or HCT116 IDH1 R132C/+ 2A9 cells were suspended in sterile PBS, and injected at 5 ÃŮ 10^6, 5 x 10^6, or 10 x 10^6 cells, respectively, into the flanks of nu/nu mice. Tumor growth was monitored by caliper measurement in two dimensions and tumor volume was estimated by the equation V $= (\pi/6)(L*W^2)$. Mice were prepared for glutamine infusions when tumors reached a minimum diameter of 0.8cm. Chronic venous catheters were implanted into the jugular vein of animals with xenograft tumors 5-7 days before performing glutamine infusion experiments. After surgical recovery, mice were fasted overnight before [1-^{13}C]glutamine was reconstituted in saline and infused into conscious mice for 360 min following a bolus to achieve steady-state enrichments, as previously reported (Marin-Valencia et al., 2012). Next, mice were anesthetized with sodium pentobarbital injection and tissue harvested within 5 minutes, snap frozen in liquid nitrogen using Biosqueezer (BioSpec Products), and stored at -80°C for subsequent analysis and metabolite extraction. All animal procedures followed protocols approved by MIT's Committee on Animal Care. Data are expressed at means $\pm$ S.E.M. Metabolites were extracted by finely grinding tissue at liquid nitrogen temperatures using a Retsch Cryomill. Tissues were resuspended in 3:1:2 methanol, water, chloroform and phase extracted. Polar metabolites were dried under nitrogen gas and frozen at -80°C for subsequent derivitization and analysis by gas-chromatography mass-spectrometry.

Synthesis of IDH1i A

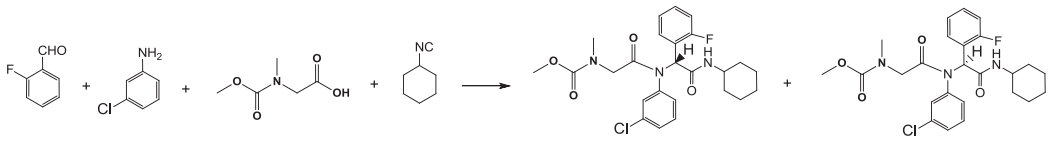

Figure S2.2: Chemical Synthesis Scheme for IDH1i A.

A mixture of 2-fluorobenzaldehyde (250 mg, 2.014 mmol) and 3-chloro aniline (257 mg, 2.014 mmol) was stirred at room temperature in a 50 mL reaction tube for 30 minutes. The resulting beige solid was dissolved by the addition of toluene (8 ml) and warming at 60°C. 2-(methoxycarbonyl(methyl)amino)-acetic acid (296 mg, 2.014 mmol) and cyclohexylisocyanide (0.250 ml, 2.014 mmol) were added and the reaction stirred at 60°C for 20 hours. The resulting amber solution was cool to room temperature and poured into water. The aqueous mixture was extracted with CH_2Cl_2 and organic layer was washed with brine, dried over $MgSO_4$ and concentrated under reduced pressure to give a brown oil. The crude material was purified via HPLC (Sunfire Prep C18 column, OBO 5µm, 19x100 mm, 10-80% acetonitrile/water gradient over 15 min) to give methyl (2-((3-chlorophenyl)(2-(cyclohexylamino)-1-(2-fluorophenyl)-2-oxoethyl)amino)-2-oxoethyl)(methyl)carbamate as a white solid (110 mg). The enantiomers of this compound were separated via chiral HPLC (Chirapak IA column, 5µm particle size, 20x250 mm, 20% MeOH + 5mM NH_4OH in CO_2) To give the individual enantiomers:

(R)-methyl(2-((3-chlorophenyl)(2-(cyclohexylamino)-1-(2-fluorophenyl)-2-oxoethyl)amino)-2-oxoethyl)(methyl)carbamate: 25 mg, white solid, HPLC (chiral prep) t_R = 1.85 min (λ = 220 nm). This compound was presumed to be the (R) enantiomer based on a comparison of the biochemical activity versus the enantiomer below and comparison of these results to the results of an analogous set of compounds prepared in a chirally specific manner. This enantiomer is less active than the (S) enantiomer, and was not used for these studies.

(S)-methyl(2-((3-chlorophenyl)(2-(cyclohexylamino)-1-(2-fluorophenyl)-2-

oxoethyl)amino)-2-oxoethyl)(methyl)carbamate: 17 mg, , white solid, HPLC (chiral prep) t_R = 2.65 min (λ = 220 nm). ^{1}H NMR (400 MHz, CD_2Cl_2) (mixture of rotamers) δ 7.12-7.33 (m, 4H), 6.88-7.12 (m, 4H), 6.37 (s, 0.6H), 6.34 (s, 0.4H), 6.18 (d, J = 7.53 Hz, 0.6H), 5.72 (d, J = 7.53 Hz, 0.4H), 3.68-3.96 (m, 3H), 3.70 (s, 2H), 3.63 (s, 1H), 2.92 (s, 2H), 2.89 (s, 1H), 1.84-2.12 (m, 2H), 1.58-1.84 (m, 4H), 1.05-1.46 (m, 4H); ^{13}C NMR (101 MHz, CD_2Cl_2) major rotamer δ 169.19, 167.67, 161.41 (d, J = 247 Hz), 157.70, 140.13, 134.73, 132.26 (d, J = 3 Hz), 131.16 (d, J = 8 Hz), 130.48, 129.15, 129.18, 128.73, 124.36 (d, J = 3 Hz), 122.10 (d, J = 14 Hz), 115.59 (d, J = 22 Hz), 58.68, 53.15, 52.40, 49.37, 35.99, 33.10 (2C), 25.95, 25.41, 25.30, minor rotamer δ 169.00, 167.83, 161.35 (d, J = 247 Hz), 157.07, 139.93, 134.73, 131.89 (d, J = 3 Hz), 131.25 (d, J = 8 Hz), 130.48, 129.15, 129.18, 128.73, 124.54 (d, J = 3 Hz), 121.81 (d, J = 13 Hz), 115.67 (d, J = 21 Hz), 58.32, 52.96, 51.76, 49.30, 36.14, 33.18 (2C), 25.87, 25.25, 25.16; HRMS (ESI-MS) m/z calcd for C25H29ClFN3O4 [M + H]+ 490.1909, found 490.1884; HPLC t_R = 2.70 min. This compound was presumed to be the (S) enantiomer based on a comparison of the biochemical activity versus the enantiomer below and comparison of these results to the results of an analogous set of compounds prepared in a chirally specific manner. For the studies presented in this paper, only the (S) enantiomer was used. Biochemical assays using IDH1i A were performed as previously described in Patent WO2013046136 A1.

Supplemental Figures and Tables

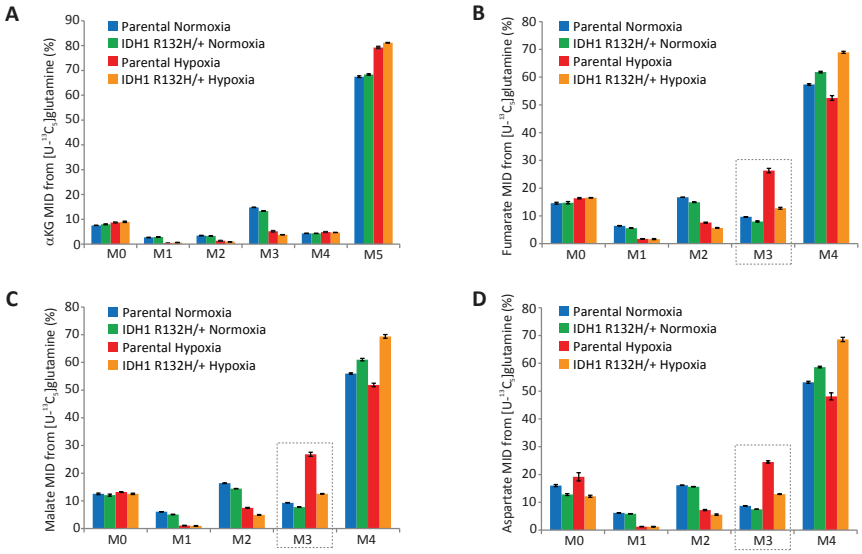

Figure S2.3: Isogenic IDH1 Mutation Compromises Metabolic Reprogramming Under Hypoxia. (A, B, C and D) α-Ketoglutarate (A), Fumarate (B), Malate (C) and Aspartate (D) MIDS labeling from [U-$^{13}C_5$]glutamine for HCT116 Parental and HCT116 IDH1 R132H/+ clone 2H1 cells cultured in normoxia or hypoxia (2% oxygen) for 72 hours.

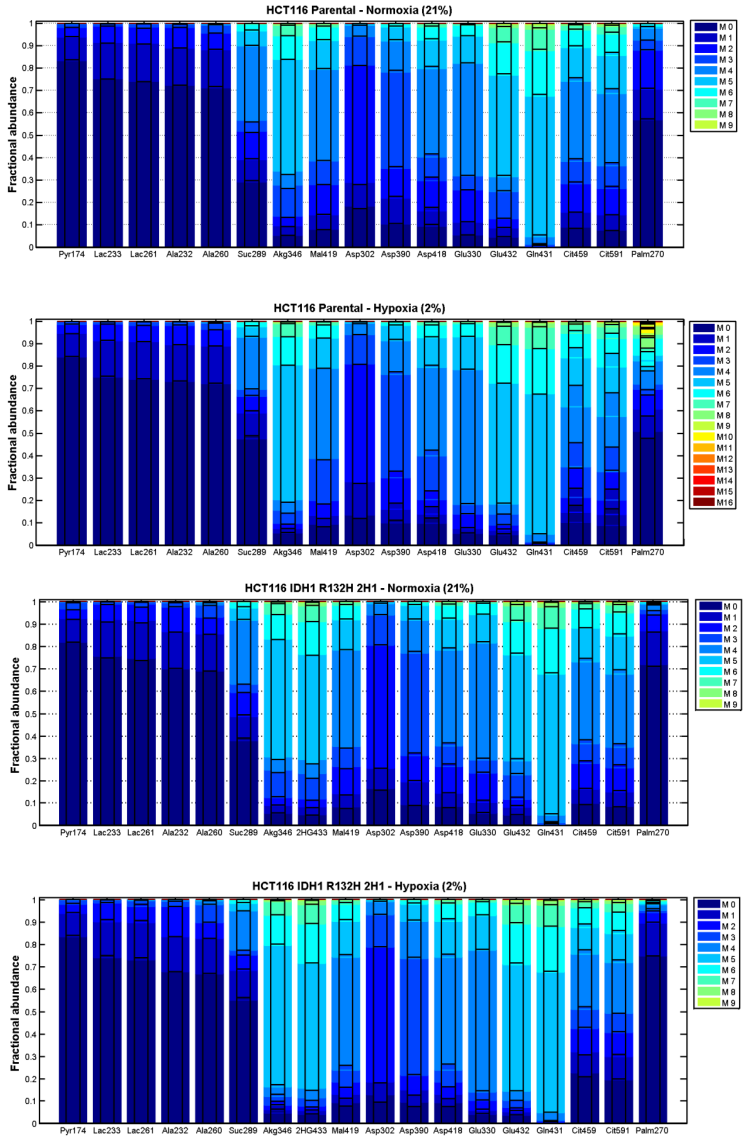

Figure S2.4: Simulated and Measured Uncorrected MIDs. Simulated and measured uncorrected MIDs; outside and inside (black-outlined) bars, respectively; for HCT116 parental and HCT116 IDH1 R132H/+ 2H1 cells cultured in either hypoxic (2%) or normoxic (21%) conditions. Simulated MIDs were extracted from best model fit listed in Tables S2.2-S2.5.

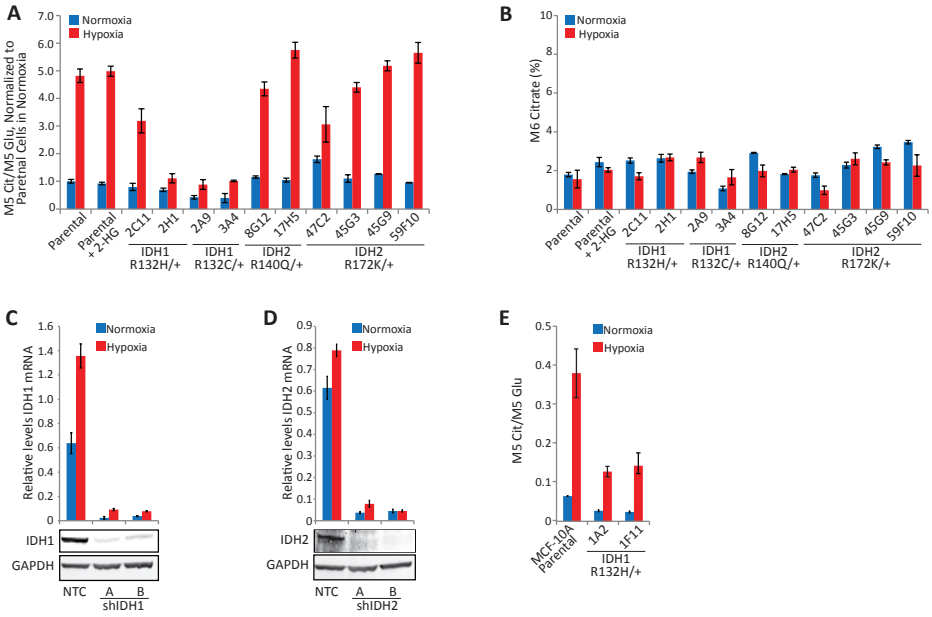

Figure S2.5: Compromised Reductive TCA Metabolism is Specific to Cells with Mutant IDH1. (A) Relative level of reductive glutamine metabolism, determined by M5 labeling of citrate normalized to M5 labeling of glutamate from [U-$^{13}C_5$]glutamine in HCT116 Parental cells with or without 10mM 2-HG, or HCT116 IDH1/2-mutant isogenic cells cultured in normoxia or hypoxia (2% oxygen) for 72 hours. (B) M6 labeling of citrate from [U-$^{13}C_5$]glutamine in cells cultured as in Figure S2.5A. (C and D) Relative levels of IDH1 and IDH2 mRNA and protein from cells cultured as in Figure 2.2F. (E) Relative level of glutamine reductive carboxylation, determined by M5 labeling of citrate normalized to M5 labeling of glutamate from [U-$^{13}C_5$]glutamine of cells cultured as in Figure 2.2G.

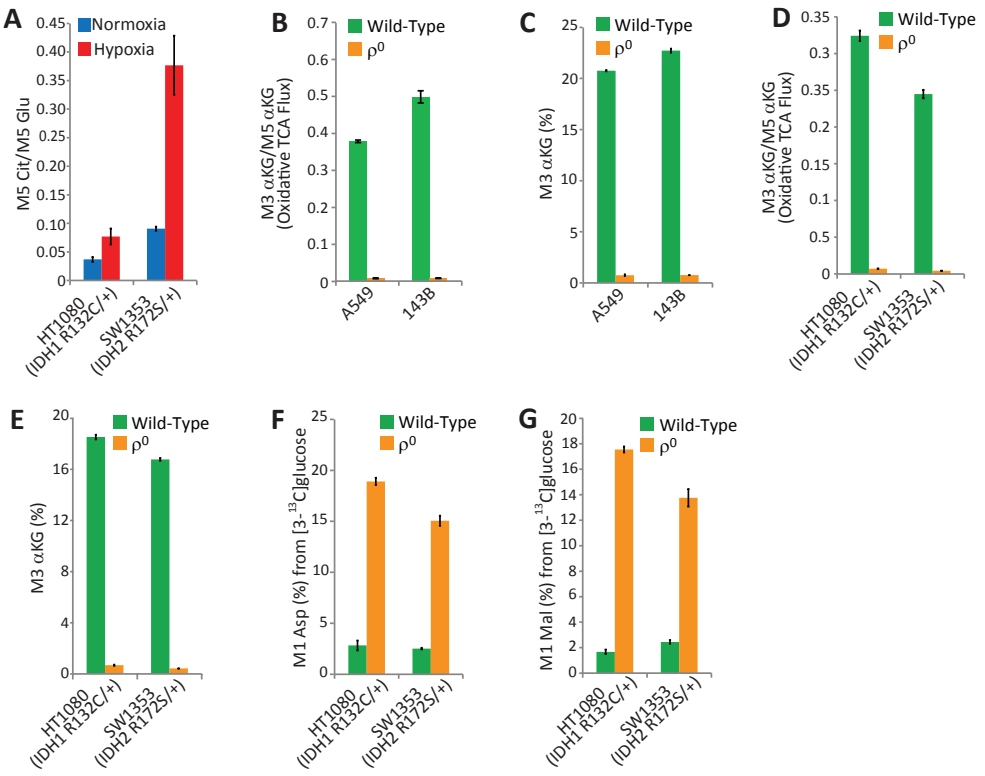

Figure S2.6: Cells with Endogenous IDH1 and IDH2 Mutations Respond Differently to Mitochondrial Stress. (A) Glutamine reductive metabolism, as determined by M5 labeling of citrate relative to M5 labeling of glutamate from [U-$^{13}C_5$]glutamine in cells cultured as in Figure 2.4A. (B) Relative level of oxidative TCA flux, determined by M3 labeling of αKG relative to M5 labeling of αKG from [U-$^{13}C_5$]glutamine in A549 and 143B wild-type or ρ^0 cells. (C) Relative level of oxidative TCA flux, determined by % M3 labeling of αKG from [U-$^{13}C_5$]glutamine in A549 and 143B wild-type or ρ^0 cells. (D) Relative level of oxidative TCA flux, determined by M3 labeling of αKG relative to M5 labeling of αKG from [U-$^{13}C_5$]glutamine in HT-1080 and SW1353 wild-type or ρ^0 cells. (E) Relative level of oxidative TCA flux, determined by % M3 labeling of αKG from [U-$^{13}C_5$]glutamine in HT-1080 and SW1353 wild-type or ρ^0 cells. (F and G) Relative level of pyruvate carboxylase activity, as determined by M1 labeling of aspartate (F) and malate (G) from [3-^{13}C]glucose in HT-1080 and SW1353 wild-type or ρ^0 cells.

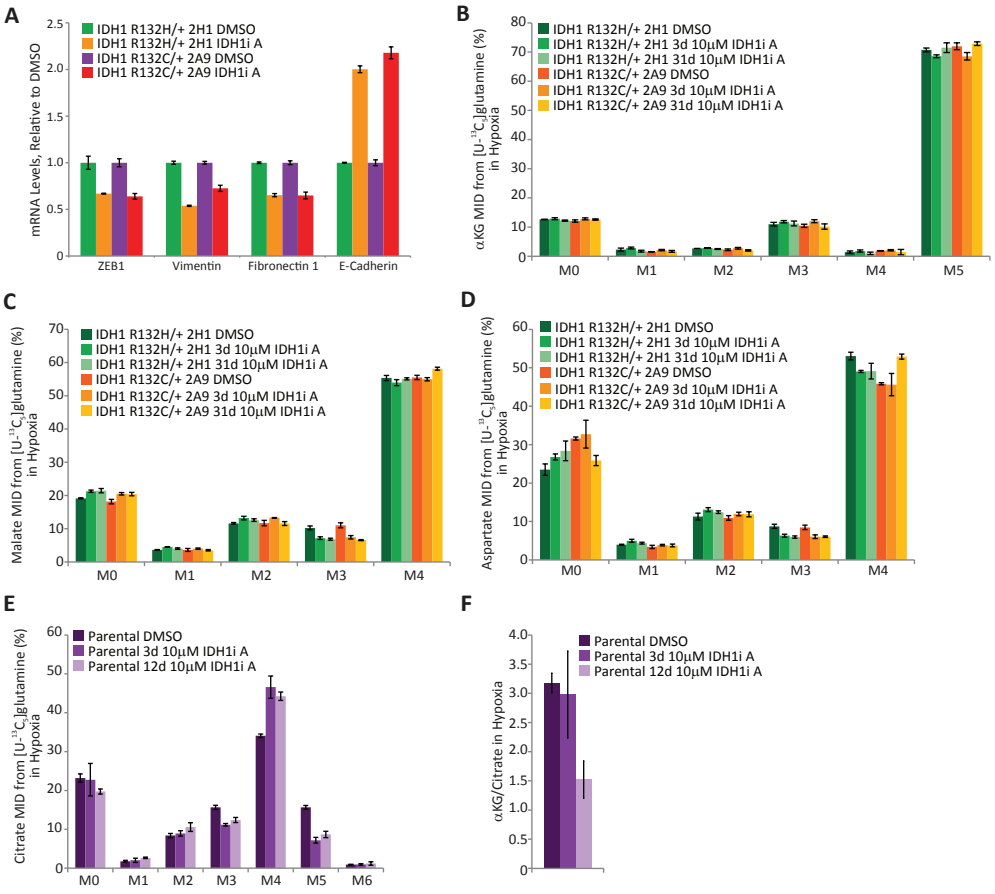

Figure S2.7: Inhibition of Mutant IDH1 Does Not Rescue Reprogramming of TCA Metabolism. (A) mRNA levels of EMT markers (which have been previously shown to be modulated by 2-HG levels (Grassian et al., 2012)) in HCT116 IDH1 R132H/+ 2H1 and HCT116 IDH1 R132C/+ 2A9 cells which were cultured in the presence or absence of 10μM IDH1i A for 28 days. Expression is normalized to DMSO control for each cell line. (B-D) αKG (B), Malate (C), and Aspartate (D) MID labeling from [U-$^{13}C_5$]glutamine from cells cultured as in Figure 2.6D. (E) Citrate MID labeling from [U-$^{13}C_5$]glutamine from HCT116 Parental cells cultured in the presence or absence of 10μM of IDH1i A for 3 or 12 days, the final 72 hours of which the cells are grown in hypoxia (2% oxygen). (F) αKG/citrate ratio from cells cultured as in Figure S2.7E.

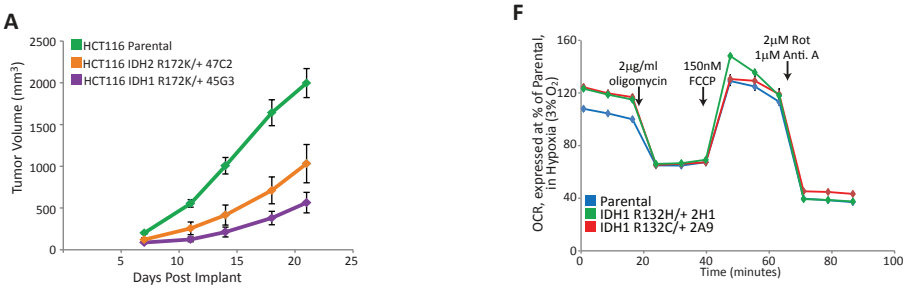

Figure S2.8: Cells Expressing Mutant IDH1 are Sensitive to Pharmacological Inhibition of Mitochondrial Oxidative Metabolism. (A) Growth curves for HCT116 Parental and IDH2 mutant xenografts. (B) Maximal respiration rate for the indicated cells in Normoxia. (C) Respiratory capacity (ratio of maximal respiration to ATP-linked respiration) of the indicated cells in Normoxia. (D) Representative trace of oxygen consumption rates in Normoxia for the indicated cell lines. Data is presented as percentage of HCT116 Parental cells setting the third measurement as 100%. (E) Representative trace of O_2 levels for HCT116 IDH1 R132H/+ 2H1 cells in Normoxia. Data is presented as percentage of background. (F) Representative trace of oxygen consumption rates in Hypoxia (3% O2) for the indicated cell lines. Data is presented as percentage of HCT116 Parental cells setting the third measurement as 100%. (G) Representative trace of O_2 levels for HCT116 IDH1 R132H/+ 2H1 cells in Hypoxia (3% O2). Data is presented as percentage of background. (H) Growth charts from cells cultured as indicated. Images were acquired every 12 hours to measure confluency. (I) Relative level of oxidative TCA flux, determined by M3 labeling of αKG relative to M5 labeling of αKG from [U-$^{13}C_5$]glutamine in HCT116 parental, HCT116 IDH1 R132H/+ 2H1, or HCT116 IDH1 R132C/+ 2A9 cells cultured in the presence or absence of 100nM Rotenone for 72 hours. (J) Reductive glutamine metabolism, determined by M5 Citrate labeling from [U-$^{13}C_5$]glutamine of cells cultured as in Figure S2.8I. (K) Ratio of α-ketoglutarate to citrate from cells cultured as in Figure S2.8I. (L) Relative level of oxidative TCA flux, determined by %M3 αKG labeling from [U-$^{13}C_5$]glutamine from cells cultured in the presence or absence of 1µM Rotenone or 1µM Antimycin for 6 hours. (M and N) Reductive glutamine metabolism, determined by M3 Fumarate (M) and Malate (N) from [U-$^{13}C_5$]glutamine of cells cultured as in Figure S2.8L. (O) M4 labeling of Succinate from [U-$^{13}C_5$]glutamine from cells cultured as in Figure S2.8L. (P and Q) Growth charts from cells cultured as indicated. Images were acquired every 12 hours to measure confluency. (R) Average IC_{50}'s of the CCLE cell panel across all compounds tested. HT-1080 and SW1353 are indicated. Dotted lines represent +/- 1 standard deviation (SD), and +/- 2 SD.

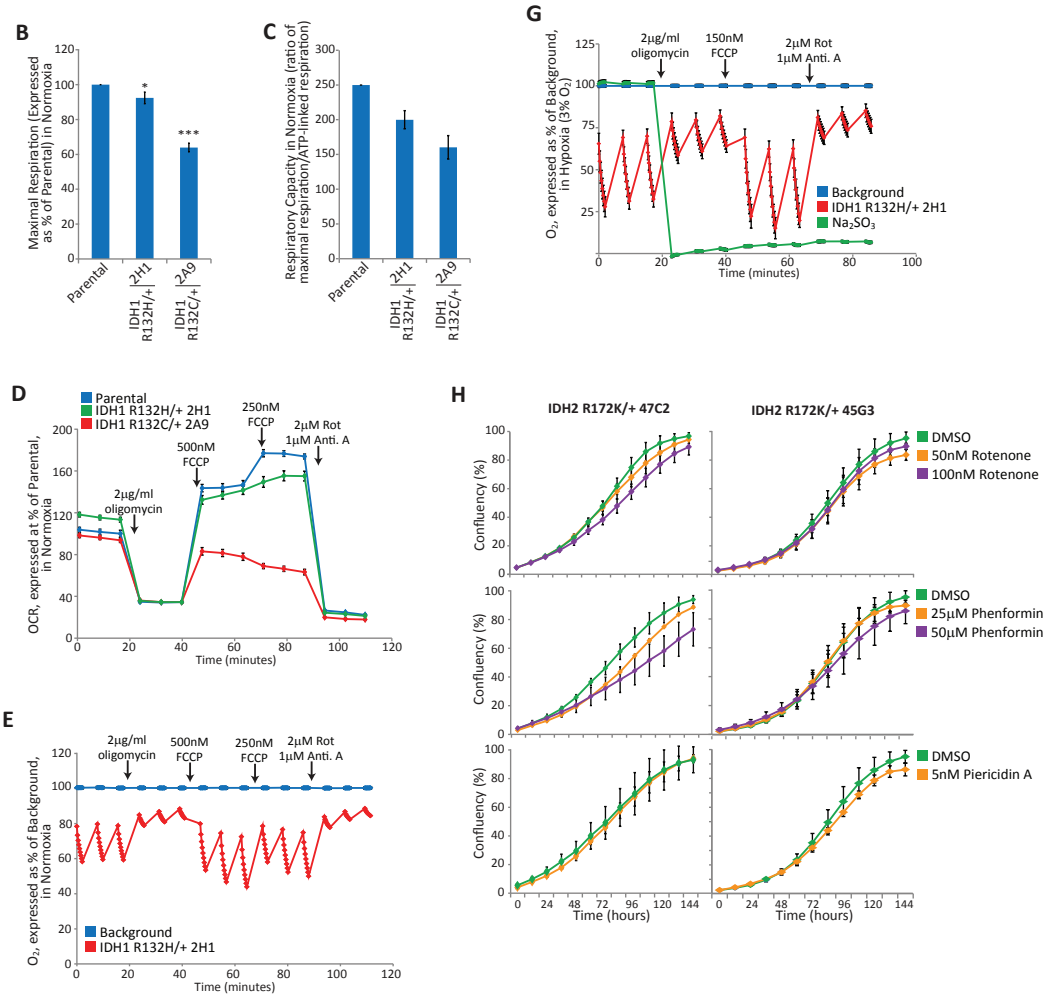

Figure S2.8: Cells Expressing Mutant IDH1 are Sensitive to Pharmacological Inhibition of Mitochondrial Oxidative Metabolism, *continued*.

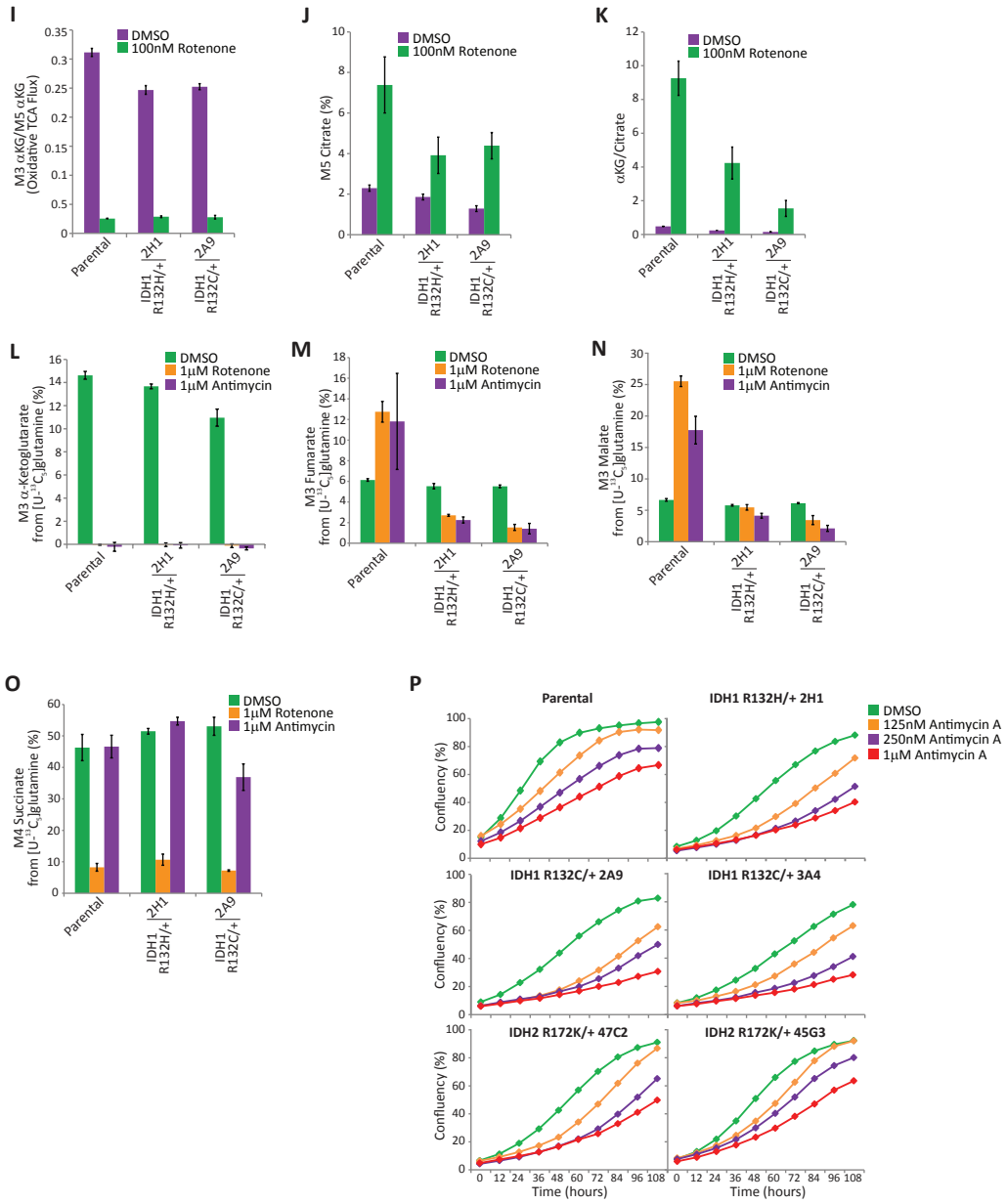

Figure S2.8: Cells Expressing Mutant IDH1 are Sensitive to Pharmacological Inhibition of Mitochondrial Oxidative Metabolism, *continued*.

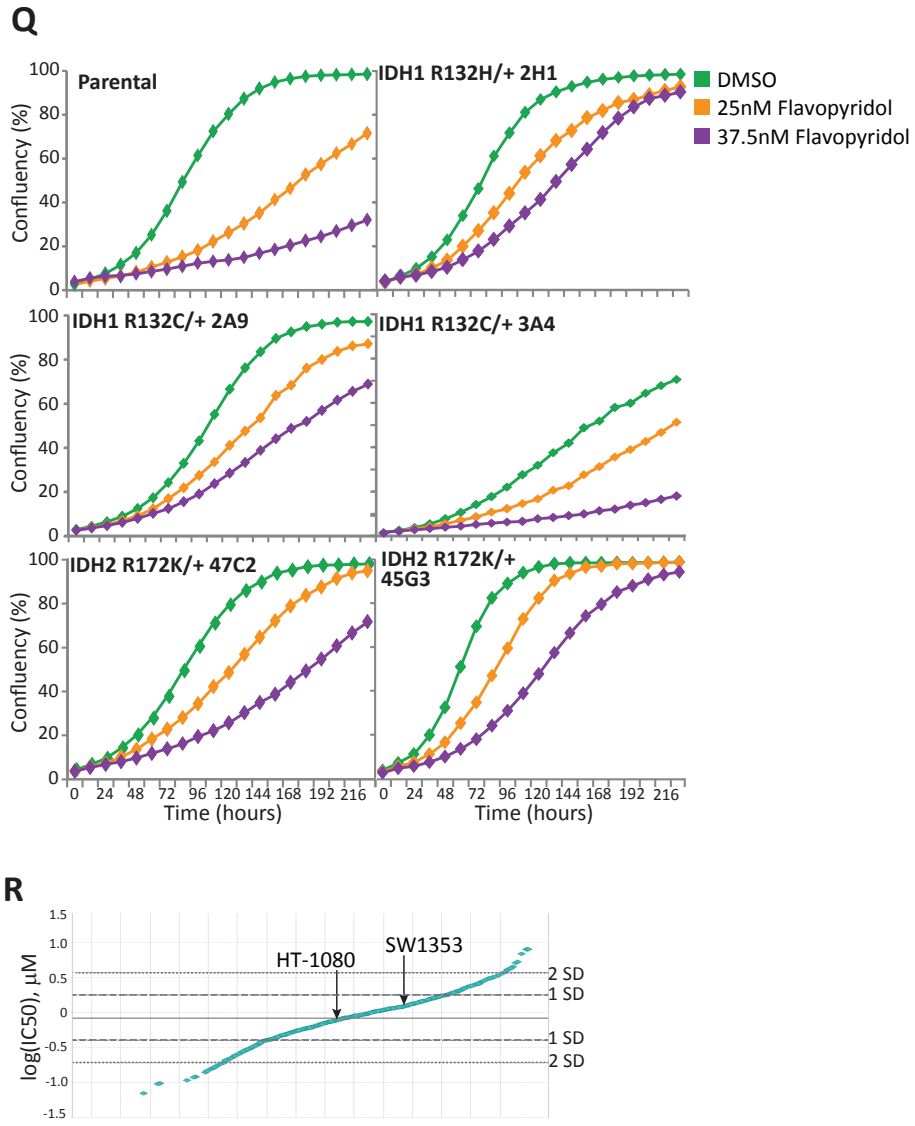

Figure S2.8: Cells Expressing Mutant IDH1 are Sensitive to Pharmacological Inhibition of Mitochondrial Oxidative Metabolism, *continued*.

Table S2.2: Estimated Fluxes from MFA model for HCT116 Parental Cells in Normoxia. Analysis, assumptions and model described in Supplementary Experimental Procedures. Data are presented as averages of three replicates from a single experiment and representative of three independent experiments.

HCT116 Parental - Normoxia (21%)

	Flux	95% Confidence Interval	
Pathway/Reaction	(fmol/cell/hr)	Lower	Upper
Glycolysis			
Glc.x -> G6P	302.20	295.60	308.90
G6P -> F6P	289.20	282.50	295.90
F6P -> G6P	0.00	0.00	Inf
F6P -> DHAP + GAP	296.10	289.50	302.70
DHAP -> GAP	296.10	289.50	302.70
GAP -> DHAP	0.19	0.00	Inf
GAP -> 3PG	595.60	582.50	608.70
3PG -> GAP	1.05	0.00	Inf
3PG -> Pyr.c	595.60	582.50	608.70
Pyr.c -> Lac	498.60	484.90	512.30
Lac -> Pyr.c	26.73	0.00	Inf
Lac -> Lac.x	498.60	484.90	512.30
Pyr.c -> Ala	2.80	-221.40	266.00
Ala -> Pyr.c	0.11	0.00	271.70
Pyr.m -> Ala	8.94	-254.50	232.90
Ala -> Pyr.m	0.00	0.00	Inf
Pyr.c -> Pyr.x	49.08	47.70	50.46
Ala -> Ala.x	4.74	4.39	5.09
Pentose Phosphate			
G6P -> P5P + CO2	13.04	12.19	13.89
P5P + P5P -> S7P + GAP	3.44	3.10	3.77
S7P + GAP -> P5P + P5P	0.11	0.00	Inf
S7P + GAP -> F6P + E4P	3.44	3.10	3.77
F6P + E4P -> S7P + GAP	0.11	0.00	Inf
P5P + E4P -> F6P + GAP	3.44	3.10	3.77
F6P + GAP -> P5P + E4P	0.50	0.00	Inf
Anaplerotic Reactions			
Pyr.c -> Pyr.m	45.08	-221.10	266.10
Pyr.m -> Pyr.c	63.21	0.00	221.40
Pyr.m + CO2 -> Oac.m	1.84	1.32	2.44
Mal.m -> Pyr.m + CO2	6.71	3.00	11.06
Pyr.m -> AcCoA.m + CO2	41.01	34.85	47.27
Glu -> Akg	8.24	4.66	12.26
Akg -> Glu	607.30	285.90	Inf
Gln -> Glu	30.17	26.37	34.16
Glu -> Gln	1.89	0.00	5.09
Gln.x -> Gln	33.92	29.78	38.16
Glu -> Glu.x	18.58	18.37	18.79

Table S2.2: Estimated Fluxes from MFA model for HCT116 Parental Cells in Normoxia, *continued*.

HCT116 Parental - Normoxia (21%)

	Flux	95% Confidence Interval	
Pathway/Reaction	(fmol/cell/hr)	Lower	Upper
TCA Cycle			
AcCoA.m + Oac.m -> Cit	41.01	34.85	47.27
Cit -> Akg + CO2	12.35	10.68	14.27
Akg + CO2 -> Cit	2.47	1.85	3.18
Akg -> Suc + CO2	20.59	15.45	26.35
Suc -> Fum.m	20.59	15.45	26.35
Fum.m -> Suc	6.04	0.00	Inf
Fum.m -> Mal.m	20.59	15.45	26.35
Mal.m -> Fum.m	1.63E+05	0.00	Inf
Mal.m -> Oac.m	39.16	33.20	45.25
Oac.m -> Mal.m	0.00	0.00	69.35
Oac.m -> Asp.m	0.00	0.00	0.00
Asp.m -> Oac.m	0.00	0.00	Inf
Oac.c -> Mal.c	-8988.00	-Inf	30.30
Mal.c -> Oac.c	9.99E+06	0.00	Inf
Oac.c -> Asp.c	9016.00	2.72	Inf
Asp.c -> Oac.c	0.00	0.00	Inf
Asp.c -> Fum.c	9013.00	0.00	Inf
Mal.c -> Fum.c	-9013.00	-Inf	0.00
Fum.c -> Mal.c	9.99E+06	0.00	Inf
Mal.c -> Mal.m	25.28	20.41	30.30
Mal.m -> Mal.c	26.82	0.00	Inf
Biomass			
Cit -> AcCoA.c + Oac.c	28.65	23.13	34.33
0*AcCoA.c + 0*AcCoA.c + …	0.11	0.00	Inf
Palm.d -> Palm.s	0.08	0.00	Inf
114*Asp.c + 152*Glu +	0.03	0.02	0.04
Dilution/Mixing			
0*Pyr.c -> Pyr.mnt	0.66	0.24	1.00
0*Pyr.m -> Pyr.mnt	0.34	0.00	0.76
0*Mal.c -> Mal.mnt	0.11	0.00	Inf
0*Mal.m -> Mal.mnt	0.22	0.00	Inf
0*Asp.c -> Asp.mnt	0.49	0.00	1.00
0*Asp.m -> Asp.mnt	0.51	0.00	1.00
Suc.d -> Suc.mnt	0.34	0.27	0.40
0*Suc -> Suc.mnt	0.66	0.60	0.73
0*Fum.m -> Fum.mnt	0.48	0.00	1.00
0*Fum.c -> Fum.mnt	0.52	0.00	1.00

Table S2.2: Estimated Fluxes from MFA model for HCT116 Parental Cells in Normoxia, *continued*.

HCT116 Parental - Normoxia (21%)

	Flux	95% Confidence Interval	
Pathway/Reaction	(fmol/cell/hr)	Lower	Upper
Glu.d -> Glu	1.14	0.63	1.68
Pyr.mnt -> Pyr.fix	1.00	1.00	1.00
Suc.mnt -> Suc.fix	1.00	1.00	1.00
Asp.mnt -> Asp.fix	1.00	1.00	1.00
Fum.mnt -> Fum.fix	1.00	1.00	1.00
Neomorphic reactions			
Akg -> 2HG	-	-	-
2HG -> 2HG.x	-	-	-

SSE = 87.1
Expected SSE = [45.5, 129.5] (99.9% confidence, 81 DOF)

Table S2.3: Estimated Fluxes from MFA model for HCT116 IDH1 R132H/+ 2H1 Cells in Normoxia. Analysis, assumptions and model described in Supplementary Experimental Procedures. Data are presented as averages of three replicates from a single experiment and representative of three independent experiments.

HCT116 IDH1 R132H 2H1 - Normoxia (21%)

	Flux	**95% Confidence Interval**	
Pathway/Reaction	(fmol/cell/hr)	Lower	Upper
Glycolysis			
Glc.x -> G6P	304.40	299.30	309.60
G6P -> F6P	288.10	282.80	294.60
F6P -> G6P	0.00	0.00	Inf
F6P -> DHAP + GAP	297.60	292.60	303.70
DHAP -> GAP	297.60	292.60	303.70
GAP -> DHAP	0.35	0.00	Inf
GAP -> 3PG	600.00	590.00	612.00
3PG -> GAP	8.40	0.00	Inf
3PG -> Pyr.c	600.00	590.00	612.00
Pyr.c -> Lac	475.30	466.80	483.80
Lac -> Pyr.c	0.00	0.00	Inf
Lac -> Lac.x	475.30	466.80	483.80
Pyr.c -> Ala	0.00	-74.15	115.50
Ala -> Pyr.c	0.00	0.00	115.30
Pyr.m -> Ala	12.43	-103.00	86.73
Ala -> Pyr.m	0.05	0.00	Inf
Pyr.c -> Pyr.x	81.05	75.95	85.48
Ala -> Ala.x	7.10	6.89	7.32
Pentose Phosphate			
G6P -> P5P + CO2	16.30	14.58	18.01
P5P + P5P -> S7P + GAP	4.74	4.05	5.33
S7P + GAP -> P5P + P5P	0.00	0.00	Inf
S7P + GAP -> F6P + E4P	4.74	4.05	5.33
F6P + E4P -> S7P + GAP	0.00	0.00	Inf
P5P + E4P -> F6P + GAP	4.74	4.05	5.33
F6P + GAP -> P5P + E4P	0.02	0.00	Inf
Anaplerotic Reactions			
Pyr.c -> Pyr.m	43.62	-74.09	115.60
Pyr.m -> Pyr.c	3.04	0.00	74.17
Pyr.m + CO2 -> Oac.m	1.94	1.54	2.60
Mal.m -> Pyr.m + CO2	4.48	3.36	9.71
Pyr.m -> AcCoA.m + CO2	33.74	29.07	39.48
Glu -> Akg	7.00	4.34	11.90
Akg -> Glu	1396.00	390.40	Inf
Gln -> Glu	32.82	29.88	37.76
Glu -> Gln	2.24	0.00	6.05
Gln.x -> Gln	35.68	32.41	40.83
Glu -> Glu.x	23.83	23.08	24.69

Table S2.3: Estimated Fluxes from MFA model for HCT116 IDH1 R132H/+ 2H1 Cells in Normoxia, *continued*.

HCT116 IDH1 R132H 2H1 - Normoxia (21%)			
	Flux	**95% Confidence Interval**	
Pathway/Reaction	(fmol/cell/hr)	Lower	Upper
TCA Cycle			
AcCoA.m + Oac.m -> Cit	33.74	29.07	39.48
Cit -> Akg + CO2	11.94	10.73	13.93
Akg + CO2 -> Cit	1.52	1.17	2.07
Akg -> Suc + CO2	17.05	14.73	23.65
Suc -> Fum.m	17.05	14.73	23.65
Fum.m -> Suc	5.24	0.00	Inf
Fum.m -> Mal.m	17.05	14.73	23.65
Mal.m -> Fum.m	13.31	0.00	Inf
Mal.m -> Oac.m	31.80	27.32	37.32
Oac.m -> Mal.m	0.00	0.00	9.68
Oac.m -> Asp.m	0.00	0.00	0.00
Asp.m -> Oac.m	0.05	0.00	Inf
Oac.c -> Mal.c	-1.00E+07	-Inf	22.89
Mal.c -> Oac.c	3425.00	0.00	Inf
Oac.c -> Asp.c	1.00E+07	2.09	Inf
Asp.c -> Oac.c	9.93	0.00	Inf
Asp.c -> Fum.c	1.00E+07	0.00	Inf
Mal.c -> Fum.c	-1.00E+07	-Inf	0.00
Fum.c -> Mal.c	0.00	0.00	Inf
Mal.c -> Mal.m	19.24	15.51	22.89
Mal.m -> Mal.c	159.20	35.96	Inf
Biomass			
Cit -> AcCoA.c + Oac.c	21.80	17.58	25.93
0*AcCoA.c + 0*AcCoA.c + …	0.10	0.00	7.01E+06
Palm.d -> Palm.s	0.37	0.00	Inf
114*Asp.c + 152*Glu +	0.02	0.02	0.03
Dilution/Mixing			
0*Pyr.c -> Pyr.mnt	0.46	0.00	1.00
0*Pyr.m -> Pyr.mnt	0.54	0.00	1.00
0*Mal.c -> Mal.mnt	0.00	0.00	Inf
0*Mal.m -> Mal.mnt	0.00	0.00	Inf
0*Asp.c -> Asp.mnt	1.00	0.73	1.00
0*Asp.m -> Asp.mnt	0.00	0.00	0.27
Suc.d -> Suc.mnt	0.47	0.42	0.50
0*Suc -> Suc.mnt	0.53	0.50	0.58
0*Fum.m -> Fum.mnt	0.88	0.00	1.00
0*Fum.c -> Fum.mnt	0.12	0.00	1.00

Table S2.3: Estimated Fluxes from MFA model for HCT116 IDH1 R132H/+ 2H1 Cells in Normoxia, *continued*.

HCT116 IDH1 R132H 2H1 - Normoxia (21%)

	Flux	95% Confidence Interval	
Pathway/Reaction	(fmol/cell/hr)	Lower	Upper
Glu.d -> Glu	1.42	0.96	1.92
Pyr.mnt -> Pyr.fix	1.00	1.00	1.00
Suc.mnt -> Suc.fix	1.00	1.00	1.00
Asp.mnt -> Asp.fix	1.00	1.00	1.00
Fum.mnt -> Fum.fix	1.00	1.00	1.00
Neomorphic reactions			
Akg -> 2HG	1.89	0.00	3.79
2HG -> 2HG.x	1.89	0.00	3.79

SSE = 77.6
Expected SSE = [56.1, 147] (99.9% confidence, 95 DOF)

Table S2.4: Estimated Fluxes from MFA model for HCT116 Parental Cells in Hypoxia (2% Oxygen). Analysis, assumptions and model described in Supplementary Experimental Procedures. Data are presented as averages of three replicates from a single experiment and representative of three independent experiments.

HCT116 Parental - Hypoxia (2%)

	Flux	95% Confidence Interval	
Pathway/Reaction	(fmol/cell/hr)	Lower	Upper
Glycolysis			
Glc.x -> G6P	752.40	725.80	778.90
G6P -> F6P	719.10	692.40	745.70
F6P -> G6P	0.00	0.00	Inf
F6P -> DHAP + GAP	739.10	712.50	765.70
DHAP -> GAP	739.10	712.50	765.70
GAP -> DHAP	6.31E+06	0.00	Inf
GAP -> 3PG	1488.00	1435.00	1541.00
3PG -> GAP	0.00	0.00	Inf
3PG -> Pyr.c	1488.00	1435.00	1541.00
Pyr.c -> Lac	1416.00	1362.00	1470.00
Lac -> Pyr.c	9.53	0.00	Inf
Lac -> Lac.x	1416.00	1362.00	1470.00
Pyr.c -> Ala	-74.89	-274.00	308.10
Ala -> Pyr.c	396.30	8.06	1533.00
Pyr.m -> Ala	88.07	-300.10	287.20
Ala -> Pyr.m	3.66	0.00	431.60
Pyr.c -> Pyr.x	41.55	34.34	48.75
Ala -> Ala.x	4.81	3.27	6.33
Pentose Phosphate			
G6P -> P5P + CO2	33.31	31.22	35.39
P5P + P5P -> S7P + GAP	10.02	9.30	10.74
S7P + GAP -> P5P + P5P	1.00E+07	0.00	Inf
S7P + GAP -> F6P + E4P	10.02	9.30	10.74
F6P + E4P -> S7P + GAP	1.00E+07	0.00	Inf
P5P + E4P -> F6P + GAP	10.02	9.30	10.74
F6P + GAP -> P5P + E4P	2.36E+06	0.00	Inf
Anaplerotic Reactions			
Pyr.c -> Pyr.m	105.70	-285.50	298.70
Pyr.m -> Pyr.c	0.00	0.00	283.40
Pyr.m + CO2 -> Oac.m	3.09	2.00	4.25
Mal.m -> Pyr.m + CO2	18.50	11.27	26.15
Pyr.m -> AcCoA.m + CO2	33.01	27.18	38.99
Glu -> Akg	19.44	12.87	26.41
Akg -> Glu	292.20	110.30	Inf
Gln -> Glu	36.45	29.71	43.67
Glu -> Gln	5.43	0.00	15.23
Gln.x -> Gln	40.94	33.74	48.73
Glu -> Glu.x	14.01	13.24	14.78

Table S2.4: Estimated Fluxes from MFA model for HCT116 Parental Cells in Hypoxia (2% Oxygen), *continued*.

HCT116 Parental - Hypoxia (2%)

	Flux	95% Confidence Interval	
Pathway/Reaction	(fmol/cell/hr)	Lower	Upper
TCA Cycle			
AcCoA.m + Oac.m -> Cit	33.01	27.18	38.99
Cit -> Akg + CO2	-1.29	-2.74	-0.05
Akg + CO2 -> Cit	7.63	5.69	9.96
Akg -> Suc + CO2	18.15	12.63	24.17
Suc -> Fum.m	18.15	12.63	24.17
Fum.m -> Suc	2.09	0.00	Inf
Fum.m -> Mal.m	18.15	12.63	24.17
Mal.m -> Fum.m	1.00E+07	0.00	Inf
Mal.m -> Oac.m	29.92	24.42	35.72
Oac.m -> Mal.m	0.00	0.00	6.38
Oac.m -> Asp.m	0.00	0.00	0.00
Asp.m -> Oac.m	0.00	0.00	Inf
Oac.c -> Mal.c	30.27	-Inf	35.76
Mal.c -> Oac.c	865.70	159.50	Inf
Oac.c -> Asp.c	4.03	3.30	Inf
Asp.c -> Oac.c	1.03	0.00	Inf
Asp.c -> Fum.c	0.00	0.00	Inf
Mal.c -> Fum.c	0.00	-Inf	0.00
Fum.c -> Mal.c	1.00E+07	0.00	Inf
Mal.c -> Mal.m	30.27	24.80	35.76
Mal.m -> Mal.c	379.20	83.80	Inf
Biomass			
Cit -> AcCoA.c + Oac.c	34.30	28.10	40.53
0*AcCoA.c + 0*AcCoA.c + …	0.00	0.00	Inf
Palm.d -> Palm.s	0.00	0.00	Inf
114*Asp.c + 152*Glu +	0.04	0.03	0.04
Dilution/Mixing			
0*Pyr.c -> Pyr.mnt	0.95	0.81	1.00
0*Pyr.m -> Pyr.mnt	0.05	0.00	0.19
0*Mal.c -> Mal.mnt	0.00	0.00	Inf
0*Mal.m -> Mal.mnt	0.44	0.00	Inf
0*Asp.c -> Asp.mnt	0.99	0.58	1.00
0*Asp.m -> Asp.mnt	0.01	0.00	0.42
Suc.d -> Suc.mnt	0.61	0.57	0.66
0*Suc -> Suc.mnt	0.39	0.34	0.43
0*Fum.m -> Fum.mnt	0.39	0.00	1.00
0*Fum.c -> Fum.mnt	0.61	0.00	1.00

Table S2.4: Estimated Fluxes from MFA model for HCT116 Parental Cells in Hypoxia (2% Oxygen), *continued*.

HCT116 Parental - Hypoxia (2%)

	Flux	**95% Confidence Interval**	
Pathway/Reaction	(fmol/cell/hr)	Lower	Upper
Glu.d -> Glu	2.37	1.81	3.04
Pyr.mnt -> Pyr.fix	1.00	1.00	1.00
Suc.mnt -> Suc.fix	1.00	1.00	1.00
Asp.mnt -> Asp.fix	1.00	1.00	1.00
Fum.mnt -> Fum.fix	1.00	1.00	1.00
Neomorphic reactions			
Akg -> 2HG	-	-	-
2HG -> 2HG.x	-	-	-

SSE = 135.5
Expected SSE = [54.5, 144.5] (99.9% confidence, 93 DOF)

Table S2.5: Estimated Fluxes from MFA model for HCT116 IDH1 R132H/+ 2H1 Cells in Hypoxia (2% Oxygen). Analysis, assumptions and model described in Supplementary Experimental Procedures. Data are presented as averages of three replicates from a single experiment and representative of three independent experiments.

HCT116 IDH1 R132H 2H1 - Hypoxia (2%)

	Flux	**95% Confidence Interval**	
Pathway/Reaction	(fmol/cell/hr)	Lower bound	Upper bound
Glycolysis			
Glc.x -> G6P	766.00	650.60	884.20
G6P -> F6P	724.80	607.60	844.50
F6P -> G6P	0.02	0.00	Inf
F6P -> DHAP + GAP	751.40	636.10	869.60
DHAP -> GAP	751.40	636.10	869.60
GAP -> DHAP	0.00	0.00	Inf
GAP -> 3PG	1516.00	1286.00	1751.00
3PG -> GAP	10.57	0.00	Inf
3PG -> Pyr.c	1516.00	1286.00	1751.00
Pyr.c -> Lac	1415.00	1183.00	1653.00
Lac -> Pyr.c	0.00	0.00	Inf
Lac -> Lac.x	1415.00	1183.00	1653.00
Pyr.c -> Ala	6.14	-316.30	323.10
Ala -> Pyr.c	4.42	0.00	617.30
Pyr.m -> Ala	13.90	-302.80	336.40
Ala -> Pyr.m	0.00	0.00	1003.00
Pyr.c -> Pyr.x	97.22	83.27	111.00
Ala -> Ala.x	16.77	14.39	19.11
Pentose Phosphate Pathway			
G6P -> P5P + CO2	41.15	18.09	64.23
P5P + P5P -> S7P + GAP	13.29	5.56	20.98
S7P + GAP -> P5P + P5P	0.63	0.00	Inf
S7P + GAP -> F6P + E4P	13.29	5.56	20.98
F6P + E4P -> S7P + GAP	0.27	0.00	Inf
P5P + E4P -> F6P + GAP	13.29	5.56	20.98
F6P + GAP -> P5P + E4P	0.25	0.00	Inf
Anaplerotic Reactions			
Pyr.c -> Pyr.m	-2.59	-324.40	315.20
Pyr.m -> Pyr.c	232.70	0.00	314.50
Pyr.m + CO2 -> Oac.m	9.71	7.93	11.61
Mal.m -> Pyr.m + CO2	48.00	37.90	59.01
Pyr.m -> AcCoA.m + CO2	21.79	17.86	25.86
Glu -> Akg	40.32	31.53	50.07
Akg -> Glu	413.50	151.80	Inf
Gln -> Glu	62.24	53.22	72.06
Glu -> Gln	12.33	0.00	37.29
Gln.x -> Gln	63.99	54.71	74.04
Glu -> Glu.x	21.22	19.04	23.42

Table S2.5: Estimated Fluxes from MFA model for HCT116 IDH1 R132H/+ 2H1 Cells in Hypoxia (2% Oxygen), *continued*.

HCT116 IDH1 R132H 2H1 - Hypoxia (2%)

	Flux	95% Confidence Interval	
Pathway/Reaction	(fmol/cell/hr)	Lower bound	Upper bound
TCA Cycle			
AcCoA.m + Oac.m -> Cit	21.79	17.86	25.86
Cit -> Akg + CO2	8.40	6.66	10.46
Akg + CO2 -> Cit	0.93	0.45	1.48
Akg -> Suc + CO2	48.26	38.17	59.52
Suc -> Fum.m	48.26	38.17	59.52
Fum.m -> Suc	60.13	0.00	Inf
Fum.m -> Mal.m	48.26	38.17	59.52
Mal.m -> Fum.m	1.00E+07	0.00	Inf
Mal.m -> Oac.m	12.08	9.79	14.46
Oac.m -> Mal.m	0.00	0.00	1.13
Oac.m -> Asp.m	0.00	0.00	0.00
Asp.m -> Oac.m	0.85	0.00	Inf
Oac.c -> Mal.c	0.00	-Inf	14.34
Mal.c -> Oac.c	1.00E+07	0.00	Inf
Oac.c -> Asp.c	13.40	< 13.36	Inf
Asp.c -> Oac.c	0.00	0.00	Inf
Asp.c -> Fum.c	11.82	0.00	Inf
Mal.c -> Fum.c	-11.82	-Inf	0.00
Fum.c -> Mal.c	0.59	0.00	Inf
Mal.c -> Mal.m	11.82	9.36	14.34
Mal.m -> Mal.c	1.00E+07	485.80	Inf
Biomass			
Cit -> AcCoA.c + Oac.c	13.39	10.61	16.25
0*AcCoA.c + 0*AcCoA.c + … -> Palm.s	0.15	0.00	3.24E+06
Palm.d -> Palm.s	1.23	0.00	Inf
114*Asp.c + 152*Glu + 237*Ala + 127*Gln + 970*AcCoA.c + 92*P5P -> Biomass	0.01	0.01	0.02
Dilution/Mixing			
0*Pyr.c -> Pyr.mnt	1.00	0.92	1.00
0*Pyr.m -> Pyr.mnt	0.00	0.00	0.08
0*Mal.c -> Mal.mnt	0.00	0.00	Inf
0*Mal.m -> Mal.mnt	0.00	0.00	Inf
0*Asp.c -> Asp.mnt	1.00	0.98	1.00
0*Asp.m -> Asp.mnt	0.00	0.00	0.02
Suc.d -> Suc.mnt	0.72	0.67	0.77
0*Suc -> Suc.mnt	0.28	0.23	0.33
0*Fum.m -> Fum.mnt	0.02	0.00	1.00
0*Fum.c -> Fum.mnt	0.98	0.00	1.00

Table S2.5: Estimated Fluxes from MFA model for HCT116 IDH1 R132H/+ 2H1 Cells in Hypoxia (2% Oxygen), *continued*.

HCT116 IDH1 R132H 2H1 - Hypoxia (2%)

	Flux	**95% Confidence Interval**	
Pathway/Reaction	(fmol/cell/hr)	Lower bound	Upper bound
Glu.d -> Glu	1.40	0.59	2.26
Pyr.mnt -> Pyr.fix	1.00	1.00	1.00
Suc.mnt -> Suc.fix	1.00	1.00	1.00
Asp.mnt -> Asp.fix	1.00	1.00	1.00
Fum.mnt -> Fum.fix	1.00	1.00	1.00
Neomorphic reactions			
Akg -> 2HG	0.46	0.31	0.61
2HG -> 2HG.x	0.46	0.31	0.61

SSE = 141.2

Expected SSE = [53.0, 142.0] (99.9% confidence, 91 DOF)

Supplement to Chapter 3

Materials and Methods

LC-MS/MS Analysis of NAD(H) and NADP(H)

For analysis of NAD(H) and NADP(H) using a Q Exactive Benchtop LC-MS/MS (Thermo Fisher Scientific), chromatographic separation was achieved by injecting 2µL of sample on a SeQuant ZIC-pHILIC Polymeric column (2.1x150mm 5µM, EMD Millipore). Flow rate was set to 100µL/min, column compartment was set to 25°C, and autosampler sample tray was set to 4°C. Mobile Phase A consisted of 20mM Ammonium Carbonate, 0.1% Ammonium Hydroxide in 100% Water. Mobile Phase B was 100% Acetonitrile. The mobile phase gradient (%B) was as follows: 0 min 80%, 5 min 80%, 30 min 20%, 31 min 80%, 42 min 80%. All mobile phase was introduced into the Ion Max source equipped with a HESI II probe set with the following parameters: Sheath Gas = 40, Aux Gas = 15, Sweep Gas = 1, Spray Voltage = 3.1 kV, Capillary Temperature = 275°C, S-lens RF level = 40, Heater Temp = 350°C. NAD+, NADP+, NADH, and NADPH were monitored in negative mode using a targeted selected ion monitoring (tSIM) method with the quadropole centred on the M-H ion m+2 mass. Isolation window was 5 amu, resolution was set to 140,000, and AGC target was set to 1e5 ions. Data were acquired and analysed using Xcalibur v2.2 software (Thermo Fisher Scientific). Raw counts were corrected for quadropole bias by measuring the quadropole bias experimentally in a set of adjacent runs of samples at natural abundance. Quadropole bias was measured for all species by monitoring the measured vs. theoretical m1/m0 ratio at natural abundance of all species with m-1, m0, m1, and m2 centred scans. Quadropole bias-corrected counts were additionally corrected for natural

abundance to obtain the final mass isotopomer distribution for each compound in each sample.

Chromatographic separation of NAD(H) and NADP(H) using a XSELECT HSS XP (Waters, Milford, MA) with an UFLC XR HPLC (Shimadzu, Columbia, MD) was operated as follows. Mobile phase A was composed of 10 mM tributylamine (TBA), 10 mM acetic acid (pH 6.86), 5% methanol, and 2% 2-propanol; mobile phase B was 2-propanol. Oven temperature was 40°C. The chromatographic conditions are as follows: 0, 0, 0.4; 5, 0, 0.4; 9, 2, 0.4; 9.5, 6, 0.4; 11.5, 6, 0.4; 12, 11, 0.4; 13.5, 11, 0.4; 15.5, 28, 0.4; 16.5, 53, 0.15; 22.5, 53, 0.15; 23, 0, 0.15; 27, 0, 0.4; 33, 0, 0.4; (Total time [min], Eluent B [vol%], Flow rate [mL*min^{-1}]). The autosampler temperature was 10°C and the injection volume was 10 µL with full loop injection. An AB SCIEX Qtrap 5500 mass spectrometer (AB SCIEX, Framingham, MA) was operated in negative mode. Electrospray ionization parameters were optimized for 0.4 mL/min flow rate, and are as follows: electrospray voltage of -4500 V, temperature of 500°C, curtain gas of 40, CAD gas of 12, and gas 1 and 2 of 50 and 50 psi, respectively. Analyser parameters were optimized for each compound using manual tuning. The instrument was mass calibrated with a mixture of polypropylene glycol (PPG) standards. Samples were acquired using the scheduled MRM pro algorithm in Analyst 1.6.2. The acquisition method consisted of a multiple reaction monitoring (MRM) survey scan coupled to an information dependent acquisition (IDA) consisting of an enhanced resolution (ER) and an enhanced product ion (EPI) scan for compound isotopomer distribution and compound identity confirmation. MRMs were processed using Multiquant 2.1.1. Enhanced production ion (EPI) scans and enhanced resolution scans were processed using Analyst. The identity of each compound was previously determined running pure standards. Linearity of each compound was determined by running calibration curves that spanned the upper and lower limits of detection. Quality controls and carry-over checks were included with each batch.

Supplemental Figures and Tables

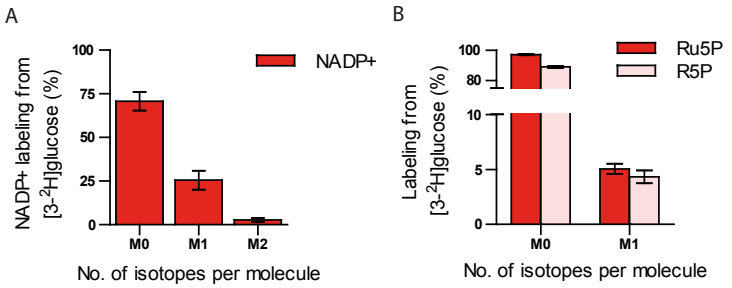

Figure S3.1: 1-^{2}Hglucose and 3-^{2}Hglucose Label Cytosolic NADPH via G6PD and 6PGD. (A) NADP+ labeling in parental H1299 cells incubated for 24 hours with [3-^{2}H]glucose measured via LC-MS/MS. (B) Labeling of ribose 5-phosphate (R5P) and ribulose 5-phosphate (Ru5P) from [3-^{2}H]glucose measured via LC-MS/MS in parental H1299 cells after 24 hour incubation. (C) NAD+ (top panel) and NADH (bottom panel) labeling in parental H1299 cells incubated over a course of 30 minutes and for 24 hours with [3-^{2}H]glucose measured via LC-MS/MS. (D) Atom-transition map depicting a model of deuterium transfer from [1-^{2}H]glucose through glycolysis and the pentose phosphate pathway. Open large circles represent carbon and small blue circles indicate deuterium label from [1-^{2}H]glucose. Enrichments of M1 isotopomer (%) for glycolytic intermediates from [1-^{2}H]glucose in parental H1299 cells measured via GC-MS are indicated below specific metabolites. (E) Labeling of NADP+ and NADPH in parental H1299 cells incubated for 24 hours with [1-^{2}H]glucose measured via LC-MS/MS. (F) Labeling of ribose 5-phosphate (R5P) and ribulose 5-phosphate (Ru5P) in parental H1299 cells incubated for 24 hours with [1-^{2}H]glucose measured via LC-MS/MS. (G) Glucose 6-phosphate (G6P) labeling in parental H1299 cells incubated for 24 hours with either [1-^{2}H]glucose or [3-^{2}H]glucose measured via LC-MS/MS. Lower G6P labeling from [1-^{2}H]glucose is due to deuterium exchange with hydrogen from water from phosphoglucose isomerase (PGI) reversibility. (H) Saturated fatty acid labeling (myristate, palmitate, and stearate) in parental H1299 cells incubated for 72 hours with [1-^{2}H]glucose. Due to label from [1-^{2}H]glucose on citrate, some fatty acid labeling arises from deuterium on lipogenic acetyl-CoA. Data shown represent mean ± SD of at least three biological replicates.

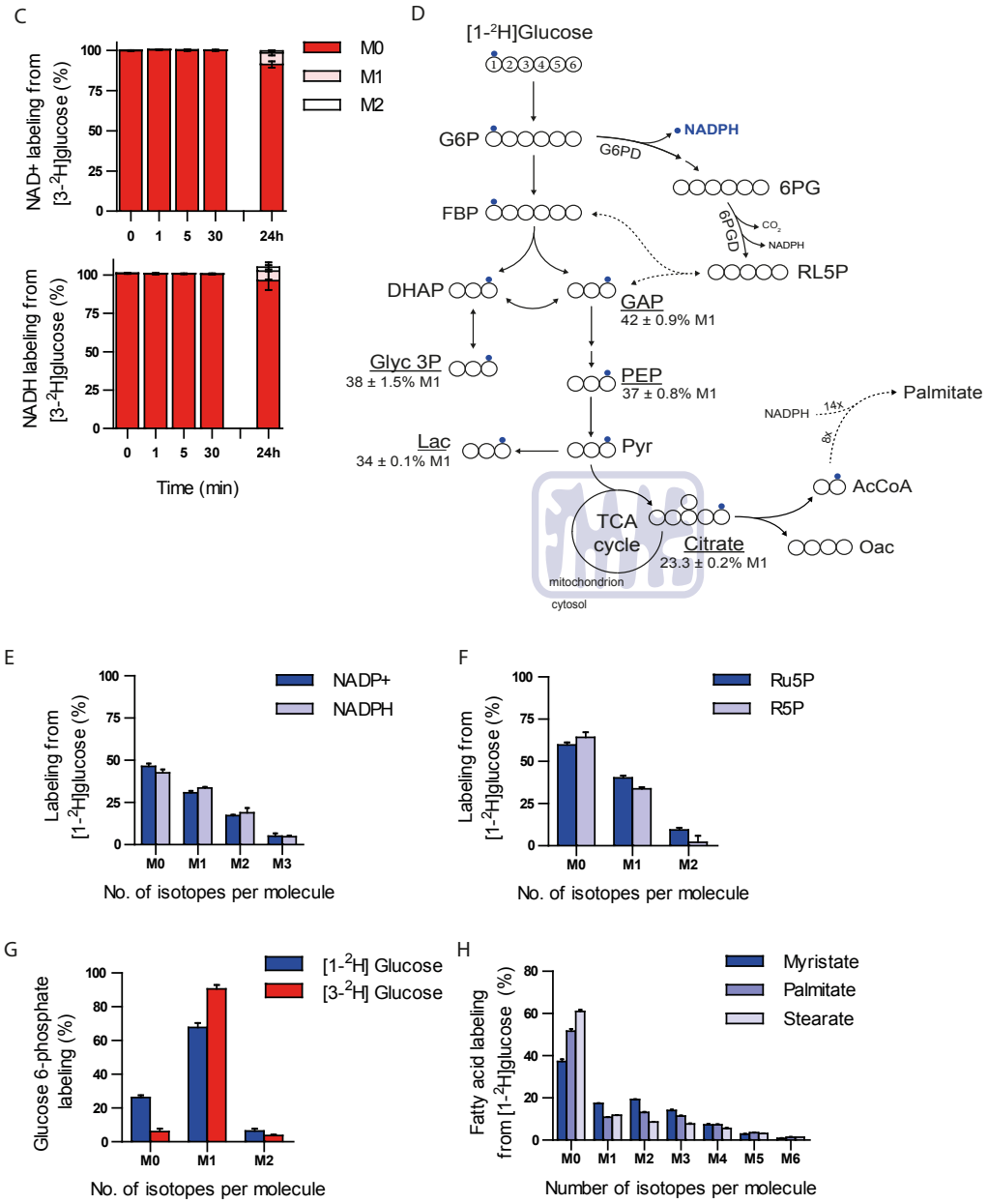

Figure S3.1: 1-^{2}Hglucose and 3-^{2}Hglucose Label Cytosolic NADPH via G6PD and 6PGD, *continued*.

Table S3.1: Metabolite fragment ions used for GCMS and LCMS analysis.

Metabolite	Carbons	Formula	Mass (m/z)
GCMS:	--	--	--
Pyruvate	123	$C_6H_{12}O_3NSi$	174
Lactate	23	$C_{10}H_{25}O_2Si_2$	233
Lactate	123	$C_{11}H_{25}O_3Si_2$	261
Citrate	123456	$C_{20}H_{39}O_6Si_3$	459
Citrate	123456	$C_{26}H_{55}O_7Si_4$	591
Isocitrate	123456	$C_{20}H_{39}O_6Si_3$	459
Isocitrate	123456	$C_{26}H_{55}O_7Si_4$	591
αKG	12345	$C_{14}H_{28}O_5NSi_2$	346
Succinate	1234	$C_{12}H_{25}O_4Si_2$	289
Fumarate	1234	$C_{12}H_{23}O_4Si_2$	287
Malate	1234	$C_{18}H_{39}O_5Si_3$	419
Glyceraldehyde 3-phosphate	123	$C_{18}H_{43}O_6NSi_3P$	484
Phosphoenolpyruvate	123	$C_{17}H_{38}O_6Si_3P$	453
3-phosphoglycerate	123	$C_{23}H_{54}O_7Si_4P$	585
Glycerol 3-phosphate	123	$C_{23}H_{56}O_6Si_4P$	571
Alanine	23	$C_{10}H_{26}ONSi_2$	232
Alanine	123	$C_{11}H_{26}O_2NSi_2$	260
Aspartate	12	$C_{14}H_{32}O_2NSi_2$	302
Aspartate	234	$C_{17}H_{40}O_3NSi_3$	390
Aspartate	1234	$C_{18}H_{40}O_4NSi_3$	418
Glutamate	2345	$C_{16}H_{36}O_2NSi_2$	330
Glutamate	12345	$C_{19}H_{42}O_4NSi_3$	432
Glutamine	12345	$C_{19}H_{43}N_2O_3Si_3$	431
Glycine	2	$C_9H_{24}ONSi_2$	218
Glycine	12	$C_{10}H_{24}O_2NSi_2$	246
Serine	23	$C_{14}H_{34}NOSi_2$	288
Serine	12	$C_{14}H_{32}O_2NSi_2$	302
Serine	23	$C_{16}H_{40}O_2NSi_3$	362
Serine	123	$C_{17}H_{40}O_3NSi_3$	390
2HG	12345	$C_{19}H_{41}O_5Si_3$	433
Myristate	1-14	$C_{15}H_{30}O_2$	242
Palmitate	1-16	$C_{17}H_{34}O_2$	270
Stearate	1-18	$C_{19}H_{38}O_2$	298
LCMS:	--	--	--
6-phospogluconate	123456	$C_6H_{13}O_{10}P$	276
Ribulose 5-phosphate	12345	$C_5H_{11}O_8P$	230
Ribose 5-phosphate	12345	$C_5H_{11}O_8P$	230
NAD+	1-21	$C_{21}H_{26}N_7O_{14}P_2$	662
NADH	1-21	$C_{21}H_{27}N_7O_{14}P_2$	663
NADP+	1-21	$C_{21}H_{28}N_7O_{17}P_3$	743
NADPH	1-21	$C_{21}H_{29}N_7O_{17}P_3$	744

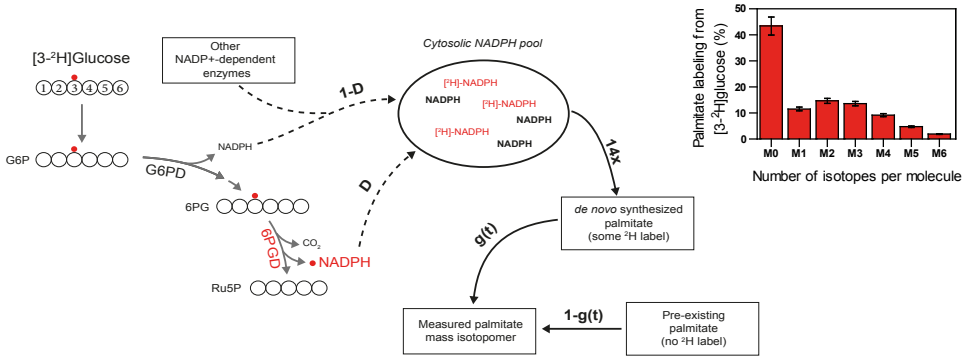

Figure S3.2: Overview of ^{2}Hglucose Isotopomer Spectral Analysis (ISA). The ISA method applied to palmitate synthesis provides estimates for the relative enrichment of lipogenic NADPH from a particular source (*e.g.* [3-^{2}H]glucose labels NADPH via 6PGD), the D parameter, and the fraction of the fatty acid pool that was synthesized *de novo*, the g(t) parameter. Parameters are estimated by comparing simulated to measured palmitate mass isotopomer distributions, and the 95% confidence interval is determined by sensitivity analysis.

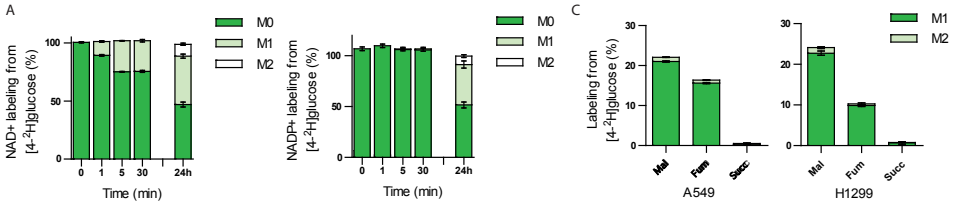

Figure S3.3: 4-^{2}H-glucose Labels NADH via GAPDH. (A) NAD+ (left panel) and NADP+ (right panel) labeling over 24 hours in parental H1299 cells incubated with [4-^{2}H]glucose. (B) Atom-transition map depicting a model of label transfer from ^{2}H-labeled NADH to malate, via malate dehydrogenase, and subsequent labeling of TCA intermediates. Malate labeling enters the TCA cycle via the malate-aspartate shuttle (small black circles) and labeling is scrambled due to the symmetry of fumarate and reversibility of fumarase (small green circles). Open large circles represent carbon and small coloured circles (black/green) indicated deuterium label from ^{2}H-labeled NADH. No deuterium labels lipogenic acetyl-CoA. (C) M1 and M2 labeling of malate (Mal), fumarate (Fum), and succinate (Succ) in parental A549 (left panel) and H1299 (right panel) cells from [4-^{2}H]glucose. (D) M1 labeling of aspartate (Asp), citrate (Cit), isocitrate (ICT), and alpha-ketoglutarate (aKG) in parental A549 (left panel) and H1299 (right panel) cells from [4-^{2}H]glucose. (E) Labeling of ribose 5-phosphate (R5P) and ribulose 5-phosphate (Ru5P) in parental H1299 cells incubated for 24 hours with [4-^{2}H]glucose. Data represent mean $\pm$ SD of three biological replicates. (F) Possible mechanisms for [4-^{2}H]glucose labeled NADH transferring to cytosolic and mitochondrial NADPH. Labeling of malate and TCA intermediates are described in Figure S3.3B. Labeled malate can label cytosolic NADPH through malic enzyme 1 (ME1) or label mitochondrial NAD(P)H through either ME2 or ME3. Mitochondrial NADH can transfer H^- to mitochondrial NADPH via transhydrogenase (NNT). Due to fumarate symmetry, label from [4-^{2}H]glucose can transfer to citrate, as described in Figure S3.3B, and label mitochondrial NAD(P)H via isocitrate dehydrogenase 2 or 3 (IDH2/3) or label cytosolic NADPH via IDH1.

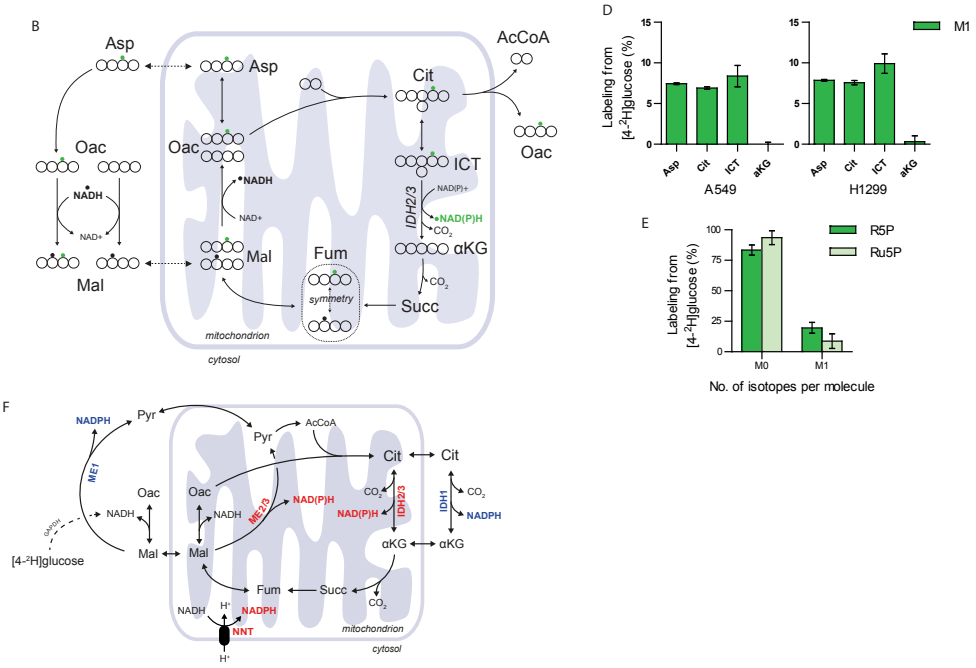

Figure S3.3: 4-^{2}H-glucose Labels NADH via GAPDH, *continued*.

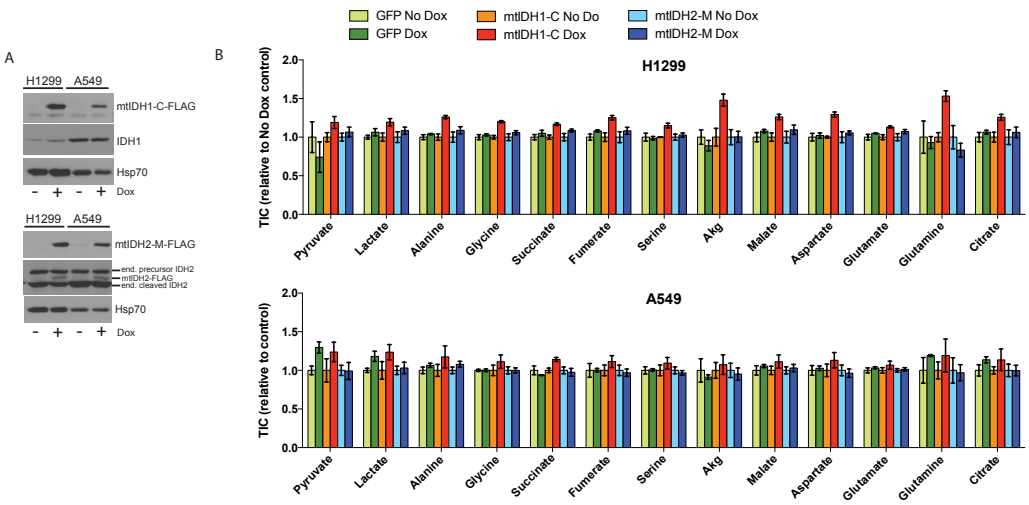

Figure S3.4: Characterization of Cell Lines Expressing Inducible mtIDH1-C and mtIDH2-M. (A) Flag-tagged exogenous mutant IDH proteins (mtIDH1-C and mtIDH2-M) induced by doxycycline are not overexpressed when compared to endogenous IDH levels. (B) Doxycyline does not affect pool sizes of central carbon metabolites as measured by GCMS and compared to vehicle (water) treated (No Dox) H1299 (upper panel) and A549 (lower panel) cells. (C) Doxycyline does not affect proliferation rates of H1299 (upper panels) or A549 (lower panels) cell lines. (D) Doxycyline addition and 2HG production does not affect pool sizes of NAD+, NADH, NADP+ or NADPH in H1299 mtIDH1-C cells (upper panel) or mtIDH2-M cells (lower panel). (E) NADPH production from the pentose phosphate pathway (as shown by [3-^{2}H]glucose tracing) occurs in cells harboring endogenous IDH1 mutations (HT1080) but not endogenous IDH2 mutations (SW1353). (F) [4-^{2}H]glucose labels mostly 2HG in SW1353 cells (IDH2 R172S/+) and not in HT1080 (IDH1 R132C/+) cells. Data shown are mean $\pm$ SEM of three biological replicates (B-D). (E-F): data shown represent mean $\pm$ SD of three biological replicates. (G) Enrichment of lipogenic NADPH from [3-^{2}H]glucose in A549 cells expressing either GFP, mtIDH1-C, or mtIDH2-M following incubation with tracer for 24 hours prior to dox-induction (0.1 μg/mL) for 48 hours. Data plotted as mean $\pm$ 95% confidence interval of at least three biological replicates.

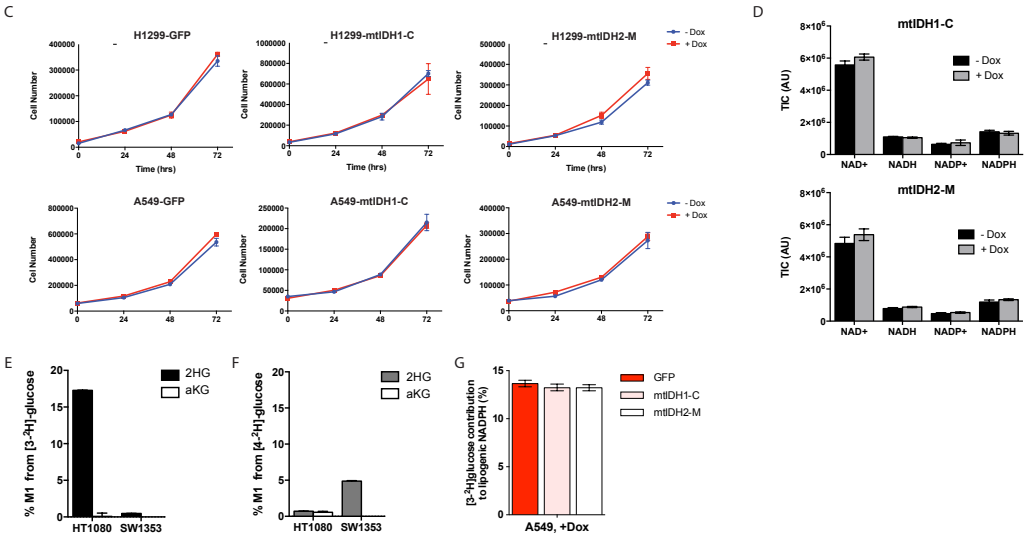

Figure S3.4: Characterization of Cell Lines Expressing Inducible mtIDH1-C and mtIDH2-M, *continued*.

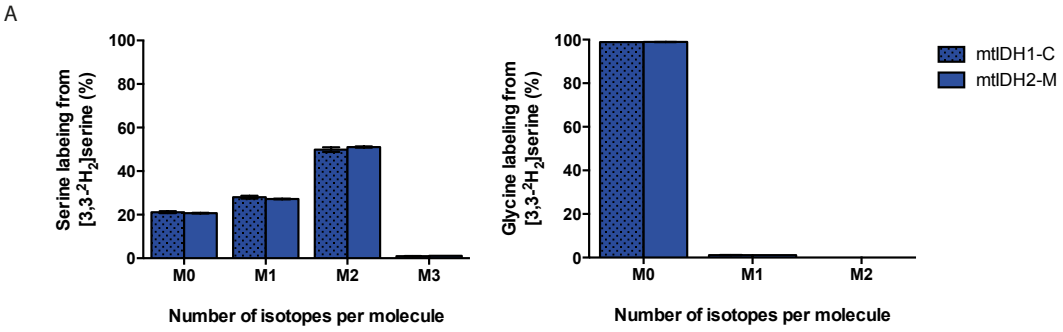

Figure S3.5: Directionality of Folate-Mediated Serine and Glycine Metabolism. (A) Serine and glycine labeling in A549 mtIDH1-C and mtIDH2-M cells cultured with [3,3-$^2H_2$]serine for 24 hours plus 48 hours mtIDH induction (0.1 μg/mL dox). (B) Serine and glycine labeling in A549 mtIDH1-C and mtIDH2-M cells cultured with [2,3,3-$^2H_3$]serine for 24 hours plus 48 hours mtIDH induction (0.1 μg/mL dox). (C) Serine and glycine labeling in A549 mtIDH1-C and mtIDH2-M cells cultured with [2,2-$^2H_2$]glycine for 24 hours prior to 48 hours mtIDH induction (0.1 μg/mL dox). Data shown represent mean ± SEM of three biological replicates. (D) Serine fragment (C_1C_2 or C_2C_3) labeling in A549 mtIDH1-C and mtIDH2-M cells cultured with [3-^2H]glucose for 24 hours plus 48 hours mtIDH induction (0.1 μg/mL dox). Presence of label on the C_2C_3 fragment but not the C_1C_2 fragment of serine reveals that label arises from transfer of H^- from NADPH to 5,10-methylene-THF. Data shown represent mean ± SEM of at least three biological replicates.

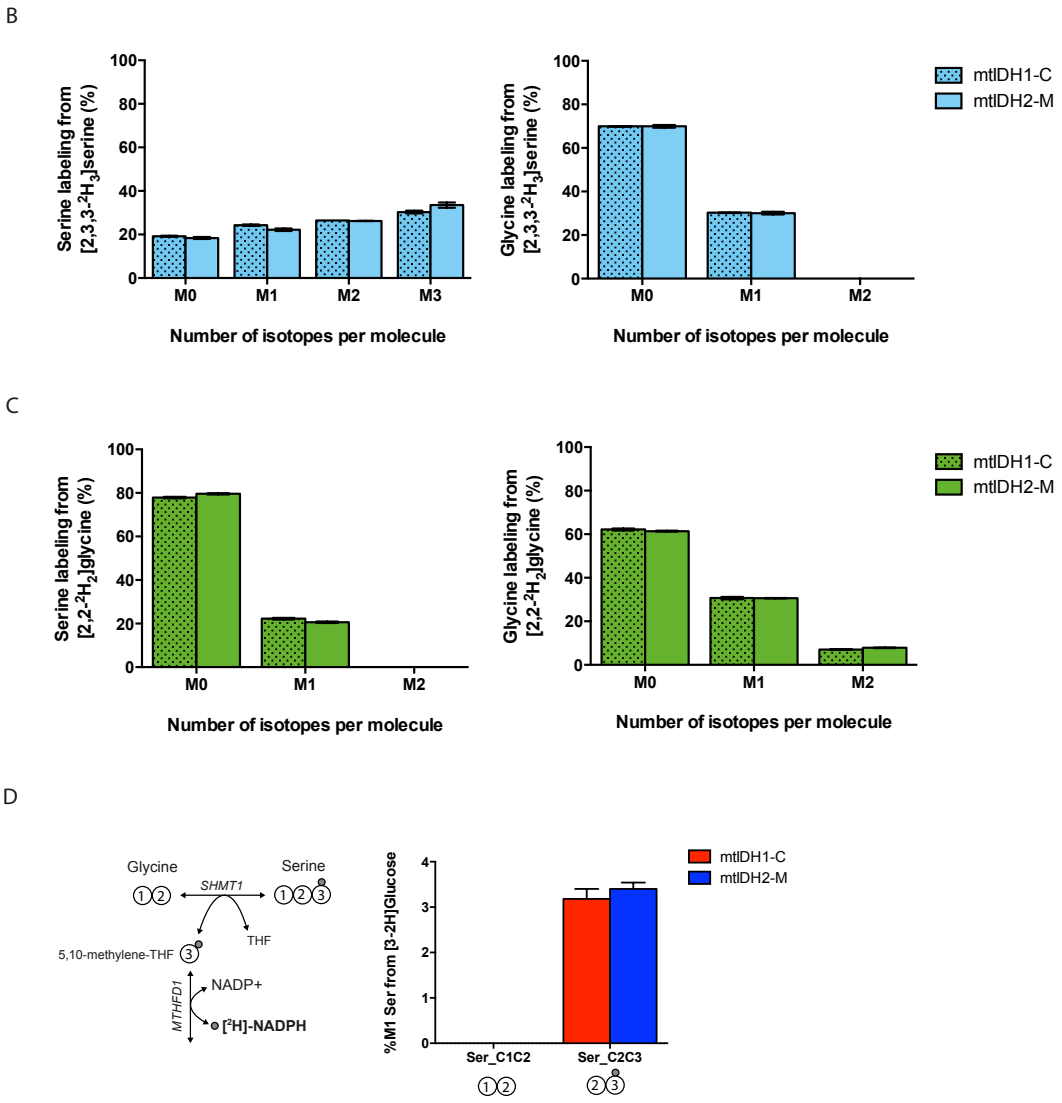

Figure S3.5: Directionality of Folate-Mediated Serine and Glycine Metabolism, *continued*.

References

Ahler, E., Sullivan, W. J., Cass, A., Braas, D., York, A. G., Bensinger, S. J., Graeber, T. G., and Christofk, H. R. (2013). Doxycycline alters metabolism and proliferation of human cell lines. *PloS one*, 8(5):e64561.

Ahn, W. S. and Antoniewicz, M. R. (2011). Metabolic flux analysis of cho cells at growth and non-growth phases using isotopic tracers and mass spectrometry. *Metab Eng*, 13(5):598–609.

Amary, M. F., Bacsi, K., Maggiani, F., Damato, S., Halai, D., Berisha, F., Pollock, R., O'Donnell, P., Grigoriadis, A., Diss, T., Eskandarpour, M., Presneau, N., Hogendoorn, P. C., Futreal, A., Tirabosco, R., and Flanagan, A. M. (2011). Idh1 and idh2 mutations are frequent events in central chondrosarcoma and central and periosteal chondromas but not in other mesenchymal tumours. *J Pathol*, 224(3):334–43.

Anderson, D. D., Quintero, C. M., and Stover, P. J. (2011). Identification of a de novo thymidylate biosynthesis pathway in mammalian mitochondria. *Proceedings of the National Academy of Sciences of the United States of America*, 108(37):15163–15168.

Antoniewicz, M. R., Kelleher, J. K., and Stephanopoulos, G. (2006). Determination of confidence intervals of metabolic fluxes estimated from stable isotope measurements. *Metab Eng*, 8(4):324–37.

Antoniewicz, M. R., Kelleher, J. K., and Stephanopoulos, G. (2007). Elementary metabolite units (emu): a novel framework for modeling isotopic distributions. *Metab Eng*, 9(1):68–86.

Arai, M., Nobusawa, S., Ikota, H., Takemura, S., and Nakazato, Y. (2012). Frequent idh1/2 mutations in intracranial chondrosarcoma: a possible diagnostic clue for its differentiation from chordoma. *Brain Tumor Pathol*, 29(4):201–6.

Balendiran, G. K., Dabur, R., and Fraser, D. (2004). The role of glutathione in cancer. *Cell Biochem Funct*, 22(6):343–52.

Balss, J., Meyer, J., Mueller, W., Korshunov, A., Hartmann, C., and von Deimling, A. (2008). Analysis of the idh1 codon 132 mutation in brain tumors. *Acta Neuropathol*, 116(6):597–602.

Banhegyi, G., Csala, M., and Benedetti, A. (2009). Hexose-6-phosphate dehydrogenase: linking endocrinology and metabolism in the endoplasmic reticulum. *Journal of molecular endocrinology*, 42(4):283–9.

Barlowe, C. K. and Appling, D. R. (1988). In vitro evidence for the involvement of mitochondrial

folate metabolism in the supply of cytoplasmic one-carbon units. *BioFactors*, 1(2):171–6.

Barretina, J., Caponigro, G., Stransky, N., Venkatesan, K., Margolin, A. A., Kim, S., Wilson, C. J., Lehar, J., Kryukov, G. V., Sonkin, D., Reddy, A., Liu, M., Murray, L., Berger, M. F., Monahan, J. E., Morais, P., Meltzer, J., Korejwa, A., Jane-Valbuena, J., Mapa, F. A., Thibault, J., Bric-Furlong, E., Raman, P., Shipway, A., Engels, I. H., Cheng, J., Yu, G. K., Yu, J., Aspesi, P., J., de Silva, M., Jagtap, K., Jones, M. D., Wang, L., Hatton, C., Palescandolo, E., Gupta, S., Mahan, S., Sougnez, C., Onofrio, R. C., Liefeld, T., MacConaill, L., Winckler, W., Reich, M., Li, N., Mesirov, J. P., Gabriel, S. B., Getz, G., Ardlie, K., Chan, V., Myer, V. E., Weber, B. L., Porter, J., Warmuth, M., Finan, P., Harris, J. L., Meyerson, M., Golub, T. R., Morrissey, M. P., Sellers, W. R., Schlegel, R., and Garraway, L. A. (2012). The cancer cell line encyclopedia enables predictive modelling of anticancer drug sensitivity. *Nature*, 483(7391):603–7.

Ben-Yoseph, O., Kingsley, P. B., and Ross, B. D. (1994). Metabolic loss of deuterium from isotopically labeled glucose. *Magnetic resonance in medicine : official journal of the Society of Magnetic Resonance in Medicine / Society of Magnetic Resonance in Medicine*, 32(3):405–9.

Berwick, D. C., Hers, I., Heesom, K. J., Moule, S. K., and Tavare, J. M. (2002). The identification of atp-citrate lyase as a protein kinase b (akt) substrate in primary adipocytes. *J Biol Chem*, 277(37):33895–900.

Birner, P., Pusch, S., Christov, C., Mihaylova, S., Toumangelova-Uzeir, K., Natchev, S., Schoppmann, S. F., Tchorbanov, A., Streubel, B., Tuettenberg, J., and Guentchev, M. (2014). Mutant idh1 inhibits pi3k/akt signaling in human glioma. *Cancer*, 120(16):2440–7.

Bissell, M. J., Rambeck, W. A., White, R. C., and Bassham, J. A. (1976). Glycerol phosphate shuttle in virus-transformed cells in culture. *Science*, 191(4229):856–8.

Bleau, A. M., Hambardzumyan, D., Ozawa, T., Fomchenko, E. I., Huse, J. T., Brennan, C. W., and Holland, E. C. (2009). Pten/pi3k/akt pathway regulates the side population phenotype and abcg2 activity in glioma tumor stem-like cells. *Cell Stem Cell*, 4(3):226–35.

Bleeker, F. E., Atai, N. A., Lamba, S., Jonker, A., Rijkeboer, D., Bosch, K. S., Tigchelaar, W., Troost, D., Vandertop, W. P., Bardelli, A., and Van Noorden, C. J. (2010). The prognostic idh1(r132) mutation is associated with reduced nadp+-dependent idh activity in glioblastoma. *Acta Neuropathol*, 119(4):487–94.

Bordbar, A., Monk, J. M., King, Z. A., and Palsson, B. O. (2014). Constraint-based models predict metabolic and associated cellular functions. *Nat Rev Genet*, 15(2):107–20.

Borger, D. R., Tanabe, K. K., Fan, K. C., Lopez, H. U., Fantin, V. R., Straley, K. S., Schenkein, D. P., Hezel, A. F., Ancukiewicz, M., Liebman, H. M., Kwak, E. L., Clark, J. W., Ryan, D. P., Deshpande, V., Dias-Santagata, D., Ellisen, L. W., Zhu, A. X., and Iafrate, A. J. (2012). Frequent mutation of isocitrate dehydrogenase (idh)1 and idh2 in cholangiocarcinoma identified through broad-based tumor genotyping. *Oncologist*, 17(1):72–9.

Bralten, L. B., Kloosterhof, N. K., Balvers, R., Sacchetti, A., Lapre, L., Lamfers, M., Leenstra, S., de Jonge, H., Kros, J. M., Jansen, E. E., Struys, E. A., Jakobs, C., Salomons, G. S., Diks, S. H., Peppelenbosch, M., Kremer, A., Hoogenraad, C. C., Smitt, P. A., and French, P. J.

(2011). Idh1 r132h decreases proliferation of glioma cell lines in vitro and in vivo. *Ann Neurol*, 69(3):455–63.

Cairns, R. A., Harris, I. S., and Mak, T. W. (2011). Regulation of cancer cell metabolism. *Nat Rev Cancer*, 11(2):85–95.

Cairns, R. A., Iqbal, J., Lemonnier, F., Kucuk, C., de Leval, L., Jais, J. P., Parrens, M., Martin, A., Xerri, L., Brousset, P., Chan, L. C., Chan, W. C., Gaulard, P., and Mak, T. W. (2012). Idh2 mutations are frequent in angioimmunoblastic t-cell lymphoma. *Blood*, 119(8):1901–3.

Cairns, R. A. and Mak, T. W. (2013). Oncogenic isocitrate dehydrogenase mutations: mechanisms, models, and clinical opportunities. *Cancer Discov*, 3(7):730–41.

Carmeliet, P. and Jain, R. K. (2000). Angiogenesis in cancer and other diseases. *Nature*, 407(6801):249–57.

Ceccarelli, C., Grodsky, N. B., Ariyaratne, N., Colman, R. F., and Bahnson, B. J. (2002). Crystal structure of porcine mitochondrial nadp+-dependent isocitrate dehydrogenase complexed with mn2+ and isocitrate. insights into the enzyme mechanism. *J Biol Chem*, 277(45):43454–62.

Chan, S. M., Thomas, D., Corces-Zimmerman, M. R., Xavy, S., Rastogi, S., Hong, W. J., Zhao, F., Medeiros, B. C., Tyvoll, D. A., and Majeti, R. (2015). Isocitrate dehydrogenase 1 and 2 mutations induce bcl-2 dependence in acute myeloid leukemia. *Nat Med*, 21(2):178–84.

Chandel, N. S., McClintock, D. S., Feliciano, C. E., Wood, T. M., Melendez, J. A., Rodriguez, A. M., and Schumacker, P. T. (2000). Reactive oxygen species generated at mitochondrial complex iii stabilize hypoxia-inducible factor-1alpha during hypoxia: a mechanism of o2 sensing. *J Biol Chem*, 275(33):25130–8.

Chaumeil, M. M., Larson, P. E., Woods, S. M., Cai, L., Eriksson, P., Robinson, A. E., Lupo, J. M., Vigneron, D. B., Nelson, S. J., Pieper, R. O., Phillips, J. J., and Ronen, S. M. (2014). Hyperpolarized [1-13c] glutamate: a metabolic imaging biomarker of idh1 mutational status in glioma. *Cancer Res*, 74(16):4247–57.

Chen, R., Nishimura, M. C., Kharbanda, S., Peale, F., Deng, Y., Daemen, A., Forrest, W. F., Kwong, M., Hedehus, M., Hatzivassiliou, G., Friedman, L. S., and Phillips, H. S. (2014). Hominoid-specific enzyme glud2 promotes growth of idh1r132h glioma. *Proc Natl Acad Sci U S A*, 111(39):14217–22.

Cheng, T., Sudderth, J., Yang, C., Mullen, A. R., Jin, E. S., Mates, J. M., and DeBerardinis, R. J. (2011). Pyruvate carboxylase is required for glutamine-independent growth of tumor cells. *Proc Natl Acad Sci U S A*, 108(21):8674–9.

Chesnelong, C., Chaumeil, M. M., Blough, M. D., Al-Najjar, M., Stechishin, O. D., Chan, J. A., Pieper, R. O., Ronen, S. M., Weiss, S., Luchman, H. A., and Cairncross, J. G. (2014). Lactate dehydrogenase a silencing in idh mutant gliomas. *Neuro Oncol*, 16(5):686–95.

Chou, W. C., Lei, W. C., Ko, B. S., Hou, H. A., Chen, C. Y., Tang, J. L., Yao, M., Tsay, W., Wu, S. J., Huang, S. Y., Hsu, S. C., Chen, Y. C., Chang, Y. C., Kuo, K. T., Lee, F. Y.,

Liu, M. C., Liu, C. W., Tseng, M. H., Huang, C. F., and Tien, H. F. (2011). The prognostic impact and stability of isocitrate dehydrogenase 2 mutation in adult patients with acute myeloid leukemia. *Leukemia*, 25(2):246–53.

Chowdhury, R., Yeoh, K. K., Tian, Y. M., Hillringhaus, L., Bagg, E. A., Rose, N. R., Leung, I. K., Li, X. S., Woon, E. C., Yang, M., McDonough, M. A., King, O. N., Clifton, I. J., Klose, R. J., Claridge, T. D., Ratcliffe, P. J., Schofield, C. J., and Kawamura, A. (2011). The oncometabolite 2-hydroxyglutarate inhibits histone lysine demethylases. *EMBO Rep*, 12(5):463–9.

da Silva, C. G., Ribeiro, C. A., Leipnitz, G., Dutra-Filho, C. S., Wyse, A. A., Wannmacher, C. M., Sarkis, J. J., Jakobs, C., and Wajner, M. (2002). Inhibition of cytochrome c oxidase activity in rat cerebral cortex and human skeletal muscle by d-2-hydroxyglutaric acid in vitro. *Biochim Biophys Acta*, 1586(1):81–91.

Dang, C. V. (2013). Role of aerobic glycolysis in genetically engineered mouse models of cancer. *BMC Biol*, 11:3.

Dang, C. V., Kim, J. W., Gao, P., and Yustein, J. (2008). The interplay between myc and hif in cancer. *Nat Rev Cancer*, 8(1):51–6.

Dang, L., White, D. W., Gross, S., Bennett, B. D., Bittinger, M. A., Driggers, E. M., Fantin, V. R., Jang, H. G., Jin, S., Keenan, M. C., Marks, K. M., Prins, R. M., Ward, P. S., Yen, K. E., Liau, L. M., Rabinowitz, J. D., Cantley, L. C., Thompson, C. B., Vander Heiden, M. G., and Su, S. M. (2009). Cancer-associated idh1 mutations produce 2-hydroxyglutarate. *Nature*, 462(7274):739–44.

DeBerardinis, R. J., Lum, J. J., Hatzivassiliou, G., and Thompson, C. B. (2008). The biology of cancer: metabolic reprogramming fuels cell growth and proliferation. *Cell Metab*, 7(1):11–20.

DeBerardinis, R. J. and Thompson, C. B. (2012). Cellular metabolism and disease: what do metabolic outliers teach us? *Cell*, 148(6):1132–44.

Diehn, M., Cho, R. W., Lobo, N. A., Kalisky, T., Dorie, M. J., Kulp, A. N., Qian, D., Lam, J. S., Ailles, L. E., Wong, M., Joshua, B., Kaplan, M. J., Wapnir, I., Dirbas, F. M., Somlo, G., Garberoglio, C., Paz, B., Shen, J., Lau, S. K., Quake, S. R., Brown, J. M., Weissman, I. L., and Clarke, M. F. (2009). Association of reactive oxygen species levels and radioresistance in cancer stem cells. *Nature*, 458(7239):780–3.

Dubbink, H. J., Taal, W., van Marion, R., Kros, J. M., van Heuvel, I., Bromberg, J. E., Zonnenberg, B. A., Zonnenberg, C. B., Postma, T. J., Gijtenbeek, J. M., Boogerd, W., Groenendijk, F. H., Smitt, P. A., Dinjens, W. N., and van den Bent, M. J. (2009). Idh1 mutations in low-grade astrocytomas predict survival but not response to temozolomide. *Neurology*, 73(21):1792–5.

Eales, K. L., Hollinshead, K. E., and Tennant, D. A. (2016). Hypoxia and metabolic adaptation of cancer cells. *Oncogenesis*, 5:e190.

Elstrom, R. L., Bauer, D. E., Buzzai, M., Karnauskas, R., Harris, M. H., Plas, D. R., Zhuang, H., Cinalli, R. M., Alavi, A., Rudin, C. M., and Thompson, C. B. (2004). Akt stimulates aerobic glycolysis in cancer cells. *Cancer Res*, 64(11):3892–9.

Engelman, J. A. (2009). Targeting pi3k signalling in cancer: opportunities, challenges and limitations. *Nat Rev Cancer*, 9(8):550–62.

Esmaeili, M., Hamans, B. C., Navis, A. C., van Horssen, R., Bathen, T. F., Gribbestad, I. S., Leenders, W. P., and Heerschap, A. (2014). Idh1 r132h mutation generates a distinct phospholipid metabolite profile in glioma. *Cancer Res*, 74(17):4898–907.

Fan, J., Kamphorst, J. J., Mathew, R., Chung, M. K., White, E., Shlomi, T., and Rabinowitz, J. D. (2013). Glutamine-driven oxidative phosphorylation is a major atp source in transformed mammalian cells in both normoxia and hypoxia. *Mol Syst Biol*, 9:712.

Fan, J., Ye, J., Kamphorst, J. J., Shlomi, T., Thompson, C. B., and Rabinowitz, J. D. (2014). Quantitative flux analysis reveals folate-dependent nadph production. *Nature*, 510(7504):298–302.

Fendt, S. M., Bell, E. L., Keibler, M. A., Davidson, S. M., Wirth, G. J., Fiske, B., Mayers, J. R., Schwab, M., Bellinger, G., Csibi, A., Patnaik, A., Blouin, M. J., Cantley, L. C., Guarente, L., Blenis, J., Pollak, M. N., Olumi, A. F., Vander Heiden, M. G., and Stephanopoulos, G. (2013a). Metformin decreases glucose oxidation and increases the dependency of prostate cancer cells on reductive glutamine metabolism. *Cancer Res*, 73(14):4429–38.

Fendt, S. M., Bell, E. L., Keibler, M. A., Olenchock, B. A., Mayers, J. R., Wasylenko, T. M., Vokes, N. I., Guarente, L., Vander Heiden, M. G., and Stephanopoulos, G. (2013b). Reductive glutamine metabolism is a function of the alpha-ketoglutarate to citrate ratio in cells. *Nat Commun*, 4:2236.

Fernandez, C. A., Des Rosiers, C., Previs, S. F., David, F., and Brunengraber, H. (1996). Correction of 13c mass isotopomer distributions for natural stable isotope abundance. *Journal of mass spectrometry : JMS*, 31(3):255–62.

Field, M. S., Kamynina, E., Watkins, D., Rosenblatt, D. S., and Stover, P. J. (2015). Human mutations in methylenetetrahydrofolate dehydrogenase 1 impair nuclear de novo thymidylate biosynthesis. *Proc Natl Acad Sci U S A*, 112(2):400–5.

Figueroa, M. E., Abdel-Wahab, O., Lu, C., Ward, P. S., Patel, J., Shih, A., Li, Y., Bhagwat, N., Vasanthakumar, A., Fernandez, H. F., Tallman, M. S., Sun, Z., Wolniak, K., Peeters, J. K., Liu, W., Choe, S. E., Fantin, V. R., Paietta, E., Lowenberg, B., Licht, J. D., Godley, L. A., Delwel, R., Valk, P. J., Thompson, C. B., Levine, R. L., and Melnick, A. (2010). Leukemic idh1 and idh2 mutations result in a hypermethylation phenotype, disrupt tet2 function, and impair hematopoietic differentiation. *Cancer Cell*, 18(6):553–67.

Finkel, T. and Holbrook, N. J. (2000). Oxidants, oxidative stress and the biology of ageing. *Nature*, 408(6809):239–47.

Frezza, C., Zheng, L., Tennant, D. A., Papkovsky, D. B., Hedley, B. A., Kalna, G., Watson, D. G., and Gottlieb, E. (2011). Metabolic profiling of hypoxic cells revealed a catabolic signature required for cell survival. *PLoS One*, 6(9):e24411.

Gaglio, D., Metallo, C. M., Gameiro, P. A., Hiller, K., Danna, L. S., Balestrieri, C., Alberghina,

L., Stephanopoulos, G., and Chiaradonna, F. (2011). Oncogenic k-ras decouples glucose and glutamine metabolism to support cancer cell growth. *Mol Syst Biol*, 7:523.

Gameiro, P. A., Yang, J., Metelo, A. M., Perez-Carro, R., Baker, R., Wang, Z., Arreola, A., Rathmell, W. K., Olumi, A., Lopez-Larrubia, P., Stephanopoulos, G., and Iliopoulos, O. (2013). In vivo hif-mediated reductive carboxylation is regulated by citrate levels and sensitizes vhl-deficient cells to glutamine deprivation. *Cell Metab*, 17(3):372–85.

Gess, B., Hofbauer, K. H., Deutzmann, R., and Kurtz, A. (2004). Hypoxia up-regulates triosephosphate isomerase expression via a hif-dependent pathway. *Pflugers Arch*, 448(2):175–80.

Go, M. K., Amyes, T. L., and Richard, J. P. (2009). Hydron transfer catalyzed by triosephosphate isomerase. products of the direct and phosphite-activated isomerization of [1-(13)c]-glycolaldehyde in d(2)o. *Biochemistry*, 48(24):5769–78.

Grassian, A. R., Lin, F., Barrett, R., Liu, Y., Jiang, W., Korpal, M., Astley, H., Gitterman, D., Henley, T., Howes, R., Levell, J., Korn, J. M., and Pagliarini, R. (2012). Isocitrate dehydrogenase (idh) mutations promote a reversible zeb1/microrna (mir)-200-dependent epithelial-mesenchymal transition (emt). *J Biol Chem*, 287(50):42180–94.

Grassian, A. R., Metallo, C. M., Coloff, J. L., Stephanopoulos, G., and Brugge, J. S. (2011). Erk regulation of pyruvate dehydrogenase flux through pdk4 modulates cell proliferation. *Genes Dev*, 25(16):1716–33.

Grassian, A. R., Parker, S. J., Davidson, S. M., Divakaruni, A. S., Green, C. R., Zhang, X., Slocum, K. L., Pu, M., Lin, F., Vickers, C., Joud-Caldwell, C., Chung, F., Yin, H., Handly, E. D., Straub, C., Growney, J. D., Vander Heiden, M. G., Murphy, A. N., Pagliarini, R., and Metallo, C. M. (2014). Idh1 mutations alter citric acid cycle metabolism and increase dependence on oxidative mitochondrial metabolism. *Cancer Res*, 74(12):3317–31.

Gravel, S. P., Hulea, L., Toban, N., Birman, E., Blouin, M. J., Zakikhani, M., Zhao, Y., Topisirovic, I., St-Pierre, J., and Pollak, M. (2014). Serine deprivation enhances antineoplastic activity of biguanides. *Cancer Res*, 74(24):7521–33.

Guo, D., Reinitz, F., Youssef, M., Hong, C., Nathanson, D., Akhavan, D., Kuga, D., Amzajerdi, A. N., Soto, H., Zhu, S., Babic, I., Tanaka, K., Dang, J., Iwanami, A., Gini, B., Dejesus, J., Lisiero, D. D., Huang, T. T., Prins, R. M., Wen, P. Y., Robins, H. I., Prados, M. D., Deangelis, L. M., Mellinghoff, I. K., Mehta, M. P., James, C. D., Chakravarti, A., Cloughesy, T. F., Tontonoz, P., and Mischel, P. S. (2011). An lxr agonist promotes glioblastoma cell death through inhibition of an egfr/akt/srebp-1/ldlr-dependent pathway. *Cancer Discov*, 1(5):442–56.

Hagedorn, C. H. and Phang, J. M. (1983). Transfer of reducing equivalents into mitochondria by the interconversions of proline and delta 1-pyrroline-5-carboxylate. *Archives of biochemistry and biophysics*, 225(1):95–101.

Hatzivassiliou, G., Zhao, F., Bauer, D. E., Andreadis, C., Shaw, A. N., Dhanak, D., Hingorani, S. R., Tuveson, D. A., and Thompson, C. B. (2005). Atp citrate lyase inhibition can suppress tumor cell growth. *Cancer Cell*, 8(4):311–21.

Hayden, J. T., Fruhwald, M. C., Hasselblatt, M., Ellison, D. W., Bailey, S., and Clifford, S. C. (2009). Frequent idh1 mutations in supratentorial primitive neuroectodermal tumors (spnet) of adults but not children. *Cell Cycle*, 8(11):1806–7.

Hellerstein, M. K., Greenblatt, D. J., and Munro, H. N. (1986). Glycoconjugates as noninvasive probes of intrahepatic metabolism: pathways of glucose entry into compartmentalized hepatic udp-glucose pools during glycogen accumulation. *Proceedings of the National Academy of Sciences of the United States of America*, 83(18):7044–8.

Higashimura, Y., Nakajima, Y., Yamaji, R., Harada, N., Shibasaki, F., Nakano, Y., and Inui, H. (2011). Up-regulation of glyceraldehyde-3-phosphate dehydrogenase gene expression by hif-1 activity depending on sp1 in hypoxic breast cancer cells. *Arch Biochem Biophys*, 509(1):1–8.

Hockel, M. and Vaupel, P. (2001). Tumor hypoxia: definitions and current clinical, biologic, and molecular aspects. *J Natl Cancer Inst*, 93(4):266–76.

Hollinshead, K. E. and Tennant, D. A. (2016). Mitochondrial metabolic remodeling in response to genetic and environmental perturbations. *Wiley Interdiscip Rev Syst Biol Med*, 8(4):272–85.

Houillier, C., Wang, X., Kaloshi, G., Mokhtari, K., Guillevin, R., Laffaire, J., Paris, S., Boisselier, B., Idbaih, A., Laigle-Donadey, F., Hoang-Xuan, K., Sanson, M., and Delattre, J. Y. (2010). Idh1 or idh2 mutations predict longer survival and response to temozolomide in low-grade gliomas. *Neurology*, 75(17):1560–6.

Izquierdo-Garcia, J. L., Cai, L. M., Chaumeil, M. M., Eriksson, P., Robinson, A. E., Pieper, R. O., Phillips, J. J., and Ronen, S. M. (2014). Glioma cells with the idh1 mutation modulate metabolic fractional flux through pyruvate carboxylase. *PLoS One*, 9(9):e108289.

Jain, M., Nilsson, R., Sharma, S., Madhusudhan, N., Kitami, T., Souza, A. L., Kafri, R., Kirschner, M. W., Clish, C. B., and Mootha, V. K. (2012). Metabolite profiling identifies a key role for glycine in rapid cancer cell proliferation. *Science*, 336(6084):1040–4.

Jeon, S. M., Chandel, N. S., and Hay, N. (2012). Ampk regulates nadph homeostasis to promote tumour cell survival during energy stress. *Nature*, 485(7400):661–5.

Jiang, L., Shestov, A. A., Swain, P., Yang, C., Parker, S. J., Wang, Q. A., Terada, L. S., Adams, N. D., McCabe, M. T., Pietrak, B., Schmidt, S., Metallo, C. M., Dranka, B. P., Schwartz, B., and DeBerardinis, R. J. (2016). Reductive carboxylation supports redox homeostasis during anchorage-independent growth. *Nature*, 532(7598):255–8.

Jiang, P., Du, W., Mancuso, A., Wellen, K. E., and Yang, X. (2013). Reciprocal regulation of p53 and malic enzymes modulates metabolism and senescence. *Nature*, 493(7434):689–93.

Jin, G., Reitman, Z. J., Duncan, C. G., Spasojevic, I., Gooden, D. M., Rasheed, B. A., Yang, R., Lopez, G. Y., He, Y., McLendon, R. E., Bigner, D. D., and Yan, H. (2013). Disruption of wild-type idh1 suppresses d-2-hydroxyglutarate production in idh1-mutated gliomas. *Cancer Res*, 73(2):496–501.

Jin, G., Reitman, Z. J., Spasojevic, I., Batinic-Haberle, I., Yang, J., Schmidt-Kittler, O., Bigner,

D. D., and Yan, H. (2011). 2-hydroxyglutarate production, but not dominant negative function, is conferred by glioma-derived nadp-dependent isocitrate dehydrogenase mutations. *PLoS One*, 6(2):e16812.

Juratli, T. A., Peitzsch, M., Geiger, K., Schackert, G., Eisenhofer, G., and Krex, D. (2013). Accumulation of 2-hydroxyglutarate is not a biomarker for malignant progression in idh-mutated low-grade gliomas. *Neuro Oncol*, 15(6):682–90.

Kaelin, W. G., J. and McKnight, S. L. (2013). Influence of metabolism on epigenetics and disease. *Cell*, 153(1):56–69.

Kardon, T., Senesi, S., Marcolongo, P., Legeza, B., Banhegyi, G., Mandl, J., Fulceri, R., and Benedetti, A. (2008). Maintenance of luminal nadph in the endoplasmic reticulum promotes the survival of human neutrophil granulocytes. *FEBS letters*, 582(13):1809–15.

Katz, J., Landau, B. R., and Bartsch, G. E. (1966). The pentose cycle, triose phosphate isomerization, and lipogenesis in rat adipose tissue. *The Journal of biological chemistry*, 241(3):727–40.

Katz, J. and Rognstad, R. (1976). Futile cycles in the metabolism of glucose. *Current topics in cellular regulation*, 10:237–89.

Katz, J. and Rognstad, R. (1978). Futile cycling in glucose-metabolism. *Trends in Biochemical Sciences*, 3(8):171–174.

Katz, J., Rognstad, R., and Kemp, R. G. (1965). Isotope discrimination effects in the metabolism of tritiated glucose. *The Journal of biological chemistry*, 240:PC1484–6.

Kharroubi, A. T., Masterson, T. M., Aldaghlas, T. A., Kennedy, K. A., and Kelleher, J. K. (1992). Isotopomer spectral analysis of triglyceride fatty acid synthesis in 3t3-l1 cells. *Am J Physiol*, 263(4 Pt 1):E667–75.

Kikuchi, G., Motokawa, Y., Yoshida, T., and Hiraga, K. (2008). Glycine cleavage system: reaction mechanism, physiological significance, and hyperglycinemia. *Proceedings of the Japan Academy. Series B, Physical and biological sciences*, 84(7):246–63.

Kim, H., Won, S. J., Fabian, C., Kang, M., Szardenings, M., and Shin, M. (2015). Mitochondrial dna aberrations and pathophysiological implications in hematopoietic diseases, chronic inflammatory diseases, and cancers. *Ann Lab Med*, 35(1):1–14.

Kim, J. W., Gao, P., Liu, Y. C., Semenza, G. L., and Dang, C. V. (2007). Hypoxia-inducible factor 1 and dysregulated c-myc cooperatively induce vascular endothelial growth factor and metabolic switches hexokinase 2 and pyruvate dehydrogenase kinase 1. *Mol Cell Biol*, 27(21):7381–93.

Kim, J. W., Tchernyshyov, I., Semenza, G. L., and Dang, C. V. (2006). Hif-1-mediated expression of pyruvate dehydrogenase kinase: a metabolic switch required for cellular adaptation to hypoxia. *Cell Metab*, 3(3):177–85.

King, A., Selak, M. A., and Gottlieb, E. (2006). Succinate dehydrogenase and fumarate hydratase: linking mitochondrial dysfunction and cancer. *Oncogene*, 25(34):4675–82.

Koivunen, P., Lee, S., Duncan, C. G., Lopez, G., Lu, G., Ramkissoon, S., Losman, J. A., Joensuu, P., Bergmann, U., Gross, S., Travins, J., Weiss, S., Looper, R., Ligon, K. L., Verhaak, R. G., Yan, H., and Kaelin, W. G., J. (2012). Transformation by the (r)-enantiomer of 2-hydroxyglutarate linked to egln activation. *Nature*, 483(7390):484–8.

Koul, D. (2008). Pten signaling pathways in glioblastoma. *Cancer Biol Ther*, 7(9):1321–5.

Kranendijk, M., Struys, E. A., van Schaftingen, E., Gibson, K. M., Kanhai, W. A., van der Knaap, M. S., Amiel, J., Buist, N. R., Das, A. M., de Klerk, J. B., Feigenbaum, A. S., Grange, D. K., Hofstede, F. C., Holme, E., Kirk, E. P., Korman, S. H., Morava, E., Morris, A., Smeitink, J., Sukhai, R. N., Vallance, H., Jakobs, C., and Salomons, G. S. (2010). Idh2 mutations in patients with d-2-hydroxyglutaric aciduria. *Science*, 330(6002):336.

Labussiere, M., Idbaih, A., Wang, X. W., Marie, Y., Boisselier, B., Falet, C., Paris, S., Laffaire, J., Carpentier, C., Criniere, E., Ducray, F., El Hallani, S., Mokhtari, K., Hoang-Xuan, K., Delattre, J. Y., and Sanson, M. (2010). All the 1p19q codeleted gliomas are mutated on idh1 or idh2. *Neurology*, 74(23):1886–90.

Lai, A., Kharbanda, S., Pope, W. B., Tran, A., Solis, O. E., Peale, F., Forrest, W. F., Pujara, K., Carrillo, J. A., Pandita, A., Ellingson, B. M., Bowers, C. W., Soriano, R. H., Schmidt, N. O., Mohan, S., Yong, W. H., Seshagiri, S., Modrusan, Z., Jiang, Z., Aldape, K. D., Mischel, P. S., Liau, L. M., Escovedo, C. J., Chen, W., Nghiemphu, P. L., James, C. D., Prados, M. D., Westphal, M., Lamszus, K., Cloughesy, T., and Phillips, H. S. (2011). Evidence for sequenced molecular evolution of idh1 mutant glioblastoma from a distinct cell of origin. *J Clin Oncol*, 29(34):4482–90.

Lai, K., Selinger, D. W., Solomon, J. M., Wu, H., Schmitt, E., Serluca, F. C., Curtis, D., and Benson, J. D. (2013). Integrated compound profiling screens identify the mitochondrial electron transport chain as the molecular target of the natural products manassantin, sesquicillin, and arctigenin. *ACS Chem Biol*, 8(1):257–67.

LaNoue, K. F., Meijer, A. J., and Brouwer, A. (1974). Evidence for electrogenic aspartate transport in rat liver mitochondria. *Archives of biochemistry and biophysics*, 161(2):544–50.

LaNoue, K. F. and Schoolwerth, A. C. (1979). Metabolite transport in mitochondria. *Annual review of biochemistry*, 48:871–922.

Le, A., Lane, A. N., Hamaker, M., Bose, S., Gouw, A., Barbi, J., Tsukamoto, T., Rojas, C. J., Slusher, B. S., Zhang, H., Zimmerman, L. J., Liebler, D. C., Slebos, R. J., Lorkiewicz, P. K., Higashi, R. M., Fan, T. W., and Dang, C. V. (2012). Glucose-independent glutamine metabolism via tca cycling for proliferation and survival in b cells. *Cell Metab*, 15(1):110–21.

Leonardi, R., Subramanian, C., Jackowski, S., and Rock, C. O. (2012). Cancer-associated isocitrate dehydrogenase mutations inactivate nadph-dependent reductive carboxylation. *J Biol Chem*, 287(18):14615–20.

Levintow, L. and Eagle, H. (1961). Biochemistry of cultured mammalian cells. *Annual review of biochemistry*, 30:605–.

Lewis, C. A., Parker, S. J., Fiske, B. P., McCloskey, D., Gui, D. Y., Green, C. R., Vokes, N. I., Feist, A. M., Vander Heiden, M. G., and Metallo, C. M. (2014). Tracing compartmentalized nadph metabolism in the cytosol and mitochondria of mammalian cells. *Mol Cell*, 55(2):253–63.

Li, S., Chou, A. P., Chen, W., Chen, R., Deng, Y., Phillips, H. S., Selfridge, J., Zurayk, M., Lou, J. J., Everson, R. G., Wu, K. C., Faull, K. F., Cloughesy, T., Liau, L. M., and Lai, A. (2013). Overexpression of isocitrate dehydrogenase mutant proteins renders glioma cells more sensitive to radiation. *Neuro Oncol*, 15(1):57–68.

Locasale, J. W., Grassian, A. R., Melman, T., Lyssiotis, C. A., Mattaini, K. R., Bass, A. J., Heffron, G., Metallo, C. M., Muranen, T., Sharfi, H., Sasaki, A. T., Anastasiou, D., Mullarky, E., Vokes, N. I., Sasaki, M., Beroukhim, R., Stephanopoulos, G., Ligon, A. H., Meyerson, M., Richardson, A. L., Chin, L., Wagner, G., Asara, J. M., Brugge, J. S., Cantley, L. C., and Vander Heiden, M. G. (2011). Phosphoglycerate dehydrogenase diverts glycolytic flux and contributes to oncogenesis. *Nature genetics*, 43(9):869–874.

Losman, J. A. and Kaelin, W. G., J. (2013). What a difference a hydroxyl makes: mutant idh, (r)-2-hydroxyglutarate, and cancer. *Genes Dev*, 27(8):836–52.

Losman, J. A., Looper, R. E., Koivunen, P., Lee, S., Schneider, R. K., McMahon, C., Cowley, G. S., Root, D. E., Ebert, B. L., and Kaelin, W. G., J. (2013). (r)-2-hydroxyglutarate is sufficient to promote leukemogenesis and its effects are reversible. *Science*, 339(6127):1621–5.

Lu, C., Venneti, S., Akalin, A., Fang, F., Ward, P. S., Dematteo, R. G., Intlekofer, A. M., Chen, C., Ye, J., Hameed, M., Nafa, K., Agaram, N. P., Cross, J. R., Khanin, R., Mason, C. E., Healey, J. H., Lowe, S. W., Schwartz, G. K., Melnick, A., and Thompson, C. B. (2013). Induction of sarcomas by mutant idh2. *Genes Dev*, 27(18):1986–98.

Lu, C., Ward, P. S., Kapoor, G. S., Rohle, D., Turcan, S., Abdel-Wahab, O., Edwards, C. R., Khanin, R., Figueroa, M. E., Melnick, A., Wellen, K. E., O'Rourke, D. M., Berger, S. L., Chan, T. A., Levine, R. L., Mellinghoff, I. K., and Thompson, C. B. (2012). Idh mutation impairs histone demethylation and results in a block to cell differentiation. *Nature*, 483(7390):474–8.

Lunt, S. Y. and Vander Heiden, M. G. (2011). Aerobic glycolysis: meeting the metabolic requirements of cell proliferation. *Annu Rev Cell Dev Biol*, 27:441–64.

Ma, S., Jiang, B., Deng, W., Gu, Z. K., Wu, F. Z., Li, T., Xia, Y., Yang, H., Ye, D., Xiong, Y., and Guan, K. L. (2015). D-2-hydroxyglutarate is essential for maintaining oncogenic property of mutant idh-containing cancer cells but dispensable for cell growth. *Oncotarget*, 6(11):8606–20.

MacKenzie, E. D., Selak, M. A., Tennant, D. A., Payne, L. J., Crosby, S., Frederiksen, C. M., Watson, D. G., and Gottlieb, E. (2007). Cell-permeating alpha-ketoglutarate derivatives alleviate pseudohypoxia in succinate dehydrogenase-deficient cells. *Mol Cell Biol*, 27(9):3282–9.

Maddocks, O. D., Berkers, C. R., Mason, S. M., Zheng, L., Blyth, K., Gottlieb, E., and Vousden, K. H. (2013). Serine starvation induces stress and p53-dependent metabolic remodelling in cancer cells. *Nature*, 493(7433):542–6.

Maddocks, O. D., Labuschagne, C. F., Adams, P. D., and Vousden, K. H. (2016). Serine

metabolism supports the methionine cycle and dna/rna methylation through de novo atp synthesis in cancer cells. *Mol Cell*, 61(2):210–21.

Mahon, P. C., Hirota, K., and Semenza, G. L. (2001). Fih-1: a novel protein that interacts with hif-1alpha and vhl to mediate repression of hif-1 transcriptional activity. *Genes Dev*, 15(20):2675–86.

Mardis, E. R., Ding, L., Dooling, D. J., Larson, D. E., McLellan, M. D., Chen, K., Koboldt, D. C., Fulton, R. S., Delehaunty, K. D., McGrath, S. D., Fulton, L. A., Locke, D. P., Magrini, V. J., Abbott, R. M., Vickery, T. L., Reed, J. S., Robinson, J. S., Wylie, T., Smith, S. M., Carmichael, L., Eldred, J. M., Harris, C. C., Walker, J., Peck, J. B., Du, F., Dukes, A. F., Sanderson, G. E., Brummett, A. M., Clark, E., McMichael, J. F., Meyer, R. J., Schindler, J. K., Pohl, C. S., Wallis, J. W., Shi, X., Lin, L., Schmidt, H., Tang, Y., Haipek, C., Wiechert, M. E., Ivy, J. V., Kalicki, J., Elliott, G., Ries, R. E., Payton, J. E., Westervelt, P., Tomasson, M. H., Watson, M. A., Baty, J., Heath, S., Shannon, W. D., Nagarajan, R., Link, D. C., Walter, M. J., Graubert, T. A., DiPersio, J. F., Wilson, R. K., and Ley, T. J. (2009). Recurring mutations found by sequencing an acute myeloid leukemia genome. *N Engl J Med*, 361(11):1058–66.

Marin-Valencia, I., Yang, C., Mashimo, T., Cho, S., Baek, H., Yang, X. L., Rajagopalan, K. N., Maddie, M., Vemireddy, V., Zhao, Z., Cai, L., Good, L., Tu, B. P., Hatanpaa, K. J., Mickey, B. E., Mates, J. M., Pascual, J. M., Maher, E. A., Malloy, C. R., Deberardinis, R. J., and Bachoo, R. M. (2012). Analysis of tumor metabolism reveals mitochondrial glucose oxidation in genetically diverse human glioblastomas in the mouse brain in vivo. *Cell Metab*, 15(6):827–37.

Matsunaga, H., Futakuchi-Tsuchida, A., Takahashi, M., Ishikawa, T., Tsuji, M., and Ando, O. (2012). Idh1 and idh2 have critical roles in 2-hydroxyglutarate production in d-2-hydroxyglutarate dehydrogenase depleted cells. *Biochemical and biophysical research communications*, 423(3):553–6.

McClintock, D. S., Santore, M. T., Lee, V. Y., Brunelle, J., Budinger, G. R., Zong, W. X., Thompson, C. B., Hay, N., and Chandel, N. S. (2002). Bcl-2 family members and functional electron transport chain regulate oxygen deprivation-induced cell death. *Mol Cell Biol*, 22(1):94–104.

Medes, G., Thomas, A., and Weinhouse, S. (1953). Metabolism of neoplastic tissue. iv. a study of lipid synthesis in neoplastic tissue slices in vitro. *Cancer Res*, 13(1):27–9.

Metallo, C. M., Gameiro, P. A., Bell, E. L., Mattaini, K. R., Yang, J., Hiller, K., Jewell, C. M., Johnson, Z. R., Irvine, D. J., Guarente, L., Kelleher, J. K., Vander Heiden, M. G., Iliopoulos, O., and Stephanopoulos, G. (2012). Reductive glutamine metabolism by idh1 mediates lipogenesis under hypoxia. *Nature*, 481(7381):380–4.

Metallo, C. M. and Vander Heiden, M. G. (2013). Understanding metabolic regulation and its influence on cell physiology. *Mol Cell*, 49(3):388–98.

Metallo, C. M., Walther, J. L., and Stephanopoulos, G. (2009). Evaluation of 13c isotopic tracers for metabolic flux analysis in mammalian cells. *J Biotechnol*, 144(3):167–74.

Molenaar, R. J., Radivoyevitch, T., Maciejewski, J. P., van Noorden, C. J., and Bleeker, F. E.

(2014). The driver and passenger effects of isocitrate dehydrogenase 1 and 2 mutations in oncogenesis and survival prolongation. *Biochim Biophys Acta*, 1846(2):326–41.

Moroni, I., Bugiani, M., D'Incerti, L., Maccagnano, C., Rimoldi, M., Bissola, L., Pollo, B., Finocchiaro, G., and Uziel, G. (2004). L-2-hydroxyglutaric aciduria and brain malignant tumors: a predisposing condition? *Neurology*, 62(10):1882–4.

Mullen, A. R. and DeBerardinis, R. J. (2012). Genetically-defined metabolic reprogramming in cancer. *Trends Endocrinol Metab*, 23(11):552–9.

Mullen, A. R., Wheaton, W. W., Jin, E. S., Chen, P. H., Sullivan, L. B., Cheng, T., Yang, Y., Linehan, W. M., Chandel, N. S., and DeBerardinis, R. J. (2012). Reductive carboxylation supports growth in tumour cells with defective mitochondria. *Nature*, 481(7381):385–8.

Murphy, T. A., Dang, C. V., and Young, J. D. (2013). Isotopically nonstationary 13c flux analysis of myc-induced metabolic reprogramming in b-cells. *Metab Eng*, 15:206–17.

Mustafa, D. A., Swagemakers, S. M., Buise, L., van der Spek, P. J., and Kros, J. M. (2014). Metabolic alterations due to idh1 mutation in glioma: opening for therapeutic opportunities? *Acta Neuropathol Commun*, 2:6.

Nikiforov, A., Dolle, C., Niere, M., and Ziegler, M. (2011). Pathways and subcellular compartmentation of nad biosynthesis in human cells: from entry of extracellular precursors to mitochondrial nad generation. *The Journal of biological chemistry*, 286(24):21767–78.

Nilsson, R., Jain, M., Madhusudhan, N., Sheppard, N. G., Strittmatter, L., Kampf, C., Huang, J., Asplund, A., and Mootha, V. K. (2014). Metabolic enzyme expression highlights a key role for mthfd2 and the mitochondrial folate pathway in cancer. *Nature communications*, 5:3128.

Noguchi, Y., Young, J. D., Aleman, J. O., Hansen, M. E., Kelleher, J. K., and Stephanopoulos, G. (2009). Effect of anaplerotic fluxes and amino acid availability on hepatic lipoapoptosis. *J Biol Chem*, 284(48):33425–36.

Ozturk, S. S. and Palsson, B. O. (1990). Chemical decomposition of glutamine in cell culture media: effect of media type, ph, and serum concentration. *Biotechnol Prog*, 6(2):121–8.

Papandreou, I., Cairns, R. A., Fontana, L., Lim, A. L., and Denko, N. C. (2006). Hif-1 mediates adaptation to hypoxia by actively downregulating mitochondrial oxygen consumption. *Cell Metab*, 3(3):187–97.

Parker, S. J. and Metallo, C. M. (2015). Metabolic consequences of oncogenic idh mutations. *Pharmacol Ther*, 152:54–62.

Parsons, D. W., Jones, S., Zhang, X., Lin, J. C., Leary, R. J., Angenendt, P., Mankoo, P., Carter, H., Siu, I. M., Gallia, G. L., Olivi, A., McLendon, R., Rasheed, B. A., Keir, S., Nikolskaya, T., Nikolsky, Y., Busam, D. A., Tekleab, H., Diaz, L. A., J., Hartigan, J., Smith, D. R., Strausberg, R. L., Marie, S. K., Shinjo, S. M., Yan, H., Riggins, G. J., Bigner, D. D., Karchin, R., Papadopoulos, N., Parmigiani, G., Vogelstein, B., Velculescu, V. E., and Kinzler, K. W. (2008). An integrated genomic analysis of human glioblastoma multiforme. *Science*, 321(5897):1807–12.

Perry, C., Yu, S., Chen, J., Matharu, K. S., and Stover, P. J. (2007). Effect of vitamin b6 availability on serine hydroxymethyltransferase in mcf-7 cells. *Archives of biochemistry and biophysics*, 462(1):21–7.

Pollak, N., Dolle, C., and Ziegler, M. (2007a). The power to reduce: pyridine nucleotides–small molecules with a multitude of functions. *Biochem J*, 402(2):205–18.

Pollak, N., Niere, M., and Ziegler, M. (2007b). Nad kinase levels control the nadph concentration in human cells. *The Journal of biological chemistry*, 282(46):33562–71.

Popovici-Muller, J., Saunders, J. O., Salituro, F. G., Travins, J. M., Yan, S., Zhao, F., Gross, S., Dang, L., Yen, K. E., Yang, H., Straley, K. S., Jin, S., Kunii, K., Fantin, V. R., Zhang, S., Pan, Q., Shi, D., Biller, S. A., and Su, S. M. (2012). Discovery of the first potent inhibitors of mutant idh1 that lower tumor 2-hg in vivo. *ACS Med Chem Lett*, 3(10):850–5.

Porstmann, T., Santos, C. R., Griffiths, B., Cully, M., Wu, M., Leevers, S., Griffiths, J. R., Chung, Y. L., and Schulze, A. (2008). Srebp activity is regulated by mtorc1 and contributes to akt-dependent cell growth. *Cell Metab*, 8(3):224–36.

Pusch, S., Schweizer, L., Beck, A. C., Lehmler, J. M., Weissert, S., Balss, J., Miller, A. K., and von Deimling, A. (2014). D-2-hydroxyglutarate producing neo-enzymatic activity inversely correlates with frequency of the type of isocitrate dehydrogenase 1 mutations found in glioma. *Acta Neuropathol Commun*, 2:19.

Quek, L. E., Dietmair, S., Kromer, J. O., and Nielsen, L. K. (2010). Metabolic flux analysis in mammalian cell culture. *Metab Eng*, 12(2):161–71.

Rardin, M. J., Wiley, S. E., Naviaux, R. K., Murphy, A. N., and Dixon, J. E. (2009). Monitoring phosphorylation of the pyruvate dehydrogenase complex. *Anal Biochem*, 389(2):157–64.

Reitman, Z. J., Duncan, C. G., Poteet, E., Winters, A., Yan, L. J., Gooden, D. M., Spasojevic, I., Boros, L. G., Yang, S. H., and Yan, H. (2014). Cancer-associated isocitrate dehydrogenase 1 (idh1) r132h mutation and d-2-hydroxyglutarate stimulate glutamine metabolism under hypoxia. *J Biol Chem*, 289(34):23318–28.

Reitman, Z. J., Jin, G., Karoly, E. D., Spasojevic, I., Yang, J., Kinzler, K. W., He, Y., Bigner, D. D., Vogelstein, B., and Yan, H. (2011). Profiling the effects of isocitrate dehydrogenase 1 and 2 mutations on the cellular metabolome. *Proc Natl Acad Sci U S A*, 108(8):3270–5.

Rendina, A. R., Hermes, J. D., and Cleland, W. W. (1984). Use of multiple isotope effects to study the mechanism of 6-phosphogluconate dehydrogenase. *Biochemistry*, 23(25):6257–62.

Rendina, A. R., Pietrak, B., Smallwood, A., Zhao, H., Qi, H., Quinn, C., Adams, N. D., Concha, N., Duraiswami, C., Thrall, S. H., Sweitzer, S., and Schwartz, B. (2013). Mutant idh1 enhances the production of 2-hydroxyglutarate due to its kinetic mechanism. *Biochemistry*, 52(26):4563–77.

Rohle, D., Popovici-Muller, J., Palaskas, N., Turcan, S., Grommes, C., Campos, C., Tsoi, J., Clark, O., Oldrini, B., Komisopoulou, E., Kunii, K., Pedraza, A., Schalm, S., Silverman, L.,

Miller, A., Wang, F., Yang, H., Chen, Y., Kernytsky, A., Rosenblum, M. K., Liu, W., Biller, S. A., Su, S. M., Brennan, C. W., Chan, T. A., Graeber, T. G., Yen, K. E., and Mellinghoff, I. K. (2013). An inhibitor of mutant idh1 delays growth and promotes differentiation of glioma cells. *Science*, 340(6132):626–30.

Rose, N. R., McDonough, M. A., King, O. N., Kawamura, A., and Schofield, C. J. (2011). Inhibition of 2-oxoglutarate dependent oxygenases. *Chem Soc Rev*, 40(8):4364–97.

Ru, P., Williams, T. M., Chakravarti, A., and Guo, D. (2013). Tumor metabolism of malignant gliomas. *Cancers (Basel)*, 5(4):1469–84.

Ruhl, M., Le Coq, D., Aymerich, S., and Sauer, U. (2012). 13c-flux analysis reveals nadph-balancing transhydrogenation cycles in stationary phase of nitrogen-starving bacillus subtilis. *The Journal of biological chemistry*, 287(33):27959–70.

Rzem, R., Vincent, M. F., Van Schaftingen, E., and Veiga-da Cunha, M. (2007). L-2-hydroxyglutaric aciduria, a defect of metabolite repair. *J Inherit Metab Dis*, 30(5):681–9.

Sabharwal, S. S. and Schumacker, P. T. (2014). Mitochondrial ros in cancer: initiators, amplifiers or an achilles' heel? *Nat Rev Cancer*, 14(11):709–21.

Sasaki, M., Knobbe, C. B., Itsumi, M., Elia, A. J., Harris, I. S., Chio, I., Cairns, R. A., McCracken, S., Wakeham, A., Haight, J., Ten, A. Y., Snow, B., Ueda, T., Inoue, S., Yamamoto, K., Ko, M., Rao, A., Yen, K. E., Su, S. M., and Mak, T. W. (2012a). D-2-hydroxyglutarate produced by mutant idh1 perturbs collagen maturation and basement membrane function. *Genes Dev*, 26(18):2038–49.

Sasaki, M., Knobbe, C. B., Munger, J. C., Lind, E. F., Brenner, D., Brustle, A., Harris, I. S., Holmes, R., Wakeham, A., Haight, J., You-Ten, A., Li, W. Y., Schalm, S., Su, S. M., Virtanen, C., Reifenberger, G., Ohashi, P. S., Barber, D. L., Figueroa, M. E., Melnick, A., Zuniga-Pflucker, J. C., and Mak, T. W. (2012b). Idh1(r132h) mutation increases murine haematopoietic progenitors and alters epigenetics. *Nature*, 488(7413):656–9.

Sazanov, L. A. and Jackson, J. B. (1994). Proton-translocating transhydrogenase and nad- and nadp-linked isocitrate dehydrogenases operate in a substrate cycle which contributes to fine regulation of the tricarboxylic acid cycle activity in mitochondria. *FEBS letters*, 344(2-3):109–16.

Schafer, Z. T., Grassian, A. R., Song, L., Jiang, Z., Gerhart-Hines, Z., Irie, H. Y., Gao, S., Puigserver, P., and Brugge, J. S. (2009). Antioxidant and oncogene rescue of metabolic defects caused by loss of matrix attachment. *Nature*, 461(7260):109–13.

Scott, D. A., Richardson, A. D., Filipp, F. V., Knutzen, C. A., Chiang, G. G., Ronai, Z. A., Osterman, A. L., and Smith, J. W. (2011). Comparative metabolic flux profiling of melanoma cell lines: beyond the warburg effect. *J Biol Chem*, 286(49):42626–34.

Scotti, M., Stella, L., Shearer, E. J., and Stover, P. J. (2013). Modeling cellular compartmentation in one-carbon metabolism. *Wiley interdisciplinary reviews. Systems biology and medicine*, 5(3):343–65.

Selak, M. A., Armour, S. M., MacKenzie, E. D., Boulahbel, H., Watson, D. G., Mansfield, K. D., Pan, Y., Simon, M. C., Thompson, C. B., and Gottlieb, E. (2005). Succinate links tca cycle dysfunction to oncogenesis by inhibiting hif-alpha prolyl hydroxylase. *Cancer Cell*, 7(1):77–85.

Seltzer, M. J., Bennett, B. D., Joshi, A. D., Gao, P., Thomas, A. G., Ferraris, D. V., Tsukamoto, T., Rojas, C. J., Slusher, B. S., Rabinowitz, J. D., Dang, C. V., and Riggins, G. J. (2010). Inhibition of glutaminase preferentially slows growth of glioma cells with mutant idh1. *Cancer Res*, 70(22):8981–7.

Semenza, G. L., Jiang, B. H., Leung, S. W., Passantino, R., Concordet, J. P., Maire, P., and Giallongo, A. (1996). Hypoxia response elements in the aldolase a, enolase 1, and lactate dehydrogenase a gene promoters contain essential binding sites for hypoxia-inducible factor 1. *J Biol Chem*, 271(51):32529–37.

Semenza, G. L., Roth, P. H., Fang, H. M., and Wang, G. L. (1994). Transcriptional regulation of genes encoding glycolytic enzymes by hypoxia-inducible factor 1. *J Biol Chem*, 269(38):23757–63.

Shechter, I., Dai, P., Huo, L., and Guan, G. (2003). Idh1 gene transcription is sterol regulated and activated by srebp-1a and srebp-2 in human hepatoma hepg2 cells: evidence that idh1 may regulate lipogenesis in hepatic cells. *J Lipid Res*, 44(11):2169–80.

Sheikh, K., Forster, J., and Nielsen, L. K. (2005). Modeling hybridoma cell metabolism using a generic genome-scale metabolic model of mus musculus. *Biotechnol Prog*, 21(1):112–21.

Shi, J., Sun, B., Shi, W., Zuo, H., Cui, D., Ni, L., and Chen, J. (2014). Decreasing gsh and increasing ros in chemosensitivity gliomas with idh1 mutation. *Tumour Biol*.

Shin, K. J., Wall, E. A., Zavzavadjian, J. R., Santat, L. A., Liu, J., Hwang, J. I., Rebres, R., Roach, T., Seaman, W., Simon, M. I., and Fraser, I. D. (2006). A single lentiviral vector platform for microrna-based conditional rna interference and coordinated transgene expression. *Proceedings of the National Academy of Sciences of the United States of America*, 103(37):13759–64.

Sjoblom, T., Jones, S., Wood, L. D., Parsons, D. W., Lin, J., Barber, T. D., Mandelker, D., Leary, R. J., Ptak, J., Silliman, N., Szabo, S., Buckhaults, P., Farrell, C., Meeh, P., Markowitz, S. D., Willis, J., Dawson, D., Willson, J. K., Gazdar, A. F., Hartigan, J., Wu, L., Liu, C., Parmigiani, G., Park, B. H., Bachman, K. E., Papadopoulos, N., Vogelstein, B., Kinzler, K. W., and Velculescu, V. E. (2006). The consensus coding sequences of human breast and colorectal cancers. *Science*, 314(5797):268–74.

Son, J., Lyssiotis, C. A., Ying, H., Wang, X., Hua, S., Ligorio, M., Perera, R. M., Ferrone, C. R., Mullarky, E., Shyh-Chang, N., Kang, Y., Fleming, J. B., Bardeesy, N., Asara, J. M., Haigis, M. C., DePinho, R. A., Cantley, L. C., and Kimmelman, A. C. (2013a). Glutamine supports pancreatic cancer growth through a kras-regulated metabolic pathway. *Nature*, 496(7443):101–5.

Son, J., Lyssiotis, C. A., Ying, H., Wang, X., Hua, S., Ligorio, M., Perera, R. M., Ferrone, C. R., Mullarky, E., Shyh-Chang, N., Kang, Y., Fleming, J. B., Bardeesy, N., Asara, J. M., Haigis, M. C., DePinho, R. A., Cantley, L. C., and Kimmelman, A. C. (2013b). Glutamine supports

pancreatic cancer growth through a kras-regulated metabolic pathway. *Nature*, 496(7443):101–5.

SongTao, Q., Lei, Y., Si, G., YanQing, D., HuiXia, H., XueLin, Z., LanXiao, W., and Fei, Y. (2012). Idh mutations predict longer survival and response to temozolomide in secondary glioblastoma. *Cancer Sci*, 103(2):269–73.

Struys, E. A. (2006). D-2-hydroxyglutaric aciduria: unravelling the biochemical pathway and the genetic defect. *J Inherit Metab Dis*, 29(1):21–9.

Szaraz, P., Banhegyi, G., and Benedetti, A. (2010). Altered redox state of luminal pyridine nucleotides facilitates the sensitivity towards oxidative injury and leads to endoplasmic reticulum stress dependent autophagy in hepg2 cells. *The international journal of biochemistry cell biology*, 42(1):157–66.

Tarhonskaya, H., Rydzik, A. M., Leung, I. K., Loik, N. D., Chan, M. C., Kawamura, A., McCullagh, J. S., Claridge, T. D., Flashman, E., and Schofield, C. J. (2014). Non-enzymatic chemistry enables 2-hydroxyglutarate-mediated activation of 2-oxoglutarate oxygenases. *Nat Commun*, 5:3423.

Tedeschi, P. M., Markert, E. K., Gounder, M., Lin, H., Dvorzhinski, D., Dolfi, S. C., Chan, L. L., Qiu, J., Dipaola, R. S., Hirshfield, K. M., Boros, L. G., Bertino, J. R., Oltvai, Z. N., and Vazquez, A. (2013). Contribution of serine, folate and glycine metabolism to the atp, nadph and purine requirements of cancer cells. *Cell death disease*, 4:e877.

Tennant, D. A., Duran, R. V., and Gottlieb, E. (2010). Targeting metabolic transformation for cancer therapy. *Nat Rev Cancer*, 10(4):267–77.

Tibbetts, A. S. and Appling, D. R. (2010). Compartmentalization of mammalian folate-mediated one-carbon metabolism. *Annu Rev Nutr*, 30:57–81.

Tonjes, M., Barbus, S., Park, Y. J., Wang, W., Schlotter, M., Lindroth, A. M., Pleier, S. V., Bai, A. H., Karra, D., Piro, R. M., Felsberg, J., Addington, A., Lemke, D., Weibrecht, I., Hovestadt, V., Rolli, C. G., Campos, B., Turcan, S., Sturm, D., Witt, H., Chan, T. A., Herold-Mende, C., Kemkemer, R., Konig, R., Schmidt, K., Hull, W. E., Pfister, S. M., Jugold, M., Hutson, S. M., Plass, C., Okun, J. G., Reifenberger, G., Lichter, P., and Radlwimmer, B. (2013). Bcat1 promotes cell proliferation through amino acid catabolism in gliomas carrying wild-type idh1. *Nat Med*, 19(7):901–8.

Turcan, S., Rohle, D., Goenka, A., Walsh, L. A., Fang, F., Yilmaz, E., Campos, C., Fabius, A. W., Lu, C., Ward, P. S., Thompson, C. B., Kaufman, A., Guryanova, O., Levine, R., Heguy, A., Viale, A., Morris, L. G., Huse, J. T., Mellinghoff, I. K., and Chan, T. A. (2012). Idh1 mutation is sufficient to establish the glioma hypermethylator phenotype. *Nature*, 483(7390):479–83.

Van Schaftingen, E., Rzem, R., Marbaix, A., Collard, F., Veiga-da Cunha, M., and Linster, C. L. (2013). Metabolite proofreading, a neglected aspect of intermediary metabolism. *J Inherit Metab Dis*, 36(3):427–34.

Vander Heiden, M. G., Cantley, L. C., and Thompson, C. B. (2009). Understanding the warburg

effect: the metabolic requirements of cell proliferation. *Science*, 324(5930):1029–33.

Vander Heiden, M. G., Chandel, N. S., Williamson, E. K., Schumacker, P. T., and Thompson, C. B. (1997). Bcl-xl regulates the membrane potential and volume homeostasis of mitochondria. *Cell*, 91(5):627–37.

Wajne, M., Vargas, C. R., Funayama, C., Fernandez, A., Elias, M. L., Goodman, S. I., Jakobs, C., and van der Knaap, M. S. (2002). D-2-hydroxyglutaric aciduria in a patient with a severe clinical phenotype and unusual mri findings. *J Inherit Metab Dis*, 25(1):28–34.

Wakimoto, H., Tanaka, S., Curry, W. T., Loebel, F., Zhao, D., Tateishi, K., Chen, J., Klofas, L. K., Lelic, N., Kim, J. C., Dias-Santagata, D., Ellisen, L. W., Borger, D. R., Fendt, S. M., Vander Heiden, M. G., Batchelor, T. T., Iafrate, A. J., Cahill, D. P., and Chi, A. S. (2014). Targetable signaling pathway mutations are associated with malignant phenotype in idh-mutant gliomas. *Clin Cancer Res*, 20(11):2898–909.

Wallace, D. C. (2012). Mitochondria and cancer. *Nat Rev Cancer*, 12(10):685–98.

Wallace, D. C. and Fan, W. (2010). Energetics, epigenetics, mitochondrial genetics. *Mitochondrion*, 10(1):12–31.

Wallace, D. C., Fan, W., and Procaccio, V. (2010). Mitochondrial energetics and therapeutics. *Annu Rev Pathol*, 5:297–348.

Wang, F., Travins, J., DeLaBarre, B., Penard-Lacronique, V., Schalm, S., Hansen, E., Straley, K., Kernytsky, A., Liu, W., Gliser, C., Yang, H., Gross, S., Artin, E., Saada, V., Mylonas, E., Quivoron, C., Popovici-Muller, J., Saunders, J. O., Salituro, F. G., Yan, S., Murray, S., Wei, W., Gao, Y., Dang, L., Dorsch, M., Agresta, S., Schenkein, D. P., Biller, S. A., Su, S. M., de Botton, S., and Yen, K. E. (2013). Targeted inhibition of mutant idh2 in leukemia cells induces cellular differentiation. *Science*, 340(6132):622–6.

Wang, P., Wu, J., Ma, S., Zhang, L., Yao, J., Hoadley, K. A., Wilkerson, M. D., Perou, C. M., Guan, K. L., Ye, D., and Xiong, Y. (2015). Oncometabolite d-2-hydroxyglutarate inhibits alkbh dna repair enzymes and sensitizes idh mutant cells to alkylating agents. *Cell Rep*, 13(11):2353–61.

Warburg, O. (1956). On respiratory impairment in cancer cells. *Science*, 124(3215):269–70.

Ward, P. S., Cross, J. R., Lu, C., Weigert, O., Abel-Wahab, O., Levine, R. L., Weinstock, D. M., Sharp, K. A., and Thompson, C. B. (2012). Identification of additional idh mutations associated with oncometabolite r(-)-2-hydroxyglutarate production. *Oncogene*, 31(19):2491–8.

Ward, P. S., Lu, C., Cross, J. R., Abdel-Wahab, O., Levine, R. L., Schwartz, G. K., and Thompson, C. B. (2013). The potential for isocitrate dehydrogenase mutations to produce 2-hydroxyglutarate depends on allele specificity and subcellular compartmentalization. *J Biol Chem*, 288(6):3804–15.

Ward, P. S., Patel, J., Wise, D. R., Abdel-Wahab, O., Bennett, B. D., Coller, H. A., Cross, J. R., Fantin, V. R., Hedvat, C. V., Perl, A. E., Rabinowitz, J. D., Carroll, M., Su, S. M., Sharp,

K. A., Levine, R. L., and Thompson, C. B. (2010). The common feature of leukemia-associated idh1 and idh2 mutations is a neomorphic enzyme activity converting alpha-ketoglutarate to 2-hydroxyglutarate. *Cancer Cell*, 17(3):225–34.

Watanabe, T., Nobusawa, S., Kleihues, P., and Ohgaki, H. (2009). Idh1 mutations are early events in the development of astrocytomas and oligodendrogliomas. *Am J Pathol*, 174(4):1149–53.

Williams, S. C., Karajannis, M. A., Chiriboga, L., Golfinos, J. G., von Deimling, A., and Zagzag, D. (2011). R132h-mutation of isocitrate dehydrogenase-1 is not sufficient for hif-1alpha upregulation in adult glioma. *Acta Neuropathol*, 121(2):279–81.

Wise, D. R., Ward, P. S., Shay, J. E., Cross, J. R., Gruber, J. J., Sachdeva, U. M., Platt, J. M., DeMatteo, R. G., Simon, M. C., and Thompson, C. B. (2011). Hypoxia promotes isocitrate dehydrogenase-dependent carboxylation of alpha-ketoglutarate to citrate to support cell growth and viability. *Proc Natl Acad Sci U S A*, 108(49):19611–6.

Xiao, M., Yang, H., Xu, W., Ma, S., Lin, H., Zhu, H., Liu, L., Liu, Y., Yang, C., Xu, Y., Zhao, S., Ye, D., Xiong, Y., and Guan, K. L. (2012). Inhibition of alpha-kg-dependent histone and dna demethylases by fumarate and succinate that are accumulated in mutations of fh and sdh tumor suppressors. *Genes Dev*, 26(12):1326–38.

Xu, W., Yang, H., Liu, Y., Yang, Y., Wang, P., Kim, S. H., Ito, S., Yang, C., Wang, P., Xiao, M. T., Liu, L. X., Jiang, W. Q., Liu, J., Zhang, J. Y., Wang, B., Frye, S., Zhang, Y., Xu, Y. H., Lei, Q. Y., Guan, K. L., Zhao, S. M., and Xiong, Y. (2011). Oncometabolite 2-hydroxyglutarate is a competitive inhibitor of alpha-ketoglutarate-dependent dioxygenases. *Cancer Cell*, 19(1):17–30.

Xu, X., Zhao, J., Xu, Z., Peng, B., Huang, Q., Arnold, E., and Ding, J. (2004). Structures of human cytosolic nadp-dependent isocitrate dehydrogenase reveal a novel self-regulatory mechanism of activity. *J Biol Chem*, 279(32):33946–57.

Yan, H., Parsons, D. W., Jin, G., McLendon, R., Rasheed, B. A., Yuan, W., Kos, I., Batinic-Haberle, I., Jones, S., Riggins, G. J., Friedman, H., Friedman, A., Reardon, D., Herndon, J., Kinzler, K. W., Velculescu, V. E., Vogelstein, B., and Bigner, D. D. (2009). Idh1 and idh2 mutations in gliomas. *N Engl J Med*, 360(8):765–73.

Ye, J., Fan, J., Venneti, S., Wan, Y. W., Pawel, B. R., Zhang, J., Finley, L. W., Lu, C., Lindsten, T., Cross, J. R., Qing, G., Liu, Z., Simon, M. C., Rabinowitz, J. D., and Thompson, C. B. (2014). Serine catabolism regulates mitochondrial redox control during hypoxia. *Cancer Discov*, 4(12):1406–17.

Yen, K., Wang, F., Travins, J., Chen, Y., Hua, Y., Straley, K., Choe, S., Dorsch, M., Schenkein, D. P., Agresta, S., Biller, S., and Su, M. (2013). Ag-221 offers a survival advantage in a primary human idh2 mutant aml xenograft model. *Blood*, 122(21):1.

Yen, K. E. and Schenkein, D. P. (2012). Cancer-associated isocitrate dehydrogenase mutations. *Oncologist*, 17(1):5–8.

Yizhak, K., Benyamini, T., Liebermeister, W., Ruppin, E., and Shlomi, T. (2010). Integrating quantitative proteomics and metabolomics with a genome-scale metabolic network model. *Bioinformatics*, 26(12):i255–60.

You, K. S. (1985). Stereospecificity for nicotinamide nucleotides in enzymatic and chemical hydride transfer reactions. *CRC critical reviews in biochemistry*, 17(4):313–451.

Young, J. D. (2014). Inca: a computational platform for isotopically non-stationary metabolic flux analysis. *Bioinformatics*.

Young, J. D., Walther, J. L., Antoniewicz, M. R., Yoo, H., and Stephanopoulos, G. (2008). An elementary metabolite unit (emu) based method of isotopically nonstationary flux analysis. *Biotechnol Bioeng*, 99(3):686–99.

Zamboni, N. (2011). 13c metabolic flux analysis in complex systems. *Curr Opin Biotechnol*, 22(1):103–8.

Zhao, S., Lin, Y., Xu, W., Jiang, W., Zha, Z., Wang, P., Yu, W., Li, Z., Gong, L., Peng, Y., Ding, J., Lei, Q., Guan, K. L., and Xiong, Y. (2009). Glioma-derived mutations in idh1 dominantly inhibit idh1 catalytic activity and induce hif-1alpha. *Science*, 324(5924):261–5.

Zheng, B., Yao, Y., Liu, Z., Deng, L., Anglin, J. L., Jiang, H., Prasad, B. V., and Song, Y. (2013). Crystallographic investigation and selective inhibition of mutant isocitrate dehydrogenase. *ACS Med Chem Lett*, 4(6):542–546.